2007

Probing the Association Behavior of Hydrophobic Organic Compounds with Dissolved Humic Materials

Hadi M. Marwani
Louisiana State University and Agricultural and Mechanical College, hmarwa1@lsu.edu

PROBING THE ASSOCIATION BEHAVIOR OF HYDROPHOBIC ORGANIC COMPOUNDS WITH DISSOLVED HUMIC MATERIALS

A Dissertation

Submitted to the Graduate Faculty of the
Louisiana State University and
Agricultural and Mechanical College
in partial fulfillment of the
requirements for the degree of
Doctor of Philosophy

in

The Department of Chemistry

by
Hadi M. Marwani
B.S., King Abdulaziz University, 1998
December 2007

DEDICATION

I dedicate this work to my wife Nouf Alrobi and my parents. I thank all of you for your love, help, confidence in me, constant prayers, and guidance that gave me the strength throughout this challenging journey and made one of my dreams come true. Nouf, thank you for understanding and cheering me on especially during the hard times. Your love and passion has been the oasis of my encouragement and endurance in my academic pursuits.

ACKNOWLEDGMENTS

I acknowledge the following people for their support and contributions:

My parents, for all your love, constant encouragement, support, and prayers that have brought me this far.

Dr. Isiah M. Warner, for your wisdom, guidance, professional advice, patience, support and confidence in me. Thank you for encouraging me to explore different scientific aspects. You are an excellent mentor. I benefited greatly from the way you challenge your students on scientific thinking and from your enthusiasm and professionalism on exploring new and interesting scientific fields.

Dr. Robert L. Cook, for your professional advice, guidance, support, patience, and your helpful scientific discussions. Thank you for encouraging me to finish what I started. I am indebted to you for teaching me a great deal about the environmental field. Your influence on my research contributed to every accomplishment presented here.

My Committee Members, for your helpful comments and contribution towards my dissertation.

Dr. Dale Treleaven, for your teaching and help with nuclear magnetic resonance (NMR) spectroscopy and for helpful scientific discussions.

Dr. Mark Lowry, for your contributions to my research. Your intelligence, talent, and expertise really inspired me.

Dr. Sayo Fakayode, Dr. Kristin Fletcher, and Ms. Elmonia Collins, for useful research discussions, advice, and editing my research work.

Warner and Cook research groups, for your friendship and support. I will cherish the moments we spent together.

King Abdulaziz University, for your financial support and contributions to the achievement of my dream.

My loving wife, Nouf Alrobi, for your love, care, and encouragement. You were always there when I needed someone to talk to. This is also your doctorate.

My son and daughter, Morad and Nadine, you are great gifts to my life. May you grow to be full of wisdom and knowledge.

TABLE OF CONTENTS

LIST OF TABLES

Table **Page**

LIST OF FIGURES

LIST OF ABBREVIATIONS

Abbreviation	Name
AHA	Amherst humic acid
BAHA	bleached Amherst humic acid
BNF	1,1'-bi-2-naphthol bis (trifluoro - methanesulfonate)
Al^{3+}	aluminum ion
$C_{18}H_{37}Si$-	octadecylsilyl groups
Ca^{2+}	calcium ion
$CFCl_3$	trichlorofluoromethane
CH_3F	fluoromethane
Cl^-	chloride ion
CMC	critical micelle concentration
CO_2	carbon dioxide
CR	combined run
D_2	deuterium
DHM	dissolved humic materials
DMSO	dimethyl sulfoxide
DOC	dissolved organic carbons
FA	fulvic acids
Fe^{3+}	ferric ion
Fl	fluorescein
FPHAS	Florida peat humic acid standard
H^+	proton ion

H_2	hydrogen
HA	humic acids
HCl	hydrochloric acid
HETP	height equivalent to one theoretical plate
HF	hydrofluoric acid
HM	humic materials
HOC	hydrophobic organic compounds
HPLC	high performance liquid chromatography
HS	humic substances
IHSS	international humic substances society
LHAS	Leonardite humic acid standard
LR	long run
Mg^{2+}	magnesium ion
N	nitrogen
$Na_4P_2O_7$	sodium pyrophosphate
NaCl	sodium chloride
NaOH	sodium hydroxide
NLLS	non-linear least squares
NMR	nuclear magnetic resonance
NOM	natural organic matter
OM	organic matter
P	phosphorus
PAHs	polycyclic aromatic hydrocarbons

PMT	photomultiplier tubes
RhB	rhodamine B
S	sulfur
S/N	signal to noise ratio
SRFAR	Suwannee River fulvic acid reference
TCSPC	time-correlated single photon counting
TFAE	1-(9-anthryl)-2,2,2-trifluoroethanol
UV-Vis	Ultraviolet-Visible
XAD	poly(methyl methacrylate)

ABSTRACT

The association mechanism between hydrophobic organic compounds (HOC) and dissolved humic materials (DHM) has continued to be one of the interesting areas in environmental applications. The goal of the research reported in this dissertation is to investigate the association behavior of HOC with DHM. The first part of this research involves steady-state fluorescence measurements of these multi-component systems to study the effect of DHM content on the association mechanism of HOC, in particular using pyrene as a model. Results showed that steady-state fluorescence alone may not provide enough information about the quenching mechanism of pyrene with DHM. Lifetime based fluorescence measurements allow for a deeper mechanistic understanding as compared to the traditional steady-state technique. However, photobleaching, dissolved oxygen, and HOC adsorption to cell walls are problems encountered in lifetime measurements. These effects can directly complicate the interpretation of fluorescence lifetime results. Therefore, a new approach to frequency-domain lifetime measurements, based on frequency segmentation and recombination, was developed during the second part of this dissertation research to address these experimental considerations. The frequency segmentation and recombination method was evaluated using a simple two component system consisting of fluorescein and rhodamine B mixture. Comparison of experimental data collected in traditional and segmented fashion with simulated data demonstrated the validity of the technique. The newly developed method was applied to mixtures of pyrene and DHM to further investigate the pyrene quenching mechanism with DHM. Finally, the chemical effect of chiral pesticides (coumachlor, difenacoum, warfarin, and napropamide) in the presence of Leonardite humic acid standard (LHAS) was investigated by use of steady-state fluorescence spectroscopy. In addition, the chiral recognition ability and enantiomeric selectivity of LHAS with pure enantiomers of

1,1'-bi-2-naphthol bis (trifluoro - methanesulfonate) and 1-(9-anthryl)-2,2,2-trifluoroethanol, used as probes of the interaction, were investigated using liquid-state ^{19}F NMR spectroscopy. To further study DHM enantioselectivity with chiral compounds, the interaction of *R* or *S*-1-(9-anthryl)-2,2,2-trifluoroethanol with LHAS was evaluated for samples monitored in the dark and exposed to light for different time periods by use of high performance liquid chromatography.

CHAPTER 1

INTRODUCTION

1.1 Humic Materials

Humic Materials (HM) are heterogeneous mixtures and constitute a series of relatively high molecular weight aggregates, yellow to black organic compounds of aliphatic and aromatic nature.[1, 2] HM are found in soils, natural waters, sewage, marine and lake sediments, compost heaps, peat bogs, lignites, brown coals, and miscellaneous other deposits.[3] Their abundance in soils is two to three times higher as compared to the living mass of organic matter (OM).[4] They contained approximately 60-70% of the total organic carbon in soils, 40-60% of dissolved organic carbon in natural waters, and are the largest fraction of natural organic matter (NOM) in water.[2] HM are very important in the environment because they have physical, chemical, and biological benefits, such as increasing water holding capacity, increasing nitrogen content of soils, possessing a high ion exchange, increasing the vitamin content of plants, acting as redox reagents and pH buffers, and reducing the toxicity of some heavy metals.[5]

Many studies were performed in order to classify HM based on their chemical nature between 1900 and 1940.[3] HM are operationally classified based on aqueous solubility into three major fractions: humic acids (HA), fulvic acids (FA), and humins. HA are soluble in alkaline media but participate at pH 2. FA are soluble in water at any pH value, and humins are insoluble in water under any condition.[3, 6] Humins are thought to be HM associated with hydroxides or mineral oxides. As an alternative, they may be strongly associated with hydrocarbons and lipids, leading to water-insoluble humins.[7] In general, HA and humins are found mostly in soils and sediments as a portion of the solid phase. FA are more mobile in aqueous environments and

considered to be a major part of dissolved humic materials (DHM) in natural waters.[3] However, HA are also a major component of DHM in natural systems.

1.1.1 Formation of Humic Materials

In all terrestrial and aquatic environments, HM are formed during the decay of biomatter. The term biomatter refers to biologically synthesized matter that is no longer considered to be portion of a living cell. The formation of HM takes place in the early period of biomatter digenesis in comparison to coal and petroleum formation, which are produced under harsher conditions and over a longer geological period. Substances do not originate from biomatter decay in soils, natural waters, or sediments should not be counted as HM even though they may exhibit the same color and acid/base solubility behaviors as HM.[8]

The decay of plant and animal residues in soil represents the basic biological process in which carbon is redistributed to the environment (Figure 1.1).

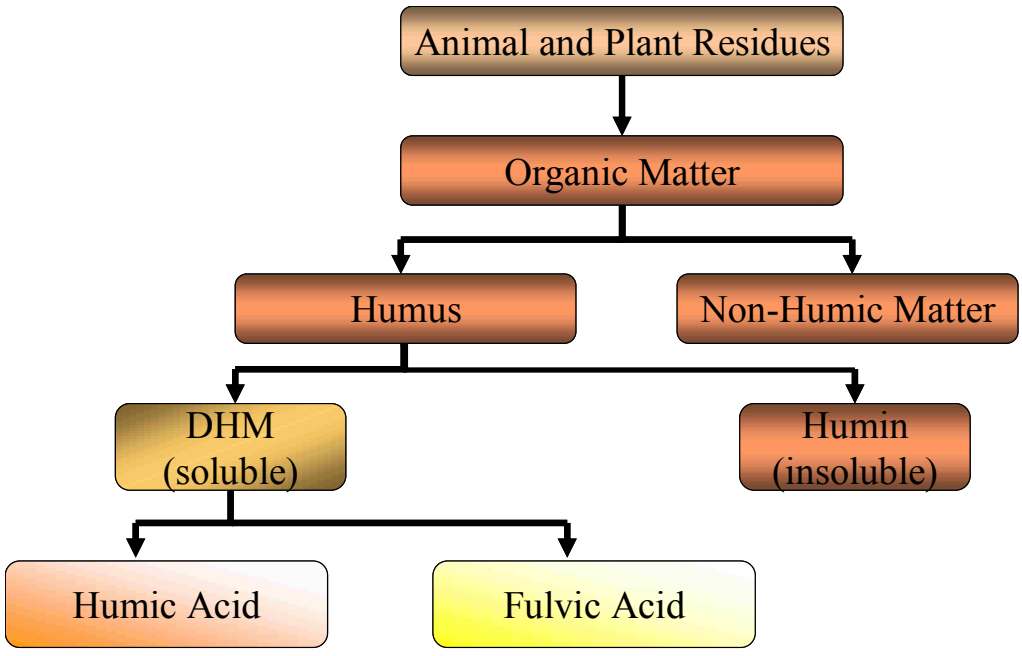

Figure 1.1 Proposed mechanism for HM formation.

Carbon is transformed into carbon dioxide (CO_2) in most environments as a result of the mineralization process, which is defined as the microbial transformation of an element from an organic to inorganic form.[3] Other elements, such as nitrogen (N), phosphorus (P), sulfur (S), and several micronutrients, are in forms needed by higher plants. However, the mineralization process is seldom completed; consequently, organic matter (OM) gathers in the form of HM. The accumulation stage is dependent on turnover times, weather, parent mineral materials, topography, cropping, and vegetation. The formation of HM is not constrained by reactions that occur within living organisms. Alternatively, a collection of some chemicals, including microbial intermediates and none biologically directed reactions, generates a complex mixture of organic compounds. A portion of these organic compounds are converted into stable humus, which is then fully decomposed into humins and DHM. HA and FA are then fractionated from DHM based on their water-solubility (Figure 1.1).

1.1.2 Isolation of Humic Materials from Soils and Waters

Several analytical separation methods, ranging from fractional precipitation to more advanced separation methods such as all types of chromatography, electrophoresis, and field-flow fractionation, have been used for the isolation of HM. However, even when the most advanced isolation methods are used, the isolated fractions are very complex mixtures.[8] In this section, the isolation of HM from soils and waters is discussed in detail.

1.1.2.1 Isolation of Humic Materials from Soils

Solubility of HM is accomplished by solvation of ions. The protonation of ions increases with an increase in the pH.[4, 9] Characteristics of proton ion (H^+) exchanged HM are the same as neutral polar macromolecules, which are bound to each other by hydrogen bonding. Hydrogen bonding, with associated non-polar moieties via hydrophobic association or van der Waals

forces, and charge transfer processes yield HM with similar properties to those of high molecular weight materials. The least associated and most polar HM can only be dissolved in water. The strongest acidic groups are dissociated first at higher pH, and conjugated bases, generally carboxylates, are then solvated. Finally, the weakest acidic groups, such as phenols and enols, dissociate and solvate.

Di- and tri-valent cations, particularly calcium ion (Ca^{2+}), magnesium ion (Mg^{2+}), ferric ion (Fe^{3+}), and aluminum ion (Al^{3+}), are the dominant exchangeable cations. Anionic groups in HM strongly bind these cations. As a result, cations are able to form inter- and intramolecular bridges between anionic sites. However, the mono-valent cation does not support such bridging. Consequently, repulsion takes place between charged species, and the configuration of the molecules is expanded, allowing solvation to take place. Hydrogen bonding, cation bridging, hydrophobic association, or van der Waals association effects can easily lead to a condensed conformation of HM, with water being partially excluded from the matrix. These effects can be resolved by exchanging the di-valent or polyvalent cations with mono-valent species other than H^{+}. Consequently, the addition of sodium pyrophosphate ($Na_4P_2O_7$) to the system allows the pyrophosphate to complex polyvalent cations, and negatively charged ions of HM are neutralized by the sodium. Charged species are then solvated in water.

An alternative approach is the extraction with sodium hydroxide pyro (NaOH/Pyro) and elution at different pH values using XAD [poly(methyl methacrylate)] resins. HM extraction with dimethyl sulfoxide and hydrochloric acid (DMSO/HCl) should follow after exhaustive extraction with base. International humic substances society (IHSS) standards are extracted by using a 0.1 M HCl and 0.3 M hydrofluoric acid (HF) to remove inorganic soil colloids, resulting in humic substances with acceptable ash content. The use of HCl and HF is applied repeatedly as

needed in order to lower the ash content to < 1%. However, these treatments can also result in losses of the humic fraction.[3, 9, 10]

1.1.2.2 Isolation of Humic Materials from Waters

The isolation of HM from waters involves different procedures from those used for HM isolation from soils and sediments, such as filtration and co-precipitation, ultrafiltration, reverse osmosis, solvent extraction, ion exchange, and sorption, including the use of alumina, carbon, and nonionic macroporous and weak anion exchange resins.[11] The most commonly used methods involve XAD resin and reverse osmosis.

In the XAD resin procedure, six fractions of dissolved organic carbons (DOC) can be isolated: the hydrophobic acids, bases, and neutrals, and the hydrophilic acids, bases, and neutrals.[12] The hydrophobic fractions are retained by a XAD-8 resin column, while the hydrophilic fractions can be retained by an XAD-4 resin column. The IHSS aquatic HA and FA standards are isolated by this method, but only the hydrophobic fractions are collected. Samples are prefiltered through a 0.45 μm or 0.2 μm filter, and the filtrate is adjusted to pH 2 in order to suppress acidic group ionization. The acidified filtrate is then passed over the resin by addition of water. The binding mechanism is a combination of weak hydrogen bonding between HM and the resin ester functionalities and hydrophobic or van der Waals forces. By back elution of the XAD-8 resin with 0.1 M NaOH, the sorbed fraction of HM is recovered and immediately acidified to avoid materials oxidation. HM materials are then re-concentrated using a smaller XAD-8 resin column until the DOC is greater than 500 mg/L. Adjusting the pH to 1.0 with HCl precipitates the HA, at which point the HA is filtered off. The precipitated fraction of HA is rinsed to remove chloride ion (Cl^-). An appropriate amount of 0.1 M NaOH is used to dissolve HA, and HA is H^+ exchanged by using a cation exchange resin. The remaining supernatant from the HA filtrate

contains and passed over the XAD-8 resin at pH 2, desalted by washing the column with distilled water, and eluted with 0.1 M NaOH. The eluate is H^+ exchanged. The HA and FA are finally isolated in a solid form by freeze dried. Hydrophobic neutrals can be eluted by the use of solvents such as ethanol.[4]

The second method for isolating HM from waters is reverse osmosis. The reverse osmosis process concentrates OM by the use of large amounts of water.[13] The resulting concentrate need to be further processed because all solutes including organic salts and non-HM are concentrated. The reverse osmosis concentrate can undergo the previously discussed procedure to yield humic fractions.

1.1.3 Fractionation of Humic Materials

Fractionation of HM is an important step in the characterization of HM. The main objective of fractionation is to alleviate the inherent complexity of HM. This can only be done by minimizing the heterogeneity of the extracted materials. HA, FA, and humins are commonly recovered fractions. Other recoverable fractions are hymatomelanic acid and the gray and brown HA.[3, 9] In this section, the fractionation of terrestrial and aquatic HM is discussed.

1.1.3.1 Fractionation of Terrestrial Humic Materials

Many chemical and physical methods have been used for the fractionation of terrestrial HM. The chemical methods used are usually based upon physico-chemical characteristics. For example, some of these methods are solubility differences in a chemical reagent, charge properties, adsorption differences, density, particle size, and molecular weight. The most applied physical methods beyond those in the isolation of HA, FA, and humins involve the use of filtration and centrifugation.[10]

In the chemical method, the difference in the solubility of the HA in chemical reagent, for instance, in neutral salt and ethanol solutions, is primarily used for fractionation of HA into subfractions. Fractionation that is based on charge characteristics is performed by the electrophoretic and ion exchange technique. Fractioning procedures using adsorption differences are widely varied and ranged from the use of anion exchange resins to gel chromatography. For instance, anion exchange resins are selected to attract negatively charged humic species. Other adsorption resins are employed for non-charged humic molecules in gel chromatography. These molecules are then fractionated into different molecular weight. In addition to the chemical method, ultrafiltration is one the most applied physical methods for HA fractionation. In general, filters separate on the basis of linear size or dimension but not by molecular sizes. Colloidal sizes are expressed in terms of linear sizes (μm or nm) or mass by the use of molecular weights or daltons. The choice is dependent upon the studies purpose, and there is no direct statistical conversion of linear dimentions into mass. A few daltons, however, are generally believed to be equivalent to 1 nm diameter. The size of colloids corresponds to a continuum, ranging from 0.001 to 1.0 μm. Filters with pore sizes of 0.45 μm are commonly used based on the assumption that humic colloids are in the size range of < 0.45 μm, and that living entities will be filtered out.

Fractionation of FA has attracted less research attention than that of HA because of the small size or molecular weight of FA. There have been few attempts to separate FA into subfractions. In general, the used method for fractionation of FA is similar to the physical and chemical methods applied to the fractionation of HA.

1.1.3.2 Fractionation of Aquatic Humic Materials

Aquatic HM fractionation can be adopted from that of terrestrial HM. However, fractionation of aquatic HM usually yields very low concentrations. As a result, fractionation is

only possible if aquatic HM have been properly extracted and collected in reasonable amounts. For fractionation of aquatic HM, filters with very good pore sizes are suggested. Methods applying filters with pore size ranging from 0.001 up to 0.0025 μm can generate FA fractions by molecular weights ranging from 10^3 to 30×10^3 daltons; however, additional studies are needed for verification.[10]

Hallow-fiber has been recently used for fractionation of aquatic HA and FA.[14] Hallow-fiber ultrafilters are able to fractionate humic molecules with a size ranging from 0.001 to 0.45 μm. These filters are different from flatbed filters because they prevent filter polarization, pilling up of the filtered humic molecules, when processing large volumes. In hallow-fiber filtration, water is pumped from inside to outside of the filter during filtration, by flowing water parallel to the hallow-fiber filters.

1.1.4 Purification of Humic Materials

Recovered HM usually contain significant amounts of inorganic components, such as salts, silicon, sesquioxides, and clay. These species, however, should be removed before characterization studies of HM. In addition, there is the issue of removing organic impurities, for example, carbohydrates and proteins.[3] It is thought that organic impurities are covalently bound to HA. The most commonly used methods for removing carbohydrate and protein constituents involve hydrolysis with mineral acids, gel filtration, and phenol extraction. For example, treatment of HA with aqueous phenol, using phenol extraction method, has resulted in the separation of protein-rich components.[15] HA and FA boiling with water has also been described to extract polysaccharides, polypeptides, and small amounts of phenolic acid and aldehydes.[16] At this point, the problem of removing organic impurities from HM has not been resolved.

In addition, HA always have high content of ash, usually exceeding 30%. The ash content can be reduced by repeated precipitation with mineral acids followed by passing through ion exchange resins. An effective way of removing clay from HA is by high-speed centrifugation, after redissolving the HA in a dilute base and adjusting the pH to 7. The use of a dilute HF allows one to obtain HA with low ash content, by dissolving hydrated clay minerals and by di- and tri-valent cations exchange to liberate complexed HM.[3] In general, the FA fraction is disposed in most characterization studies, and only precipitated materials with HA are kept for investigation. Typically, the fraction of FA is lost in the filtrate (or supernatant) after the initial precipitation step in the HA isolation. If the FA fraction is desired, it can be recovered with difficulty in a manner very similar to that used for isolation of aquatic HM.

1.1.5 Composition of Humic Materials

The composition of HM relates to the elemental composition, functional groups, and molecules, which frame the HM structure. Typically, the carbon content of HM is greater than 50 % even though some soil FA have less, while the hydrogen content of soil and freshwater samples is approximately 5%. Marine samples, however, have higher hydrogen content due to their aliphatic nature. In general, the content of oxygen is in the range of 30-40% in soil and aquatic HM, but groundwater samples have the lowest values.[1] The elemental composition and the average charge density of acidic and phenolic functional groups in soil and aquatic HM are shown in Tables 1.1 and 1.2.[2] In general, the carbon content of aquatic HM is greater than that in soil HM, but opposite is seen for oxygen content. The C/N ratios for aquatic HA (18-30:1) and FA (45-55:1) are comparatively greater than those for soil HA (average 10:1) and FA (average 20:1) and for HM from aquatic sediments.

The phenolic content (1-2 meq/g) in aquatic HM is lower than that in soil HM. The phenolic group is one of the major contributors to the total HM acidity. However, the most important moiety in HM is the carboxylic group because of its functionality for buffering activity, metal ion complexation, water retention, exchange capacity, and acidity.[2, 6] The level of oxygen and oxygen containing groups, such as carboxyl, in soil FA is greater while the aromatic content is lower than those of soil HA.[17]

Table 1.1 The average percentage of elemental compositions in soil and aquatic HM.[2]

HM	C	H	O	N	P	S	Ash
Soil FA	48.0	4.5	45.0	1.0	-	0.4	1.2
Soil HA	56.0	4.5	37.0	1.6	-	0.3	2.4
Lake water FA	52.0	5.2	39.0	1.3	0.1	1.0	5.0
Groundwater FA	59.7	5.9	31.6	0.9	0.3	0.6	1.2
Groundwater HA	62.1	4.9	23.5	3.2	0.5	1.0	5.1
Seawater FA	50.0	6.8	36.4	6.4	-	0.5	3.4
River water FA	51.9	5.0	40.3	1.1	0.2	0.6	1.5
River water HA	50.5	4.7	39.6	2.0	-	-	5.0
Wetland water FA	51.0	4.3	40.2	0.7	0.2	0.4	2.0
Wetland water HA	51.2	4.4	40.9	0.6	0.1	0.6	2.0

Table 1.2 The average charge density of major acidic and phenolic functional groups in soil and aquatic HM.[2]

HM	Carboxyl (meq/g)	Phenolic (meq/g)
Soil FA	5.2-11.2	0.3-5.7
Soil HA	1.5-5.7	2.1-5.7
Lake water FA	5.5-6.2	0.3-0.5
Groundwater FA	5.1-5.5	1.4-1.6
Seawater FA	5.5	-
River water FA	5.5-6.0	1.5
River water HA	4.0-4.5	2.0
Wetland water FA	5.0-5.5	2.5
Wetland water HA	4.0-4.5	2.5

The aromaticity is a function of group molecule percentages, which provides information on how much of the aromatic molecules relative to aliphatic compounds are present in the HM molecular structure.[10] The most commonly used method for determination of aromaticity is ^{13}C nuclear magnetic resonance spectroscopy, which provides the percentage of functional group compositions. The value of aromaticity can be obtained by use of the weight percentages, which can be displayed as follows:

$$Aromaticity = \frac{Aromatic\ \ C\%}{Total\ \ C\%} \times 100\% \tag{1.1}$$

Aromaticity or aliphaticity data are very useful for evaluating not only the source, stability, and chemical property of HM, but they are also used for differentiating between several types of HM.[18] An example of the average percentage of aliphaticity and aromaticity for soil, black water, and geologic deposit HM is shown in Table 1.3.[10]

Table 1.3 The average percentage of aliphaticity and aromaticity for soil, black water, and geologic deposit HM.[10]

HM	Aliphatic (C)	Aromatic (C)	Aliphaticity (C)	Aromaticity (C)
Soil FA	61.6	20.7	74.8	25.2
Soil HA	37.3	51.6	42.0	58.0
Black water FA	61.6	22.3	73.4	26.6
Geologic deposit FA	45.7	34.9	56.6	43.4
Geologic deposit HA	27.2	63.8	29.9	70.1

It is interesting to note that there is a significant difference in aromaticity between HA and FA. HA seem to be twice as aromatic as FA. The higher aromatic content in HA may be due to the humification process. In this process, it is thought that the amount of aromatic and alkyl carbons increases with a reduction in carbohydrates. Soil microbes break carbohydrates down, leading to a relative increase in the ecologically stable aromatic and alkyl fractions.[19]

1.1.6 Molecular Structure of Humic Materials

The molecular structure of HM is complex and problematic. Many efforts have been made and a monograph was accomplished by IHSS in 1989. Various structural models of HM have been proposed according to different concepts.[10] Some of these structural models are simple, while others are very complex. Stevenson[3] has also given a detailed review of the HM molecular structure. The IHSS monograph has much information on degradation methods, such as oxidative, hydrolytic, reductive cleavage, and thermal degradation techniques. Studies based on these techniques always indicate that the structure of HM contains phenol or benzoic-like units, such as, methoxy-benzaldehydes, methoxybenzenecarboxylic acid, and hydroxybenzene.

In general, most structural designs of HM are in the category of the phenol protein concept. These designs represent a complex network of phenol units bound together by other carbon units. For example, a tangled web of phenolic units weaving around from the whole page bottom to top has been suggested for the structural design of HA. In addition, less complex structures of HM has been proposed by Schnitzer[20] and Orlov[21] based on the phenol polymer concept (Figure 1.2).

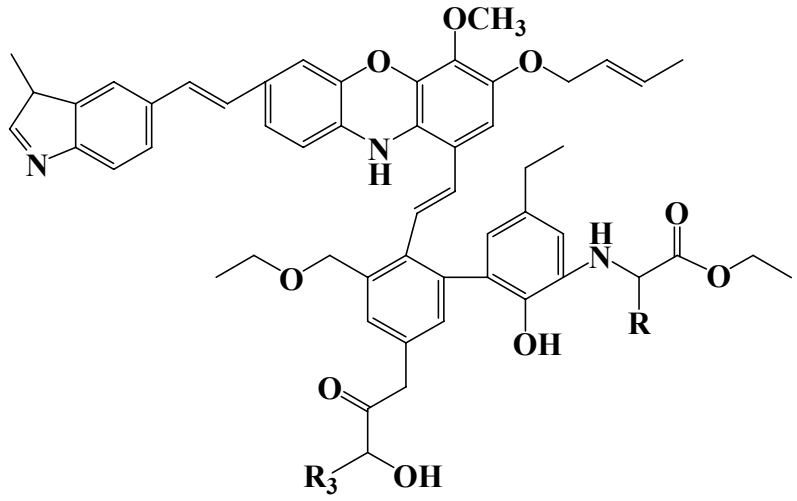

Figure 1.2 Proposed molecular structure for soil HA by Orlov.[21]

For example, the molecular structure of HA suggested by Orlov is shown in Figure 1.2. However, the proposed structure of HA by Stevenson[3], based on the phenol dimer concept, is the simplest design. Stevenson assumes the linkage of two phenol units to which a protein is connected as the basic or smallest unit of the humic molecule. In this assumption, the dimer is an excellent unit for illustrating the chemical reaction property of HM. Figure 1.3 shows a structure for soil HA, which is proposed by Stevenson. In general, the structure of HA is thought to be complex aromatic macromolecules with amino acids, amino sugars, peptides, aliphatic compounds involved in linkages between the aromatic groups.

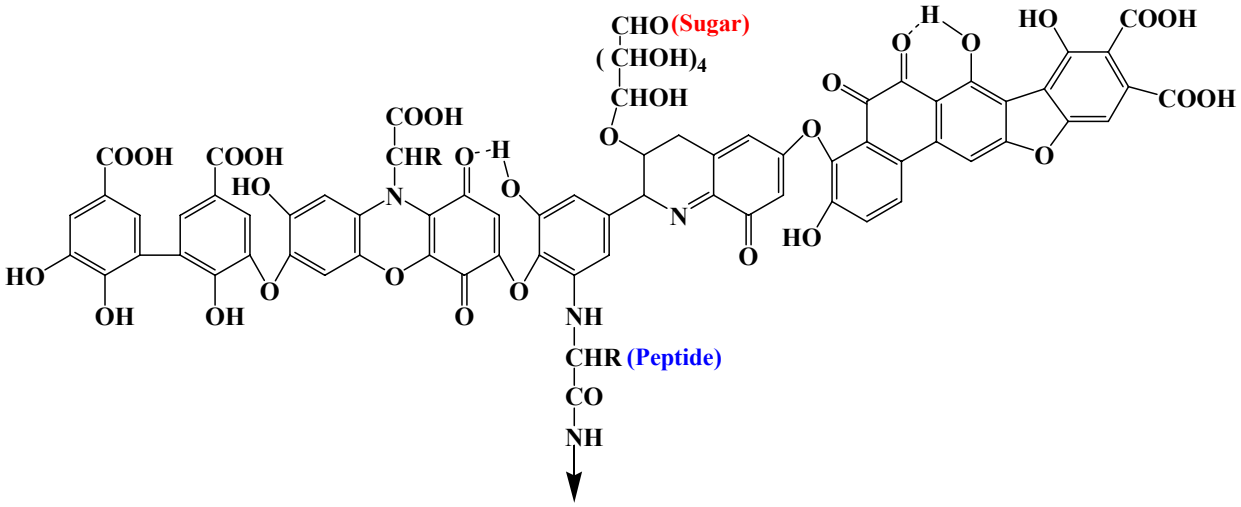

Figure 1.3 Proposed molecular structure for soil HA by Stevenson.[3]

Intensive research into the molecular structure of Suwannee River FA has also been performed. For example, Leenheer et al.[22] have proposed several structures of FA, which are shown in Figure 1.4. These structures are in agreement with elemental composition, nuclear magnetic resonance, and titration data. Even though these molecules are based on the same molecular grouping, larger and more complex molecules are also expected. The structural design of FA contains both aromatic and aliphatic moieties that are extensively substituted with oxygen-

containing functional groups. The molecular structure of FA is less complex and has somewhat higher carboxylic group content than that of HA. In general, carboxylic and phenolic functional groups are the most abundant functional moieties within FA and HA. However, the structure of FA may fold and bring those functional groups together, generating multidentate sites that allow metal ions to associate with more than one single group.[1, 3]

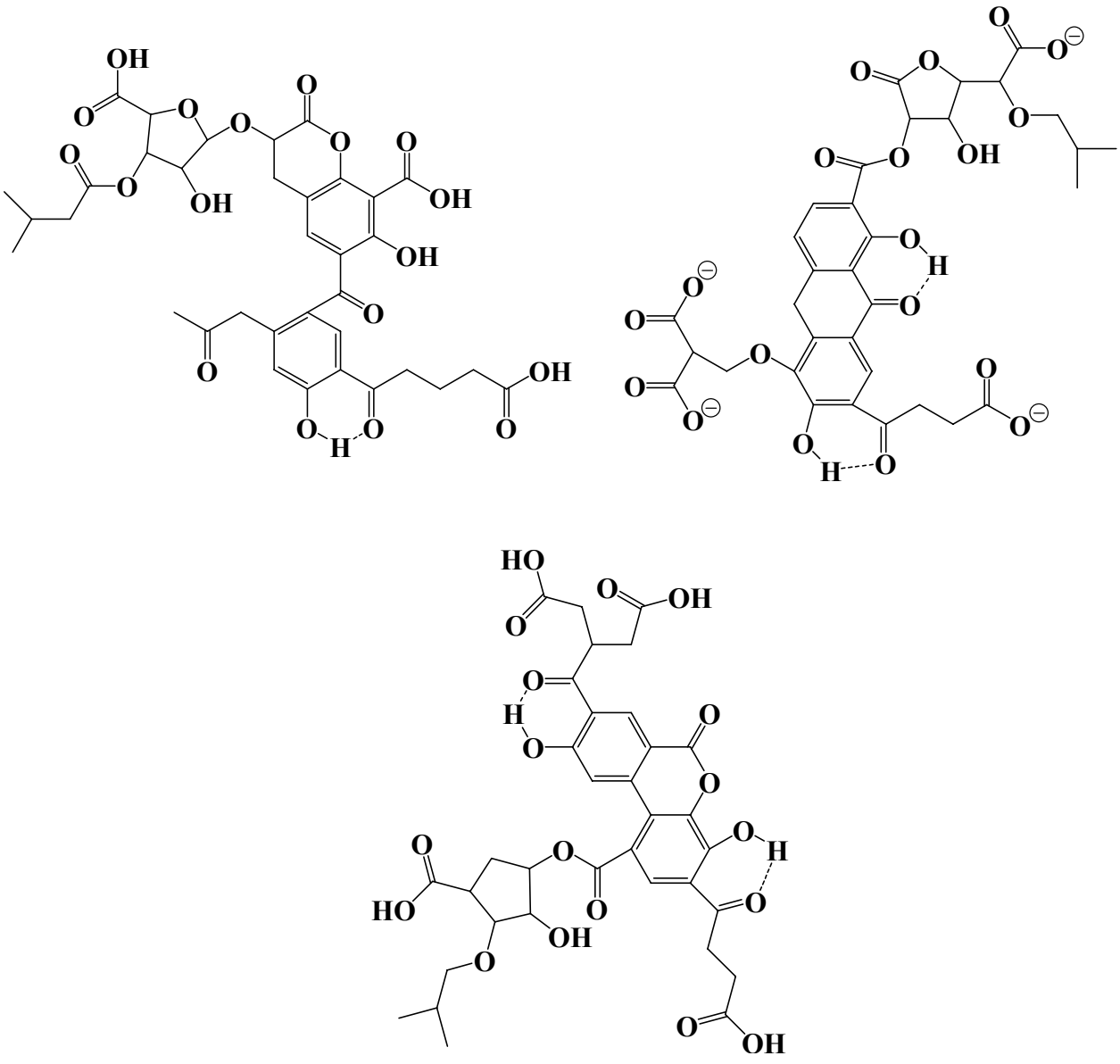

Figure 1.4 Proposed molecular structures for Suwannee River FA by Leenheer.[22]

1.1.7 Molecular Weight of Humic Materials

Different challenges have been encountered when determining the molecular weight of HM. In fact, it is of no surprise that complications have been encountered in measuring the molecular weight of HM due to their polyelectrolytic, heterogeneous, and polydisperse nature.[6] Many experimental studies have been proposed in order to measure the molecular weight of HM, for example, sedimentation,[23] ultracentrifugation,[24, 25] and gel permeation chromatography.[26] However, each technique has advantages and disadvantages and shows a range of the molecular weight for HM. For instance, data are only obtained when the centrifuge column reached equilibrium in the sedimentation method. As a result, larger molecules tend to sediment out of the column and are excluded from the measurement.[27] In addition, gel permeation chromatography gives the molecular weight distributions, but serious problems were encountered because of the charge-repulsion effect and solute adsorption. Weight-average molecular weight values obtained from these methods range from 2×10^3 to 4×10^5 dalton.[6] However, Stevenson[3] suggested that the highest molecular weight values may have been a result of HM aggregation.

The molecular weight of HM is based on average values because HM are mixtures. The number-average (M_n) and weight-average (M_w) are the most commonly used for the molecular weight of HM, which can be expressed as follows:

$$M_n = \frac{\sum_i n_i M_i}{\sum_i n_i} \tag{1.2}$$

$$M_w = \frac{\sum_i c_i M_i}{\sum_i c_i} \tag{1.3}$$

where n_i and c_i denote the number and weight concentration of different HM fractions, respectively. The ratio of M_n and M_w is the polydispersity. The M_n and M_w are equivalent, and hence polydispersity is unity for the pure compound. The molecular weight of FA is a few thousand at the most. Table 1.4 shows an example of both M_n and M_w values for FA and HA.[1] The M_n and M_w values for FA are around 800 and 1600, respectively, so that the polydispersity is approximately two. The molecular weight of unfractionated HA differs from a thousand to a few hundred thousand. The polydispersity is apparently high when both M_n and M_w values are available.[1, 10]

Table 1.4 Some reported M_n and M_w values for FA and HA.[1]

HM	M_n ($\times 10^2$)	M_w ($\times 10^3$)
Freshwater FA	6.0-14.0	1.0-2.3
Freshwater HA	-	4.0-8.0
Marine FA	5.0-8.0	-
Soil FA	6.0-10.0	-
Aldrich chemical HA	15.0-31.0	4.0-20.0
Soil HA	-	25.0-200.0
Peat HA	-	8.0-17.0

1.1.8 Micellar Properties and Polymeric Structure of Humic Materials

HM are heterogeneous mixtures of naturally-occurring organic compounds that are surface active. The molecules that constitute HM are also known to build aggregates of colloidal dimensions. In addition, FA and HA can solubilize various hydrophobic organic compounds (HOC) in a fashion that is consistent with micelle-forming surfactants.[28] Micelles are defined as colloidal particles formed by a concentration-dependent aggregation of surfactant molecules.[29]

In aqueous environments, micelles are formed when the hydrophobic portions of surfactant molecules start to associate at a surfactant concentration that is related to the critical micelle concentration (CMC) caused by hydrophobic effects. Micelles have a hydrophobic

domain and charged surface due to the orientation of hydrophilic (or ionized) functional groups out into the bulk solution. At a concentration lower than the CMC, surfactant molecules move toward the solution air-interface disturbing the structure of water molecules and resulting in a decrease in the solution's surface tension.[30] At a concentration higher than the CMC, however, increasing the amount of surfactant leads to the formation of additional micelles, while the surface tension stays constant. Typically, the surface tension of a surfactant will go through an abrupt conversion to a constant value at the CMC.

Many approaches have shown that the spontaneous aggregation of aqueous HM can be intramolecular (a single polymer chain) or intermolecular (multiple chains) polymer chain nature.[31-36] In the intramolecular case, it is thought that HM can fold and twist generating knots in a string. The external domain is more hydrophilic, while the internal domain of HM is relatively hydrophobic. This configuration is similar to that of the surfactant micelle. Figure 1.5 displays the manner in which the surfactant forms micelles.

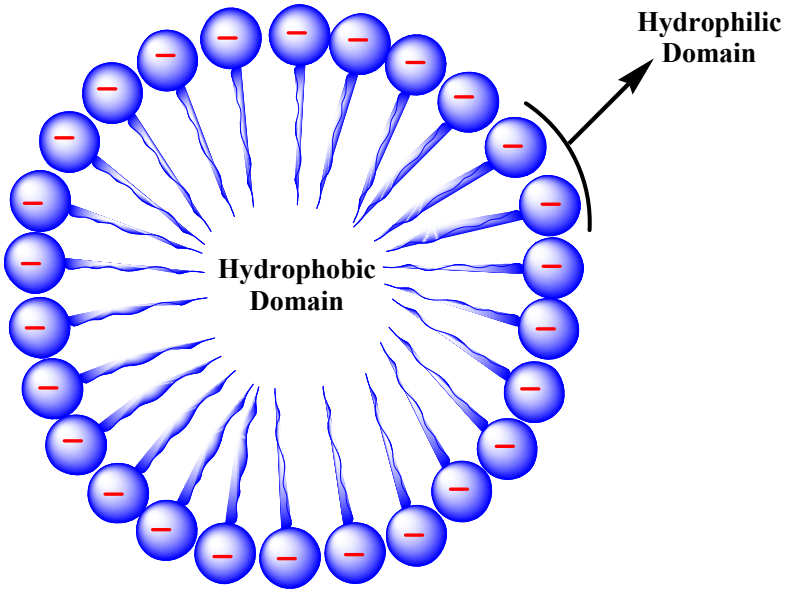

Figure 1.5 Representation of surfactant micelles.

Despite the fact that the structure of HM is controlled by their intramolecular nature of the arrangement and their polydispersity, it is similar to that of a surfactant micelle. Therefore, the term pseudomicelle is more suitable for describing HM structure. For example, von Wandruszka et al.[37] indicated that metal ions, particularly polyvalent ions, have an effect on the aggregation of HA and formation of humic pseudomicelles. It is believed to be the result of the cations capability to neutralize the negative charge of HM and engage in bridging interactions.

Alternatively, the structural conformation of HM currently can be described via a polymer view. In this model, the molecular structure of HM is thought to fold and twist at low pH, high concentrations, and high ionic strength, but this configuration is expanded and stretched to sheet-like structures at neutral or higher pH, low ionic strength, and low concentration.[38, 39] In addition, the structure of HM is considered to consist of supramolecular assemblies instead of macromolecular polymers. In the supramolecular associations, it is suggested that small and heterogeneous units of HM are self-assembled into supramolecular configurations primarily stabilized by weak intermolecular forces, such as van der Waals, π-π, or CH-π bonds. These supramolecular configurations are thought to form large molecular dimensions.[40-49] The use of organic acids, in particular mono- and di-carboxylic acids, can result in a disaggregation of this large conformation into smaller molecular associations.[41, 47]

1.2 The Effect of Pollutants on the Environment

Soils and waters are hosts to large quantities of organic chemicals, which are presented either intentionally or accidentally in our environment. Organic pollutants may interact with soils and waters via many sources, such as municipal and industrial wastes and landfill effluent. When these chemicals reach soil surfaces, their degradation will be subject to several fates. They may be sorbed by the soil or transport to the aquatic environment through run-off into surface waters.

These organic chemicals are aliphatic and aromatic derivatives of petrol and plastics, such as polycyclic aromatic hydrocarbons (PAHs) and pesticides and their biological, chemical, and photochemical degradation products.[2, 50]

PAHs contain many classes of organic compounds. They are divided into two categories known as alternant and non-alternant. Alternant PAHs contain only six membered rings, while non-alternant PAHs contain both six and odd membered rings. These classes of compounds are named based on how the rings are fused together. When bezenoid rings are fused to each other in a linear manner, the compound name is ended with acene, for example, anthracene, naphthacene, and pentacene. The end of the compound name can also be phene when bezenoid rings are fused together in an angular fashion, for instance, pentaphene.[51] PAHs are one of the most hazardous classes of HOC found in nature. PAHs are usually found in regions contaminated with creosote (or coal tar) and places where crude oil spillage has occurred. They may also be found due to incomplete combustion in incinerators, power plants, etc.[52] PAHs have carcinogenic, mutagenic, and toxic effects on the living organisms.[53] These properties make them of continual interest for environmental monitoring. HM can facilitate the transport of these contaminants, and the association of PAHs with HM can result in an increase of the contaminant mobility and a decrease in toxicity and bioavailability of PAHs.[53-58]

In addition to PAHs, pesticides are one of the major problems that contributes to the contamination in the environment. For example, the presence of these compounds in drinking water can result in carcinogenic and health risks to the living organisms.[59] These compounds vary in their level of ionization, polarity, and solubility in water. In addition, they contain a large number of organic compounds which are geometrical, positional, and optical isomers.[60] Optically active molecules are able to rotate plane of polarized light to different degrees. Molecules

rotating light to the left [or right] are known as levorotatory (L) [or dextrorotatory (D)], and they have the negative sign (–) [or positive (+)]. These molecules are called chiral compounds, which have an asymmetric carbon atom.[61] The term chirality is defined as a physical object that is non-superimposable on its mirror image. This property was first discovered by Louis Pasteur in 1848.[62]

Chirality is an important consideration in the design of pesticides and in determining their behavior in a biological environment. Pesticide effectiveness relies on the geometry and magnitudes of that portion of the pesticide that interacts with the recipient.[63] In nature, the pesticide biological interest is limited to a single enantiomer, and only one enantiomer of the racemic mixture pesticide is usually effective. The other enantiomer may have toxic effects and/or act in response with non-living organic materials to produce other undesirable side effects. Steric properties of pesticides are important with respect to their biological interest. Not only is the toxicity important, but also the environmental factors such as association to soils. Synthetic organic pesticides are applied in large quantities over large regions and eradicate the requirement for manual weeding. HM play an important role in accumulation, mobilization and transformation processes of these pollutants.[64] The association of pesticides with HM may facilitate their activity through soils and waters. The shortcomings of using large quantities of pesticides become obvious because most pesticides go through transformations in our environment through various degradation processes, such as hydrolysis, photolysis, oxidation, biodegradation, etc.[63, 65-67]

The chemical reactivity of HM is a very important property. HM contain carboxylic functional groups, weakly acidic phenolic groups, and are redox active. Carboxylic groups and weakly acidic phenolic groups are contributors to the complexation and ion exchange

characteristic of HM. These properties are very important in geochemical and environment processes. They can associate small molecules via both hydrogen bonding and non-polar interactions.[8] HM may affect the fate of organic chemicals in various ways, including adsorption and partitioning, solubilization, degradation via hydrolysis, and photodecomposition. In addition, the surface activity of HM is an important characteristic, which prompts interactions, particularly with HOC. Several organic chemicals have been observed in aqueous phases, which can associate with HM. As a result, this can significantly impact the dissolution rate of organic chemicals, volatilization, transfer to sediments, biological uptake and bioaccumulation, or chemical degradation.[2]

1.3 Association of Hydrophobic Organic Compounds with Humic Materials

The association of HOC with DHM present in soils and waters is of continual concern in environmental areas because of the high affinity of HOC to DHM and the potential risks to the environment. DHM are involved in the fate and transport of these contaminants, and the association of HOC with DHM can result in an increase of the contaminants mobility and a decrease in their toxicity and bioavailability.[58, 68] The sorption behavior between HOC and DHM is likely the result of weak associations such as hydrophobic interactions between HOC and DHM. Yet, this process is poorly understood. In addition, this association is dependent upon various factors, for example, the pH, ionic strength, temperature, and nature and concentration of DHM.[69]

There has been a large focus in studying the association mechanism between HOC, such as PAHs and pesticides, and DHM. Several methods have been developed for investigating the association behavior of HOC with DHM.[70-73] The most commonly used analytical methods involve dialysis,[74, 75] liquid chromatography,[59, 71] solubility enhancement,[76-78] and fluorescence

quenching.[79, 80] Each method, however, has its advantages and disadvantages. In addition, there is no universal agreement in the preference of one technique over the others. In general, the association constant values of HOC with DHM obtained by different techniques are sometimes significantly different from each other. In one such example, Kukkonen and Pellinen[81] have reported that the association constant values obtained by the dialysis method are always higher as compared to those of reverse phase separation. In addition, one of the major problems encountered in studying the association behavior of HOC with DHM was that the association sites on the DHM are heterogeneous.[3, 82, 83] Therefore, it was indicated that different association sites presented in DHM can result in significantly different association constants values.

Fluorescence spectroscopy is one of the popular techniques and has been used to gain insight into the interaction of HOC with DHM. Studies in the past have shown the promise of fluorescence based measurements as one can study these systems at environmentally relevant concentrations. In the literature, static quenching of HOC with DHM has generally been assumed based on steady-state fluorescence measurements;[73, 79] however, dynamic quenching has also been implied by some studies.[32, 76, 80] There are numerous other problems associated in fluorescence spectroscopy for monitoring HOC interaction with DHM. For example, Danielsen et al.[84] showed that the method of fluorescence quenching tends to overestimate the association constant values as compared to the solubility enhancement method. In addition, Tiller and Jones[85] have also indicated that oxygen and long exposure to radiation, or photobleaching, can overestimate association constants of HOC with DHM. In most studies, the problem of photobleaching has only been addressed by simply controlling the fluorometer shutter between measurements in order to gain deeper insight into what fluorescence spectroscopy is actually monitoring. Other researchers have used fluorescence lifetime measurements in order to resolve

the debate over the quenching mechanism of HOC with DHM.[86, 87] Although time-resolved measurements addressed some issues associated with the steady-state fluorescence technique, these efforts have not completely resolved the effect of photobleaching. Thus, the seemingly simple question of whether the quenching mechanism of HOC with DHM is static, dynamic, or both is still open. In addition to the effect of photobleaching, the adsorption of HOC to cell walls has been reported to be one of the encountered problems when measuring fluorescence.[88-90] It was indicated that the cell walls adsorption of HOC can cause a decrease in the fluorescence intensity and complicate the interpretation of fluorescence results.

Additionally, there has also been a large discussion on the sorption behavior of HOC to DHM. Various models have been proposed, as exemplified by the "glassy/rubber" (hard/soft or condensed/non-condensed) model.[91-96] But, none of these models has been universally accepted. Only one point that was almost universally agreed upon was that HOC sorb into aromatic domains within DHM.[32, 76, 87, 97, 98] However, based on the recent work of Chefetz et al.,[99] Hu et al.,[100] and Wang and Xing,[101] this point of view has come under question, and aliphatic domains within HM have been proposed to sorb HOC. Thus, the seemingly simple question of whether HOC interact with aliphatic, aromatic, or both domains is still open.

In accordance, the first part of the research presented in this dissertation focused on the investigation of the effect of DHM content on the association with pyrene, a common fluorescence probe, by use of steady-state fluorescence spectroscopy. Stern-Volmer plots and the effect of temperature on the pyrene fluorescence quenching ratio were also evaluated. The variable temperature results indicated that steady-state technique alone may not provide enough information about the quenching mechanism of pyrene with DHM. Thus, an additional technique is needed to resolve the quenching mechanism of pyrene by DHM.

Lifetime based fluorescence measurements allow for a deeper mechanistic understanding as compared to traditional steady-state fluorescence measurements. Therefore, in the second part of this dissertation, a new approach to frequency-domain lifetime measurements based on frequency segmentation and recombination was developed in order to address the effect of photobleaching in multi-component systems. The validation of the method was performed using a simple two component system consisting of fluorescein and rhodamine B. The comparison of experimental data collected in traditional and segmented fashion was also evaluated. In addition, the frequency segmentation and recombination method was applied to a more complex system containing pyrene and DHM in order to evaluate the quenching mechanism of pyrene with DHM. Experimental considerations, such as the effect of oxygen, wall adsorption, and photobleaching within the pyrene and DHM system, were also addressed in order to carefully quantify recovered lifetimes and fractional intensity contributions.

While a great deal of time has been spent on investigating the association behavior between achiral HOC, not much is known about the enantiomeric selectivity chiral recognition ability of DHM and their association behavior with chiral compounds. Therefore, the last part of this dissertation focuses on the effect of chiral pollutants on the association with Leonardite humic acid standard, used as a DHM model, by use of steady-state fluorescence spectroscopy. In addition, pure enantiomers of 1-(9-anthryl)-2,2,2-trifluoroethanol and 1,1'-bi-2-naphthol bis (trifluoro - methanesulfonate) were used to investigate the enantioselectivity of Leonardite humic acid standard by use of liquid-state fluorine nuclear magnetic resonance spectroscopy. To further investigate the enantiomeric selectivity of Leonardite humic acid standard, the interaction of *R*- or *S*-1-(9-anthryl)-2,2,2-trifluoroethanol with Leonardite humic acid standard was evaluated for

samples monitored in the dark and exposed to light for different time periods by use of high performance liquid chromatography.

1.4 Ultraviolet-Visible Absorption Spectroscopy

Spectroscopy is a branch of science in which radiation is resolved into its component wavelengths. As a result, a spectrum is produced for theoretical and structural studies. The spectrum is displayed by the intensity of absorbed, emitted, or scattered radiation of the molecule versus a quantity related to photon energy, such as wavelength or frequency. Spectroscopy across-the-board involves not only the use of light but also other types of electromagnetic radiation. It has many forms, including gamma-rays, X-rays, ultraviolet, visible, infrared, microwave, and radio-frequency radiation.[102, 103] Many types of these interactions occur as a result of transition between specific energy states of chemical species and are observed by monitoring the absorption or emission of electromagnetic radiation. Electromagnetic radiation consists of discrete packets of energy, known as photons. In addition, electromagnetic radiation has a wave property in which the energy of a photon can be related to its wavelength and frequency as follows:

$$E = h\nu = \frac{hc}{\lambda} \tag{1.4}$$

where E denotes the energy in joules (J), ν is the frequency (Hz or s^{-1}), h is the Planck's constant (6.63×10^{-34} J s), c denotes the speed of light (2.99792×10^{8} m/s in a vacuum), and λ is the wavelength (m).

Ultraviolet-Visible (UV-Vis) absorption spectroscopy is an instrumental method which measures the absorption by a molecule as a function of wavelength for UV or Vis radiation. UV-Vis radiation has enough energy to promote the outer electrons to higher energy levels. In the UV-Vis wavelength region, absorption radiation leads to electronic transitions at different

wavelengths for a given molecular structure. Molecules absorb light at different wavelengths and to different extents, yielding an absorption spectrum. This spectrum displays different absorption bands, which corresponds to structural groups within the molecule.[103]

In UV-Vis spectroscopy, a beam of monochromatic radiation with a radiant power (I_0) passes through the sample in a cell with path length (b), which can be depicted in Figure 1.6.

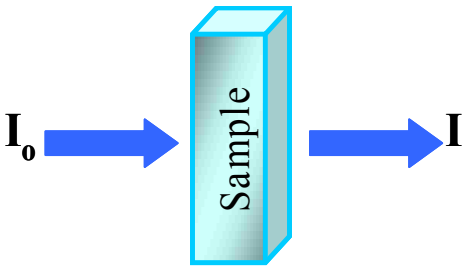

Figure 1.6 A beam of radiation passing through the solution.

As a result, absorption occurs and the beam of radiation at radiant power (I) will leave the sample. The transmittance (T) of the sample is the fraction of the incident beam that passes through the sample and can be expressed as follows:

$$T = \frac{I}{I_o} \tag{1.5}$$

The absorbance (A) is related to the transmittance as follows:

$$A = -\log T = \log \frac{I_o}{I} \tag{1.6}$$

The Beer-Lambert law is the linear relationship between the absorbance and absorbing species concentration. This can be expressed as follows:

$$A = \varepsilon bc \tag{1.7}$$

where ε is the molar absorptivity ($Lmol^{-1}cm^{-1}$), c denotes the concentration of the sample (mol/l), and b is the optical path length of the cell.

The absorbance spectrum (absorbance versus wavelength) is usually measured by a dedicated absorption spectrometer. A typical UV-Vis spectrometer consists of a radiation source, wavelength selector, sample container, detector, signal processor, and readout devices as shown in Figure 1.7. UV-Vis instrumentations are configured for single- or double-beam measurements and can be based on single or multi-channel detectors.

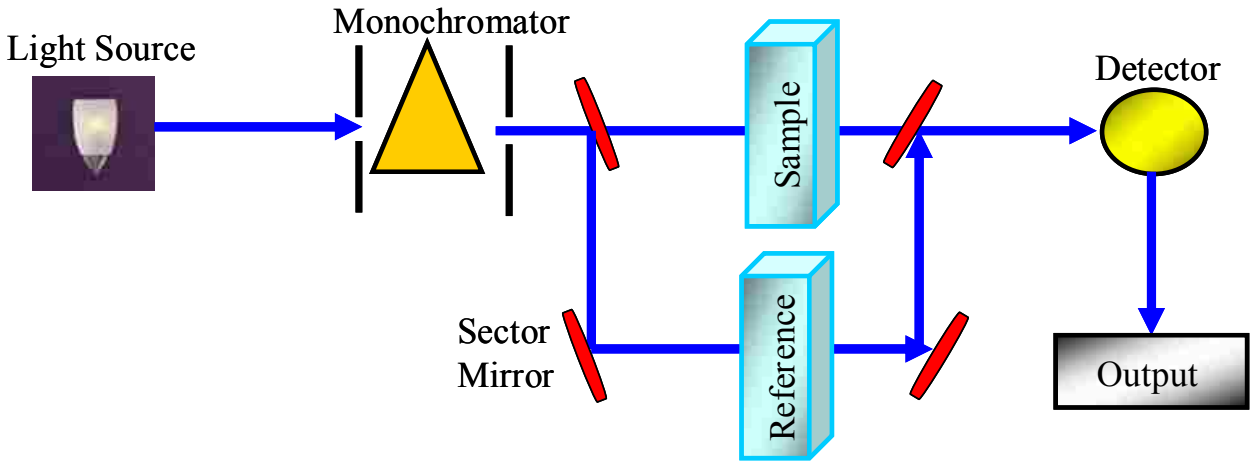

Figure 1.7 A double-beam UV-Vis absorption spectrometer with a single detector.

The most economical design is a UV-Vis spectrometer equipped with a single detector. In this approach, a specific wavelength band of the radiation source is transmitted by the wavelength selector to the detector through the sample cell. In the single-beam spectrometer, one beam passes through a single cell and is incident on the detector. In case of the double-beam spectrometer, the radiation is split into two radiation paths by a rotating sector mirror, passing through both the sample and reference cells. Consequently, the beam from the sample and reference are recombined to be incident on the single detector.

Radiation sources in UV-Vis spectrometers are usually a tungsten or tungsten-halogen lamp, which can produce a continuum radiation over the whole Vis region. Deuterium (D_2) and

hydrogen (H_2) arc lamps are also used in UV-Vis spectrometers. Arc lamps are used at a wavelength region below approximately 350 nm. The D_2 lamp is more popular than the H_2 lamp because its radiance is about three times greater than that of the H_2 lamp. The radiation is collected and pointed to the wavelength selector with mirrors. In UV-Vis spectrometers with a single-beam detector, the wavelength selector is positioned before the sample cell to reduce the sample photodecomposition by radiation. Vacuum phototubes and photodiodes are commonly used detectors in many UV-Vis spectrometers with a large spectral bandpass. Photomultiplier tubes (PMT) are also used, providing a higher signal to noise ratio (S/N).[102, 103]

In this dissertation, UV-Vis measurements were performed for characterization of both organic chemicals and HM. HM absorb radiation in the UV-Vis region. For instance, a 10 ppm solution of a fulvic acid in a 10 mm path length cell possesses an absorbance value of 0.1 at 300 nm. Absorption spectra of HM are approximately exponential with increasing the wavelength. The absorption characteristic of HM is due to the presence of mixture of chromophores, which are thought to be aromatic, quinone, and conjugated structures. At wavelengths longer than 400 nm, charge transfer bands and light scattering can be more pronounced. HA usually have a higher absorbance than FA.[1] The molar absorptivity of HA at 280 nm is strongly related to the aromaticity.[104] In general, UV-Vis absorption spectroscopy has limited practical applications in HM science. This is attributed to the fact that the peaks of absorption spectra are broad and give little interpretable information.[4]

1.5 Fluorescence Spectroscopy

Luminescence is the emission of radiation from any molecule, after promotion to an electronic excited state. Both fluorescence and phosphorescence are similar to each other in that excitation is achieved by photons absorption. However, fluorescence occurs between states of the

same multiplicity, which are usually singlet to singlet transitions for organic molecules. The fluorescence emission rate is 10^8 s^{-1}, and the lifetime is approximately 10^{-8} s. In contrast, phosphorescence takes place between states of different multiplicities, which are usually triplet to singlet transitions. Phosphorescence has an emission rate of 10^3-10^0 s^{-1} and its lifetime is from milliseconds to seconds and can even be longer.[103, 105]

Various processes associated with absorption and emission radiation by molecules are best illustrated by use of a Jablonski energy diagram (Figure 1.8). When molecules absorb radiation in the UV-Vis range, electronic transition will occur from the lowest vibrational level of the ground electronic state (S_o), at room temperature, to the first excited singlet or higher order state (S_1 or S_n). From there, these excited molecules will undergo a loss of energy with a rapid relaxation from a higher to the lowest vibrational level of the excited electronic singlet state.

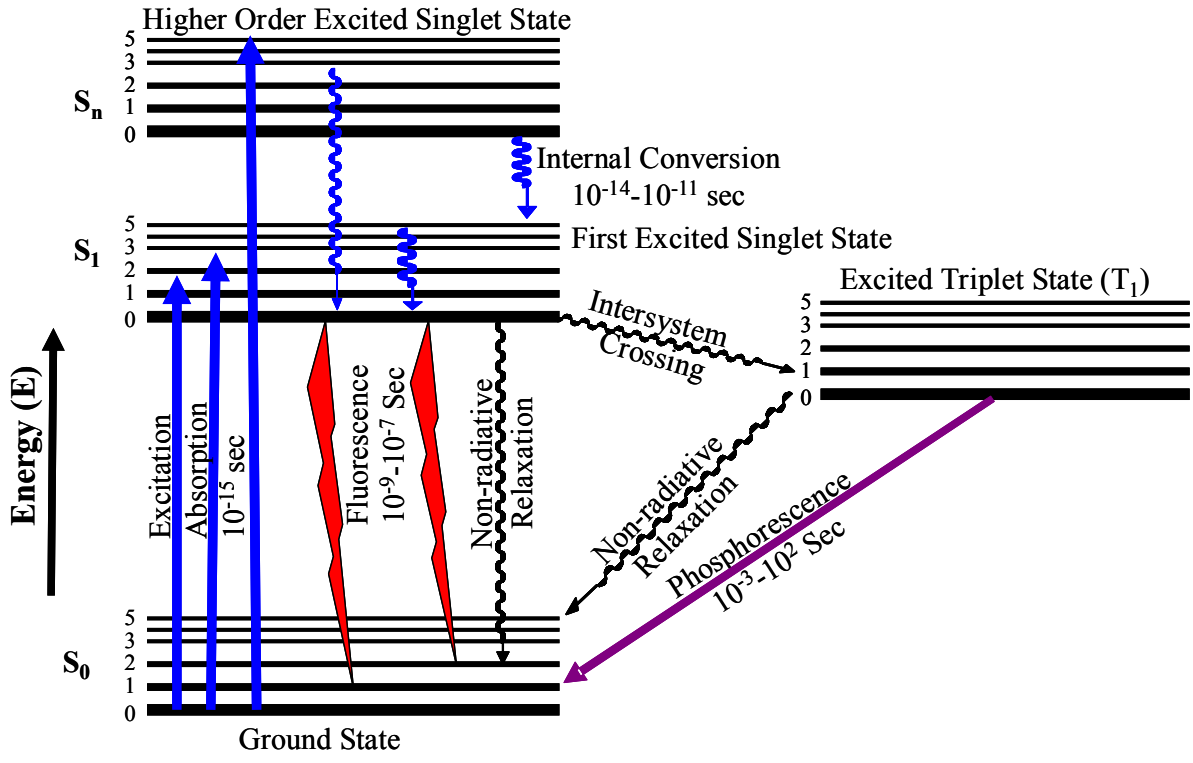

Figure 1.8 Jablonski energy diagram.

This process is a non-radiative process and is known as internal conversion. The process of internal conversion can take place in 10^{-12} s or less and is usually completed before fluorescence occurs. Molecules are then de-excited back to the ground state by either a non-radiative process or photon emission, the latter of which is known as fluorescence.

However, molecules in the excited singlet state may also undergo a forbidden transition to the excited triplet state (T_1) by intersystem crossing. Molecules then relax from a higher to the lowest vibrational in the excited triplet state or go back to the excited singlet state via intersystem crossing. In the former case, molecules may be de-excited from the excited triplet state to the ground electronic state by either non-radiative processes or emission of photons by a phosphorescence process. Phosphorescence has a longer wavelength (lower energy) shift than fluorescence because the triplet excited state has lower energy than the excited electronic singlet state. In the latter case, molecules will be de-excited back to the ground electronic state by emission of photons, resulting in delayed fluorescence which is identical to prompt fluorescence but exhibits the longer decay related to phosphorescence.[105, 106]

In general, fluorescence occurs at longer wavelength (lower energy) than the absorption as can be observed in Jablonski energy diagram. This is due to the energy loss in the excited electronic state via the internal conversion process and to the difference in the molecular geometry and solvation between the ground and excited electronic states.[107] Typically, the molecule has a specific geometry and solvation in the electronic ground state. The excited molecule also maintains its ground state geometry and solvation in the excited singlet state. However, the geometry and solvation of the molecule very shortly after excitation return to their most preferable values in the excited singlet state, resulting in lower energy of the excited molecule. When the molecule fluoresces, it returns back to the electronic ground state but retains

its excited singlet state geometry and solvation. Thus, the emission energy is less than that of excitation. In general, this phenomenon is known as Stokes' shift and was first discovered in 1852 by G. G. Stokes.[105] In Stokes' experiment, a sunlight and blue glass filter were used as the UV excitation source (Figure 1.9). The filter used was able to transmit radiation below 400 nm, which can be absorbed by quinine solution. A yellow glass of wine was used as a filter in order to block the excitation light from reaching the observer (or detector). As a result, fluorescence of quinine was observed near 450 nm.

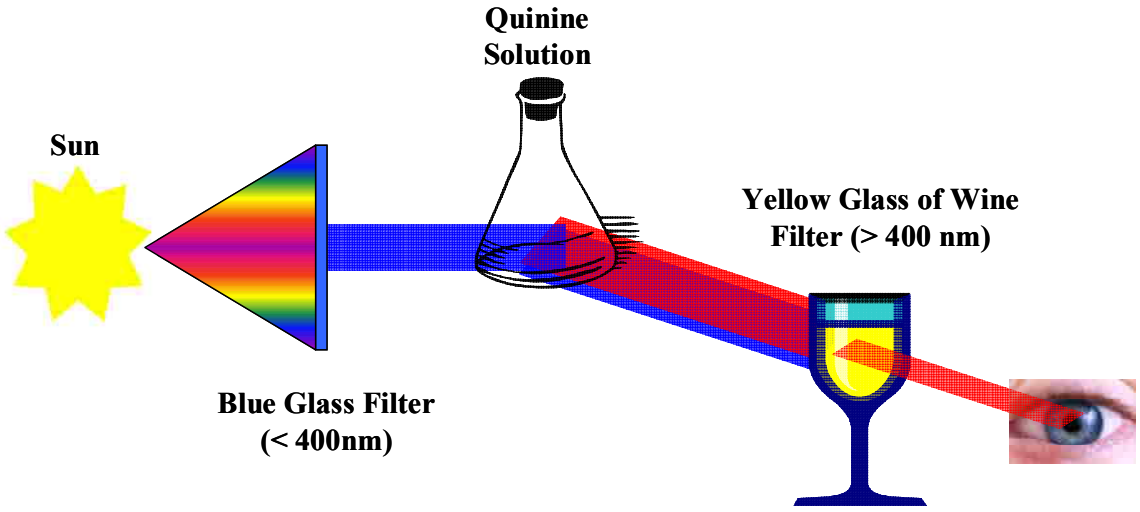

Figure 1.9 Experimental design used by G. G. Stokes.

In addition to Stokes' shift, the emission spectrum is typically similar to the excitation spectrum of the electronic transition from ground to excited singlet states ($S_o \rightarrow S_1$), which is known as the mirror image rule. This symmetric phenomenon is due to the fact that the same excitation and emission transitions are involved, and the difference between vibrational levels in the ground and excited singlet states is similar. Alterations of vibrational levels, in many molecules, are not substantial when electronic distributions of the ground and excited singlet

states differ. Based on the Frank-Condon principle, all electronic transitions occur vertically without alterations of the nuclei position in the molecular entity and its environment (Figure 1.10). For example, absorption of electronic transitions between the zeroth (ν_o) and second (ν_2) vibrational levels of the ground and excited singlet states, respectively, will probably result in similar electronic transitions for emission.

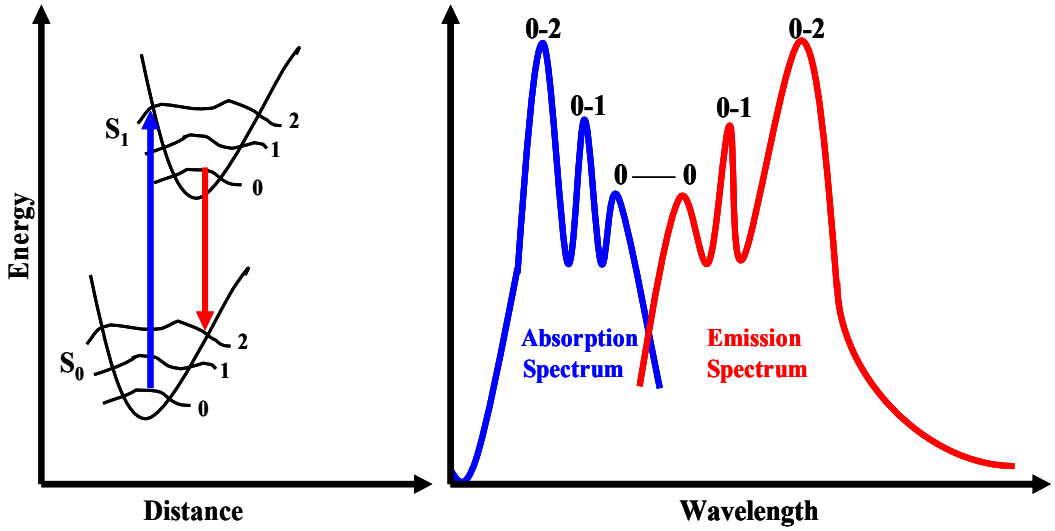

Figure 1.10 Mirror image rule and Frank-Condon factors.

In fact, emission spectra of PAHs generally exhibit the mirror image rule relationship to absorption spectra, and both emission and absorption spectra posses a single wavelength in common that corresponds to the 0-0 band. Normally, this band is less intense than other bands in both absorption and emission spectra. It is also related to the absorption and emission between the lowest vibrational levels of the ground and excited states. There are, however, many exceptions to the mirror image rule even though this rule holds most of the time. The deviation from the mirror image rule usually occurs as a result of different geometric placements for nuclei in the excited state as compared to the ground state. The displacement of nuclei occurs before fluorescence because of the long lifetime of the excited state.[105, 108, 109]

1.5.1 Deactivation Processes

The absorption of radiation prompts the molecule to one of the possible vibrational levels in the excited state. In spite of the fact that the absorption is very rapid, approximately 10^{-15} s, events involved in returning the excited molecule to its ground state are substantially slower, about 10^{-14} s to several seconds. Fluorescence of the molecule is the slowest process, approximately 10^{-10} s to a few seconds, among electronically excited states. Both fluorescence and phosphorescence are radiative processes from the thermally equilibrated excited molecules. The thermal equilibration occurs by the vibrational energy loss and is much faster, taking from 10^{-14} to 10^{-12} s.[103, 109] In this section, the events (or non-radiative processes) in the lifetime of the electronically excited state molecule, including vibrational relaxation, internal and external conversion, intersystem crossing, and delayed fluorescence, will be discussed in detail.

1.5.1.1 Vibrational Relaxation

During the excitation process, the molecule may be promoted to any number of various vibrational levels in the excited state. Nevertheless, the excess vibrational energy is immediately lost due to collision between molecules of the excited species and those of the solvent molecules. Consequently, this results in an energy transfer and temperature increase of the solvent. This process is known as vibrational relaxation. This relaxation process is very effective and takes place on the time scale of 10^{-12} s or less.

1.5.1.2 Internal and External Conversion

Internal conversion is the crossover between states of the same multiplicity. This process takes place when the potential energy curves of two electronic states cross in a way that the lower vibrational levels of the higher electronic state are around the same energy as the higher vibrational levels of the lower electronic state. Internal conversion may take place between

excited electronic states, e.g. $S_2 \rightarrow S_1$, or between the first excited state and ground state, e.g. $S_1 \rightarrow S_o$. On the other hand, external conversion occurs when excited states transport their excess energy to other species, for example solvent and solute molecules. Dynamic quenching is the primary mechanism of the external conversion. During collisions, dynamic quenching involves the energy transfer from excited species to other molecules. Consequently, the dynamic quenching rate is minimized by cooling the sample.

1.5.1.3 Intersystem Crossing

Intersystem Crossing is the crossover between states of different multiplicity, which is usually $S_1 \rightarrow T_1$. Even though some molecules may exhibit weak absorption, absorption transitions to the excited triplet state are forbidden. As was previously mentioned via the Jablonski diagram, the molecule in the excited triplet state can be de-activated by vibrational relaxation to the lowest vibrational level in the excited triplet state or by going back to the excited singlet state via intersystem crossing.

1.5.1.4 Delayed Fluorescence

Delayed fluorescence possesses a longer lifetime than fluorescence because the first excited electronic state is populated by an indirect mechanism. Recall that the molecule in the excited triplet state may be de-activated by moving back to the excited singlet state via intersystem crossing. Thus, delayed fluorescence occurs when molecules are de-excited to the ground electronic state by emission of photons.

1.5.2 Quantum Yield

The quantum yield, or quantum efficiency, is defined as the ratio of the number of emitted molecules to the number of excited molecules per unit time. It can be less than or equal to 1 (≤ 1) under some conditions. The quantum yield approaches unity for highly fluorescent

molecules, while it is close to zero for non-fluorescent molecules. Fluorescence quantum yield (ϕ) can be expressed by rate constants of fluorescence (k_f), intersystem crossing (k_{isc}), internal conversion (k_{ic}), external conversion (k_{ec}), pre-dissociation (k_{pd}), and dissociation (k_d) as follows:

$$\phi = \frac{k_f}{k_f + k_{isc} + k_{ic} + k_{ec} + k_{pd} + k_d} \tag{1.8}$$

The absolute quantum yield measurement is difficult, involving the use of specific instrumentations. It is also important to determine the amount of excited radiation received by the molecule. Therefore, it is frequently acceptable to determine the relative quantum yield. This can be obtained by relating the unknown fluorescence efficiency to that of the standard, which can be expressed as follows:

$$\phi_{F(x)} = \left(\frac{A_s}{A_x}\right)\left(\frac{F_x}{F_s}\right)\left(\frac{n_x}{n_s}\right)^2 \phi_{F(s)} \tag{1.9}$$

where ϕ_F denotes the fluorescence quantum yield, A is the absorbance at the excitation wavelength, F is the fluorescence intensity of the corrected emission peak, n is referred to the solvent refractive index, and subscripts x and s are the unknown and standard, respectively.[102, 110]

1.5.3 Environmental Effects on Fluorescence

Fluorescence spectral positions and intensities are significantly influenced by many factors. These effects involve the molecular structure and chemical environment, such as, oxygen, temperature, solvent, pH, and concentration effects. Some of these factors are discussed in this section.

1.5.3.1 Effect of Molecular Structure

Molecules containing aromatic groups are found to be the most fluorescence compounds. A few highly unsaturated aliphatic compounds, however, are also fluorescent. In general, increase in the degree of π-electron system may result in a shift of both absorption and emission

spectra to a longer wavelength and an enhancement of the fluorescence quantum yield. For example, naphthalene, anthracene, naphthacene, and pentacene can fluoresce in the UV, blue, green, and red regions, respectively. In addition, substitution with an electron-donating group, such as, -OH, -OR, $-NH_2$, and $–NR_2$ causes an increase and shift in the absorption and emission spectra and often produces structured and broad spectra. Electron lone pairs on oxygen and nitrogen atoms do not alter π-π* nature transitions. They are actually involved in π bonding with the aromatic system. In contrast, substitution with an electron-withdrawing group, such as aldehyde, carbonyl, nitro, or carboxyl, shows a low fluorescent quantum yield because of the low-lying n-π* excited state.[108]

In addition, it has been found that molecules with rigid structures do exhibit strong fluorescence. For instance, fluorene (rigid structure) and biphenyl (non-rigid structure) have approximately 1.0 and 0.2 quantum efficiencies. The higher quantum efficiency of fluorene is due to the methylene group bridging, which makes its structure rigid. However, molecules with less structural rigidity have low fluorescence, which is likely the result of an increase in the internal conversion rate. The non-rigid portion of the compound shows low frequency vibrations with respect to the rigid portion.[102]

1.5.3.2 Effect of Oxygen

Fluorescence intensities of molecules, particularly PAHs, often decrease in the presence of dissolved oxygen. It has been established that molecular oxygen is an effective quencher for a number of fluorescent molecules.[85, 111, 112] This may be attributed to a photochemical oxidation of fluorescent species. Commonly, quenching by oxygen occurs as a result of the paramagnetic characteristics of molecular oxygen.[102, 105] It is thought that molecular oxygen is capable of quenching fluorescence by promoting intersystem crossing of the excited molecules ($^1M^*$) to the

excited triplet state ($^3M^*$). Excited molecules can then return from the excited triplet state to the ground state (^0M) by the non-radiative process. Dynamic quenching takes place only when the sample is excited by UV radiation because dynamic quenching requires the interaction with excited molecules.[113] However, it has become a common practice to ensure a complete removal of oxygen from oxygen sensitive systems. This is because the presence of oxygen in such systems can complicate the interpretation of fluorescence results.

1.5.3.3 Effect of Temperature and Solvent

In general, fluorescence quantum efficiencies of molecules decrease with an increase in temperature. This is ascribed to the frequency increase of collisions at high temperature, increasing the probability for deactivation by external conversion. In addition, an increase in the solvent viscosity can prompt external conversion, leading to the same result. Solvents and fluorophores containing heavy atoms may also demonstrate a decrease in fluorescence quantum efficiencies. This is because the interaction of the orbital spin leads to an increase in the intersystem crossing rate.[102]

The polarity of solvents also affects the absorption and/or emission spectra. For instance, solvatochromic fluorophores show a shift in the absorption and/or emission spectra with solvents of different polarities.[114-117] This shift is dependent on the dielectric and dipolar properties of solvatochromic fluorophores microenvironment. Some PAHs, particularly pyrene, have been used extensively for probing the local polarity.[118-124] PAHs do not exhibit spectral shifts like solvatochromic molecules. Instead, they display a variation in the band intensities ratio of emission, which is related to the PAHs polarity. For example, pyrene is one of fluorescent probes of polarity in organized media. It has been established that the first and third band intensity ratio of pyrene emission peak provides information about the solvent polarity, which is known as the

polarity ratio of pyrene (I_1/I_3). The effect of the solvent on pyrene polarity is known as the Ham effect which is a non-covalent dipole moment interaction between the excited fluorophore and solvent molecules.[121]

1.5.3.4 Effect of pH

Fluorescence of aromatic molecules substituted with an acidic or basic group is usually pH dependent.[125, 126] Fluorescence intensity and wavelength tend to be different for the ionized and non-ionized form of the fluorophore. This variation in the emission for some compounds, such as phenol and aniline, is attributed to a different number of resonance species that is linked to both the acidic and basic forms. A more stable first excited state due to additional resonance forms leads to fluorescence in the UV region. In addition, some fluorophores exhibit a shift in their emission spectra at different pH. This is due to the differences in the acid dissociation constant between the excited and ground state fluorophore. Therefore, fluorescence based measurements need a close control of pH.[102]

1.5.3.5 Effect of Concentration

Fluorescence radiation (F) is directly proportional to the power of absorption radiation, which is absorbed by the molecule. This can be expressed as follow:

$$F = K\left(I_o - I\right) \tag{1.10}$$

where K is a constant that depends on the fluorescence quantum yield. By substituting equation 1.7 into equation 1.6, the Beer-Lambert law can be written in the following format in order to relate fluorescence to the concentration:

$$\frac{I}{I_o} = 10^{-\varepsilon bc} \tag{1.11}$$

By substituting equation 1.11 into equation 1.10, one can obtain the following equation:

$$F = K I_o \left(1 - 10^{-\varepsilon bc}\right) \tag{1.12}$$

The exponential term in equation 1.12 can be expressed based on a Maclaurin series as follows:

$$F = K I_o \left[2.303\varepsilon bc - \frac{(2.303\varepsilon bc)^2}{2!} + \frac{(2.303\varepsilon bc)^3}{3!} ..... \right] \tag{1.13}$$

All terms within the brackets become small with respect to the first term, which provides that $2.303\varepsilon bc < 0.05$. In this case, the maximum relative error in equation 1.13, by eliminating all terms except the first term in the brackets, is 2.5%. As a result, equation 1.13 can be written as follows:

$$F = K I_o 2.303\varepsilon bc \tag{1.14}$$

or it can be in this form at constant I_o,

$$F = Kc \tag{1.15}$$

A linear plot can be obtained at low fluorophores concentration by plotting fluorescence intensity verses the concentration. However, higher order terms in equation 1.13 become important and linearity will be lost when the concentration is high enough to make $2.303\varepsilon bc > 0.05$.

Linearity can be affected not only by the high concentration but also by self-quenching and self-absorption. Self-quenching occurs as a result of the dynamic collision between excited fluorophores and solvent molecules via external conversion. It can be expected that self-quenching increases with an increase in the concentration, leading to a higher probability of the dynamic collision. On the other hand, self-absorption takes place when the emission wavelength overlaps the excitation wavelength. Consequently, there will be a decrease in fluorescence when the emitted radiation traverses the solution. There are primary and secondary absorption effects. The primary (or secondary) absorption effect is a significant absorption of the excitation (or emission) radiation. The secondary absorption effect resulting from the fluorophore is

specifically referred to the self-absorption phenomenon. These effects together are known as the inner-filter effect.[102, 103]

In this dissertation, fluorescence measurements were used to investigate the association behavior between HOC and DHM. Fluorescence of HOC was monitored in the presence of DHM in order to investigate this association. Recall, however, that DHM absorb light in the UV-Vis region, hence they usually absorb radiation at both excitation and emission regions of the fluorophore. As a result, this can cause fluctuations on the observed fluorescence intensities of the fluorophore due to the inner-filter effect. This effect has been reported to be an obstruction when investigating the association mechanism of HOC with DHM.[68, 79, 80, 127-130] In spite of the sensitivity advantage of fluorescence spectroscopy, the inner-filter effect can easily interfere with the fluorescence intensities of the fluorophore at both excitation and emission wavelength region. Therefore, correction for the inner-filter effect is very critical in order to carefully interpret fluorescence data. This can be achieved by correcting the measured fluorescence intensities based on the following equation[105]:

$$F_{corr.} = F_{obs.} 10^{\frac{\left(A_{ex}L_{ex} + A_{em}L_{em}\right)}{2}} \tag{1.16}$$

where $F_{corr.}$ denotes the corrected fluorescence intensity, A and L are the absorption and cuvette pathlength, respectively, for both excitation (*ex*) and emission (*em*) wavelengths, and $F_{obs.}$ is the observed fluorescence intensity.

1.5.4 Fluorescence Quenching

Fluorescence quenching is defined as the process that induces a decrease in the fluorophore fluorescence intensity. Several molecular processes may result in fluorescence quenching, including excited-state reactions, molecular rearrangements, energy transfer, ground-state complex formation, and dynamic (or collisional) quenching. Dynamic quenching is

encountered as a result of collision between the fluorophore and quencher, while static quenching occurs due to a ground-state complex formation. In addition, fluorescence quenching can take place as a result of the fluorophore optical characteristics, such as high optical density or turbidity.[105] In this section, detailed insights into dynamic and static quenching are discussed.

1.5.4.1 Dynamic Quenching Theory[105]

The Stern-Volmer equation is typically used to describe dynamic quenching process and can be obtained by the fluorescence intensities in the absence and presence of the quencher. In the excited state, the fluorescence intensity of the fluorophore is directly proportional to its concentration [*F**]. A constant population of the excited fluorophores is achieved when using continuous radiation. In the absence of the quencher, the equation of [*F**] is given by:

$$\frac{d[F^*]}{dt} = f(t) - \gamma[F^*]_o = 0 \tag{1.17}$$

In the presence of the quencher, equation 1.17 can be written in this format:

$$\frac{d[F^*]}{dt} = f(t) - \left(\gamma + k_q[Q]\right)[F^*] = 0 \tag{1.18}$$

where *f(t)* denotes the constant function of excitation, γ is the fluorophore decay rate in the absence of the quencher, and k_q is the bimolecular quenching constant. The decay rate of the excited state population in the absence of the quencher can be described as follows:

$$\gamma = \left(\Gamma + \Gamma_{NR}\right) \tag{1.19}$$

where Γ and Γ_{NR} are the radiative and non-radiative decay rates. Under continuous excitation, the excited state population is constant. Therefore, the derivative can be deleted, and the Stern-Volmer equation can be obtained by the division of equation 1.18 by equation 1.17:

$$\frac{F_o}{F} = \frac{\gamma + k_q[Q]}{\gamma} = 1 + k_q\tau_o[Q] = 1 + K_D[Q] \tag{1.20}$$

where F_o and F are fluorescence intensities of the fluorophore in the absence and presence of the quencher, respectively, [Q] is the quencher concentration, and K_D is the Stern-Volmer constant. The Stern-Volmer constant (K_{sv}) is equivalent to $k_q\tau_o$, and is described by K_D when the quenching of the fluorophore is known to be dynamic. Because dynamic quenching depopulates the excited state, the lifetime in the absence (τ_o) and presence (τ) of the quencher can be expressed as follows:

$$\tau_o = \frac{1}{\gamma} \tag{1.21}$$

$$\tau = \frac{1}{\gamma + k_q[Q]} \tag{1.22}$$

By dividing equation 1.21 by equation 1.22, one can obtain the following equation:

$$\frac{\tau_o}{\tau} = 1 + k_q\tau_o[Q] = 1 + K_D[Q] \tag{1.23}$$

From equations 1.20 and 1.23, an important property of the dynamic quenching can be observed. This characteristic is an equivalent decrease in the fluorophore fluorescence intensity and in its lifetime, which can be displayed as follows:

$$\frac{F_o}{F} = \frac{\tau_o}{\tau} \tag{1.24}$$

Since dynamic quenching process is an additional rate depopulating the excited state in the absence of fluorescence emission, the reduction in the lifetime takes place. No such decrease in the lifetime is observed when static quenching occurs. This is because only unbound fluorophores can be observed and have the unquenched lifetime τ_o.

A plot of F_o/F versus [Q], based on equation 1.20, is expected to be linear with a slope equal to K_D and an intercept, on the y-axis, of 1. The linearity is dependent upon the quencher concentration. It is of interest to observe that K_D^{-1} is equivalent to the concentration of the

quencher when the fluorophore fluorescence intensity is decreased by 50% (or F_o/F= 2). Typically, a linear Stern-Volmer plot shows that a single class of fluorophores is equally accessible to the quencher. A deviation in the linearity toward the x-axis indicates that two portions of fluorophores are present, and one class is not accessible to the quencher.

1.5.4.2 Static Quenching Theory[105]

Static quenching occurs as a result of the non-fluorescent complex formation between the fluorophore and quencher in the ground state. The fluorophore fluorescence intensity depends on the concentration of the quencher, and the association constant of the complex formation can be expressed as follows:

$$K_S = \frac{[F-Q]}{[F][Q]} \tag{1.25}$$

where [F – Q] is the complex concentration and [F] denotes the unbound fluorophore concentration. If the bound molecules are non-fluorescent, the remaining fluorescence fraction (F/F_o) is presented by the fraction of the total fluorescent molecules ($f_i = F/F_o$) and the total fluorophore concentration [F_o] can be displayed as follows:

$$[F_o] = [F] + [F-Q] \tag{1.26}$$

By substituting equation 1.26 into equation 1.25, K_S can be obtained as follows:

$$K_S = \frac{[F_o]-[F]}{[F][Q]} = \frac{[F_o]}{[F][Q]} - \frac{1}{[Q]} \tag{1.27}$$

The substitution of fluorescence intensities by the fluorophore concentration, followed by rearrangements of equation 1.27, yields the Stern-Volmer equation, which can be displayed as follows:

$$\frac{F_o}{F} = 1 + K_S[Q] \tag{1.28}$$

The Stern-Volmer equation for static quenching is similar to that for dynamic quenching, the only one exception being that the quenching constant (K_D) is now the association constant (K_S). A linear relationship can also be obtained from the Stern-Volmer plot for static quenching, which is identical to that of dynamic quenching. The linearity in the Stern-Volmer plot, however, does not show if the quenching mechanism is either static or dynamic. In fact, both dynamic and static quenching can result in a linear relationship. The most favorable method for distinguishing dynamic from static quenching is the lifetime measurement. In addition, dynamic and static quenching can behave differently based on the temperature or viscosity. In dynamic quenching, a faster diffusion rate and more collisional quenching result at higher temperatures so that there will be an increase of K_D and k_q. In the static quenching case, a decrease in the stability of complexes results at higher temperatures, leading to a decrease in K_s. Another way for distinguishing static from dynamic quenching is to examine the fluorophore absorption spectrum. Dynamic quenching affects only the fluorophore excited state; therefore, no changes can be observed in the absorption spectra. In contrast, static quenching often results in changes in the fluorophore absorption spectrum due to the formation of the ground-state complex.

1.5.4.3 Combined Dynamic and Static Quenching[105]

In many cases, the quenching of the fluorophore fluorescence may take place as a result of the combination of dynamic and static quenching. Consequently, an upward curvature toward the y-axis is observed in the Stern-Volmer plot. The remaining fraction of fluorescence (F/F_o) is given by the fraction of unbound fluorophores (f_i) and the fraction of unquenched fluorophores by collisional encounters, which can be expressed as follows:

$$\frac{F}{F_o} = f_i \frac{\gamma}{\gamma + k_q[Q]} \tag{1.29}$$

Reorganization of the last term on the right and inversion of equation 1.29 gives a modified form of the Stern-Volmer equation, which is given by:

$$\frac{F_o}{F} = \left(1 + K_D[Q]\right)\left(1 + K_S[Q]\right) \tag{1.30}$$

This equation is a second order in [Q], accounting for the resulted upward curvature when both dynamic and static quenching of the fluorophore occur. Using lifetime measurements, the dynamic portion of equation 1.30 is obtained from equation 1.23. However, equation 1.30 can be modified, allowing a graphical separation of K_S and K_D, when the lifetime measurement is not available. The multiplication of terms in the parentheses yields the following equation:

$$\frac{F_o}{F} = 1 + \left(K_D + K_S\right)[Q] + K_D K_S [Q]^2 = 1 + K_{app}[Q] \tag{1.31}$$

where K_{app} denotes the apparent quenching constant and is given by:

$$K_{app} = \left(\frac{F_o}{F} - 1\right)\frac{1}{[Q]} = \left(K_D + K_S\right) + K_D K_S [Q] \tag{1.32}$$

A linear relationship, with a slope of $K_D K_S$ and an intercept of $(K_D + K_S)$, can be obtained from a plot of K_{app} versus $[Q]$.

1.5.5 Fluorescence Spectroscopy Instrumentation

Almost all fluorescence instruments are designed with double beam optics in order to compensate for the power fluctuations in the excitation source. Figure 1.11 shows a typical configuration for the fluorometer basic components. As shown in Figure 1.11, the excitation radiation first passes through an excitation monochromator in order to transmit the beam, which will excite the sample. Consequently, fluorescence takes place in all directions from the cell and can be collected at any angle to the incident radiation. Fluorescence measurements, however, are usually performed at a right angle (90^o) to the direction of the incident radiation in order to eliminate any possible interference from the exciting radiation and minimize the reflection from

cell walls and scattering from the solution. After passing through a second emission monochromator, the emitted beam is then collected at the PMT for measurement. On the other side, the reference radiation will pass through an attenuator. The attenuator minimizes its power to roughly that of the emitted radiation. The reduction of the power by the attenuator is usually a factor of 100 or more. Finally, signals from both reference and sample PMT are sent into a ratio amplifier. The output of the ratio amplifier is represented by a meter or recorder.[102]

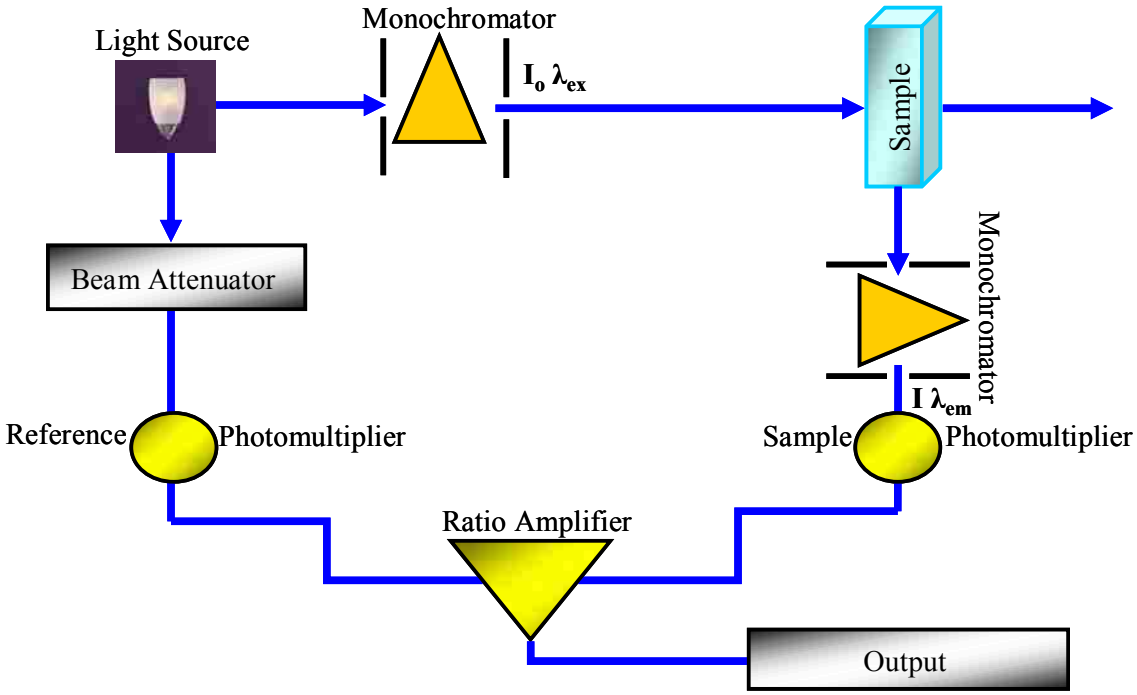

Figure 1.11 Fluorescence basic instrumental components.

Fluorescence instrumentations in most applications are configured with a more intense excitation source than the tungsten, deuterium, or hydrogen arc lamps used for a UV-Vis absorption spectrometer. Typically, a mercury or xenon lamp is employed with fluorometers. A low pressure mercury lamp, equipped with a fused silica window, is a line excitation source and is most often used in filter fluorometers. It provides a spectrum containing intense lines at 254,

366, 405, 436, 546, 577, 691, and 773 nm. A high pressure xenon lamp, 75 to 450 W, is a continuous radiation source and requires a large power supply, which can produce a voltage of 15 to 30 V and direct current of 5 to 20 A. The xenon lamp provides a continuous spectrum from 3×10^2 to 13×10^2 nm and is most often used in fluorometers. Various laser excitation sources, for example, a tunable dye laser using a pulsed nitrogen laser as a primary radiation source, were also used in fluorometers starting in the 1970s. Radiation monochromators between 360 and 650 nm are also developed, which eliminate the need for excitation monochromators.

As was previously mentioned, fluorescent signals are of low intensity; therefore, large amplification factors for fluorescence measurement are needed. Typically, PMT are widely used as detectors in fluorescence instruments because of their sensitivity. PMT consist of a photosensitive cathode and a collection anode. The cathode and anode, however, are isolated by several electrodes, known as dynodes, which produce electron multiplication or gain. As long as anode currents do not exceed their maximum rating, typically < 1 μA, PMT usually show linear responses to a few percent. PMT must also be operated with a very stable power supply in order to keep the total gain constant. PMT are useful in detecting a low radiation level because of their high gain. The rise time of PMT is dependent mostly upon the electron spread in the transit time during the multiplication process. The electron spread is typically around 10 ns, but some specific electron optics can minimize the transit time to below 1 ns.[102, 103]

1.5.6 Time-Resolved Fluorescence Measurements

Time-resolved fluorescence measurements are widely used in fluorescence spectroscopy, particularly for biological macromolecules application. This is due to the fact that time-resolved measurements provide more information than steady-state fluorescence measurements. For instance, a protein possesses two tryptophan residues and each one has its own distinct lifetime

decay. It is not easy to resolve fluorescence spectra from the two residues because of the overlap between their absorption and emission spectra. Using time-resolved fluorescence measurements, one can obtain a lifetime for each residue and resolve their fluorescence spectra.[105]

In addition, time-resolved measurements are employed as a supplemental tool for selectivity enhancement and multi-component system determinations in analytical applications. They provide important information such as the rate of excited-state reactions and energy transfer between a donor and acceptor molecules in a bimolecular process. It has also been established that time-resolved measurements are one of the most powerful tools for distinguishing static from dynamic quenching. As was previously discussed, the lifetime of unbound fluorophores does not decrease when static (formation of ground-state complexes) quenching takes place. This is attributed to the fact that only unbound fluorophores can be detected in a fluorescence experiment. On the other hand, the dynamic quenching process decreases the decay time by acting on the entire excited-state population.[103, 105, 109] In this section, two methods of time-resolved measurements will be discussed in detail, namely time- and frequency-domain fluorescence lifetime measurements and their data analysis.

1.5.6.1 Time-Domain Fluorescence Lifetime

In time-domain fluorescence lifetime measurements, the fluorophore is excited by a pulsed radiation source. The width of the pulsed radiation source needs to be as short as possible and much shorter than the measured fluorescence decay time of the fluorophore. The time duration between this excitation pulse and the arrival of the first emitted photon is measured by the detector for a large number of emitted photons. As a result, the distribution of the arrival time yields the fluorescence decay curve (Figure 1.12). The fluorescence intensity (F) of the fluorophore is dependent upon the time (t) and is measured after the excitation pulse.

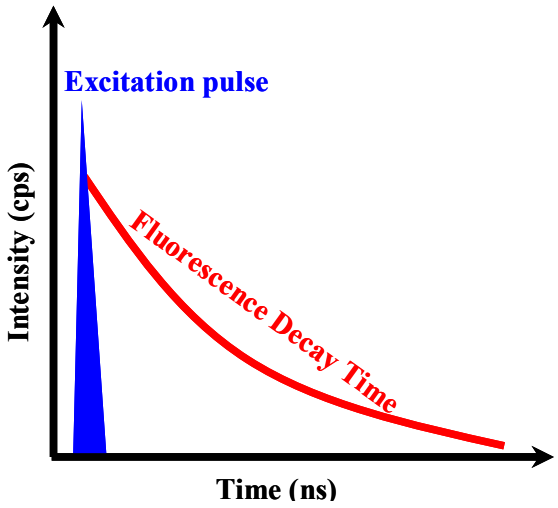

Figure 1.12 Fluorescence decay time in time-domain fluorescence lifetime.

The fluorophore fluorescence lifetime (τ) is then calculated from the slope of a plot of log $F(t)$ versus t. Currently, time-domain fluorescence measurements are performed using time-correlated single photon counting (TCSPC).[105, 131]

For a single fluorophore which decays exponentially, the time-dependent fluorescence intensity can be expressed as follows:

$$F(t) = \alpha e^{-t/\tau} \tag{1.33}$$

where α is a pre-exponential factor, which represents the fluorophore fractional contribution in each environment. When the fluorescence decay curve cannot be described by a single exponential, the fluorescence decay can be fitted by a multi-exponential decay curve in terms of an average relaxation time as follows:

$$F(t) = \sum_{i}^{n} \alpha_i e^{-t/\tau_i} \tag{1.34}$$

where n denotes the number of components for ith (i) data points and the $\sum\alpha_i$ is normalized to unity. From equation 1.34, the fluorescence intensity, in the multi-exponential decay, is assumed to decay as the summation of individual single exponential decays.

However, the values of α_i and τ_i can be used for calculation of the fractional contribution (f_i) for each fluorescence decay time to the fluorescence steady-state intensity as follows:

$$f_i = \frac{\alpha_i \tau_i}{\sum_i \alpha_i \tau_i} \tag{1.35}$$

The $\sum f_i$ is normalized to unity, and the terms $\alpha_i \tau_i$ are directly proportional to the region below the fluorescence decay curve. In fluorescence steady-state experiments, one can measure all the emission regardless to when the photon is emitted. This is why the fluorescence intensity and the terms $\alpha_i \tau_i$ are low for a short decay time. For a multi-components system, the f_i values refer to the fluorescence fractional intensity at each wavelength for each individual fluorophore component. Nevertheless, these values may not strongly relate to expected fluorescence intensities due to the difficulties in resolving the multi-exponential decay.

1.5.6.2 Frequency-Domain Fluorescence Lifetime

In the case of frequency-domain lifetime measurements, the sample is excited by a sinusoidally intensity-modulated radiation source at high frequency (Figure 1.13), instead of the pulsed light source used in time-domain lifetime. Consequently, the sample emission response is also sinusoidally modulated at the same angular modulation frequency (ω) but out of phase with the excited radiation. The sample emission is time delayed relative to the modulation excitation as a result of the time lag between the excitation and emission. This delay is known as the phase shift at each modulation frequency and increases from 0^o to 90^o with an increase in the modulation frequency. The modulation of emission results from the finite time response of the sample and decreases from 1 to 0 by increasing modulation frequency.[105]

The sample emission rapidly follows excitation, and the phase delay and modulation approach 0^o and 1 at low frequency, respectively. At high frequency, the excited state lifetime

prevents the emission from coming precisely after the excitation and the phase delay increases toward 90^{o} and the modulation decreases toward 0.

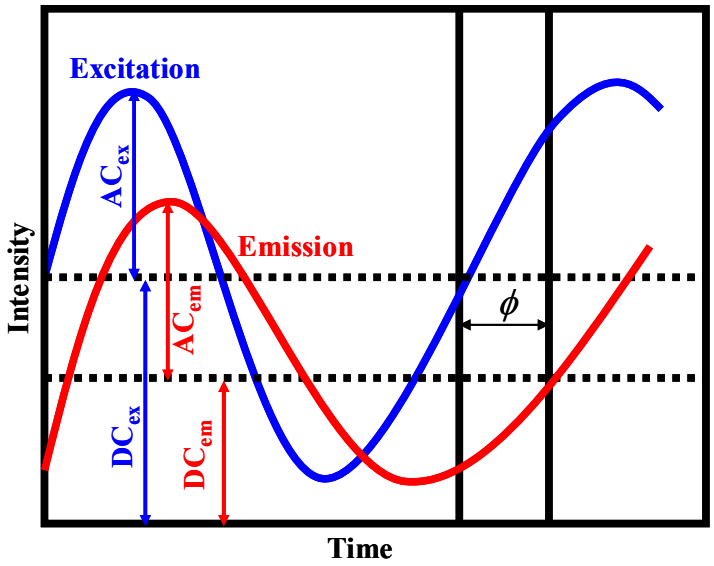

Figure 1.13 Phase and modulation of fluorescence from intensity-modulated excitation.

The modulated excitation (m_{ex}) and emission (m_{em}) are given by:

$$m_{ex} = \left(\frac{AC}{DC}\right)_{ex} \tag{1.36}$$

$$m_{em} = \left(\frac{AC}{DC}\right)_{em} \tag{1.37}$$

where AC and DC are alternative and direct currents for both excitation (ex) and emission (em), respectively. The relative modulation (m) of the emission can be expressed as follows:

$$m = \left[\frac{(AC/DC)_{em}}{(AC/DC)_{ex}}\right] \tag{1.38}$$

The phase shift (ϕ) and modulation (m) are the sum of exponential decays for a multi-component system containing multiple discrete components. The two observable parameters in

frequency-domain lifetime, ϕ and m, are functions of ω, the lifetimes of each component (τ_i), and the fractional intensity contributions (f_i):

$$\phi_\omega = \tan^{-1}\left(N_\omega / D_\omega\right) \tag{1.39}$$

$$m_\omega = \sqrt{N_\omega^2 + D_\omega^2} \tag{1.40}$$

where N_ω and D_ω are the real and imaginary portions of the signal, respectively, and can be obtained as follows:

$$N_\omega = \frac{\sum_i^n \frac{\alpha_i \omega \tau_i^2}{1+\omega^2\tau_i^2}}{\sum_i^n \alpha_i \tau_i} = \sum_i^n \frac{f_i \omega \tau_i}{1+\omega^2\tau_i^2} \tag{1.41}$$

$$D_\omega = \frac{\sum_i^n \frac{\alpha_i \tau_i}{1+\omega^2\tau_i^2}}{\sum_i^n \alpha_i \tau_i} = \sum_i^n \frac{f_i}{1+\omega^2\tau_i^2} \tag{1.42}$$

where the summation in equations 1.41 and 1.42 represents a system consisting of a finite number of components (n). The substitution of equations 1.41 and 1.42 into equations 1.39 and 1.40 yields both ϕ and m as a function of ω for a single exponential decay, containing one discrete component, as follows:

$$\phi_\omega = \tan^{-1}\left(\omega\tau_\phi\right) \tag{1.43}$$

$$m_\omega = \frac{1}{\sqrt{\left(1+\omega^2\tau_m^2\right)}} \tag{1.44}$$

where τ is the lifetime of the fluorophore. It can be observed, from equations 1.43 and 1.44, that short lifetimes require higher frequencies to interrogate the region of greatest change in ϕ and m. The opposite is true for long lifetimes.[105, 108]

In frequency-domain lifetime measurements, it is difficult in practice to measure the phase and modulation based on the excitation radiation. Alternatively, the phase and modulation are relatively measured to a reference. Typically, a scatter reference solution with a zero lifetime or a fluorophore with a known lifetime is used to monitor the modulation of the excitation radiation while also measuring the emission so that a true differential measurement is performed. In addition, the fluorescence emission usually passes through a long-pass filter at a specific wavelength in order to eliminate Rayleigh and Raman scattering in the signals.[105, 132, 133]

1.5.6.3 Data Analysis of Time-Resolved Lifetime Measurements

Several methods have been used for the analysis of time-resolved fluorescence lifetime data, such as, non-linear least squares analysis,[134-136] the method of moments,[137-139] Laplace transformation,[140-142] maximum entropy method,[143, 144] and phase plane method.[145, 146] It has been mathematically established that non-linear least squares (NLLS) method is one of the most reliable and widely used methods for the time-resolved fluorescence curve fitting.[105] In time-domain fluorescence, one can obtain the parameters that minimize the quantity that causes the mismatch between the measured $N_m(t_i)$ and calculated $N_c(t_i)$ values. This can be accomplished by minimizing the χ^2 parameter, presented in the following equation:

$$\chi^2 = \sum_{i=1}^{n}\left[\frac{N_m(t_i) - N_c(t_i)}{\sigma_i^2}\right]^2 = \sum_{i=1}^{n}\frac{\left[N_m(t_i) - N_c(t_i)\right]^2}{N_m(t_i)} \tag{1.45}$$

where N is referred to the total number of data points and σ_i is the standard deviation of i data points. In the case of frequency-domain lifetime measurements, both phase and modulation data can be analyzed and a minimized χ^2 is obtained as follows:

$$\chi^2 = \frac{1}{v}\sum_{\omega}\left[\left(\frac{\phi - \phi_{c_\omega}}{\sigma_{\phi,\omega}}\right)^2 + \left(\frac{m - m_{c_\omega}}{\sigma_{m,\omega}}\right)^2\right] \tag{1.46}$$

where v denotes the number of degree of freedom, ϕ and m are the measured phase shift and demodulation values, ϕ_{c_ω} and m_{c_ω} are the calculated phase shift and demodulation values, and $\sigma_{\phi,\omega}$ and $\sigma_{m,\omega}$ are the standard deviation of measured phase and modulation, respectively. In general, the evaluation of χ^2 minimization is performed by assuming constant error values for consistency and ease of day-to-day data interpretation.

Time-resolved decay profiles are usually analyzed using a global analysis. In the global analysis, the fluorescence lifetime is assumed to be wavelength independent. Various initial guesses of lifetime parameters are applied using NLLS analysis to evaluate the stability of the χ^2 minimization. A good fit of time-resolved decay data sets can be obtained by visual inspection of residual plots as well as by χ^2 statistics.[147-149] The value of χ^2 between 1 and 2 usually indicates that the model should be valid. It is, however, impossible to get χ^2 values within this range for many complex models. In such cases, the model can not be rejected by χ^2 statistics only, and residual plots must be considered in model discrimination.[105, 108, 150]

1.6 Nuclear Magnetic Resonance Spectroscopy

Nuclear magnetic resonance (NMR) spectroscopy deals with the measurement of absorption of electromagnetic radiation in the radio frequency region, which ranges from approximately 4 to 900 MHz. This frequency region is much lower in comparison to those in electronic, vibrational, or rotational spectroscopy. In NMR, atomic nuclei are involved in the absorption of electromagnetic radiation by the sample. The principle of NMR spectroscopy was discovered by W. Pauli in 1924. He illustrated hyperfine splitting in some atomic spectra by suggesting that certain atomic nuclei behave as spinning particles. As a result, Pauli indicated that these atomic nuclei should have spin and magnetic moment characteristics. Therefore, exposure to the magnetic field can cause splitting in the energy levels of atomic nuclei.[102, 151]

It is known that nuclei with certain isotopes have the ability to rotate about the axis so that they have the spin property and possess intrinsic angular momentum. The total magnitude of this angular momentum (p) is described as follows:

$$p = \hbar\left[I(I+1)\right]^{1/2} = \frac{h}{2\pi}\left[I(I+1)\right]^{1/2} \tag{1.47}$$

where I denotes the nuclear spin quantum number and $\hbar$ is the reduced Plank's constant ($h/2\pi$). The maximum measurable component of the angular momentum is $I\hbar$. The value of I can be integral or half integral (0, 1/2, 1, 3/2, ….). The actual value of I is dependent upon the isotope. When nuclei possess I value of 0, they have no angular momentum. The largest number of the angular momentum depends on the spin quantum number I. A nucleus can have $(2I + 1)$ discrete states and the angular momentum component of these states will have values of I, $I - 1$, $I - 2$, ……, $-I$ in any selected direction. Different states, however, have identical energies in the absence of an external field.[102, 152] Because a nucleus contains a uniform spherical charge distribution, the spin of this nucleus produces rise to the magnetic field which is parallel to the resulted field when electricity flows through a coil of wire. As a result, the magnetic moment is produced and oriented along the spin axis. The magnetic moment (μ) is proportional to the angular momentum (p) by the following relationship:

$$\mu = \gamma p \tag{1.48}$$

where γ is the magnetogyric ratio (radian.T^{-1}.s^{-1}). The magnetogyric ratio is proportionality constant and is unique to each nucleus. The measurable magnetic quantum states (m), resulting from the interrelation between the nuclear spin and magnetic moment, is given by:

$$m = I, I-1, I-2, ..., -I \tag{1.49}$$

Therefore, nuclei with $I = 1/2$ have two magnetic quantum numbers, which are aligned either parallel ($m = + 1/2$) or anti-parallel ($m = - 1/2$). When a nucleus of the spin quantum

number of one half ($I = 1/2$) is carried to an exterior magnetic field (B_o), the magnetic moment of this nucleus is oriented in one of two directions to the magnetic field, which is dependent on its magnetic quantum state (Figure 1.14).

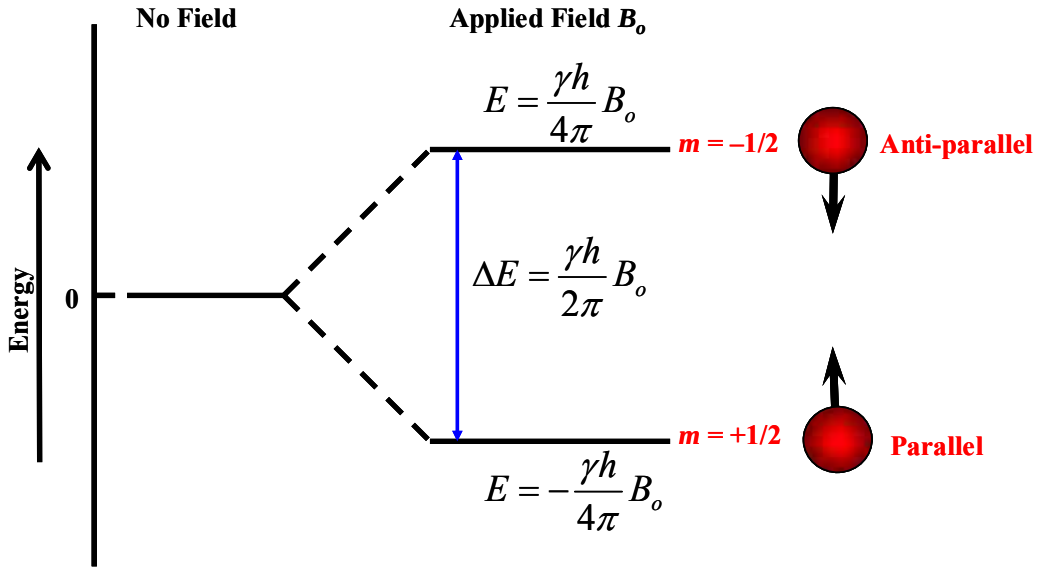

Figure 1.14 Magnetic moments and energy levels for a nucleus with a spin quantum number of ± 1/2.

The potential energy (E) of the nucleus in two orientations can be expressed by:

$$E = -\frac{\gamma m h}{2\pi} B_o \tag{1.50}$$

The potential energy of the lower ($m = +1/2$) and higher ($m = -1/2$) energy state is given by:

$$E_{+1/2} = -\frac{\gamma h}{4\pi} B_o \tag{1.51}$$

$$E_{-1/2} = \frac{\gamma h}{4\pi} B_o \tag{1.52}$$

Thus, the difference in the potential energy (ΔE) between two states can be displayed as follows:

$$\Delta E = \left(\frac{\gamma h}{4\pi} B_o\right) - \left(-\frac{\gamma h}{4\pi} B_o\right) = \frac{\gamma h}{2\pi} B_o \tag{1.53}$$

Since $\Delta E = h\nu_o$ in other types of spectroscopy, the frequency required to induce the transition from the lower to higher energy state in NMR can be obtained by substituting this relationship into equation 1.53 as follows:

$$\nu_o = \frac{\gamma B_o}{2\pi} \tag{1.54}$$

This frequency is known as the Larmor frequency. The energies of the magnetic quantum states of the nuclei are identical in the absence of a magnetic field. Therefore, nuclei will have magnetic quantum numbers of +1/2 and –1/2. However, the nuclei start to orient themselves in the presence of a magnetic field, and the lower energy state (m = +1/2) becomes more dominant. In the NMR experiment, the extent of this predominance can be calculated using the Boltzmann equation as follows:

$$\frac{N_j}{N_o} = e^{\left(\frac{-\Delta E}{kT}\right)} \tag{1.55}$$

where N_o and N_j denote the number of the nuclei in the lower (m = +1/2) and higher (m = –1/2) energy state, respectively, k is the Boltzmann constant (1.38×10^{-23} JK^{-1}), and T is the absolute temperature. The substitution of equation 1.53 into 1.55 results in the following relationship:

$$\frac{N_j}{N_o} = e^{\left(\frac{-\gamma h B_o}{2\pi kT}\right)} \tag{1.56}$$

When the temperature of the sample is at absolute zero, all magnetic moments tend to point in a parallel direction to the external magnetic field (B_o) and will be presented in the lower energy state (m = +1/2). At room temperature, however, there will be enough energy to bring some of the magnetic moments back so that they will be pointed in the opposite direction or the lower

energy state (m = –1/2). Eventually, the two energy states are equally populated at an infinitely higher temperature.[102, 151, 153]

1.6.1 Fluorine Nuclear Magnetic Resonance Spectroscopy[154, 155]

The nuclei that have received the greatest interest from chemists include proton (^{1}H), carbon (^{13}C), fluorine (^{19}F), and phosphorus (^{31}P). These nuclei possess two spin quantum numbers which correspond to I = +1/2 and –1/2. Heavier nuclei, containing several elementary particles, have nuclear spin quantum numbers ranging from zero (no net spin component) to at least 3/2. ^{19}F NMR spectroscopy has similar nuclear characteristics to ^{1}H NMR spectroscopy and there is actually not much to differentiate between the two methods. The spin lattice relaxation times for both ^{1}H and ^{19}F are short enough, a few seconds or less; therefore, resonance saturation can be easily avoided. ^{1}H and ^{19}F have natural abundances of 99.98 and 100%, respectively.[154]

Although there are similarities between ^{1}H and ^{19}F NMR spectroscopy, there is a significant difference in the NMR parameters between the two nuclei. A fluorine nucleus in a compound is surrounded by 9 electrons, compare to one electron in a proton nucleus. Therefore, the ^{19}F NMR chemical shift scale and sensitivity to the details of its microenvironment are much higher than those of ^{1}H. The ^{1}H chemical shift has a range of 10 ppm, while the chemical shift of ^{19}F is a much larger range of approximately 500 ppm. This scale can even be expanded to over 1000 ppm if inorganic fluoride is considered. The large chemical shift scale of ^{19}F is attributed to the strong paramagnetic contribution to the shielding constant originating from the fluorine atom. In fact, the diamagnetic contributions to the screening constant of ^{19}F nuclei are very low (roughly 1%). Neighboring group effects such as ring current effects or the influence of local magnetic anisotropies do not play any role in the ^{19}F chemical shift. The ^{19}F chemical shift is affected by the nature of the atoms attached to the adjacent carbon atoms. For example, the

difference in the ^{19}F chemical shift for fluoromethane (CH_3F) and trichlorofluoromethane ($CFCl_3$) is 286.7 ppm. The total scale of aromatic fluorine atoms is over 80 ppm. In addition, the solvent effect plays a much more critical role in determining the fluorine peak positions than that of ^{1}H. Shifts of 5 ppm and even more in the ^{19}F chemical shift can be expected.[154, 155]

In general practice, $CFCl_3$ is used as an internal reference. The ^{19}F chemical shift regions of most important functional groups using $CFCl_3$ as an internal reference are illustrated in Figure 1.15. Other reference compounds have also been employed; however, no uniformity rule has been established, particularly in the older literature.

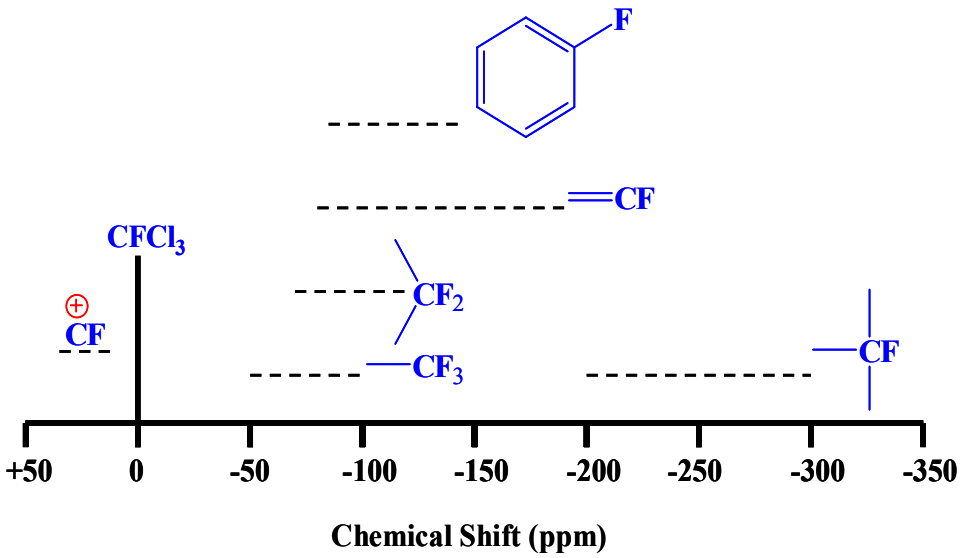

Figure 1.15 The ^{19}F chemical shift scale in organic compounds.

Moreover, most ^{19}F NMR measurements are obtained using external standards, making the comparison difficult if the corrections for different volume susceptibilities are inconceivable. However, it is frequently argued that due to the magnitude of ^{19}F chemical shift, small corrections arising from the susceptibility differences can be discounted. Most ^{19}F chemical shift values are negative due to the paramagnetic shift of the fluorine resonance in $CFCl_3$. It can be observed from Figure 1.15 that saturated compounds absorb at the highest field. In addition, the

^{19}F resonance in aliphatic, aromatic, and olefinic fluorine compounds has an extensive overlap. The subsistent electronegativity can also affect the ^{19}F chemical shift in some cases. A decrease in the electronegativity of neighboring atoms causes an increase in the shielding. For example, the ^{19}F chemical shift of NF_3, electronegativity of 3, is 142 ppm, while the chemical shift of BF_3, electronegativity of 2, is –129 ppm.[154]

1.7 High Performance Liquid Chromatography

Liquid chromatography is generally used for the separation of a multi-component mixture in a solution, with different solutes migration in a liquid (or mobile phase) passing through a packed column with solid particles (stationary phase). The mobile phase is always liquid, while the stationary phase is either a solid, porous, surface active material in a small particle form, or a thin film of liquid coated on a solid support or column wall. The technique of high performance liquid chromatography (HPLC), also known as high speed and high pressure liquid chromatography, has actually arisen from the application of liquid chromatography.[156, 157]

The HPLC technique has been widely used in different applications, such as pharmaceutical, biochemical, clinical, and environmental applications. The large contribution of HPLC is due to the fact that both stationary and mobile phases interaction can be applied, resulting in higher selectivity of the system. Developments in HPLC are related to the silica technology. The use of high operating pressure and small uniform particle sizes allows rapid diffusion rates and fast analysis times. This technique provides both qualitative and quantitative information because each compound in a mixture has its own elution time. In addition, both the area and height of each signal are proportional to the amount of the compound.[158, 159]

In HPLC, the mobile phase can traverse the column by use of a pump at a flow rate of 1 up to 5 cm^3/min. If the mobile phase composition is fixed at some percentage, the method is

known as an isocratic elution. As an alternative, the composition of the mobile phase can be changed in a predetermined manner during the separation, known as the gradient elution. The gradient elution method is important, in particular, when the range of retention times for the components in the column is very wide, or some components have high capacity factor values, resulting in a complex separation. In this case, it is recommended to decrease the range of retention times by increasing the solvent strength. For example, non-polar compounds are adsorbed relatively weakly and can be eluted with a non-polar solvent, while polar solutes are strongly adsorbed and required a polar solvent.

In addition, the separation of solutes in the column can be achieved by changing the polarity of the solvent mixture, or the gradient elution, when the sample contains a wide range of polarity. However, there are some problems encountered with the gradient elution. For example, the time is lost during reconditioning the chromatographic column for a subsequent run. In addition, a drift in the baseline can be observed because of slightly different UV absorbances for different solvents. The appearance of specious peaks can also be observed in the gradient elution due to impurities in the solvent and fluctuations in the flow rate because of the alterations in liquid compressibilities.[157-159]

1.7.1 Chromatographic Parameters

The chromatography analysis involves the introduction, separation, and detection of a multi-component mixture. The separation of this multi-component mixture is dependent upon different physicochemical and chemical interactions between the sample solutes and the stationary and mobile phases. Differences in these interactions for several components will eventually lead to their separation on the chromatographic column.[160] This can be expressed by different chromatographic parameters, which is discussed in detail in the following section.

1.7.1.1 Retention Parameters

A plot of detector signals, produced by certain analyte concentrations at the column exit, versus time or eluent (solvent) volume is known as the chromatogram. The retention volume (V_R) is defined as the volume that passes through the chromatographic column from the point of sample injection to the point where the peak maximum exits the column, representing the production of specific components. The dead volume (V_o) is considered to be the volume of eluent in the column and is defined as the retention volume of the un-retained component. The retention volume is related to the flow rate (F_v) and retention time (t_R) as follows:

$$V_R = F_v t_R \tag{1.57}$$

The retention time is more commonly used instead of the retention volume because it is easily determined and is directly visible in the chromatogram.

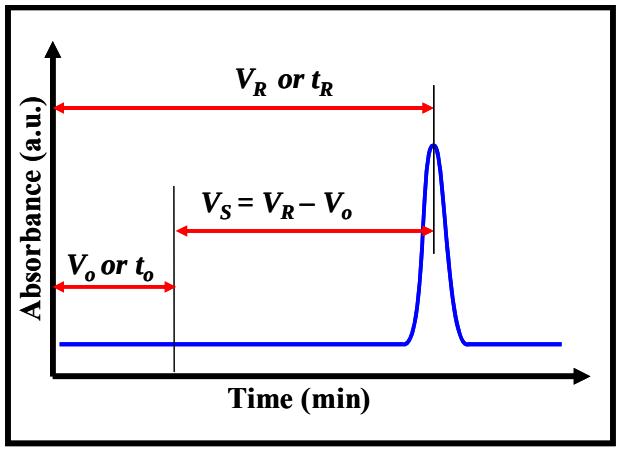

Figure 1.16 Definitions of retention time and retention volume.

The retention time is measured from the point of injection to the point of the peak maximum (Figure 1.16). The retention time or volume numerical value is mostly dependent on the chromatographic column dimension. The first moment of the Gaussian distribution (M_1) defines the retention time of the chromatographic peak, which can be expressed as follows:

$$M_1 = t_R = \frac{1}{A}\int_0^{\infty} Ct\,dt \tag{1.58}$$

where A denotes the peak area, and C is the concentration of the compound, which is correlated to the time (t) passed from the point of the solute injection.[156, 160]

1.7.1.2 Capacity Factor

The capacity factor (k') is the fundamental measurement of retention in the liquid chromatography.[156] It is defined as the ratio of number of compounds in the stationary phase (N_s) to the number of compounds in the mobile phase (N_m), which can be expressed as follows:

$$k' = \frac{N_s}{N_m} \tag{1.59}$$

The capacity factor is related to the partition coefficient (K_D) of the solute between the mobile and stationary phases by taking into account the volumes of the mobile (V_m) and stationary (V_s) phases as follows:

$$k' = K_D \frac{V_s}{V_m} \tag{1.60}$$

In addition, the capacity factor can be related to the retention time (t_R) of the solute and the elution time (t_o) of the un-retained component as follows:

$$k' = \frac{(t_R - t_o)}{t_o} = \frac{t_R}{t_o} - 1 \tag{1.61}$$

1.7.1.3 Number of Theoretical Plates

The chromatographic column efficiency is determined by the number of theoretical plates (N). This chromatographic parameter is calculated as follows:

$$N = \left(\frac{t_R}{\sigma}\right)^2 \tag{1.62}$$

where $$\sigma = \frac{w_{0.5}}{2.354} = \frac{w}{4} \quad (1.63)$$

The base width (w) of the chromatographic peak can be obtained by the tangents extrapolation at inflection points to the baseline. The symbol $w_{0.5}$ is the peak width at half of its maximum height. By the substitution of σ by either $w_{0.5}/2.354$ or $w/4$ into equation 1.62, one can obtain the following equations:

$$N = 5.54\left(\frac{t_R}{w_{0.5}}\right)^2 \quad (1.64)$$

$$N = 16\left(\frac{t_R}{w}\right)^2 \quad (1.65)$$

Both equations 1.64 and 1.65 can be used in order to calculate the column efficiency. However, equation 1.64 is generally more preferable because it does not involve extrapolation of lines at the tangent to the point of inflection.

Theoretically, the number of theoretical plates has only a small dependency on the capacity factor for packed columns. In open-tubular columns, the column efficiency decreases when the retention increases. Consequently, open-tubular liquid chromatography should be operated at a relatively low value of the capacity factor. The number of theoretical plates in the column is the measure of the dispersing amount of the solute band when it moves down the column, and the efficiency of systems is actually evaluated by the high value of the number of theoretical plates.

The number of theoretical plates is directly proportional to the column length but inversely proportional to the diameter of particles. The quality of two chromatographic columns of different length can be compared by the use of the height equivalent to one theoretical plate (HETP), or simply the plate height (H) of the column, which is given by:

$$H = \left(\frac{L}{N} \right) \tag{1.66}$$

where L is the length of the column. Efficient chromatographic columns have small values of the plate height.[156, 158]

1.7.1.4 Selectivity

The selectivity (α) of the column is the function of the thermodynamics for the mass transfer process and can be determined based on the relative peaks separation. The selectivity factor of two adjacent peaks in the chromatogram is given by:

$$\alpha = \frac{k_1'}{k_2'} \tag{1.67}$$

where k_1' and k_2' refer to capacity ratios of the first and second peaks, respectively. By the substitution of equation 1.61 into 1.67 followed by rearrangement, the selectivity can be obtained as follows:

$$\alpha = \frac{\left(t_{R2} - t_o\right)}{\left(t_{R1} - t_o\right)} \tag{1.68}$$

where t_{R1} and t_{R2} are retention times of the first and second peaks for the two solutes, respectively.[156, 160]

1.7.1.5 Resolution

The main objective of chromatography is to determine the resolution between solute bands. The resolution (R_s) of two chromatographic peaks is the evaluation of their separation and can be calculated as follows:

$$R_S = \frac{2\left(t_{R2} - t_{R1}\right)}{w_1 + w_2} \tag{1.69}$$

where w_1 and w_2 are the peak base widths of the first and second peaks (Figure 1.17).

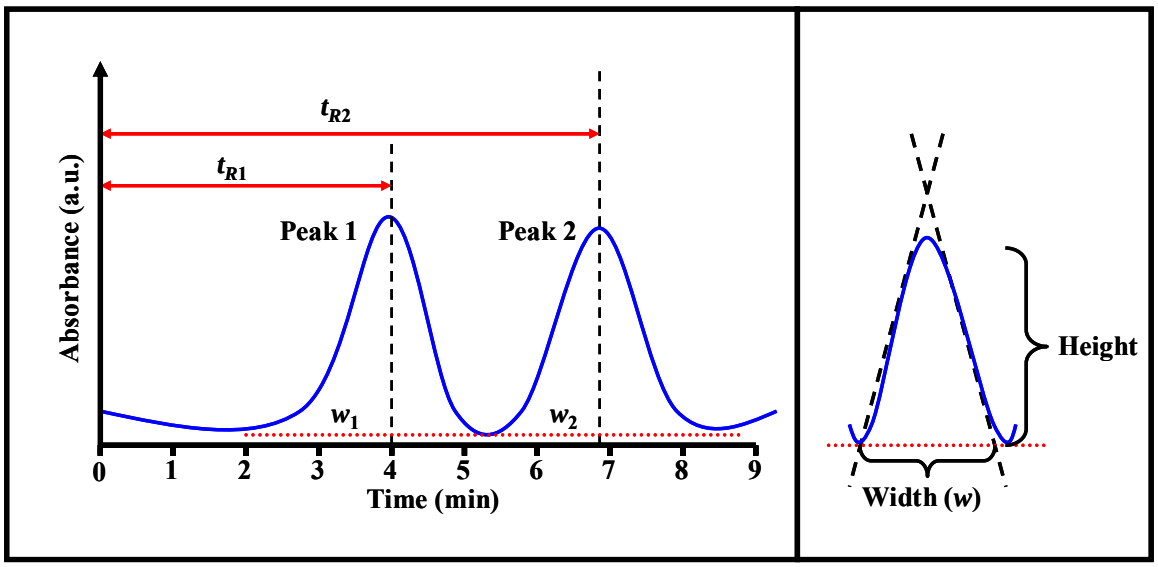

Figure 1.17 Typical chromatogram showing chromatographic parameters.

For two Gaussian peaks, the baseline resolution effectively corresponds to R_s value of 1.5 or greater. However, R_s value of 1.0 can also be obtained but for two peaks of adjacent symmetrical triangles.[158, 159] A general equation of the resolution can also be derived, which correlates the resolution to different chromatographic parameters, including selectivity, capacity factor, and the number of theoretical plates. This equation can be expressed as follows:

$$R_S = \left(\frac{\alpha - 1}{4\alpha}\right)\left(\frac{k_2'}{1 + k_2'}\right)\sqrt{N} \tag{1.70}$$

1.7.2 High Performance Liquid Chromatography Modes

The separation mechanism is based on the solutes interaction with both the mobile and stationary phases. The chromatographic separation of two components depends on the difference between their capacity factors. In addition, the capacity factor is dependent upon the distribution ration between the mobile and stationary phases. Several stationary phases used in HPLC, such as active adsorbent surfaces, polymer loaded glass, and others, result in various separation modes.[158, 160] The modes of the chromatographic separation involve adsorption or normal-

phase,[161-165] reversed–phase,[166-170] ion-exchange,[171-174] ion-pair,[175-179] size-exclusion,[180-183] and affinity[184-188] chromatography. Some practical aspects of these modes are discussed in this section.

1.7.2.1 Adsorption Chromatography

Adsorption chromatography, also known as normal-phase chromatography, is based upon highly polar stationary phases, such as water or triethyleneglycol supported on silica or alumina particles. Solute molecules move down toward an adsorbent bed (or the stationary phase) using a non-polar organic solvent as a mobile phase, such as hexane, heptane, tetrahydrofuran, *i*-propylether, and dichloromethane. The molecules are then retained based on their affinity for the adsorbent surface. Adsorption chromatography is used for separation of fairly polar organic compounds. In adsorption chromatography, the most non-polar component is eluted first since it is the most soluble in the mobile phase. The elution time, however, decreases when increasing the polarity of the mobile phase.[102, 158]

1.7.2.2 Reversed-phase Chromatography

In a reversed-phase chromatography, a non-polar stationary phase, often a hydrocarbon bonded surface, is used in conjugation with a relatively polar mobile phase, such as, water, methanol, and acetonitrile. The most commonly used stationary phase is the bonded hydrocarbon phase, formed by bonding octadecylsilyl groups ($C_{18}H_{37}Si$-). Reversed-phase chromatography is useful for separation of non-polar molecules, which have high affinity for the hydrophobic support. In the reversed-phase chromatography, polar compounds have little affinity to the hydrophobic support and high solubility in the mobile phase. As a result, the most polar molecule is eluted first. This is why this mode is referred to as reversed-phase chromatography. In addition, an increase in polarity of the mobile phase increases the elution time.[102, 158, 189]

1.7.2.3 Ion-exchange Chromatography

The very polar ionic nature of ionic compounds in fully ionized forms can actually generate various difficulties during the separation by either adsorption or reversed-phase chromatography. Alternatively, ion-exchange chromatography is suitable for separation of ionic molecules, such as, amino acids, ionic metabolic products, and organic ions. This is because the stationary phase surface contains fixed ionic charge groups, for example NR_3^+ or SO_3^-, bonded to the support. In addition, an exchangeable counter ion is close by in order to protect charge neutrality. Stationary phase ionic groups are capable of interacting with the ionic groups of sample molecules. Ionic groups of the sample molecules can be paired with the fixed charge, and the sample can not move down the column. The retention of ionic molecules is mostly dependent on their affinity for the fixed charge.

Ion-exchange chromatography can be divided into two major groups, corresponding to strong and weak ion-exchange substances. Strong ion-exchangers have functional groups that are fully ionized, leading to a constant ion-exchange capacity of the stationary phase with an applicable pH range. In the case of weak ion-exchangers, the pH of the solute is very critical because the ion-exchange capacity of ion-exchange materials is significantly dependent upon the degree of variation in the ionization.[160, 190]

1.7.2.4 Ion-pair Chromatography

Ion-pair chromatography can also be used for separation of ionic components and overcome specific problems that may be encountered in ion-exchange chromatography. In the ion-pair method, the sample ionic groups are blocked out by reasonable counter ions. The main advantage of this is that the reversed-phase system can be applied, allowing simultaneous analysis of acids, bases, and neutral products.[158, 190]

1.7.2.5 Size-exclusion Chromatography

Size-exclusion chromatography is used for separation of molecules based on differences in their sizes, or molecular weight. This mode can be divided into gel permeation and gel filtration chromatography. The term gel permeation chromatography is applied to the separation carried out by the use of organic solvents. In contrast, the separation in gel filtration chromatography is achieved using aqueous solutions. In general, size-exclusion chromatography is the best method to select when the multi-component mixture contains compounds with molecular weight difference of at least 10%.[190]

This mode takes place when the pore size of the support, such as agarose, dextran, polystyrene beads, and silica, are arranged in a fashion that can permit some of the solute molecules to enter. Very small molecules usually permeate all the internal pores of the support particle, while very large molecules are unable to enter any of the pores and are totally excluded. For example, the separation of a polymer sample containing mixed molecular weights is based on the molecular weight of the solutes. The largest molecular weight molecules, excluded solutes, are eluted first, followed by the smallest molecular weight molecules which are held back as a result of permeating the particle pores.[158, 190]

1.7.2.6 Affinity Chromatography

In affinity chromatography, the separation is achieved by highly specific biochemical interactions. The stationary phase constitutes of certain groups of molecules that adsorb only the sample if specific steric and charge correlated conditions are gratified. This mode is used for separation of complex biological molecules, such as proteins, enzymes, viruses, lipids, and nucleic acids. In affinity chromatography, a ligand is specifically bound to insoluble support, for example polystyrene beads or silica. Molecules that have an affinity for the bonded group are

retained when the biological mixture is passed down the chromatographic column. These molecules are then eluted by a change of the mobile phase of other components mixture.[158, 190]

1.7.3 Peak Shape in High Performance Liquid Chromatography

The chromatographic peak should theoretically be symmetrical based on the assumption that a single chromatographic peak has a Gaussian distribution.[191] However, peak asymmetry is commonly observed even in the most careful analytical separation. In HPLC analytical applications, it has been noted that the most common causes of peak asymmetry are linked to mixed mechanisms of retention, incompatibility of the sample mobile phase, or development of excessive undesired volume at the column head.[156, 160]

In addition to band asymmetry, band broadening can also be observed in the chromatographic separation and is considered one of the fundamental aspects in the separation science, causing a decrease in the separation efficiency. This phenomenon should be reduced in order to increase the column theoretical plate numbers. Several factors, such as the Eddy diffusion, flow distribution, solute diffusion in the mobile phase, and mass transfer between the mobile and stationary phases, may contribute to peak broadening.

In the Eddy diffusion, the column is packed with small particles of the stationary phase. The mobile phase passes through and transports the sample molecule through the chromatographic column (Figure 1.18). Multiple paths of the sample components are generated through the separation bed, and some molecules leave the column before most of others in a straight line through the chromatographic bed. However, other sample components travel later in different paths along the way. In the case of the flow distribution, the mobile phase moves in a laminar flow between the particles of the stationary phase. This flow will be faster in the center than that which is closer to the particles (Figure 1.19).

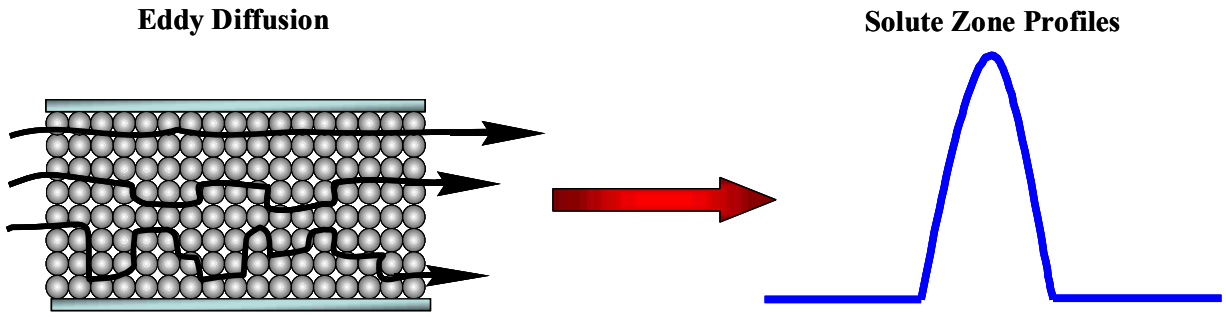

Figure 1.18 Eddy diffusion in the chromatographic column.

The yellow arrows in Figure 1.19 correspond to the mobile phase velocity. The longer is the arrow, the higher the flow velocity. Both the Eddy diffusion and flow distribution can be minimized by packing the column with evenly sized particles.

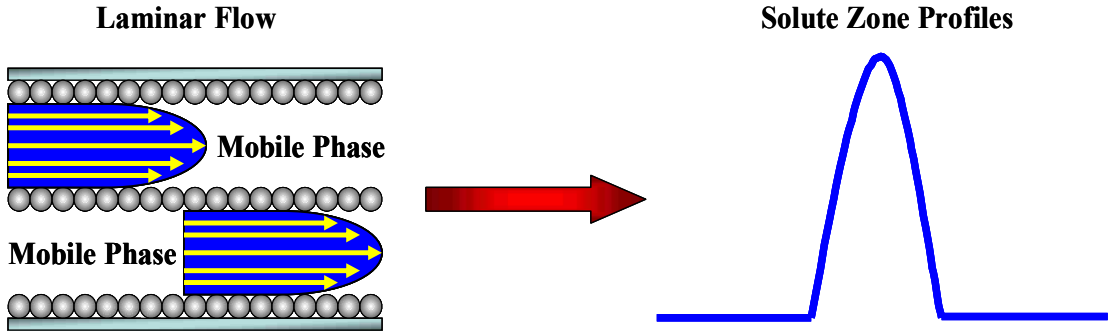

Figure 1.19 Flow distribution in the chromatographic bed.

The third cause of peak broadening is that the sample molecules diffuse in the mobile phase without any external influence, which is known as longitudinal diffusion. The longitudinal diffusion has also undesirable effects on the plate height. These effects can be encountered when small stationary phase particles, slow velocity of the mobile phase related to the particle diameter, or a relatively large diffusion coefficient of the sample is present in the HPLC system.

Finally, the slow mass transfer between phases also contributes to band broadening. The channels in the pore structure of the stationary phase are both narrow and wide (Figure 1.20).

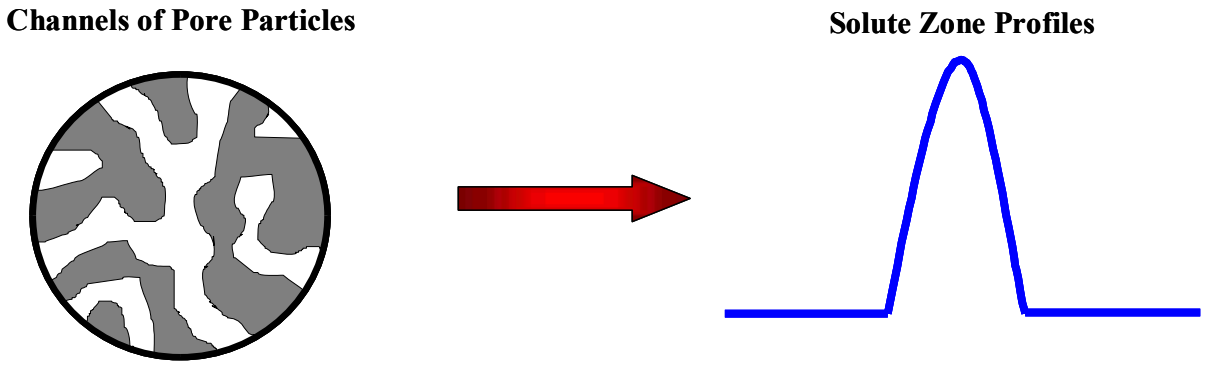

Figure 1.20 The pore structure of stationary phase particles.

Some of the channels pass through the whole particles, while others are closed off. The pores are filled by the mobile phase which does not move. Consequently, the sample molecule, entering the pore, discontinues transporting by the solvent flux and alters its location by diffusion only. This may result in the sample solute diffusing back to the mobile phase taking a long period of time. The sample solute, retained in the pores, slightly passes further. The sample component may also interact with stationary phase and is adsorbed. As a result, the sample component stays to the stationary phase and then moves on once more taking a long period of time. In both cases, peak broadening is increased with increase in the flow velocity of the mobile phase.[160, 190, 192]

1.7.4 Instrumentation of High Performance Liquid Chromatography

The HPLC instrumentation can be set of individual apparatus; however, it can also be designed as a single instrumental component. HPLC instrumental components consist of a solvent reservoir, transfer line with frit, high pressure pump, sample injection device, chromatographic column, detector, and data recorder (Figure 1.21). In the HPLC system, the mobile phase in the solvent reservoir is filtered, degassed, pressurized, and pumped through the column. The pump, which is the heart of the HPLC system, provides the mobility of the mobile phase.

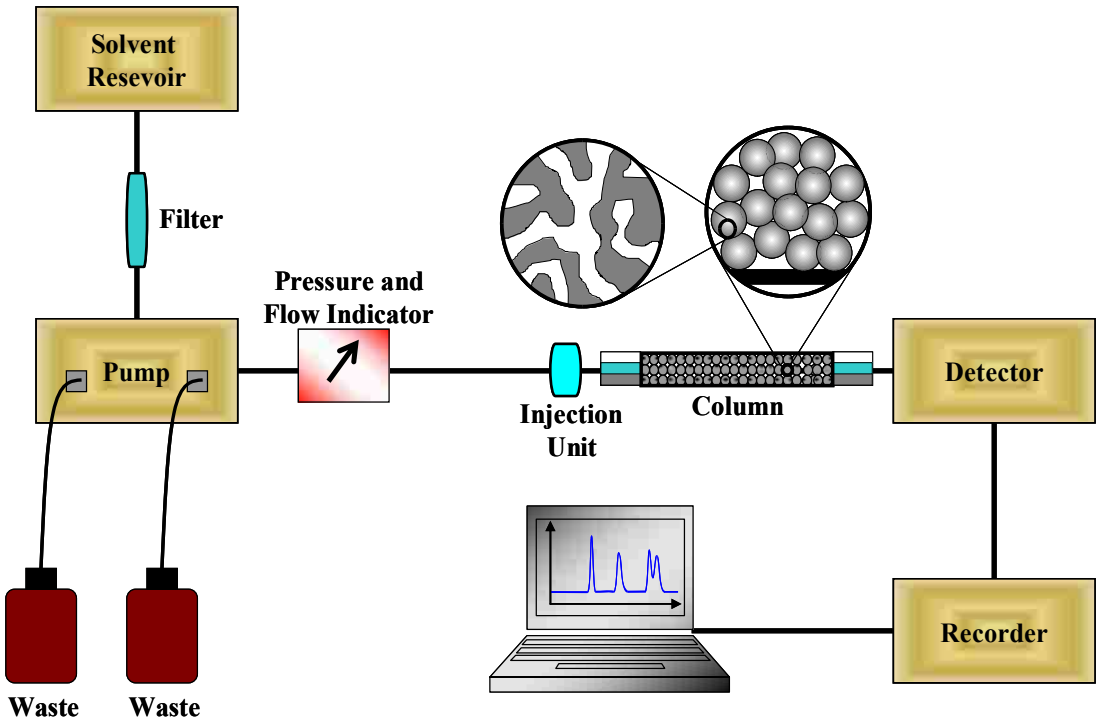

Figure 1.21 Schematic diagram of HPLC instrumentation.

It drives the mobile phase through the chromatographic column at a consistent and robust flow rate (or pressure). A mixture of solutes is introduced, using a sample injection device, to the column head and is then isolated into individual components when it passes down to the column. Even though the chromatographic column is usually small, it is considered to be one of the most important parts. It is usually enclosed in a thermostat for temperature controlled separations. The mixer and controller are both required because it is quite common to operate the separation using more than one solvent. Finally, individual components of the solutes mixture are detected and recorded as chromatographic peaks in the recorder.[156, 158, 190]

Detectors employed in the HPLC system must operate with high precision, sensitivity, and stability and do not significantly affect the chromatographic separation of the column. They should be able to detect 1 part or less in 10^6 of the isolated component and not lead to

interferences of the solute peaks. In addition, HPLC detectors should have a wide linear dynamic range in order to achieve a good quantitative analysis, low level of noise and drift, and rapid response time for recording eluting bands rapidly. They should also be insensitive to flow rate and temperature changes. However, there is no universal HPLC detector, but currently available detectors provide a wide range of applications to be performed. The output of the detectors is an electrical signal that is proportional to some property of either the solute, which is known as solute property detectors, or the solute and the mobile phase (or solvent), which is called bulk property detectors. The solute (or selective) property detectors are, for example, UV-Vis, fluorescence, infrared, electrochemical, conductivity, and atomic absorption detectors. The bulk property detectors are, for example, refractive index, fresnel and interference refractometer, and transport detectors. Other types of detectors are also used to isolate the solute from eluent before detection of the solute, such as liquid chromatography-mass spectrometry detectors.[157, 159] In this section, some practical aspects of frequently used detectors are discussed.

UV-Vis detectors are most frequently used and are one of the solute property detectors. In UV-Vis detectors, the mobile phase coming from the column passes through a small flow cell that is positioned in a path of UV-Vis radiation. These detectors are selective in detecting solutes that absorb in the UV or Vis range, such as alkenes, aromatics, and compounds with multiple bonds between atoms. In a multi-channel or diode array detector, polychromatic radiation travels through the flow cell and the released beam is diffracted by a grating; therefore, it falls on to the photodiodes array. A different narrow wavelength band is received by each photodiode. Thus, this detector can simultaneously detect a single wavelength or a number of wavelengths.

In addition, several compounds are able to absorb UV radiation and emit radiation at a longer wavelength either by fluorescence or phosphorescence (after a time delay). The absorbed

energy fraction that is re-emitted is usually quite low. However, values of 0.1 up to 1.0 can be obtained for some compounds. Such compounds are suited for fluorescence detectors. In fluorescence detectors, a radiation from the excitation source is focused on the flow cell, and interchangeable filter permits different wavelengths of excitation to be applied. Thus, fluorescence can occur and is measured at 90^{o} to the incident radiation. These detectors are selective for compounds with a conjugated cyclic structure, such as PAHs. However, other non-fluorescent compounds can be converted to fluorescent derivatives by fluorescence labeling using some suitable reagents. Electrochemical detectors can measure either the conductance of the solute or the current related to the solute oxidation or reduction. There are also multipurpose detectors, which combine UV, fluorescence, and conductivity detection capabilities. In these detectors, the function of UV is fixed at a 254 nm wavelength. Based on excitation at this wavelength, fluorescence can be monitored at an emission wavelength longer than 280 nm. Using a multipurpose detector, the detection modes can function individually or simultaneously. For example, a linear range of 10^{3} and a noise equivalent to a concentration of 5×10^{-8} gml^{-1} can be obtained in the conductivity mode using sodium chloride (NaCl).

The refractive index detector, a bulk property detector, is considered to be the closest device to a universal detector. This is because any solute can be detected as long as there is a refractive index difference between the solute and the mobile phase. However, these detectors are not as sensitive as UV-Vis detectors. The best noise level that can be obtained is approximately 10^{-7} refractive index unit, corresponding to a noise equivalent concentration of about 10^{-6} g cm^{-3} for most solutes. The linear range of most refractive index detectors is roughly 10^{4}. In addition, these detectors can not be employed when using the gradient elution because the continuous variation in the baseline with change in the solvent mixture causes differences in the

refractive index. In these detectors, the beam is focused on the cell, which contains the sample and reference chambers isolated by a glass diagonal sheet. The radiation is then divided into two portions by a beam splitter and passed into two photocells. The refractive index change of the sample stream will lead to a change in the relative amount of beam falling on the two photocells. The difference is then amplified with an error signal at the amplifier output, which controls a servomotor. This servomotor is able to rotate the beam splitter in order to minimize the error signal to zero. The movement of the beam splitter, which is proportional to the refractive index difference, is measured out by the recorder.[157, 158]

1.8 Scope of Dissertation

The research study presented in this dissertation focused on the investigation of the association behavior between hydrophobic organic compounds (HOC) and dissolved humic materials (DHM) using different analytical methods. The main objective of Chapter 2 was to examine the effect of DHM content on the association behavior with pyrene using steady-state fluorescence spectroscopy. These DHM are Leonardite (or Amherst) humic acid standard, with a high aromatic content, and Suwannee River fulvic acid reference. Stern-Volmer plots were examined to investigate the association behavior of pyrene with DHM. The fluorescence quenching mechanism was further evaluated by studying the effect of temperature on the fluorescence quenching ratio of pyrene in the presence of dissolved humic or fulvic acids. Several parameters that affect the association of pyrene with DHM, including the concentration and polarity of DHM, pH, and ionic strength, were also investigated.

Time-resolved fluorescence lifetime measurements allow for a deeper mechanistic understanding as compared to the traditional steady-state fluorescence technique. However, photobleaching is a problem encountered in fluorescence spectroscopy for biological and

environmental applications. The effect of photobleaching on multi-component systems may result in a change in the fractional intensity contribution and complicate the interpretation of fluorescence lifetime data, particularly for complex systems such as HOC and DHM. In order to address the effect of photobleaching, a new approach to frequency-domain fluorescence lifetime measurements, based on frequency segmentation and recombination, was developed in Chapter 3. This newly developed method was evaluated by simulation of a two component dye system consisting of fluorescein and rhodamine B and comparison of experimental data collected in traditional and segmented fashion. In addition, the frequency segmentation and recombination method was implemented to a more complex system containing pyrene and Suwannee River fulvic acid reference in order to carefully quantify measured fractional intensity contributions and fluorescence lifetimes. In order to further investigate the association behavior of pyrene with DHM, frequency-domain lifetime measurements via frequency segmentation and recombination method was applied to pyrene with different DHM in Chapter 4. In this study, the chemical effect of DHM on the association mechanism with pyrene was investigated. These humic materials involved three commercially available International Humic Substances Society standards (Suwannee River fulvic acid reference, Leonardite humic acid standard, and Florida peat humic acid standard), the peat derived Amherst humic acid, and a chemically bleached Amherst humic acid. In addition, experimental considerations, such as the effect of oxygen, adsorption of pyrene to cell walls, and photobleaching within the pyrene and DHM system, were addressed.

While much time has been spent on investigating the association of metal ions, hydrous oxides, clay minerals, and PAHs with DHM, little is known about the association of chiral compounds with DHM. In our environment, most of these chiral compounds undergo through

transformations by various degradation processes, such as, hydrolysis, photolysis, oxidation, biodegradation. DHM can facilitate the activity of these compounds through soils and waters. Chapter 5 outlines the chemical effect of chiral pesticides (coumachlor, difenacoum, warfarin, and napropamide) in the presence of Leonardite humic acid standard, used as DHM model, by use of steady-state fluorescence spectroscopy. The chiral recognition ability and enantiomeric selectivity of Leonardite humic acid standard were also evaluated with 1-(9-anthryl)-2,2,2-trifluoroethanol and 1,1'-bi-2-naphthol bis (trifluoro - methanesulfonate), used as probes of the interactions, by use of liquid-state ^{19}F NMR spectroscopy. In the ^{19}F NMR study, the interaction of pure enantiomers of these compounds was examined at different concentrations of Leonardite humic acid standard on a day time scale. In addition, the effect of temperature on the kinetics interaction of 1,1'-bi-2-naphthol bis (trifluoro - methanesulfonate) in the absence and presence of Leonardite humic acid standard was investigated. To further investigate the enantioselectivity of Leonardite humic acid standard with chiral compounds, the interaction of *R*- or *S*-1-(9-anthryl)-2,2,2-trifluoroethanol with Leonardite humic acid standard was evaluated for samples monitored in the dark and exposed to light for different time periods by use of HPLC. Chapter 6 summarizes the work contained in this dissertation and highlights future directions to be considered in the investigation of the association behavior of HOC with DHM.

1.9 References

(1) Tipping, E. *Cation binding by humic substances*, First ed.; Cambridge University Press: New York, 2002.

(2) Senesi, N. In *Organic Substances in Soil and Water: Natural Constituents and Their Influence on Contaminant Behavior,* First ed.; Beck, A. J., Jones, K. C., Hayes, M. H. B., Mingelgrin, U., Eds.; Royal Society of Chemistry: Cambridge, UK, 1993, pp 73–101.

(3) Stevenson, F. J. *Humus Chemistry: Genesis, Composition, Reactions*, Second ed.; John Wiley & Sons: New York, 1994.

(4) Hayes, M. H. B. In *Humic Substances in Soils, Peats and Waters Health and Environmental aspects,* First ed.; Hayes, M. H. B., Wilson, W. S., Eds.; The Royal Society of Chemistry: Cambridge, 1997, pp 3-30.

(5) Burdick, E. M. *Econ. Botany* **1965**, *19*, 152-156.

(6) Steelink, C. *Anal. Chem.* **2002**, *74*, 326A-333A.

(7) Hayes, M. H. B.; Graham, C. L. In *Humic Substances: Versatile Components of Plants, Soil and Water.,* First ed.; Ghabbour, E. A., Davies, G., Eds.; Royal Society of Chemistry: Cambridge, UK, 2000, pp 91-109.

(8) MacCarthy, P. In *Humic Substances: Structures, Models and Function,* First ed.; Ghabbour, E. A., Davies, G., Eds.; Royal Society of Chemistry: Cambridge, 2002, pp 19-30.

(9) Hayes, M. H. B. In *Humic Substances: Structures, Properties and Uses,* First ed.; Davies, G., Ghabbour, E. A., Eds.; Royal Society of Chemistry: Cambridge, 1998, pp 1-27.

(10) Tan, K. H. *Humic matter in soil and the environment: principles and controversies*, First ed.; Marcel Dekker: New York, 2003.

(11) Aiken, G. R. In *Humic substances in soil, sediment, and water: geochemistry and isolation,* First ed.; Aiken G. R., McKnight D. M., Wershaw, R. L., MacCarthy, P., Eds.; Wiley-Interscience: New York, 1985, pp 363-385.

(12) Leenheer, J. A. In *Humic Substances in Soil, Sediment and Water,* First ed.; Aiken, G. R., McKnight, D. M., Wershaw, R. L., MacCarthy, P., Eds.; Wiley: New York, 1985, pp 409-429.

(13) Deinzer, M.; Melton, R.; Mitchell, D. *Water Res.* **1975**, *9*, 799-805.

(14) Gaffney, J. S.; Marley, N. A.; Orlandini, K. A. In *Humic and Fulvic Acids. Isolation, Structure, and Environmental Role Materials in the Environment,* First ed.; Gaffney, J. S., Marley, N. A., Eds.; ACS Symposium Series 651, American Chemical Society: Washington, D.C., pp. 96-107, 1996.

(15) Biederbeck, V. O.; Paul, E. A. *Soil Sci.* **1973**, *115*, 357-366.

(16) Haworth, R. D. *Soil Sci.* **1971**, *111*, 71-79.

(17) Schnitzer, M.; Khan, S. U. *Humic Subatances in the Environment*, First ed.; Dekker: New York, 1972.

(18) Schnitzer, M.; Kodama, H.; Ripmeester, J. A. *Soil Sci. Soc. Am. J.* **1991**, *55*, 745-750.

(19) Chefetz, B.; Tarchitzky, J.; Deshmukh, A. P.; Hatcher, P. G.; Chen, Y. *Soil Sci. Soc. Am. J.* **2002**, *66*, 129-141.

(20) Schnitzer, M. In *Humic Substances: Chemistry and Reactions*; Schnitzer, M., Khan, S. U., Eds.; Elsevier: Amsterdam and New York, 1978, pp 1-64.

(21) Orlov, D. S. *Humus acids of soils*, First ed.; Amerind Pub. Co: Washington, 1985.

(22) Leenheer, J. A.; McKnight, D. M.; Thurman, E. M.; MacCarthy, P. In *Humic Substances in the Suwannee River, Georgia: Interactions, Properties, and Proposed Structures*; Averett, R. C., Leenheer, J. A., McKnight, D. M., Thorn, K. A., Eds.; U.S. Geological Survey Open-File Report 87-557: Georgia, 1989, pp 331-359.

(23) Cameron, R. S.; Thornton, B. K.; Swift, R. S.; Posner, A. M. *J. Soil Sci.* **1972**, *23*, 394-408.

(24) Posner, A. M.; Creeth, J. M. *J. Soil Sci.* **1972**, *23*, 333-341.

(25) Bryan, N. D.; Jones, M. N.; Birkett, J.; Livens, F. R. *Anal. Chim. Acta* **2001**, *437*, 281-289.

(26) Cameron, R. S.; Swift, R. S.; Thornton, B. K.; Posner, A. M. *J. Soil Sci.* **1972**, *23*, 342-349.

(27) Reid, P. M.; Wilkinson, A. E.; Tipping, E.; Jones, M. N. *Geochim. Cosmochim. Acta* **1990**, *54*, 131-138.

(28) Guetzloff, T. F.; Rice, J. A. In *Humic and fulvic acids: isolation, structure, and environmental role,* First ed.; Gaffney, J. S., Marley, N. A., Clark, S. B., Eds.; American Chemical Society: ACS Symposium Series, 651. Oxford University Press, NY, 1996, pp 18–25.

(29) Tanford, C. *The Hydrophobic Effect: Formation of Micelles and Biological Membranes*, First ed.; Wiley: New York, 1980.

(30) Popiel, W. *Introduction to Colloid Science*, First ed.; Exposition Press: New York, 1974.

(31) Wershaw, R. L. *Environ. Sci. Technol.* **1993**, *27*, 814-816.

(32) Engebretson, R. R.; von Wandruszka, R. *Environ. Sci. Technol.* **1994**, *28*, 1934-1941.

(33) Yates, L. M., III; Engebretson, R. R.; Haakenson, T. J.; von Wandruszka, R. *Anal. Chim. Acta* **1997**, *356*, 295-300.

(34) Yates, L. M., III; von Wandruszka, R. *Soil Sci. Soc. Am. J.* **1999**, *63*, 1645-1649.

(35) von Wandruszka, R.; Schimpf, M.; Hill, M.; Engebretson, R. *Org. Geochem.* **1999**, *30*, 229-235.

(36) von Wandruszka, R.; Engebretson, R. R.; Yates, L. M., III *Spec. Publ. - R. Soc. Chem.* **1999**, *247*, 79-85.

(37) von Wandruszka, R.; Ragle, C.; Engebretson, R. *Talanta* **1997**, *44*, 805-809.

(38) Ghosh, K.; Schnitzer, M. *Soil Sci.* **1980**, *129*, 266-276.

(39) Piccolo, A.; Conte, P.; Trivellone, E.; van Lagen, B.; Buurman, P. *Environ. Sci. Technol.* **2002**, *36*, 76-84.

(40) Piccolo, A.; Nardi, S.; Concheri, G. *Chemosphere* **1996**, *33*, 595-602.

(41) Piccolo, A.; Nardi, S.; Concheri, G. *Eur. J. Soil Sci.* **1996**, *47*, 319-328.

(42) Conte, P.; Piccolo, A. *Chemosphere* **1998**, *38*, 517-528.

(43) Conte, P.; Piccolo, A. *Environ. Sci. Technol.* **1999**, *33*, 1682-1690.

(44) Piccolo, A.; Conte, P.; Cozzolino, A. *Eur. J. Soil Sci.* **1999**, *50*, 687-692.

(45) Cozzolino, A.; Conte, P.; Piccolo, A. *Soil Biol. Biochem.* **2001**, *33*, 563-571.

(46) Piccolo, A. *Advances in Agronomy* **2002**, *75*, 57-134.

(47) Piccolo, A.; Conte, P.; Spaccini, R.; Chiarella, M. *Biol. Fertil. Soils* **2003**, *37*, 255-259.

(48) Peuravuori, J.; Pihlaja, K. *Environ. Sci. Technol.* **2004**, *38*, 5958-5967.

(49) Sutton, R.; Sposito, G. *Environ. Sci. Technol.* **2005**, *39*, 9009-9015.

(50) Senesi, N. In *Migration and fate of pollutants in soils and subsoils,* First ed.; Petruzzelli, D., Helfferich, F. G., Eds.; NATO-ASI Series: Springer-Verlag, Berlin, 1993, pp 47-74.

(51) Patra, D. *Appl. Spectrosc. Rev.* **2003**, *38*, 155-185.

(52) Menzie, C. A.; Potocki, B. B.; Santodonato, J. *Environ. Sci. Technol.* **1992**, *26*, 1278-1284.

(53) Perminova, I. V.; Grechishcheva, N. Y.; Kovalevskii, D. V.; Kudryavtsev, A. V.; Petrosyan, V. S.; Matorin, D. N. *Environ. Sci. Technol.* **2001**, *35*, 3841-3848.

(54) Black, M. C.; McCarthy, J. F. *Environ. Toxicol. Chem.* **1988**, *7*, 593-600.

(55) Jaffe, R. *Environ. Pollut.* **1991**, *69*, 237-257.

(56) Laor, Y.; Rebhun, M. *Environ. Sci. Technol.* **1997**, *31*, 3558-3564.

(57) Perminova, I. V.; Grechishcheva, N. Y.; Petrosyan, V. S. *Environ. Sci. Technol.* **1999**, *33*, 3781-3787.

(58) Laor, Y.; Rebhun, M. *Environ. Sci. Technol.* **2002**, *36*, 955-961.

(59) Vandecasteele, K.; Gaus, I.; Debreuck, W.; Walraevens, K. *Anal. Chem.* **2000**, *72*, 3093-3101.

(60) El Rassi, Z. *Electrophoresis* **1997**, *18*, 2465-2481.

(61) Jacques, J.; Collet, A.; Wilen, S. H. *Enantiomers, Racemates, and Resolutions*, First ed.; Krieger Pub Co: Malabar, 1991.

(62) Casey, A. F. *Medicinal Chemistry: Stereochemistry and Biological Activity*, Third ed.; Wiley-Interscience: New York, 1980.

(63) Robert Krieger, J. D., Donald Ecobichon, Derek Gammon, Ernest Hodgson, Larry Reiter, and John Ross, *Handbook of Pesticide Toxicology*, Second ed.; Academy Press, 2001.

(64) Maqueda, C.; Morillo, E.; Martin, F.; Undabeytia, T. *J. Environ. Sci. Heal. B* **1993**, *B28*, 655-670.

(65) Khan, S. U. *J. Environ. Sci. Heal. B* **1980**, *B15*, 1071-1090.

(66) Schmitt, P.; Garrison, A. W.; Freitag, D.; Kettrup, A. *J. Chromatogr. A* **1997**, *792*, 419-429.

(67) Desiderio, C.; Palcaro, C. M.; Fanali, S. *Electrophoresis* **1997**, *18*, 227-234.

(68) Gauthier, T. D.; Shane, E. C.; Guerin, W. F.; Seitz, W. R.; Grant, C. L. *Environ. Sci. Technol.* **1986**, *20*, 1162-1166.

(69) Engebretson, R. R.; von Wandruszka, R. *Environ. Sci. Technol.* **1999**, *33*, 4299-4303.

(70) Nielsen, T.; Siigur, K.; Helweg, C.; Jorgensen, O.; Hansen, P. E.; Kirso, U. *Environ. Sci. Technol.* **1997**, *31*, 1102-1108.

(71) Lobbes, J. M.; Fitznar, H. P.; Kattner, G. *Anal. Chem.* **1999**, *71*, 3008-3012.

(72) Luetzhoft, H.-C. H.; Vaes, W. H. J.; Freidig, A. P.; Halling-Sorensen, B.; Hermens, J. L. M. *Environ. Sci. Technol.* **2000**, *34*, 4989-4994.

(73) Backhus, D. A.; Golini, C.; Castellanos, E. *Environ. Sci. Technol.* **2003**, *37*, 4717-4723.

(74) Lou, T.; Xie, H.; Chen, G.; Gagne, J.-P. *Chemosphere* **2006**, *64*, 1204-1211.

(75) Li, A. Z.; Marx, K. A.; Walker, J.; Kaplan, D. L. *Environ. Sci. Technol.* **1997**, *31*, 584-589.

(76) Chin, Y.-P.; Aiken, G. R.; Danielsen, K. M. *Environ. Sci. Technol.* **1997**, *31*, 1630-1635.

(77) Johnson-Logan, L. R.; Broshears, R. E.; Klaine, S. J. *Environ. Sci. Technol.* **1992**, *26*, 2234-2239.

(78) Chiou, C. T.; Kile, D. E.; Brinton, T. I.; Malcolm, R. L.; Leenheer, J. A.; MacCarthy, P. *Environ. Sci. Technol.* **1987**, *21*, 1231-1234.

(79) Kumke, M. U.; Frimmel, F. H.; Ariese, F.; Gooijer, C. *Environ. Sci. Technol.* **2000**, *34*, 3818-3823.

(80) Puchalski, M. M.; Morra, M. J.; Von Wandruszka, R. *Environ. Sci. Technol.* **1992**, *26*, 1787-1792.

(81) Kukkonen, J.; Pellinen, J. *Sci. Total Environ.* **1994**, *152*, 19-29.

(82) Murphy, E. M.; Zachara, J. M.; Smith, S. C. *Environ. Sci. Technol.* **1990**, *24*, 1507-1516.

(83) Gu, B.; Schmitt, J.; Chen, Z.; Liang, L.; McCarthy, J. F. *Environ. Sci. Technol.* **1994**, *28*, 38-46.

(84) Danielsen, K. M.; Chin, Y.-P.; Buterbaugh, J. S.; Gustafson, T. L.; Traina, S. J. *Environ. Sci. Technol.* **1995**, *29*, 2162-2165.

(85) Tiller, C. L.; Jones, K. D. *Environ. Sci. Technol.* **1997**, *31*, 424-429.

(86) Chen, S.; Inskeep, W. P.; Williams, S. A.; Callis, P. R. *Environ. Sci. Technol.* **1994**, *28*, 1582-1588.

(87) Holbrook, R. D.; Love, N. G.; Novak, J. T. *Environ. Sci. Technol.* **2004**, *38*, 4987-4994.

(88) Backhus, D. A.; Gschwend, P. M. *Environ. Sci. Technol.* **1990**, *24*, 1214-1223.

(89) Schlautman, M. A.; Morgan, J. J. *Environ. Sci. Technol.* **1993**, *27*, 2523-2532.

(90) Herbert, B. E.; Bertsch, P. M.; Novak, J. M. *Environ. Sci. Technol.* **1993**, *27*, 398-403.

(91) Xing, B.; Pignatello, J. J.; Gigliotti, B. *Environ. Sci. Technol.* **1996**, *30*, 2432-2440.

(92) Weber, W. J., Jr.; Huang, W. *Environ. Sci. Technol.* **1996**, *30*, 881-888.

(93) Huang, W.; Young, T. M.; Schlautman, M. A.; Yu, H.; Weber, W. J., Jr. *Environ. Sci. Technol.* **1997**, *31*, 1703-1710.

(94) Huang, W.; Weber, W. J., Jr. *Environ. Sci. Technol.* **1997**, *31*, 2562-2569.

(95) Xing, B.; Pignatello, J. J. *Environ. Sci. Technol.* **1997**, *31*, 792-799.

(96) Graber, E. R.; Borisover, M. D. *Environ. Sci. Technol.* **1998**, *32*, 3286-3292.

(97) Drewes, J. E.; Croue, J. P. *Water Sci. Technol.: Water Supply* **2002**, *2*, 1-10.

(98) Chiou, C. T.; McGroddy, S. E.; Kile, D. E. *Environ. Sci. Technol.* **1998**, *32*, 264-269.

(99) Chefetz, B.; Deshmukh, A. P.; Hatcher, P. G.; Guthrie, E. A. *Environ. Sci. Technol.* **2000**, *34*, 2925-2930.

(100) Hu, W.-G.; Mao, J.; Xing, B.; Schmidt-Rohr, K. *Environ. Sci. Technol.* **2000**, *34*, 530-534.

(101) Wang, K.; Xing, B. *J. Environ. Qual.* **2005**, *34*, 342-349.

(102) Skoog, D. A., Leary, James J. *Principles of Instrumental Analysis*, Forth ed.; Harcourt Brace and Company: Orlando, 1992.

(103) Ingle, J. D.; Crouch, S. R. *Spectrochemical Analysis*, First ed.; Prentice-Hall, Inc.: Upper Saddle River, 1988.

(104) Chin, Y.-P.; Aiken, G.; O'Loughlin, E. *Environ. Sci. Technol.* **1994**, *28*, 1853-1858.

(105) Lakowicz, J. R. *Principles of Fluorescence Spectroscopy*, Second ed.; Kluwer Academic/Plenum Press: New York, 1999.

(106) McGown, L. B.; Nithipatikom, K. *Appl. Spectrosc. Rev.* **2000**, *35*, 353-393.

(107) Harris, D. C. *Quantitative Chemical Analysis*, Fifth ed.; W H Freeman & Co., 1998.

(108) Valeur, B. *Molecular Fluorescence: Principles and Applications*, First ed.; Wiley-VCH: Weinheirn, 2001.

(109) Sharma, A., Schulman, Stephen G. *Introduction to Fluorescence Spectroscopy*, First ed.; John Wiley and Sons, Inc.: New York, 1999.

(110) Fery-Forgues, S.; Lavabre, D. *J. Chem. Educ.* **1999**, *76*, 1260-1264.

(111) Wilkinson, F. *Pure Appl. Chem.* **1997**, *69*, 851-856.

(112) Lakowicz, J. R.; Weber, G. *Biochemistry* **1973**, *12*, 4161-4170.

(113) Wehry, E. L.; Rogers, L. B. In *Fluorescence and Phosphorescence Analysis,* First ed.; Hercules, D. M., Ed.; Wiley-Interscience: New York, 1966, pp 81-150.

(114) Richter-Egger, D. L.; Tesfai, A.; Tucker, S. A. *Anal. Chem.* **2001**, *73*, 5743-5751.

(115) Fletcher, K. A.; Storey, I. A.; Hendricks, A. E.; Pandey, S.; Pandey, S. *Green Chemistry* **2001**, *3*, 210-215.

(116) Fletcher, K. A.; Pandey, S. *Appl. Spectrosc.* **2002**, *56*, 1498-1503.

(117) Fletcher, K. A.; Pandey, S. *J. Phys. Chem. B* **2003**, *107*, 13532-13539.

(118) Tedeschi, C.; Moehwald, H.; Kirstein, S. *J. Am. Chem. Soc.* **2001**, *123*, 954-960.

(119) Dong, D. C.; Winnik, M. A. *Can. J. Chem.* **1984**, *62*, 2560-2565.

(120) Dong, D. C.; Winnik, M. A. *Photochem. Photobiol.* **1982**, *35*, 17-21.

(121) Kalyanasundaram, K.; Thomas, J. K. *J. Am. Chem. Soc.* **1977**, *99*, 2039-2044.

(122) Chen, S. H.; McGuffin, V. L. *Appl. Spectrosc.* **1994**, *48*, 596-603.

(123) Waris, R.; Acree, W. E., Jr.; Street, K. W., Jr. *Analyst* **1988**, *113*, 1465-1467.

(124) Waris, R.; Rembert, M. A.; Sellers, D. M.; Acree, W. E., Jr.; Street, K. W., Jr.; Fetzer, J. C. *Analyst* **1989**, *114*, 195-199.

(125) Liu, G.-D.; Liao, J.-P.; Huang, S.-S.; Shen, G.-L.; Yu, R.-Q. *Anal. Sci.* **2001**, *17*, 1031-1036.

(126) Sukul, D.; Sen, S.; Dutta, P.; Bhattacharyya, K. *Proc. - Indian Acad. Sci., Chem. Sci.* **2002**, *114*, 501-511.

(127) Coolidge, C. L.; Ryan, D. K. *Spec. Publ. - R. Soc. Chem.* **2000**, *259*, 205-214.

(128) Ganaye, V. A.; Keiding, K.; Viriot, M.-L.; Vogel, T. M.; Block, J.-C. *Environ. Sci. Technol.* **1997**, *31*, 2701-2706.

(129) Shane, E. C.; Price-Everett, M.; Hanson, T. *J. Chem. Educ.* **2000**, *77*, 1617-1618.

(130) Mackenzie, K.; Georgi, A.; Kumke, M.; Kopinke, F.-D. *Environ. Sci. Technol.* **2002**, *36*, 4403-4409.

(131) O'Connor, D. V.; Phillips, D. *Time Correlated Single Photon Counting*, First ed.; Academic Press: New York, 1984.

(132) Shaver, J. M.; McGown, L. B. *Anal. Chem.* **1996**, *68*, 9-17.

(133) Shaver, J. M.; McGown, L. B. *Anal. Chem.* **1996**, *68*, 611-620.

(134) Ware, W. R.; Doemeny, L. J.; Nemzek, T. L. *J. Phys. Chem.* **1973**, *77*, 2038-2048.

(135) Grinvald, A.; Steinberg, I. Z. *Anal. Biochem.* **1974**, *59*, 583-598.

(136) Straume, M.; Frasier-Cadoret, S. G.; Johnson, M. L. *Topics in Fluorescence Spectroscopy* **1991**, *2*, 177-240.

(137) Isenberg, I.; Dyson, R. D.; Hanson, R. *Biophys. J.* **1973**, *13*, 1090-1115.

(138) Small, E. W.; Isenberg, I. *Biopolymers* **1976**, *15*, 1093-1101.

(139) Small, E. W.; Isenberg, I. *J. Chem. Phys.* **1977**, *66*, 3347-3351.

(140) Gafni, A.; Modlin, R. L.; Brand, L. *Biophys. J.* **1975**, *15*, 263-280.

(141) Ameloot, M.; Hendrickx, H. *Biophys. J.* **1983**, *44*, 27-38.

(142) Ameloot, M.; Beechem, J. M.; Brand, L. *Biophys Chem* **1986**, *23*, 155-171.

(143) Livesey, A. K.; Brochon, J. C. *Biophys. J.* **1987**, *52*, 693-706.

(144) Kinkennon, A. E.; McGown, L. B. *J. Fluoresc.* **1997**, *7*, 201-210.

(145) Love, J. C.; Demas, J. N. *Rev. Sci. Instrum.* **1983**, *54*, 1787-1789.

(146) Carraway, E. R.; Hauenstein, B. L., Jr.; Demas, J. N.; DeGraff, B. A. *Anal. Chem.* **1985**, *57*, 2304-2308.

(147) Knutson, J. R.; Beechem, J. M.; Brand, L. *Chem. Phys. Lett.* **1983**, *102*, 501-507.

(148) Beechem, J. M.; Gratton, E. *Proc. SPIE-Int. Soc. Opt. Eng.* **1988**, *909*, 70-81.

(149) Beechem, J. M. *Chem. Phys. Lipids* **1989**, *50*, 237-251.

(150) He, Y.; Geng, L. *Anal. Chem.* **2001**, *73*, 5564-5575.

(151) Popov, A. I.; Hallenga, K. *Modern NMR Techniques and Their Application in Chemistry*, First ed.; Marcel Dekker, Inc.: New York, 1990.

(152) Akitt, J. W. *NMR and Chemistry: an introduction to modern NMR spectroscopy*, Third ed.; Chapman & Hall: New York, 1992.

(153) Bruch, M. D. *NMR spectroscopy techniques*, Second ed.; M. Dekker: New York, 1996.

(154) Günther, H. *NMR spectroscopy: an introduction*, First ed.; John Wiley & Sons Ltd: New York, 1980.

(155) Mooney, E. F. *An introduction to ^{19}F NMR spectroscopy*, First ed.; Sadtler Research Laboratories: Philadelphia, 1970.

(156) Lough, W. J.; Wainer, I. W. *High Performance Liquid Chromatography*, First ed.; Chapman & Hall Ltd.: London, 1996.

(157) Lindsay, S. *High Performance Liquid Chromatography*, First ed.; John Wiley & Sons: New York, 1987.

(158) Pryde, A.; Gilbert, M. T. *Applications of High Performance Liquid Chromatography*, First ed.; Chapman & Hall Ltd.: London, 1979.

(159) Gilbert, M. T. *High Performance Liquid Chromatography*, First ed.; IOP Publishing Ltd.: Bristol, 1987.

(160) Szepesi, G. *How to Use Reverse-Phase HPLC*, First ed.; VCH Publishers, Inc.: New York, 1992.

(161) Abbott, S. R. *J. Chromatogr. Sci.* **1980**, *18*, 540-550.

(162) Towbin, H.; Schoenenberger, C. A.; Braun, D. G.; Rosenfelder, G. *Anal. Biochem.* **1988**, *173*, 1-9.

(163) Hara, M.; Takiguchi, T.; Ashizawa, T.; Gomi, K.; Nakano, H. *J. Antibiot.* **1991**, *44*, 33-39.

(164) Ysambertt, F.; Marquez, N.; Rangel, B.; Bauza, R.; De La Cruz, C. *Sep. Sci. Technol.* **1995**, *30*, 2539-2550.

(165) Pillion, D. J.; Amsden, J. A.; Kensil, C. R.; Recchia, J. *J. Pharm. Sci.* **1996**, *85*, 518-524.

(166) Fetsch, J.; Eckart, K.; Maurer, H. R. *Eur. J. Biochem.* **1990**, *191*, 445-448.

(167) Gagliardi, D.; Penin, F.; Gautheron, D. C. *Biochim. Biophys. Acta* **1991**, *1059*, 323-331.

(168) Sluzky, V.; Shahrokh, Z.; Stratton, P.; Eberlein, G.; Wang, Y. J. *Pharm. Res.* **1994**, *11*, 485-490.

(169) Minkler, P. E.; Ingalls, S. T.; Hoppel, C. L. *Anal. Chem.* **2005**, *77*, 1448-1457.

(170) Zhang, X.; Wang, M.; Cheng, J. *Anal. Chem.* **1988**, *60*, 1670-1673.

(171) Mehta, P.; Zingde, S.; Advani, S.; Desai, H.; Gothoskar, B. *Mol. Cell. Biochem.* **1995**, *144*, 153-165.

(172) Sekar, M. C.; Scott, E. D.; Sambandam, V.; Berry, R. E. *Biochem. Mol. Med.* **1997**, *62*, 95-100.

(173) Smith, R. E. *Chromatogr. Sci. Ser.* **1998**, *78*, 365-411.

(174) Atanassova, A.; Lam, R.; Zamble, D. B. *Anal. Biochem.* **2004**, *335*, 103-111.

(175) Jost, W.; Spatz, R.; Ditz, R.; Eisenbeiss, F. *LaborPraxis* **1984**, *8*, 1016, 1019-1022.

(176) Jost, W.; Spatz, R.; Dietz, R.; Eisenbeiss, F. *LaborPraxis* **1984**, *8*, 1184-1188.

(177) Cichna, M.; Daxecker, H.; Raab, M. *Anal. Chim. Acta* **2003**, *481*, 245-253.

(178) Fritz, J. S. *J. Chromatogr. A* **2005**, *1085*, 8-17.

(179) Giovannelli, D.; Abballe, F. *J. Chromatogr. A* **2005**, *1085*, 86-90.

(180) Dauwe, C.; Reinhold, G. *LaborPraxis* **2001**, *25*, 66,68,70,73.

(181) Her, N.; Amy, G.; Foss, D.; Cho, J.; Yoon, Y.; Kosenka, P. *Environ. Sci. Technol.* **2002**, *36*, 1069-1076.

(182) Matsunaga, H.; Fu, Q.; Haginaka, J. *Anal. Sci.* **2002**, *18*, 27-30.

(183) Luykx, D. M. A. M.; Goerdayal, S. S.; Dingemanse, P. J.; Jiskoot, W.; Jongen, P. M. J. M. *J. Chromatogr. B* **2005**, *821*, 45-52.

(184) Bedair, M.; El Rassi, Z. *J. Chromatogr. A* **2005**, *1079*, 236-245.

(185) Li, R.; Jiang, F.; Zhang, X.; Chen, Y.; Fang, L. *J. Chromatogr. B* **2006**, *840*, 63-68.

(186) Puerta, A.; Vidal-Madjar, C.; Jaulmes, A.; Diez-Masa, J.-C.; De Frutos, M. *J. Chromatogr. A* **2006**, *1119*, 34-42.

(187) Besanger, T. R.; Hodgson, R. J.; Guillon, D.; Brennan, J. D. *Anal. Chim. Acta* **2006**, *561*, 107-118.

(188) Ohnmacht, C. M.; Chen, S.; Tong, Z.; Hage, D. S. *J. Chromatogr. B* **2006**, *836*, 83-91.

(189) Krstulovic, A. M.; Brown, P. R. *Reversed-Phase High-Performonce Liquid Chromatography: Theory, Practice and Biomedical Applications*, First ed.; John Wiley & Sons Inc.: New York, 1982.

(190) Meyer, V. R. *Practical High-Performance Liquid Chromatography*, Fourth ed.; John Wiley & Sons Inc.: Hoboken, 2004.

(191) Miller, J. M. *Chromatography: Concepts and Contrasts*, First ed.; Wiley-Interscience: New York, 1988.

(192) van Deemter, J. J.; Zuiderweg, F. J.; Klinkenberg, A. *Chem. Eng. Sci.* **1995**, *50*, 3869-3882.

CHAPTER 2

CHARACTERIZATION OF PYRENE ASSOCIATION BEHAVIOR WITH DISSOLVED HUMIC MATERIALS USING STEADY-STATE FLUORESCENCE SPECTROSCOPY

2.1 Introduction

Dissolved humic materials (DHM), found in subsurface and surface waters and in sedimentary porewaters, are major components in determining the transport and fate of polycyclic aromatic hydrocarbons (PAHs).[1, 2] DHM may facilitate the transport of these contaminants, and the association of PAHs with humic materials (HM) can cause an increase in the contaminants mobility and a decrease in their toxicity and bioavailability.[2-5] However, this association is constrained by a variety of solution conditions, including pH, ionic strength, temperature, and nature and concentration of HM.[6] Currently, the structural conformation of HM is best described from a polymer or supramolecular assemble point of view. In recent years, there has been a large focus on the sorption mechanism of hydrophobic organic compounds (HOC) to HM, and a series of proposed models has been investigated.[7-16] None of these models has been universally accepted, as exemplified by the "glassy/rubber" (hard/soft or condensed/non-condensed) model, and the vigorous discussion on this model that has taken place in the literature. But, one point that was almost universally agreed upon was that aromatic domains within HM are the association sites for HOC.[3, 4, 17-22]

However, based on the recent work of Chefetz et al.,[8] Hu et al.,[23] and Wang and Xing,[24] this point of view has come under question and aliphatic domains within HM have been implied in the sorption of HOC. Thus, the seemingly simple question of whether HOC interact with aliphatic, aromatic, or both is still open. The reason is that a large number of sorption studies have relied on sorption isotherms built on macroscopic mass balanced data and then relating this data to bulk ^{13}C nuclear magnetic resonance (NMR) characterization of the HM being

investigated. Such an approach does not allow for an intimate investigation of the local sorption domain.

Fluorescence spectroscopy is widely used for the analysis and investigation of the association mechanism of PAHs with DHM because it has high sensitivity and eliminates the need for sample pretreatments before measurements.[25-27] Further, fluorescence quenching is the most common method for determining the association constant of PAHs associated with DHM.[22, 27-29] However, there is a discussion in the literature concerning the fluorescence quenching mechanism of PAHs with HM. Generally, a static quenching has been assumed for PAHs with HM,[1, 30-38] while a dynamic quenching has also been implied by other studies.[21, 22, 26, 27, 29] Consequently, the question of whether complete or incomplete fluorescence quenching of PAHs with HM is still open. Thus, fluorescence quantum yields of bound PAHs have been considered in order to answer this question. Some studies have indicated that complete fluorescence quenching (static) takes place when the fluorescence quantum yield of the fluorophore in the presence of DHM approaches zero.[31, 32, 39, 40] However, Schlautman and Morgan[31] and Backhus and Gschwend[32] have observed that full fluorescence quenching is not necessarily correct for all quenchers. Backhus et al.[38] concluded that complete fluorescence quenching did not occur for all samples for perylene with Wetland colloidal organic carbon. In addition, Holbrook et al.[21] indicated that quantum yield values were greater than zero for pyrene with colloidal organic carbon.

The polarity effect of HM on the sorption behavior has also been investigated. Some approaches have indicated that the polarity of HM is positively[37, 41] or negatively[42-44] correlated to the sorption mechanism of HOC to HM. Pyrene is one of the most common fluorescent probes of polarity in organized media.[45-47] Concerning the molecular environment of pyrene, the

vibronic band intensities of fluorescence emission spectra are influenced by the polarity of the solvent.[37] This non-covalent dipole moment interaction between solvent molecule and the excited pyrene is known as the Ham effect.[48, 49] Thus, fluorescence spectra of pyrene can provide information about the polarity in DHM.

In this study, fluorescence spectroscopy was applied to examine the effect of DHM content on the association with pyrene, a common PAHs probe. The fluorescence of pyrene with dissolved humic and fulvic acids was examined at different concentrations of DHM, and Stern-Volmer plots were evaluated after correcting the measured fluorescence intensities for inner-filter effects. In addition, effects of temperature on fluorescence quenching ratios of pyrene with DHM were investigated to further evaluate the quenching mechanism of pyrene with DHM.

2.2 Experimental

2.2.1 Materials and Reagents

Amherst humic acid (AHA), a classical humic acid fraction, was a gift from professor Baoshan Xing, Department of Plant and Soil Sciences, University of Massachusetts (Amherst, MA). Leonardite humic acid standard (LHAS) and Suwannee River fulvic acid reference (SRFAR) were purchased from the International Humic Substances Society (IHSS), Department of Soil, Water, and Climate, University of Minnesota (St. Paul, MN). Pyrene (≥ 99%) was obtained from Sigma-Aldrich (Milwaukee, WI). Monobasic sodium phosphate (NaH_2PO_4), dibasic sodium phosphate (Na_2HPO_4), sodium chloride (NaCl), calcium chloride ($CaCl_2$), and sodium hydroxide (NaOH) were purchased from Fisher Scientific (Fair Lawn, NJ).

2.2.2 Sample Preparation

A stock solution of LHAS (or AHA) was prepared in 18.2 MΩ·cm distilled deionized water by first dissolving an appropriate amount of the LHAS (or AHA) solution with the aide of

a few drops of 0.1 M NaOH and then immediately upon dissolution neutralizing the solution with 0.1 M HCl. The SRFAR stock solution was also prepared in the same manner as well as LHAS and AHA but without addition of NaOH. The pyrene stock solution was prepared in ethanol. All stock solutions were stored in the dark at 4 °C. For the pyrene with DHM association study, standard solutions of 0.02 ppm pyrene, below the water solubility limit, were prepared by adding appropriate amounts of pyrene stock solution, evaporating ethanol to dryness with nitrogen gas (N_2), and followed up by adding appropriate amounts of DHM stock solution. A total of seven standard solutions were prepared in that manner in 18.2 MΩ·cm distilled deionized water. Such that DHM concentrations were 0, 4, 6, 8, 10, 12, and 16 ppm DHM and pyrene concentration remained constant at 0.02 ppm. In addition, standard reference solutions of DHM (4, 6, 8, 10, 12, and 16 ppm) were prepared under the same experimental conditions of the pyrene DHM solutions. All standard solutions were made in triplicates and adjusted to pH 4.0 with buffered aqueous solutions (1 mM NaH_2PO_4 and 1 mM Na_2HPO_4) to enhance the pyrene association with DHM. Solutions were also allowed to equilibrate in the dark for seven days.

For the ionic strength study, a stock solution of 0.1 M NaCl (or $CaCl_2$) was used to prepare a series of samples. The NaCl (or $CaCl_2$) aqueous standard solutions, with 0.02 ppm pyrene or with pyrene (0.02 ppm) and 6 ppm LHAS (or SRFAR) mixture, were also prepared and adjusted to pH 4.0 as described above to obtain final concentrations of 0.001, 0.01, 0.02, and 0.03 M NaCl (or $CaCl_2$). As in the pyrene association study, all standard solutions were purged with N_2 prior to fluorescence measurements. Fluorescence cell was rinsed three times with a fresh solution prior to the measurements to decrease the losses of pyrene to the quartz cell wall. Absorbance measurements required for inner-filter effect corrections were obtained directly following the fluorescence measurements using the same standard reference solutions.

2.2.3 Instrumentation

Steady-state fluorescence measurements were acquired in triplicate using a Spex Fluorolog-3 spectrofluorimeter (model FL3-22TAU3; Jobin Yvon, Edison, NJ, USA) equipped with a 450-W xenon lamp and R928P photomultiplier tube (PMT) detector. The excitation and emission spectra of pyrene were collected in a 10 mm quartz fluorescence cuvette with slit widths set for entrance and exit bandwidths of 4.0 and 1.5 nm on both excitation and emission monochromators, respectively. The excitation and emission wavelengths of pyrene were 333 nm and 370 nm, respectively. All fluorescence spectra were blank subtracted before proceeding with data analysis. Absorbance measurements were also performed in triplicate using a UV-3101PC (UV-Vis-NIR) scanning spectrophotometer (Shimadzu, Columbia, MD). Absorption spectra were recorded using 10 mm quartz cuvette.

2.3 Results and Discussion

2.3.1 Pyrene Association with DHM

Pyrene fluorescence emission spectra in the presence of DHM were monitored up to 600 nm, and no indications of the pyrene excimer emission were observed after subtraction from the total fluorescence intensities of pyrene with DHM. Figure 2.1 illustrates fluorescence emission spectra of pyrene in the absence and presence of LHAS, AHA, or SRFAR, respectively. As shown in Figure 2.1, pyrene fluorescence intensities decreased when increasing LHAS, AHA, or SRFAR concentration. However, more significant reduction was observed in the fluorescence intensity of pyrene with LHAS (or AHA), as shown in Figures 2.1a_1 and b_1, in contrast to that of pyrene with SRFAR (Figure 2.1c_1). Fluorescence intensities of pyrene in the absence and presence of LHAS, AHA, or SRFAR (16 ppm) were normalized as shown in Figures 2.1a_2, b_2, and c_2, respectively.

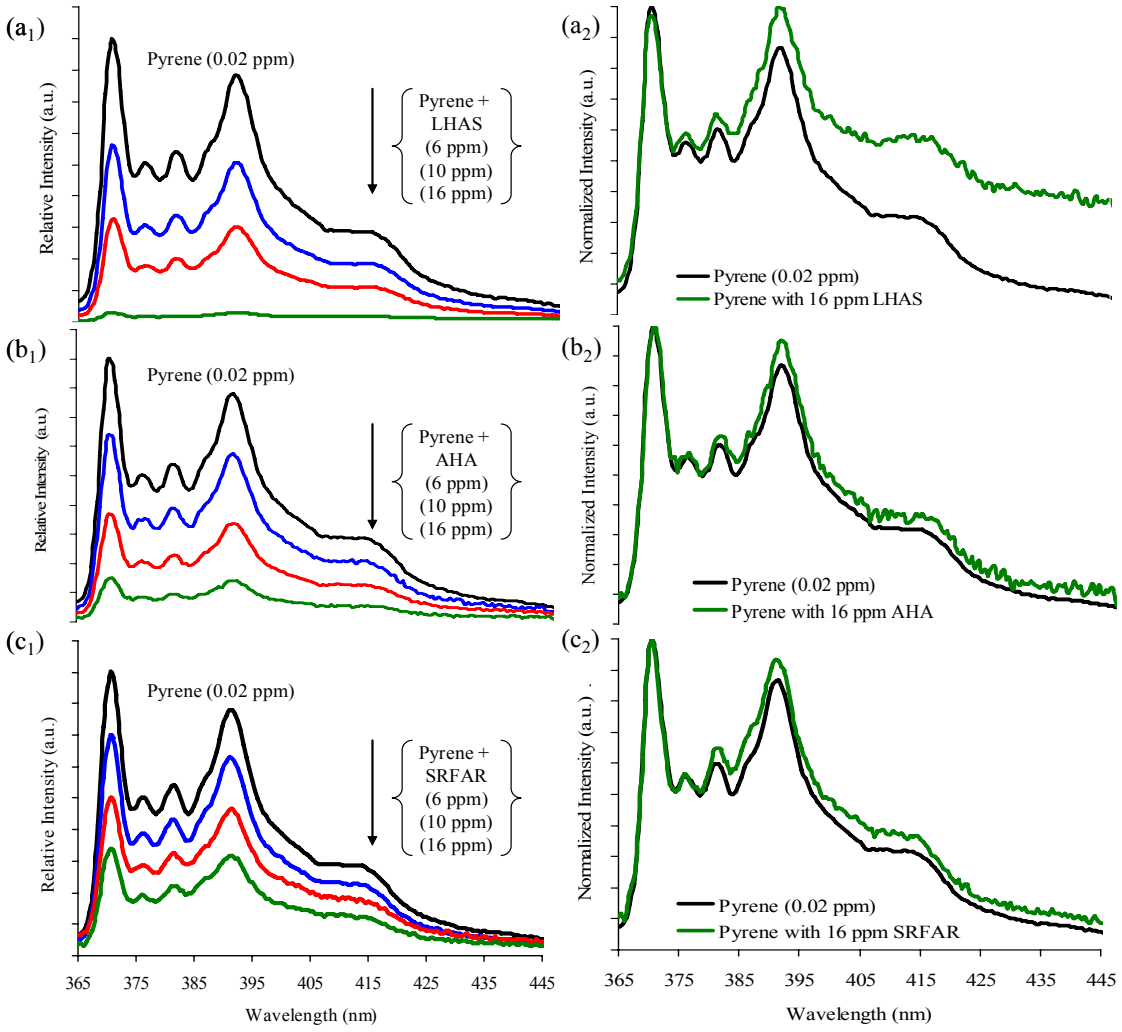

Figure 2.1 Fluorescence emission spectra of 0.02 ppm pyrene in the absence and presence of (a) LHAS, (b) AHA, or (c) SRFAR at pH 4.

A close examination of Figure 2.1 reveals that all fluorescence emissions peaks of pyrene in the presence of DHM showed marked shifts compared to those in buffer alone. This may likely be attributed to the association of pyrene with DHM.

In this study, the polarity ratio (I_1/I_3) of pyrene is shown to slightly decrease at lower concentrations of DHM (Figure 2.2). However, little or no change in the (I_1/I_3) of pyrene was observed at high concentrations of DHM.

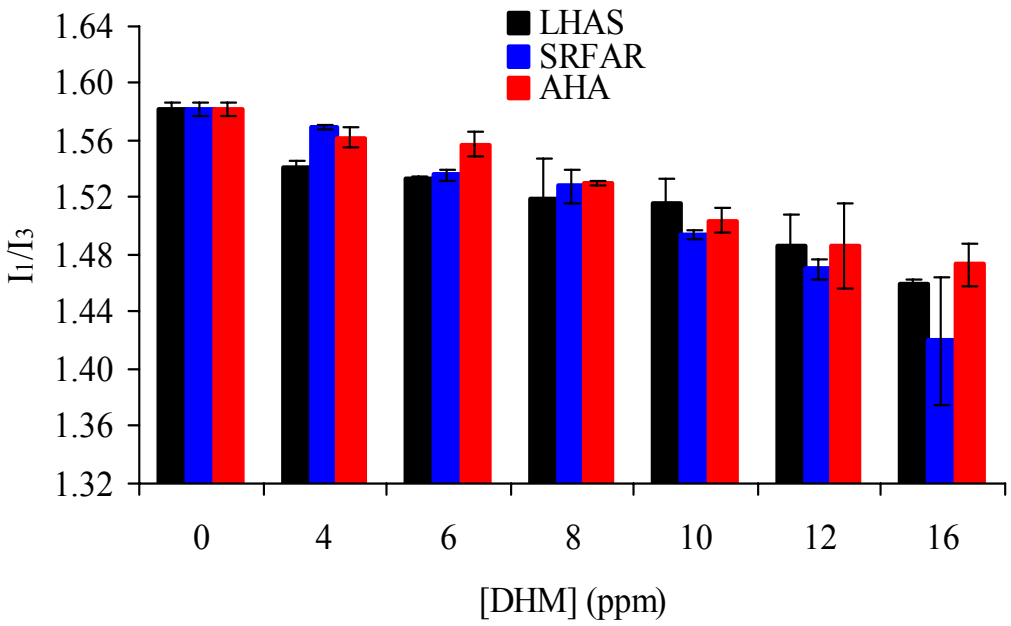

Figure 2.2 Effect of DHM concentration on the pyrene (I_1/I_3) at pH 4.

This indicates that pyrene molecules are associated more within the hydrophobic domain of DHM, and the measured pyrene (I_1/I_3) can likely be attributed to pyrene in water. Ganaye et al. [42] have shown similar findings and concluded that the quenching mechanism of pyrene with natural organic matter is not due to complete fluorescence quenching to a dark complex.

2.3.2 Quenching Mechanism of Pyrene with DHM

There was a fluctuation in the observed fluorescence intensities due to the inner-filter effect. This phenomenon can easily interfere with the measured fluorescence intensity of pyrene in the presence of DHM. The inner-filter effect occurs particularly at higher concentrations of DHM because they usually absorb light at both excitation and emission regions of pyrene. Consequently, using the molecular environment of pyrene to evaluate its association behavior with DHM is intricate due to the inner-filter effect. In this study, corrections of the measured

fluorescence intensities for primary and secondary inner-filter effects were determined using equation 1.16 in Chapter 1 of this dissertation.

The resulted Stern-Volmer plots of F_o/F versus [DHM] were examined after correcting the measured fluorescence intensities for inner-filter effects (Figure 2.3). The principles of the Stern-Volmer equation have been fully described in Chapter 1 of this dissertation. A close examination of Figure 2.3 shows that pyrene quenching in the presence of LHAS was the most efficient as compared to that of pyrene in the presence of AHA (or SRFAR).

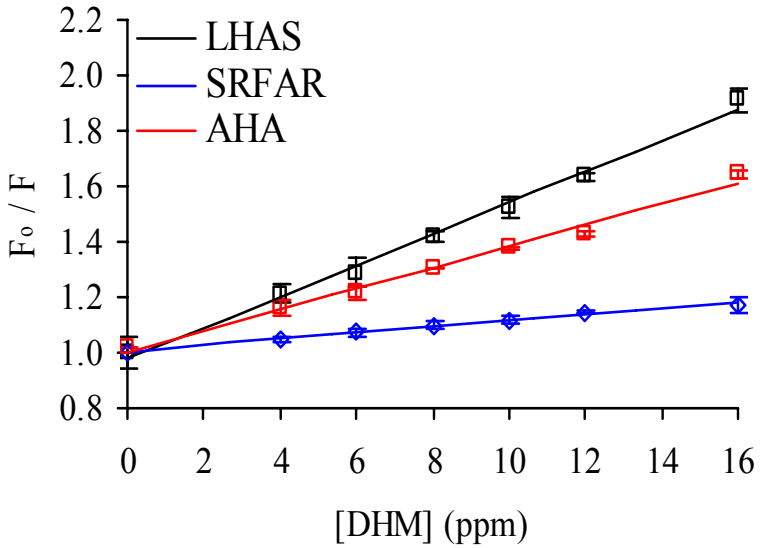

Figure 2.3 Stern-Volmer plots of 0.02 ppm pyrene with DHM at pH 4.

In addition, this indicates that fluorescence quenching efficiencies are affected by DHM content. LHAS has the highest aromatic content in contrast to AHA and SRAFR. It can also be noted from Figure 2.3 that a more reasonable linear relationship was obtained for pyrene in the presence of SRFAR as compared to that with LHAS (or AHA). This showed that the quenching mechanism of pyrene with SRFAR to be either static or dynamic quenching. Linear Stern-Volmer plots usually indicate that the quenching mechanism of the fluorophore is either static or

dynamic quenching.[50] However, an upward curvature was observed in the Stern-Volmer plot for pyrene in the presence of LHAS (or AHA), which is indicative to the contribution of both static and dynamic quenching to the association behavior of pyrene with LHAS (or AHA).

For further evaluation of the pyrene quenching mechanism with DHM, the effect of temperature on fluorescence quenching efficiencies of pyrene with LHAS (or SRFAR) at fixed concentration of DHM was examined (Figure 2.4). Because LHAS and AHA are both humic acids, only LHAS was investigated further due to its higher aromatic content as compared to that of AHA. The fluorescence quenching ratio (F_o/F) of pyrene with LHAS showed inconsistent trends when increasing the temperature from 288 K up to 318 K.

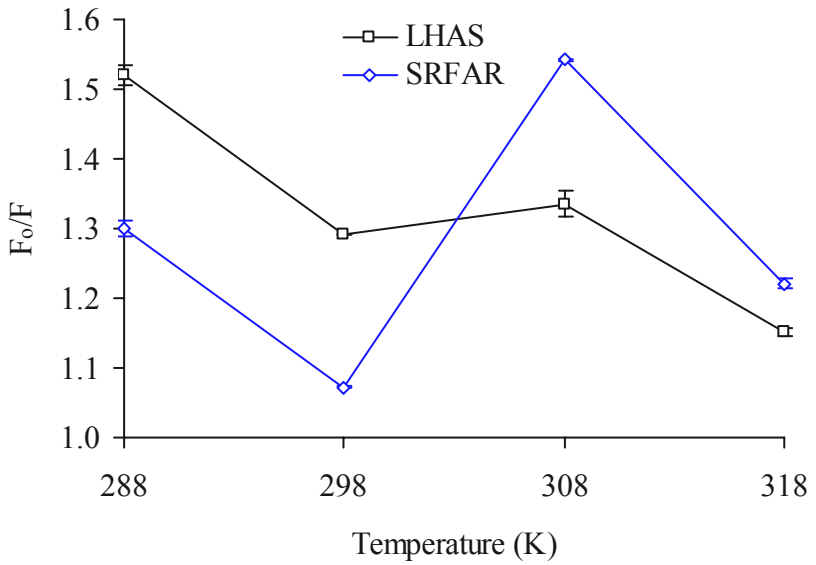

Figure 2.4 The effect of temperature on fluorescence quenching ratio (F_o/F) of 0.02 ppm pyrene with 6 ppm LHAS (or SRFAR) at pH 4.

A decrease in the pyrene fluorescence quenching ratio followed by an increase was observed with temperature. Similar trends in the fluorescence quenching ratio of pyrene with SRFAR were also observed upon increasing the temperature, from 288 K up to 308 K. In general, the increase in florescence quenching ratios of the fluorophore with an increase in the temperature may be

correlated to the decrease of water dielectric constant. Consequently, DHM can coil up and fold forcing the solvating water out. This behavior has also been observed with nonionic surfactants.[51] In addition, DHM may change their configuration from one to another with the temperature complicating the interpretation of the quenching mechanism for pyrene with DHM.

2.3.3 The Effect of pH on Pyrene Association with DHM

Because both LHAS and AHA have higher aromatic contents than SRFAR, the effect of pH on the association of pyrene with DHM was studied. Figure 2.5 shows pH effects, from pH 3 up to 8, on the (I_1/I_3) of pyrene in buffer and pyrene with LHAS (or SRFAR) at fixed DHM concentration. A close examination of Figure 2.5 reveals that the (I_1/I_3) of pyrene with LHAS (or SRFAR) generally decreased at low pH values, indicating that there may be a movement of pyrene towards hydrophobic domains within LHAS (or SRFAR).

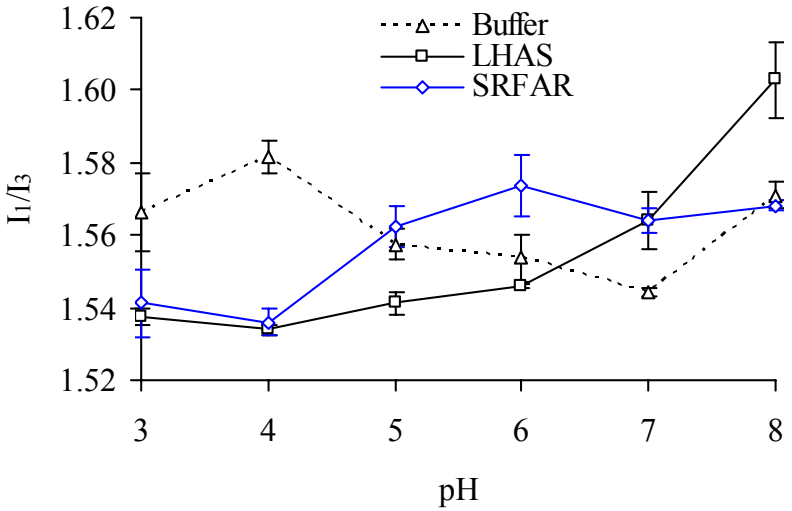

Figure 2.5 The effect of pH on the (I_1/I_3) of 0.02 ppm pyrene in buffer and pyrene in the presence of 6 ppm LHAS (or SRFAR).

Figure 2.6 presents the typical pyrene (I_1/I_3) observed in various organic solvents. In general, the pyrene (I_1/I_3) decreases (e.g., pyridine versus heptane) when the aromatic content of the solvent decreases. In addition, a reduction in the pyrene (I_1/I_3) can be noted when the solvent becomes

less polar. The calculated (I_1/I_3) of pyrene in different solvents are reported in Table 2.1, which are consistent with results published previously.[45-47]

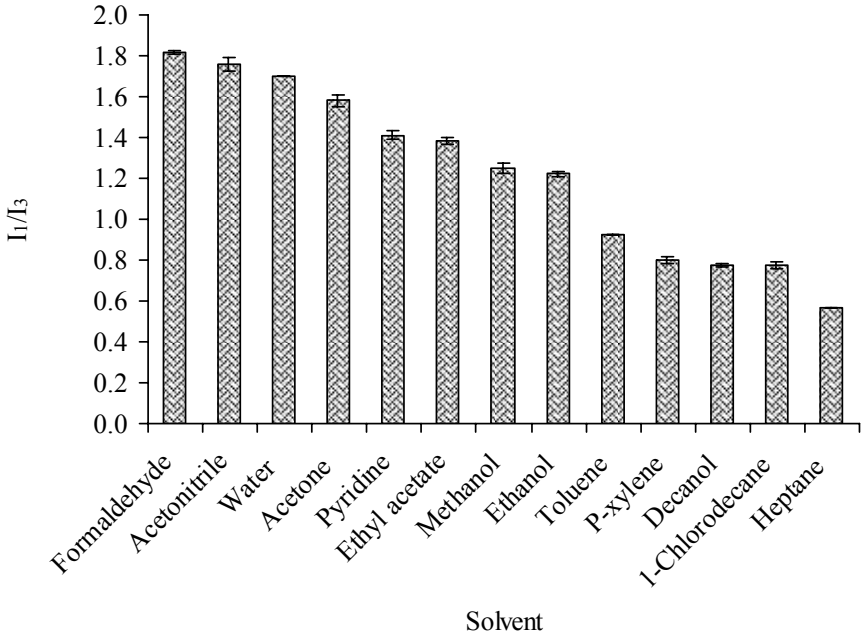

Figure 2.6 The (I_1/I_3) of 0.02 ppm pyrene in different solvents. Corresponding fitting parameters are tabulated in Table 2.1.

Table 2.1 The calculated (I_1/I_3) of pyrene when solubilized within different solvents: same as Figure 2.6.

Solvents	Pyrene Polarity Ratio (I_1/I_3)
Formaldehyde	1.817 (±0.006)
Acetonitrile	1.761 (±0.032)
Water	1.700 (±0.002)
Acetone	1.583 (±0.029)
Pyridine	1.411 (±0.020)
Ethyl acetate	1.383 (±0.016)
Methanol	1.252 (±0.024)
Ethanol	1.222 (±0.010)
Toluene	0.925 (±0.003)
P-xylene	0.802 (±0.016)
Decanol	0.775 (±0.009)
1-Chlorodecane	0.773 (±0.017)
Heptane	0.566 (±0.003)

As was previously mentioned, the results of the (I_1/I_3) of pyrene suggested that the association of pyrene within the hydrophobic domain of LHAS and/or SRFAR is maximized at low pH values. In this study, the association of pyrene with DHM was investigated at pH 4 because the (I_1/I_3) of pyrene with LHAS and/or SRFAR was the lowest as compared to other pH values.

2.3.4 The Effect of Ionic Strength on Pyrene Association with DHM

Figure 2.7 shows the effect of the ionic strength, from 0.001 M up to 0.03 M NaCl (or $CaCl_2$), on the (I_1/I_3) of pyrene in buffer and pyrene and LHAS (or SRFAR) mixture at a fixed DHM concentration and at pH 4. A close examination of Figure 2.7a shows that the pyrene (I_1/I_3) with DHM was low in the absence of NaCl. The addition of NaCl resulted in a significant increase in the (I_1/I_3) of pyrene with DHM, indicating that pyrene moved towards the water environment at the lowest concentration of NaCl (0.001 M). However, pyrene is sequestered from water via a diffusive movement within the hydrophobic domain of DHM with an increase in the ionic strength concentration from 0.001 up to 0.02 M. It is also of great significance to note that this trend was more significant for pyrene with SRFAR as compared to that with LHAS. In general, SRFAR has somewhat higher carboxylic group content than that of LHAS. In addition, the structure of SRFAR may fold and bring those functional groups together, forming multidentate sites, allowing metal ions, such as Na^{+1}, to associate with more than one single group.[52, 53] Thus, pyrene can get into more frequent association within the hydrophobic domain of SRFAR, which can be observed from the significant decrease in the (I_1/I_3) of pyrene. This may be an evidence of dynamic quenching for pyrene in the presence of SRFAR, supporting the above results obtained from Stern-Volmer plots (Figure 2.3). In contrast, the minimal effect on the pyrene (I_1/I_3) in the presence of LHAS after addition of NaCl may indicate that static is more dominant than dynamic quenching.

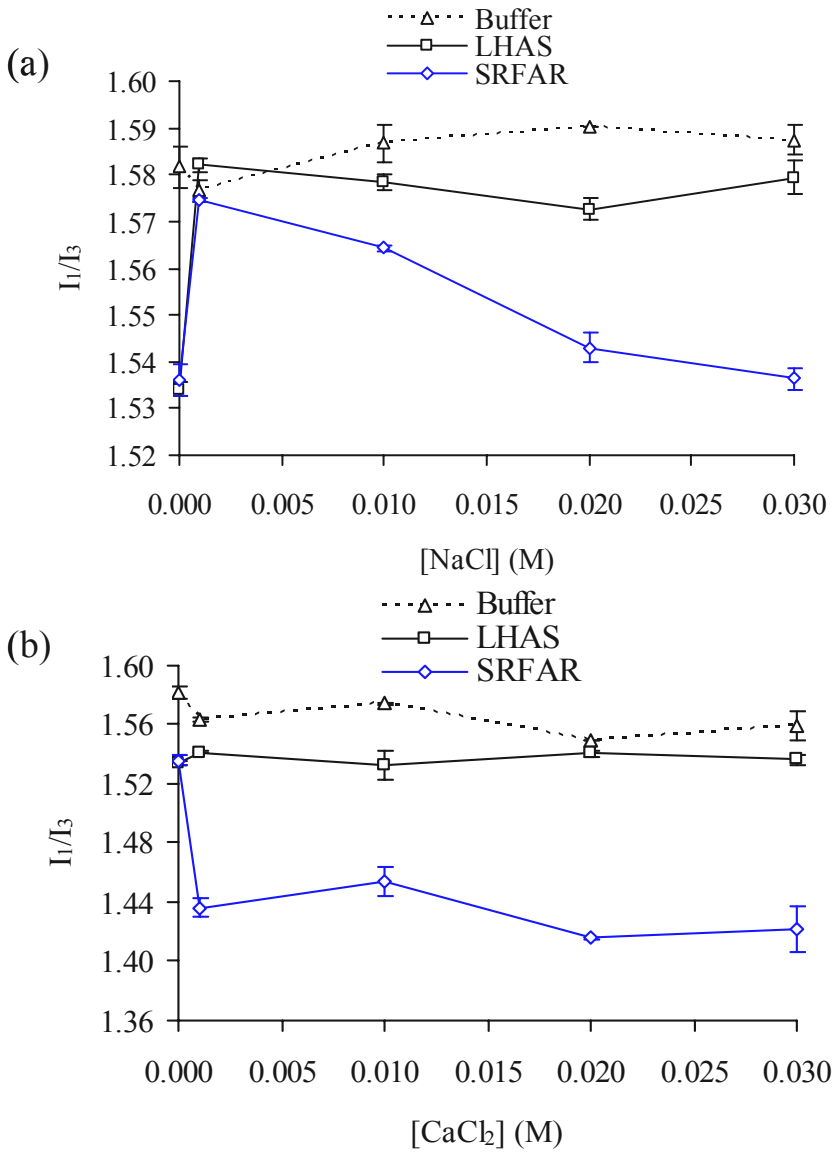

Figure 2.7 The (I_1/I_3) of 0.02 ppm pyrene in buffer and pyrene with 6 ppm LHAS (or SRFAR) after addition of (a) NaCl or (b) $CaCl_2$ at pH 4.

In the presence of $CaCl_2$, little or no change in the (I_1/I_3) of pyrene with LHAS was observed with an increase in the concentration of $CaCl_2$ (Figure 2.7b), further supporting the above findings with NaCl. However, a more significant decrease in the pyrene (I_1/I_3) with DHM, particularly SRFAR, in the presence of $CaCl_2$ as compared to those in the presence of NaCl. This implies that the movement of pyrene within the hydrophobic domain of SRFAR is maximized in

the presence of $CaCl_2$. The different trend in the (I_1/I_3) of pyrene with SRFAR in the presence of the salts can likely be attributed to the fact that the effective ionic radius of calcium ion (Ca^{+2}, 1.06 Å) is smaller than a sodium ion (Na^+, 1.24 Å).[54] Consequently, the smaller effective ionic radius and lower charge density of Ca^{+2} enhance strong binding of Ca^{+2} to SRFAR hard sites, such as carboxylic and phenolic groups. Thus, the effect of $CaCl_2$ in the polarity of SRFAR included in this study was more significant than that of NaCl.

2.4 Conclusion

The results presented in this study demonstrated clear evidence that DHM content play an important role in the association with pyrene. More significant reductions in fluorescence intensities were observed for pyrene with LHAS (or AHA) in contrast to those of pyrene with SRFAR. In general, the high aromatic content of DHM compensates for pyrene and frequently brings it into more association within their hydrophobic domains. In addition, it was observed that there was a slight decrease in the pyrene (I_1/I_3) at lower concentrations of DHM, while little or no change was noticed at higher DHM concentrations. This suggested that the pyrene quenching mechanism with DHM is not due to complete fluorescence quenching of pyrene. Stern-Volmer plots were also evaluated, and a more reasonable linear plot was obtained for pyrene with SRFAR as compared to that with LHAS (or AHA), indicating the pyrene quenching mechanism with SRFAR to be either static or dynamic. In contrast, the upward curvature in the Stern-Volmer plot of pyrene with LHAS (or AHA) suggested that both static and dynamic quenching can take place. However, results obtained from the effect of temperature on fluorescence quenching ratios of pyrene with DHM did not provide valuable information about the quenching mechanism of pyrene with DHM. Consequently, steady-state fluorescence spectroscopy alone may not provide enough information about the quenching mechanism of

pyrene with DHM. The effects of pH and ionic strength on the pyrene association with DHM were also investigated. In general, at lower pH, pyrene shifted more towards the hydrophobic domain of LHAS and/or SRFAR. In addition, the results obtained from the ionic strength study demonstrated that pyrene can get into more contact within the hydrophobic domain of SRFAR due to the smaller effective ionic radius and lower charge density of Ca^{+2} as compared to Na^{+1}.

2.5 References

(1) Gauthier, T. D.; Shane, E. C.; Guerin, W. F.; Seitz, W. R.; Grant, C. L. *Environ. Sci. Technol.* **1986**, *20*, 1162-1166.

(2) Laor, Y.; Rebhun, M. *Environ. Sci. Technol.* **2002**, *36*, 955-961.

(3) Perminova, I. V.; Grechishcheva, N. Y.; Petrosyan, V. S. *Environ. Sci. Technol.* **1999**, *33*, 3781-3787.

(4) Perminova, I. V.; Grechishcheva, N. Y.; Kovalevskii, D. V.; Kudryavtsev, A. V.; Petrosyan, V. S.; Matorin, D. N. *Environ. Sci. Technol.* **2001**, *35*, 3841-3848.

(5) Laor, Y.; Rebhun, M. *Environ. Sci. Technol.* **1997**, *31*, 3558-3564.

(6) Engebretson, R. R.; von Wandruszka, R. *Environ. Sci. Technol.* **1999**, *33*, 4299-4303.

(7) Xing, B.; Pignatello, J. J. *Environ. Toxicol. Chem.* **1996**, *15*, 1282-1288.

(8) Chefetz, B.; Deshmukh, A. P.; Hatcher, P. G.; Guthrie, E. A. *Environ. Sci. Technol.* **2000**, *34*, 2925-2930.

(9) Xing, B.; Pignatello, J. J. *Environ. Sci. Technol.* **1997**, *31*, 792-799.

(10) Xing, B.; Pignatello, J. J.; Gigliotti, B. *Environ. Sci. Technol.* **1996**, *30*, 2432-2440.

(11) Weber, W. J., Jr.; McGinley, P. M.; Katz, L. E. *Environ. Sci. Technol.* **1992**, *26*, 1955-1962.

(12) Weber, W. J., Jr.; Huang, W. *Environ. Sci. Technol.* **1996**, *30*, 881-888.

(13) Huang, W.; Young, T. M.; Schlautman, M. A.; Yu, H.; Weber, W. J., Jr. *Environ. Sci. Technol.* **1997**, *31*, 1703-1710.

(14) Huang, W.; Weber, W. J., Jr. *Environ. Sci. Technol.* **1997**, *31*, 2562-2569.

(15) Young, T. M.; Weber, W. J., Jr. *Environ. Sci. Technol.* **1995**, *29*, 92-97.

(16) Graber, E. R.; Borisover, M. D. *Environ. Sci. Technol.* **1998**, *32*, 3286-3292.

(17) Gauthier, T. D.; Seitz, W. R.; Grant, C. L. *Environ. Sci. Technol.* **1987**, *21*, 243-248.

(18) Chin, Y.-P.; Aiken, G. R.; Danielsen, K. M. *Environ. Sci. Technol.* **1997**, *31*, 1630-1635.

(19) Chiou, C. T.; McGroddy, S. E.; Kile, D. E. *Environ. Sci. Technol.* **1998**, *32*, 264-269.

(20) Drewes, J. E.; Croue, J. P. *Water Sci. Technol.: Water Supply* **2002**, *2*, 1-10.

(21) Holbrook, R. D.; Love, N. G.; Novak, J. T. *Environ. Sci. Technol.* **2004**, *38*, 4987-4994.

(22) Engebretson, R. R.; von Wandruszka, R. *Environ. Sci. Technol.* **1994**, *28*, 1934-1941.

(23) Hu, W.-G.; Mao, J.; Xing, B.; Schmidt-Rohr, K. *Environ. Sci. Technol.* **2000**, *34*, 530-534.

(24) Wang, K.; Xing, B. *J. Environ. Qual.* **2005**, *34*, 342-349.

(25) JiJi, R. D.; Cooper, G. A.; Booksh, K. S. *Anal. Chim. Acta* **1999**, *397*, 61-72.

(26) Morra, M. J.; Corapcioglu, M. O.; Von Wandruszka, R. M. A.; Marshall, D. B.; Topper, K. *Soil Sci. Soc. Am. J.* **1990**, *54*, 1283-1289.

(27) Danielsen, K. M.; Chin, Y.-P.; Buterbaugh, J. S.; Gustafson, T. L.; Traina, S. J. *Environ. Sci. Technol.* **1995**, *29*, 2162-2165.

(28) Mackenzie, K.; Georgi, A.; Kumke, M.; Kopinke, F.-D. *Environ. Sci. Technol.* **2002**, *36*, 4403-4409.

(29) Puchalski, M. M.; Morra, M. J.; Von Wandruszka, R. *Environ. Sci. Technol.* **1992**, *26*, 1787-1792.

(30) Chen, S.; Inskeep, W. P.; Williams, S. A.; Callis, P. R. *Environ. Sci. Technol.* **1994**, *28*, 1582-1588.

(31) Schlautman, M. A.; Morgan, J. J. *Environ. Sci. Technol.* **1993**, *27*, 961-969.

(32) Backhus, D. A.; Gschwend, P. M. *Environ. Sci. Technol.* **1990**, *24*, 1214-1223.

(33) Chin, Y. P.; Gschwend, P. M. *Environ. Sci. Technol.* **1992**, *26*, 1621-1626.

(34) Herbert, B. E.; Bertsch, P. M.; Novak, J. M. *Environ. Sci. Technol.* **1993**, *27*, 398-403.

(35) Traina, S. J.; McAvoy, D. C.; Versteeg, D. J. *Environ. Sci. Technol.* **1996**, *30*, 1300-1309.

(36) Tiller, C. L.; Jones, K. D. *Environ. Sci. Technol.* **1997**, *31*, 424-429.

(37) Kumke, M. U.; Frimmel, F. H.; Ariese, F.; Gooijer, C. *Environ. Sci. Technol.* **2000**, *34*, 3818-3823.

(38) Backhus, D. A.; Golini, C.; Castellanos, E. *Environ. Sci. Technol.* **2003**, *37*, 4717-4723.

(39) Schlautman, M. A.; Morgan, J. J. *Environ. Sci. Technol.* **1993**, *27*, 2523-2532.

(40) Shane, E. C.; Price-Everett, M.; Hanson, T. *J. Chem. Educ.* **2000**, *77*, 1617-1618.

(41) Engebretson, R. R.; Von Wandruszka, R. *Org. Geochem.* **1997**, *26*, 759-767.

(42) Ganaye, V. A.; Keiding, K.; Viriot, M.-L.; Vogel, T. M.; Block, J.-C. *Environ. Sci. Technol.* **1997**, *31*, 2701-2706.

(43) Kang, S.; Xing, B. *Environ. Sci. Technol.* **2005**, *39*, 134-140.

(44) Chen, Z.; Xing, B.; McGill, W. B.; Dudas, M. J. *Can. J. Soil Sci.* **1996**, *76*, 513-522.

(45) Tedeschi, C.; Moehwald, H.; Kirstein, S. *J. Am. Chem. Soc.* **2001**, *123*, 954-960.

(46) Dong, D. C.; Winnik, M. A. *Can. J. Chem.* **1984**, *62*, 2560-2565.

(47) Dong, D. C.; Winnik, M. A. *Photochem. Photobiol.* **1982**, *35*, 17-21.

(48) Kalyanasundaram, K.; Thomas, J. K. *J. Am. Chem. Soc.* **1977**, *99*, 2039-2044.

(49) Nakajima, A. *Bull. Chem. Soc. Jpn.* **1971**, *44*, 3272-3277.

(50) Lakowicz, J. R. *Principles of Fluorescence Spectroscopy*, Second ed.; Plenum Pr, 1999.

(51) Nilsson, P. G.; Wennerstroem, H.; Lindman, B. *J. Phys. Chem.* **1983**, *87*, 1377-1385.

(52) Stevenson, F. J. *Humus Chemistry : Genesis, Composition, Reactions*, Second ed.; John Wiley & Sons: New York, 1994.

(53) Tipping, E. *Cation binding by humic substances*, First ed.; Cambridge University Press: New York, 2002.

(54) Shannon, R. D. *Acta Crystall. A-Crys.* **1976**, *A32*, 751-767.

CHAPTER 3

A NEW APPROACH TO FREQUENCY-DOMAIN FLUORESCENCE LIFETIME MEASUREMENTS: ON THE EFFECTS OF PHOTOBLEACHING WITHIN A MULTI-COMPONENT SYSTEM

3.1 Introduction

Fluorescence lifetime measurements are widely used in fluorescence spectroscopy, in particular for biological application.[1] Fluorescence lifetime measurements are also used in analytical applications as a tool for selectivity enhancement and determinations in multi-component systems.[2] More valuable information can also be obtained from these measurements such as the rates of excited-state reactions, energy transfer between donor and acceptor molecules, and fluorescence quenching in bimolecular processes.[3]

However, a problem encountered in fluorescence spectroscopy is the effect of photobleaching, a chemical transformation of the fluorophore in the excited state, or long living triplet state, into a non-fluorescent species.[4, 5] Many studies have reported that photobleaching within multi-component systems can affect the observed probe's fluorescence lifetime.[6-12] For example, Nakamura et al.[6] investigated chlorophyll A in a droplet of n-octanol using time-resolved fluorescence microscopy. They observed an increase in the shorter lived fraction with increasing exposure to radiation, but observed no effect on the recovered lifetimes of two decay components. Rueck et al.[11] used time-correlated single photon counting to investigate 5-aminolevulinic acid metabolites in solutions and cell cultures, and observed a significant decrease in recovered lifetimes during illumination. Additionally, Connelly et al.[12] performed time-resolved fluorescence imaging of meta-tetra(hydroxyphenyl) chlorine (m-THPC). Their results suggested that photobleaching of m-THPC resulted in artifacts in the lifetime analysis, which shortened the recovered lifetime of m-THPC. Thus, photobleaching within multi-

component systems can affect recovered fluorescence lifetimes and fractional intensity contributions, complicating the interpretation of fluorescence lifetime results.

Furthermore, photobleaching can affect time-resolved fluorescence measurements of complex fluorescent molecules, which have more than one fluorophore, such as, collagen and elastin.[13, 14] For example, Marcu et al.[9] investigated the photobleaching characteristics of the major fluorescent components (elastin, collagen, and cholesterol) of the arterial wall during prolonged exposure to nitrogen laser pulses at various fluence levels. It was indicated that photobleaching of cholesterol was more significant than elastin. They also reported that fluorescence decays of collagen and cholesterol were altered with radiation when the fluence level of the excitation source was 21.75 $\mu W/mm^2$. It was indicated that different fluorophores usually have different photobleaching rates upon exposure to radiation. As a result, the measured lifetime can be altered with photobleching, reflecting a decrease in the fluorophores fraction because the time dependent fluorescence decay of these complex molecules consists of the decay characteristics of different fluorophores. Thus, photobleaching in artery tissue was shown to cause changes in recovered lifetimes, complicating the interpretation of the fluorescence measurements in terms of tissue composition.

Problems with photobleaching have also been encountered in environmental applications of fluorescence, as exemplified by the application of fluorescence to studies of the association mechanism between hydrophobic organic compounds and dissolved humic materials.[15-17] While time-resolved fluorescence measurement addressed some problems associated with steady-state fluorescence technique, it did not completely resolve the effect of photobleaching.[18, 19]

In general, the photobleaching effect in time-resolved measurements has been minimized by controlling the fluence level of the excitation source.[9, 12] Photobleaching has also a large

effect in fluorescence lifetime imaging microscopy investigations.[20-23] In one such example, Murata et al.[23] investigated the spatial distribution of DNA-bound donors and acceptors using frequency-domain fluorescence lifetime imaging microscopy. The sample illumination level was addressed by neutral-density filters in order to eliminate the photobleaching effect. However, this issue has not been fully resolved. Decreasing the fluence level of the excitation source reduces signal intensity, and may not be practical in all cases.

In accordance, a newly developed frequency segmentation and recombination method was applied in frequency-domain fluorescence lifetime measurements in order to address the effect of photobleaching in multi-component systems. This technique is applicable on currently available frequency-domain lifetime instruments, and can be viewed as an alternative to specialized multi-harmonic frequency instrumentation (no such instrument is currently commercially available, e.g. SLM-Amico 48000 MHF) in terms of overcoming photobleaching. The frequency segmentation and recombination method was investigated by simulation of a simple two component dye system consisting of fluorescein (Fl) and rhodamine B (RhB) and comparison of experimental data collected in traditional and segmented fashion. This method was also applied to a more complex system containing pyrene and Suwannee River fulvic acid reference in order to carefully quantify recovered lifetimes and fractional intensity contributions.

3.2 Experimental

3.2.1 Materials and Reagents

Fl (99%), RhB (~95%), and pyrene (≥ 99%) were obtained from Sigma-Aldrich (Milwaukee, WI) and used as received. Suwannee River fulvic acid reference (SRFAR) was purchased from the International Humic Substances Society (IHSS), Department of Soil, Water, and Climate, University of Minnesota (St. Paul, MN).

3.2.2 Sample Preparation

Standard reference solutions of 0.02 μM Fl, 1 μM RhB, and their mixture at the same concentrations were prepared in 0.1 M NaOH. Fluorescence measurements of Fl, RhB, and their mixture were collected on air-saturated samples to increase photobleaching as compared to deoxygenated systems.

Standard reference solutions of 0.1 ppm pyrene and 12 ppm SRFAR were prepared in 18.2 MΩ·cm distilled deionized water. The pyrene-SRFAR mixture, containing 0.04 ppm pyrene and 12 ppm SRFAR, was also prepared as above and stored in the dark at 4 °C. The mixture was allowed to equilibrate in the dark for at least seven days. Solutions were allowed to equilibrate overnight in a quartz fluorometer cell with septum cap and rinsed with fresh solutions prior to fluorescence measurements to reduce losses of pyrene to the cell wall. For such deoxygenated systems, all solutions of pyrene and DHM individual components and their mixture were purged using an argon gas for exactly 15 min, followed by 5 min of equilibration time in the sample compartment with a flow of argon gas over the course of fluorescence measurements.

3.2.3 Instrumentation

Fluorescence measurements were acquired using a Spex Fluorolog-3 spectrofluorometer (model FL3-22TAU3; Jobin Yvon, Edison, NJ, USA) equipped with a 450-W xenon lamp and R928P photomultiplier tube (PMT) detector. Fluorescence measurements were made at room temperature in a 10 mm quartz fluorometer cell with septum cap. The excitation wavelength was 490 nm for Fl, RhB, and their mixture. Pyrene, DHM, and their mixture were excited at 333 nm. Time-based fluorescence steady-state experiments used to investigate the photostability of Fl and RhB were acquired with excitation bandpass set at 8.0 nm and emission bandpass at 2.0 nm. The emission was monitored at 512 and 576 nm for Fl and RhB, respectively. Frequency-domain

fluorescence signals were passed through 370 and 500 nm long-pass filters for pyrene and dye solutions, respectively. Frequency-domain lifetime experimental details including frequency range, number of frequencies, averages, and integration times for both a single long run (LR) and combined run (CR) segments are tabulated in Table 3.1. For the LR, an integration time of 30 and 15 sec were used for Fl/RhB and Pyrene/SRFAR systems, respectively. The CR is a combination of four individual segments, with a fresh solution used for each segment.

Table 3.1 Frequency-domain fluorescence lifetime experimental details of the LR and four CR segments. The frequency range is in the logarithmic scale. The frequency range is in the logarithmic scale. Averages are calculated using the interleave function such that an average is generated each time the automated sample turret rotates.

Set	Range (MHz)	Number	Time (sec)	Averages	Time Exposed (min)
LR	0.50-275.40	39	15.0 or 30.0	5	29.25 or 58.50
CR (Segment 1)	4.30-233.30	13	15	5	9.75
CR (Segment 2)	0.50-19.30	12	15	5	9
CR (Segment 3)	0.60-3.10	6	30	5	9
CR (Segment 4)	26.90-275.40	8	7.5	5	3

All these segments were intermixed and recombined onto a single frequency-domain phase and modulation data set. Frequency-domain measurements were collected for all solutions versus ludox–a scatter reference solution– which shows a lifetime of zero. Frequency-domain phase and modulation decay profiles were analyzed using the Globals software package developed at the Laboratory for Fluorescence Dynamics at the University of Illinois at Urbana-Champaign.[24, 25] Several initial guesses of parameters were applied using non-linear least squares (NLLS) analysis to examine the stability of χ^2 minimization. Phase and modulation data sets were well fitted by appropriate models, and the quality of the fit was judged by visual inspection of residual plots as

well as by χ^2 statistics. Constant errors of 0.5° and 0.005 were used in analyses for consistency and ease of day-to-day data interpretation. The principles of the time-resolved measurements and their data analysis were described in details in Chapter 1 of this dissertation and will not be discussed further.

3.3 Results and Discussion

3.3.1 Photobleaching and Fluorescence Lifetime Measurements

In practice, commercial instrumentation for frequency-domain fluorescence lifetime measurements records the phase difference and demodulation of the sample at several modulation frequencies as the frequency is sequentially varied in a single LR. The modulation frequency typically increases from the lowest to highest frequency. Hence, frequency-domain lifetime measurements are performed on a solution which has been exposed to the greatest amount of light at the highest frequency. As a result, an alteration in fractional intensity contributions of all components over the course of the measurement can be observed due to photobleaching of one component in a multi-component system, causing errors in both measured fractions and lifetimes. The amount of radiation to which the sample is exposed must be minimized in order to reduce photobleaching.

Multi-harmonic frequency instrumentation, such as SLM-Amico 48000 MHF, can overcome the time-sensitive sampling issue (photobleaching) by scanning the entire frequency ranges in seconds. However, no such instrumentation is currently commercially available. Conventional frequency-domain fluorescence lifetime measurements, however, present a second possible strategy in that one can divide the LR into a series of overlapping segments. The number of frequencies, integration time, and number of averages specifies the total time of the sample exposure to radiation in the LR. In order to retrieve the right answer, large numbers of

data points are needed for complex systems. As such, a total of 39 frequencies ranging from 0.5 to 274.5 MHz (allowing measurement of both long and short lifetimes) was chosen for this study. At each frequency, five averages were recorded, and two integration times were selected for the LR. For the dye mixture validation study, a longer integration time of 30 sec exposed the sample to 58.50 min of radiation was chosen in order to increase the photobleaching. For pyrene and DHM system, the integration time is divided into half, minimizing the exposure to 29.25 min, in order to minimize the photobleaching. The single LR was divided into four different segments in order to reduce the total sample exposure time to radiation. Integration times were adjusted to ensure that no point was exposed to more than 10 min of radiation (Table 3.1). A fresh solution was used in the measurement of each segment, and the data from four segments were recombined onto a single frequency-domain data set for analysis. The reduction of errors associated with photobleaching justifies the larger amount of sample required. This work presents the realization of this approach 1) in terms of a proof of concept on a model system, and 2) in a real world application.

3.3.2 Proof of Concept on a Model System

- **The Model System**

The frequency segmentation and recombination method was first evaluated using a simple two component system consisting of Fl and RhB mixture. Fl and RhB were chosen because these dyes fluoresce in the same solvent system, can be excited at the same wavelength, photobleach differently, and have different lifetimes. All fluorescence measurements of the individual dye components and their mixture were obtained with air-equilibrated samples to increase photobleaching. Fluorescence steady-state emission spectra (Figure 3.1a) were collected for Fl, RhB, and their mixture before and after exposure to 30 min of radiation. The change in

fluorescence intensity of the dye mixture over time was monitored at the emission peaks of the individual components (Figure 3.1b). A close examination of Figure 3.1 reveals a marked decrease in Fl fluorescence, while little or no change was observed in RhB fluorescence intensities.

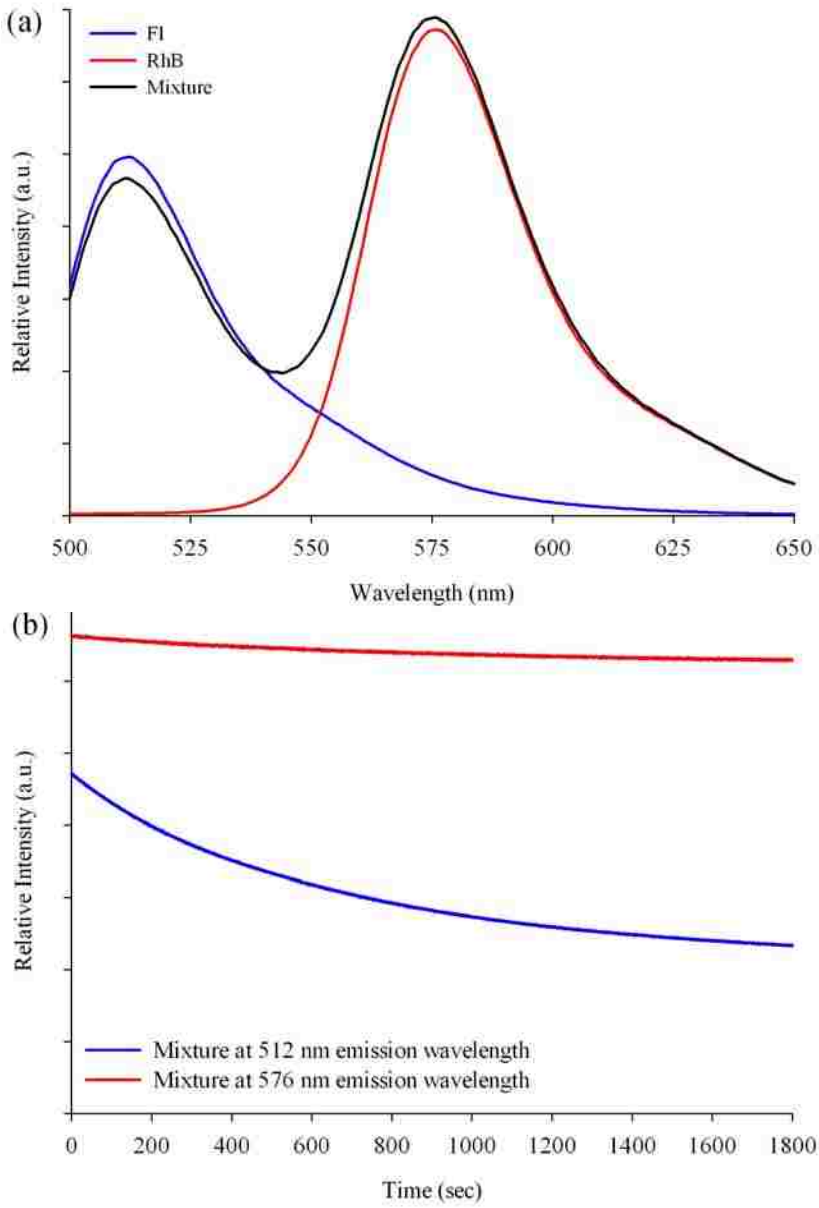

Figure 3.1 (a) Fluorescence emission spectra of Fl (0.02 μM), RhB (1 μM), and mixture in 0.1 M NaOH excited at 490 nm and (b) time-based fluorescence steady-state experiments of the dye mixture excited at 490 nm and monitored at 512 nm and 576 nm of Fl and RhB emission wavelengths, respectively.

Fl intensity decreased by approximately 55% after exposure to radiation in the dye mixture, while the intensity of RhB remained nearly constant. It was also observed in that both Fl and RhB were slightly dimmer in the mixture as compared to individual components. Fl and RhB emissions were 92.34 % and 94.68% the intensity of their individual components, respectively (Figure 3.2).

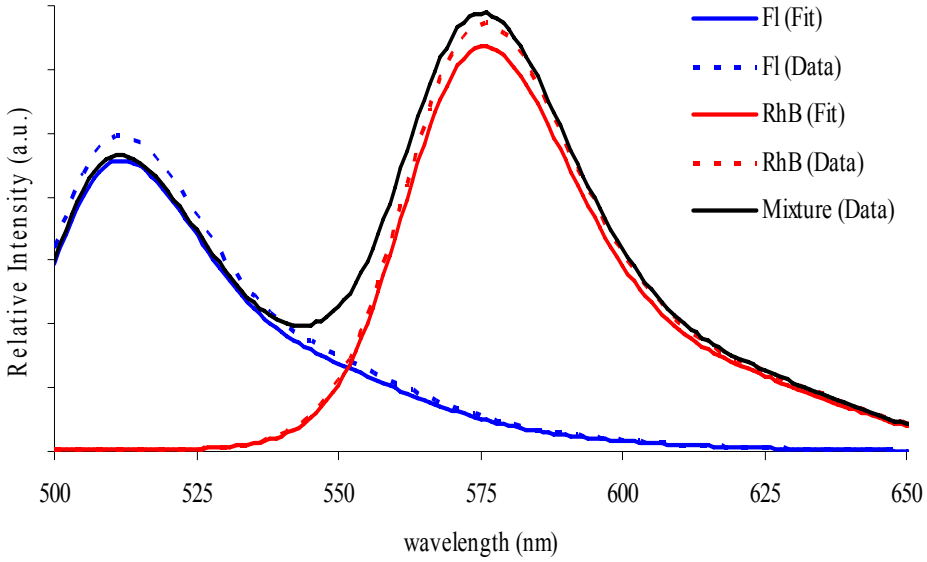

Figure 3.2 Data and fit of fluorescence emission spectra for Fl (0.02 μM), RhB (1 μM), and their mixture in 0.1 M NaOH excited at 490 nm.

The quenching of fluorescence in the mixture can be attributed to the dynamic collision between these dyes. The results in Figures 3.1 and 3.2 demonstrate that a Fl and RhB mixture is a multi-component system with a relatively large amount of bleaching for one component and allows one to study the effect of photobleaching on lifetime measurements and the effectiveness of frequency segmentation and recombination.

Figure 3.3a graphically represents the exposure of a sample to radiation as a function of integration time during the acquisition of data for the LR and segments used for the CR.

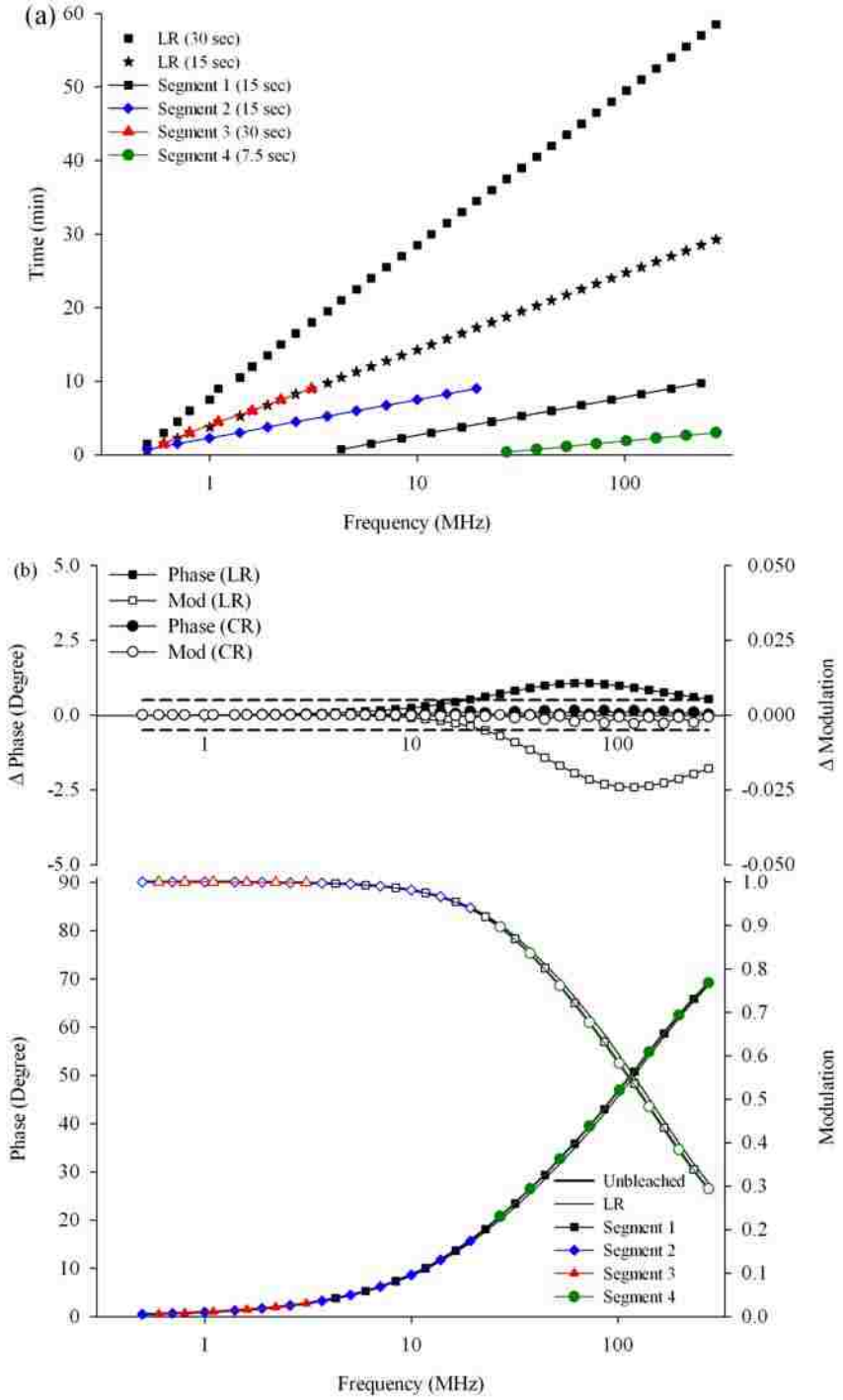

Figure 3.3 (a) Exposure time as a function of frequency for the LR and four CR segments. (b) Simulated frequency-domain LR and CR data for Fl (τ= 4.07 ns, $\alpha_{initial}$= 0.420) and RhB (τ= 1.30 ns, $\alpha_{initial}$= 0.580) mixture. A 20% Fl photobleaching was assumed in the time the LR was exposed to radiation. Solid and open symbols in (b) represent phase and modulation, respectively. Dashed lines in the residual plot represent the 0.5° and 0.005 modulation error values used in the NLLS analyses.

From this figure, it can be noticed that the frequency segmentation reduces the sample's exposure to radiation, while at the same time sampling the same frequency-domain. It should be noted, however, that modulation of the excitation light reduces the intensity of radiation that reaches the sample as compared to a steady-state measurement. Therefore, the mixture is exposed to less radiation in a frequency-domain lifetime measurements than in a steady-state measurement of equal time. The dye mixture used in the LR lifetime measurement is exposed to radiation for nearly twice as long as the mixture used in the steady-state experiment. Thus, values of 20% and 50% fluorescence intensity decrease were chosen for simulation.

- **Simulations**

Frequency-domain lifetime data (phase and modulation as a function of frequency) for the LR dye mixture were simulated assuming that Fl was photobleached by 20% (Figure 3.3b). Real and imaginary portions of the signal were calculated using equations 1.41 and 1.42, respectively, in Chapter 1 of this dissertation. In the simulation, 4.07 and 1.30 ns lifetimes were used for Fl and RhB, respectively, which are those measured for the individual components (Table 3.2). The initial fractional intensity of Fl was 0.420 based on the fractional intensity of Fl calculated from the steady-state emission spectrum of the mixture (Figure 3.1a). Based on the assumption, the intensity of the bleached component was assumed to decrease linearly with exposure time. For example, the Fl initial fractional intensity at 0.5 MHz (time = 0 min) was 0.420 and decreased to 0.367 at 275.4 MHz (time = 58.50 min). Consequently, a different set of fractional intensity values was applied in equations 1.41 and 1.42, in Chapter 1 of this dissertation, for each modulation frequency. The outputs of equations 1.41 and 1.42 were used in equations 1.39 and 1.40, in Chapter 1 of this dissertation, in order to calculate phase and modulation as a function of frequency. The individual segments of the CR were also simulated as

above with the fractional intensity contributions used in equations 1.41 and 1.42, taking into consideration a reduced exposure to radiation (<10 min).

Table 3.2 Recovered fluorescence lifetimes and fractional contributions obtained from NLLS analyses of the individual Fl and RhB components and their mixture. Bolded black parameters are fixed values: same as Figures 3.4 and 3.5.

Model	Float	Set	α_1	τ_1 (ns)	α_2	τ_2 (ns)	χ^2
D (V)	1	Fl (LR)	1.000	4.07	-	-	1.68
D (V)	1	RhB (LR)	1.000	1.30	-	-	2.29
D (V)	1	Mixture (LR)	1.000	1.89	-	-	32.81
-	-	Mixture (CR)	1.000	1.99	-	-	23.40
DD (VVFV)	3	LR1	0.405	3.79	0.595	1.19	1.07
-	-	CR1	0.413	3.69	0.587	1.29	0.93
DD (FVFV)	2	LR2	**0.420**	3.71	**0.580**	1.17	1.05
-	-	CR2	**0.420**	3.65	**0.580**	1.29	0.92
DD (VFFF)	1	LR3	0.343	**4.07**	0.657	**1.30**	1.48
-	-	CR3	0.377	**4.07**	0.623	**1.30**	1.34
DD (VFFF)	1	LR4	0.393	**3.76**	0.607	**1.23**	1.25
-	-	CR4	0.430	**3.76**	0.570	**1.23**	1.34
DD (FFFF)	0	LR5	**0.420**	**4.07**	**0.580**	**1.30**	9.51
-	-	CR5	**0.420**	**4.07**	**0.580**	**1.30**	3.81
DD (FFFF)	0	LR6	**0.420**	**3.76**	**0.580**	**1.23**	2.19
-	-	CR6	**0.420**	**3.76**	**0.580**	**1.23**	1.45
DD (FFFF)	0	LR7	**0.413**	**3.69**	**0.587**	**1.29**	4.01
-	-	CR7	**0.413**	**3.69**	**0.587**	**1.29**	0.89
DD (VFFF)	1	LR8	0.374	**3.69**	0.626	**1.29**	2.33
-	-	CR8	0.413	**3.69**	0.587	**1.29**	0.90
DD (FVFV)	2	LR9	**0.413**	3.75	**0.587**	1.18	1.04
-	-	CR9	**0.413**	3.69	**0.587**	1.29	0.92

The results for these simulations are shown in Figure 3.3b along with their residuals based on NLLS analyses of the simulated data, which represent the difference between the unbleached run and LR or (or CR). It is obvious from Figure 3.3b that the simulated LR deviated from the unbleached simulation at higher modulation frequencies, which have been exposed to the greatest amount of light. Comparing the LR with CR, it can be noted that errors resulting

from photobleaching in the CR are much smaller than those of the LR. In fact, the error caused by bleaching for the CR is now within the error values (0.5 degree, 0.005 modulation) typically used in NLLS lifetime analyses for consistency and ease of day-to-day data interpretation. These results suggest that frequency segmentation and recombination method reduced errors associated with changing fractional contributions within the multi-component system.

- **Measurements and NLLS Analyses**

In order to evaluate the photobleaching effect within the multi-component system, the results of simulations were compared to experimental LR and CR data. In addition to the 20% Fl photobleaching described above, 50% Fl, 20% RhB, and 50% RhB photobleaching were simulated for comparison. These simulations along with experimental LR and CR data are displayed together in Figure 3.4a. Figure 3.4b illustrates the effect of photobleaching on fractional intensity contributions of Fl and RhB in the mixture, which is shown in Figure 3.4a. It can be clearly noticed that fractional contribution of Fl decreased while increased for RhB when Fl intensity decreased by 20% as a result of photobleaching. The same effect can be observed but became more significant when the Fl intensity decreased by 50%. An opposite trend, however, can be observed in fractional intensity contributions of Fl and RhB when RhB intensity decreased by 20 or 50%. From Figure 3.4a, it is interesting to note that the experimental LR data's deviation from simulated unbleached data is indicative of the Fl component being photobleached, in consistency with fluorescence steady-state data. In contrast, CR experimental data matched more closely the simulated unbleached run, providing that the frequency segmentation and recombination method reduces the effect of photobleaching.

This finding is also supported by the NLLS analyses of experimental data, which are presented in Table 3.2 for Fl (LR) and RhB (LR) as well as LR and CR data for their mixture.

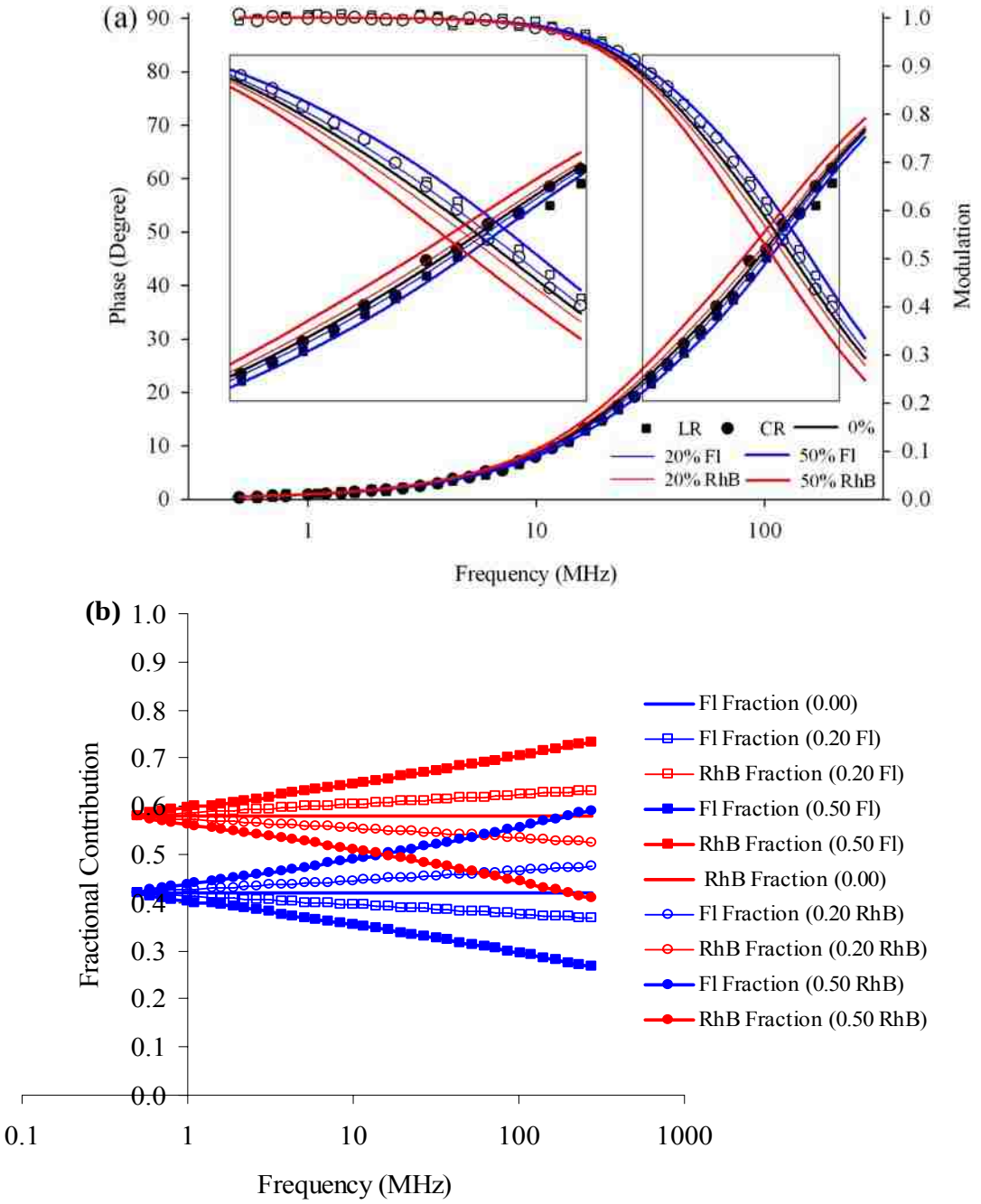

Figure 3.4 (a) Experimental and simulated frequency-domain LR and CR data for Fl (0.02 μM) and RhB (1 μM) mixture. Simulated frequency-domain LR data of the Fl (τ= 4.07 ns, $\alpha_{initial}$= 0.420) and RhB (τ= 1.30 ns, $\alpha_{initial}$= 0.580) mixture were simulated assuming (0%, 0%), (20%, 0%), (50%, 0%), (0%, 20%), and (0%, 50%) photobleaching for Fl and RhB, respectively. Solid and open symbols represent phase and modulation, respectively. Corresponding fitting parameters are tabulated in Table 3.2. (b) Effect of photobleaching on fractional intensity contributions of Fl and RhB in the mixture.

A good fitting of the phase and modulation data was obtained with a very reasonable χ^2 using a single-exponential decay (D) model for the individual components. Two-exponential decay (DD) model of both mixture LR and CR was found to provide the best fitting parameters because structured residuals and unreasonable χ^2 values were obtained when fitting the mixture data with the D model. The stability of the DD model using NLLS fitting was examined by allowing some or all lifetimes and fractional contributions to float (V) or by keeping these parameters fixed (F). Table 3.2 summarizes the results obtained from the NLLS method for both LR and CR. It can be noted that excellent fits and χ^2 values were obtained for both LR and CR data when all parameters were allowed to vary (LR1 and CR1). However, a mismatch can be observed in recovered lifetimes and fractional contributions. The Fl fractional contribution for LR1 was slightly lower than that of CR1, which is possibly indicative to the effect of photobleaching on the LR. It is also interesting to note that the recovered RhB lifetime is shorter in LR1 than CR1 indicating that NLLS analysis may compensate for bleaching of one component by changing the recovered lifetime of the other. Although analysis of both LR and CR yielded acceptable results, less confidence should be placed in recovered parameters of the LR, and it is likely the results from the CR analysis better represent the true values.

It was shown above that NLLS analysis may compensate for bleaching of one component by changing the recovered lifetime of the other. In order to eliminate this effect, the data were analyzed with the lifetimes fixed at the measured lifetimes of individual components (LR3 and CR3). For both runs, reasonable χ^2 values were obtained, but NLLS analysis compensated for Fl beaching by reducing the Fl fraction for the LR3 compared to CR3. This was observed with the first trial, but more pronounced with the lifetimes fixed. In order to further investigate how NLLS analysis compensates for photobleaching in frequency-domain lifetime measurements, the

analyses were performed by keeping all parameters fixed (LR5 and CR5). The fraction of Fl was kept fixed at 0.420, based on the emission spectrum of the dye mixture (Figure 3.1a), while the lifetimes stayed constant at recovered values for the individual components. Figures 3.5a and b display the fits and residuals for the LR and CR data, respectively. An unreasonable χ^2 value of 9.51 was observed (Figure 3.5a); however, the χ^2 value for the CR data (3.81) was butter but still high (Figure 3.5b). Structured residuals were observed for both runs. This is likely caused by a mismatch between the lifetime values fixed in the analyses and the true lifetime values for the system.

Recall that Fl and RhB in their mixture were dimmer than their individual components (Figure 3.2), indicative of both Fl and RhB lifetimes may have been affected as a result of collisional quenching in the dye mixture. By using equation 1.24, in Chapter 1 of this dissertation, recovered Fl and RhB lifetimes can be corrected for dynamic collisions in the dye mixture. These calculated lifetimes values (Fl = 3.76 ns, RhB = 1.23 ns) are similar to recovered lifetimes of the CR1 when all parameters are varied, further supporting the statement that more confidence should be placed in the CR analysis as compared to the LR analysis. For both LR6 and CR6 sets, the Fl fraction and corrected lifetimes were fixed in the NLLS analyses. NLLS analyses with lifetimes fixed at values estimated considering the effect of dynamic quenching result in better χ^2 values and residual plots, as illustrated in Table 3.2 and Figure 3.5, particularly for the CR. Based on the assumption that the results from the NLLS analysis of the CR with all variables floating (CR1) most closely represent the true values, these values were remained fixed for comparison (LR7 and CR7). It is interesting to note that a worse fit was obtained of the LR7 than LR6 described above, which can be confirmed by an increase in the χ^2 value (Table 3.2) and by visual inspection of the order within the residuals (Figure 3.5a).

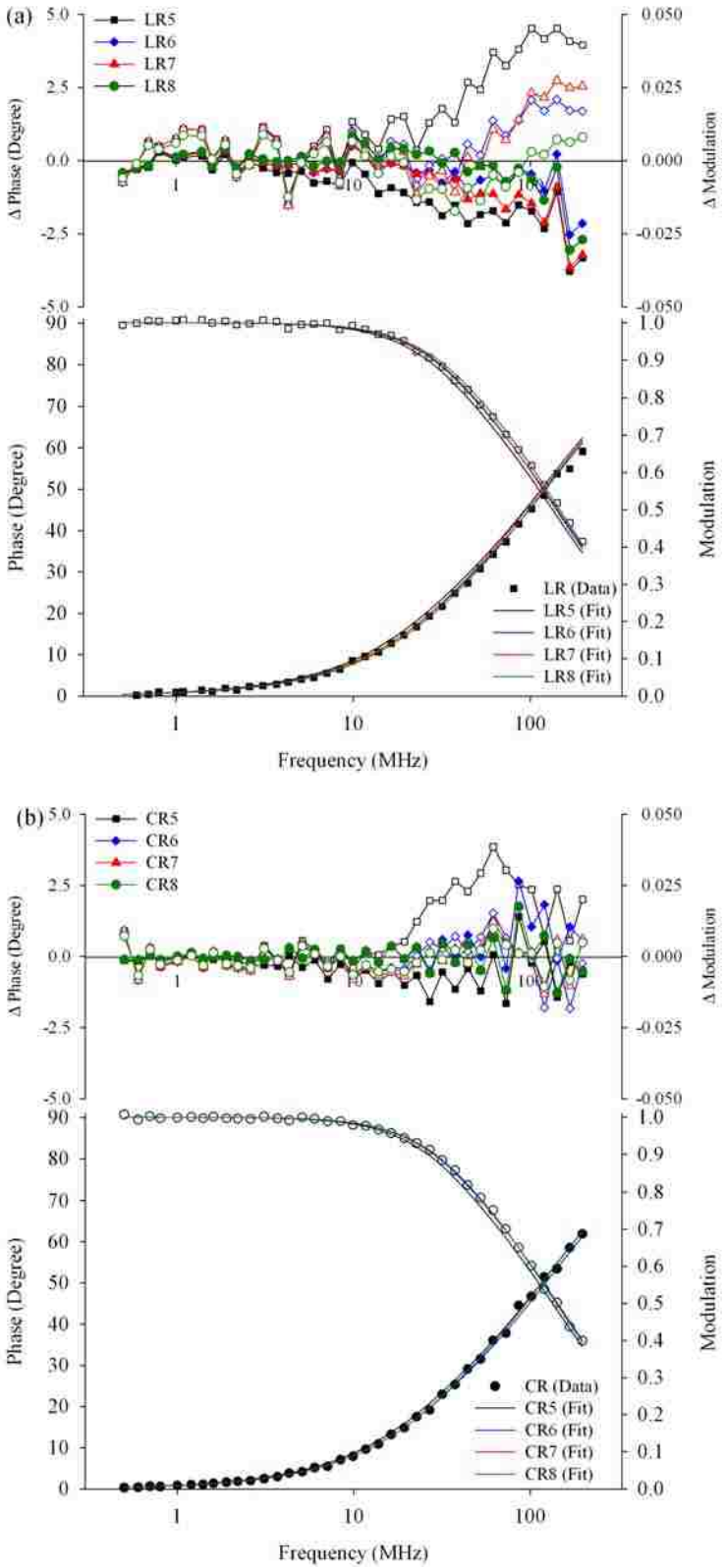

Figure 3.5 (a) LR and (b) CR experimental frequency-domain data and NLLS fits for Fl (0.02 μM) and RhB (1 μM) mixture. Solid and open symbols represent phase and modulation, respectively. Corresponding fitting parameters are tabulated in Table 3.2.

Furthermore, the RhB lifetime of the LR7 was longer than that used in LR6, further supporting that NLLS analysis accommodates for Fl photobleaching by shortening the recovered RhB lifetime. In contrast, CR7 χ^2 improved in comparison to CR6. It is also of great significance to note that χ^2 for CR7 was much lower (0.89) compared to the LR7 (4.01), and the order within LR7 residuals in Figure 3.5a was absent within CR7 residuals in Figure 3.5b.

As a final examination, Fl and RhB lifetimes were kept fixed at CR1 values, and the fractions were left to vary (LR8 and CR8). NLLS analysis yielded more acceptable χ^2 values with a lower Fl fractional contribution for the LR as compared to set 6 results discussed above (Table 3.2 and Figure 3.5). However, the LR8 fit worsened as compared to that of the LR1, where all parameters were allowed to float. These results suggest that LR data can be fitted well with NLLS analysis when all parameters are left to vary; however, recovered values may not represent the right answer. The NLLS analysis adjusted the fractions (or lifetimes) to give the best fit possible when the lifetimes (or fractions) were fixed at what were believed to be the correct values. In both cases, the resulting fits were worse than the fits when all parameters were allowed to vary. Problems associated with fitting LR data were eliminated as seen in the CR analyses presented in Table 3.2.

In general, the CR residuals randomly vibrated around zero in both phase and modulation data, while structured residuals could be noted for the LR. Larger errors in residual plots of the CR observed at higher frequencies may be ascribed to instrumental limitations. The largest standard deviations within the five averages recorded at each frequency were observed at higher modulation frequencies for all LR and CR experiments. In addition, it should be noticed that segments 1 and 4 were intermixed for interrogating the high frequency region of the CR (Figure 3.3a). Segment 4 is expected to give the largest amount of noise because it has the shortest

integration time. It can also be noticed that the small remaining effect is the greatest at highest frequencies although the segmentation and recombination method nearly eliminated the effect of photobleaching in the simulated data (Figure 3.3b). These errors, taken together, resulted in the largest residuals at highest frequencies in the CR. The fact that the errors oscillate around zero provides that no systematic errors were presented.

3.3.3 Application to Pyrene Association with SRFAR

- **Experimental Data**

Fluorescence lifetime measurements via frequency segmentation and recombination were also applied to a more complex system consisting of pyrene and SRFAR mixture. Individual components (pyrene and SRFAR) lifetimes in argon degassed aqueous solutions were measured and the results are summarized in Table 3.3.

Table 3.3 Recovered fluorescence lifetimes and fractional contributions obtained from NLLS analyses of pyrene, SRFAR, and their mixture. The f subscripts indicate the fits where SRFAR lifetimes were fixed during NLLS analyses. The F subscripts denote the fits where both SRFAR fractional intensity contributions and lifetimes were fixed during NLLS analyses. Bolded black parameters are fixed values: same as Figures 3.6, 3.7, and 3.8.

Model	Float	Set	α_{SRFAR}	α_1	τ_1 (ns)	α_2	τ_2 (ns)	α_3	τ_3 (ns)	α_4	τ_4 (ns)	χ^2
D	1	Pyrene	-	1.000	193.74	-	-	-	-	-	-	0.72
D	1	SRFAR	-	1.000	3.07	-	-	-	-	-	-	466.59
DD	3	SRFAR	-	0.472	1.05	0.528	7.61	-	-	-	-	12.05
DDD	5	SRFAR	-	0.281	0.57	0.483	3.43	0.236	13.71	-	-	1.93
D	1	LR	-	1.000	6.66	-	-	-	-	-	-	1987.38
D	1	CR	-	1.000	6.74	-	-	-	-	-	-	1936.79
DD	3	LR	-	0.531	2.12	0.469	138.55	-	-	-	-	87.29
DD	3	CR	-	0.531	2.16	0.469	131.69	-	-	-	-	84.07
DDD	5	LR	-	0.266	0.90	0.335	6.38	0.399	178.93	-	-	3.78
DDD	5	CR	-	0.254	0.88	0.345	6.11	0.401	168.89	-	-	4.78
DDDD	7	LR	-	0.162	0.51	0.239	2.75	0.208	9.21	0.391	183.77	2.80
DDDD	7	CR	-	0.173	0.56	0.281	3.34	0.157	11.02	0.389	175.84	3.55
$D_fD_fD_fD$	4	LR	-	0.179	**0.57**	0.297	**3.43**	0.142	**13.71**	0.382	189.27	3.02
$D_fD_fD_fD$	4	CR	-	0.172	**0.57**	0.306	**3.43**	0.140	**13.71**	0.382	179.76	3.57
$(D+D+D)_FD$	2	LR	0.622	**0.281**	**0.57**	**0.483**	**3.43**	**0.236**	**13.71**	0.378	192.14	3.17
$(D+D+D)_FD$	2	CR	0.621	**0.281**	**0.57**	**0.483**	**3.43**	**0.236**	**13.71**	0.379	181.89	3.55

The pyrene lifetime of 193.74 ns (Figure 3.6) is in consistency with other reports of pyrene lifetime in an aqueous degassed solution.[26, 27] The triple-exponential decay (DDD) model was used to fit the data for the argon degassed SRFAR solution is in agreement with multi-exponential lifetimes reported for dissolved organic materials.[28-30]

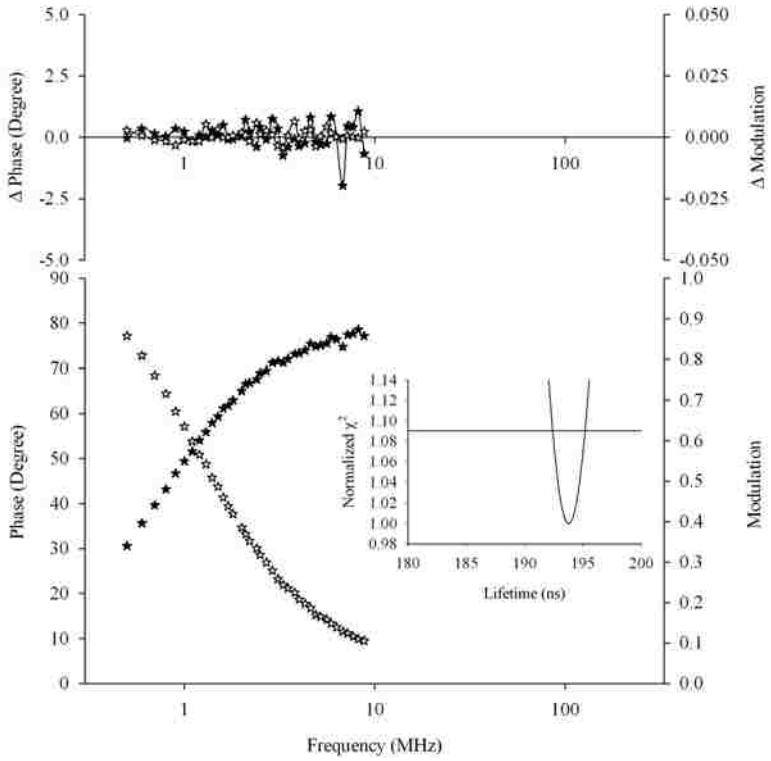

Figure 3.6 Experimental frequency-domain data of pyrene (0.1 ppm) in argon degassed aqueous solution and normalized χ^2 surface for NLLS analysis of the experimental data. Solid and open symbols, in frequency-domain data, represent phase and modulation, respectively. Horizontal dashed line: one standard deviation from the minima of the χ^2 surface. Corresponding fitting parameters are tabulated in Table 3.3.

A series of different discrete models used in NLLS analyses of experimental LR and CR data for the pyrene-SRFAR mixture are reported in Table 3.3. Models containing four lifetime components were found to give the most reasonable fits. It is expected that the mixture can display a minimum of four lifetimes comprising of the three SRFAR and one pyrene lifetime. As

with the dye validation study, both LR and CR yielded different results. The validation study demonstrated that photobleaching of one component in a multi-component mixture gave misleading results for both lifetimes and fractions for analysis of the LR. Generally, the NLLS analyses of the pyrene and SRFAR mixture produced longer pyrene lifetimes for the LR compared to CR for all models evaluated (Table 3.3). Analyses using a four-exponential decay (DDDD) model, allowed a total of 7 fitting parameters to float, yielded nearly equal pyrene fractional contributions for both LR and CR. In addition, both SRFAR fractions and lifetimes of the CR were different from those obtained with the LR (Figure 3.7a). Similar pyrene fractions were likely the result of the large number of floating parameters allowing SRFAR components to be adjusted to fit the LR data, as SRFAR lifetimes obtained from the CR were nearly the same as those for SRFAR individual component.

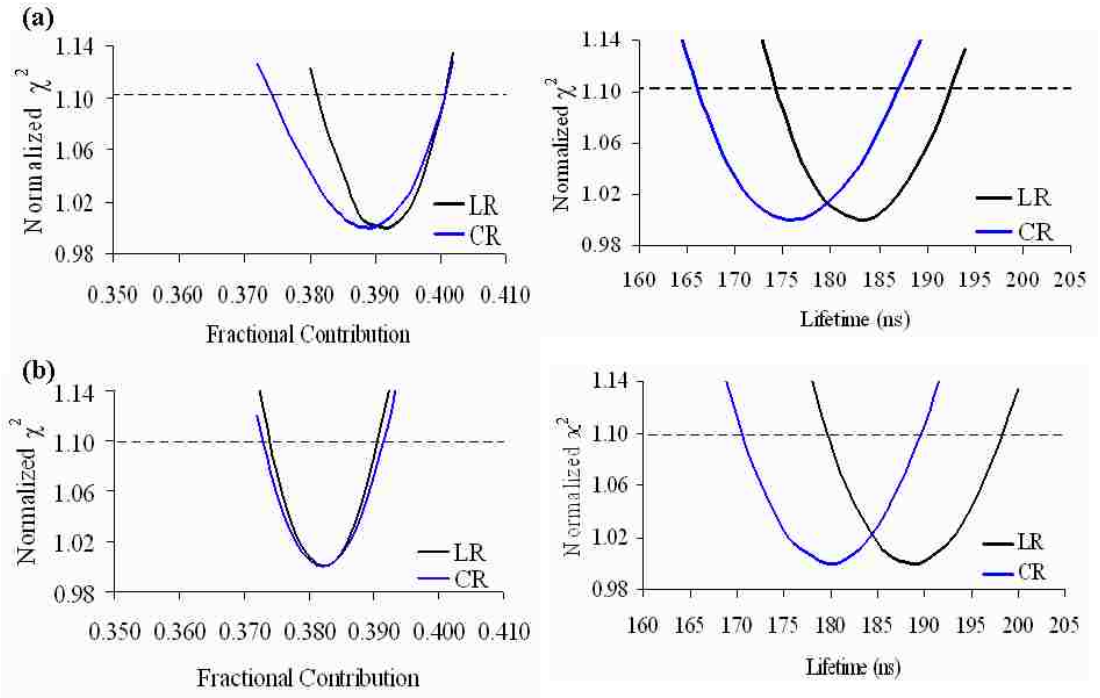

Figure 3.7 (a) Normalized χ^2 surfaces of NLLS analyses for the pyrene and SRFAR mixture experimental data for (a) DDDD and (b) $D_fD_fD_fD$ models. Horizontal dashed lines: one standard deviation from the minima of the χ^2 surface. Corresponding fitting parameters are tabulated in Table 3.3.

A second simpler model, $D_fD_fD_fD$, where SRFAR lifetimes were fixed (f) reducing the number of variable parameters to 4, recovered similar pyrene and SRFAR fractions for the LR and CR, but the floating SRFAR fractions again dominated the fit as indicated above (Figure 3.7b).

The final model, $(D+D+D)_FD$, resolved this problem. In this model, both SRFAR fractions and lifetimes were fixed (F) at measured values for SRFAR alone within the sum of three-exponential decays $(D+D+D)_F$ and allowed the pyrene fraction and lifetime to float as a discrete (D) component model. The $(D+D+D)_FD$ model minimized the total number of floating parameters to two. It was considered to be the most reasonable model, assuming that SRFAR is a single component and independent of pyrene's presence within a two component system. The experimental frequency-domain data for both LR and CR were fitted well with reasonable residual plots (Figure 3.8a). The NLLS analyses of this model resulted in different lifetimes for both runs. The recovered pyrene lifetime (192.14 ns) with the LR was approximately 10 ns longer than that (181.89 ns) of the CR. The pyrene fraction was slightly lower for the LR as compared to the CR indicating that pyrene photobleaching may be responsible for the different results.

These results are also supported by normalized χ^2 surfaces for the NLLS analysis of the experimental data (Figure 3.8b). A close examination of Figure 3.8b reveals that recovered pyrene lifetimes and fractional contributions were varied between both runs. Thus, one can conclude that the difference on the measured pyrene lifetime between both runs can easily complicate the interpretation of the fluorescence quenching mechanism of pyrene in the presence of SRFAR. In addition, it can be noticed that frequency domain fluorescence lifetime measurements using frequency segmentation and recombination minimize the effects of photobleaching in a multi-component system and provide more reliable results.

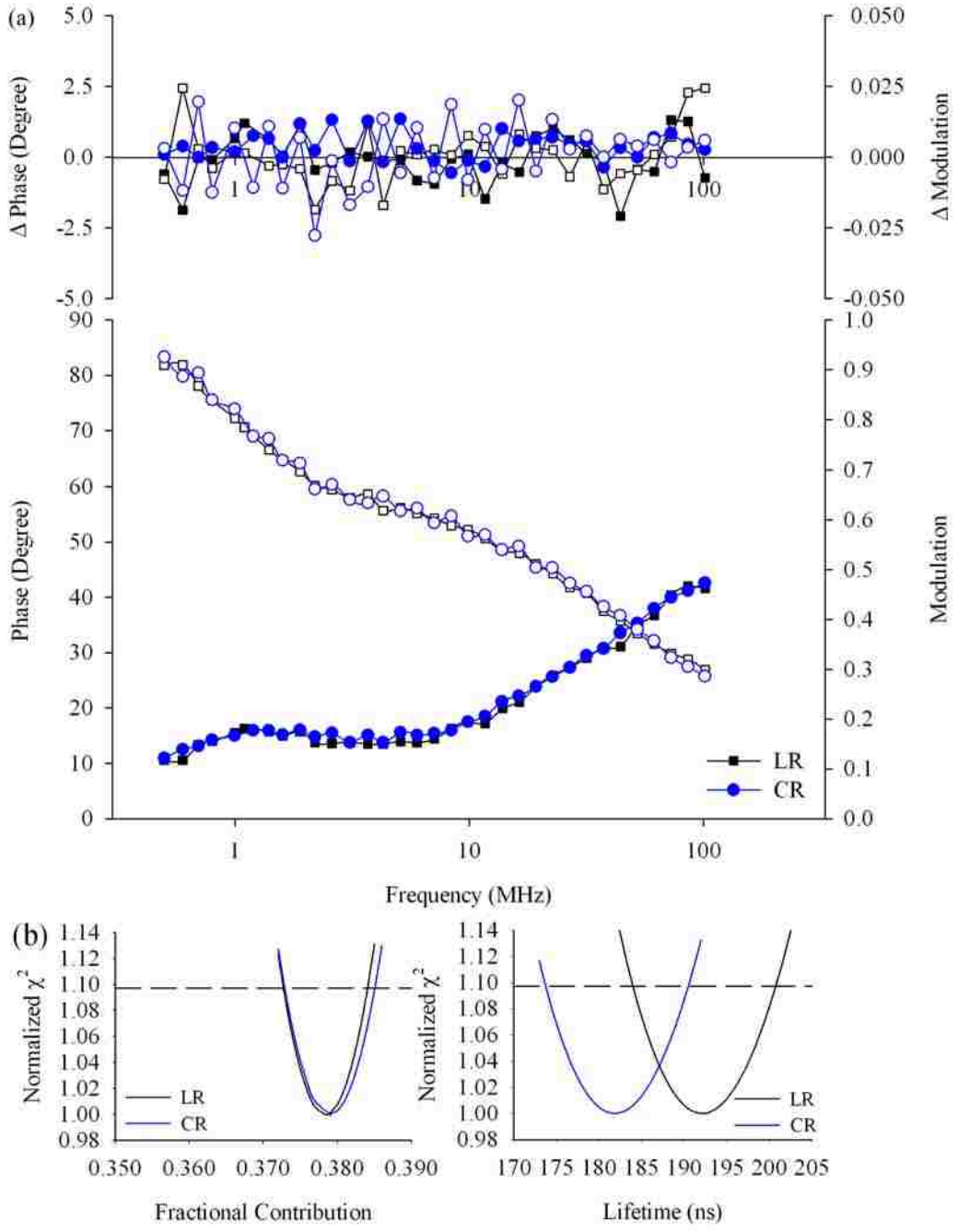

Figure 3.8 (a) Experimental frequency-domain data and NLLS fits for pyrene (0.04 ppm) and SRFAR (12 ppm) mixture. Solid and open symbols represent phase and modulation, respectively. (b) Normalized χ^2 surfaces for NLLS analyses of the experimental data. Horizontal dashed lines: one standard deviation from the minima of the χ^2 surface. Corresponding fitting parameters are tabulated in Table 3.3.

- **Simulations**

These finding were also supported by the results obtained from simulations indicating that a reduction in the pyrene intensity between the beginning and end of the LR experiment resulted in differences between the LR and CR experimental data described above. Assuming the results from the $(D+D+D)_FD$ analysis of the CR experiment (Table 3.3) most closely represents the true values, these values were used to simulate this system in the same manner as previous simulations. For the frequency domain simulation study of this system, the fluorescence intensity of pyrene was assumed to decrease linearly by 20%, while the fluorescence intensity of SRFAR remains constant after 29.25 min exposure to light. Pyrene initial fractional contribution and lifetime used in the simulation for the mixture were 0.379 and 181.89 ns, respectively, which is equal to measured values of the CR (Table 3.3). The initial fractional contribution of SRFAR in the mixture was assumed to be 0.621, which is consistent with the measured value. SRFAR fractional contributions and lifetimes in the mixture were assumed to be 0.281, 0.483, 0.236 and 0.57, 3.43, 13.71 ns, respectively, which are equivalent to reported values of the individual component. The phase and modulation data were simulated taking into account the changing fractional intensity contributions of the LR.

For the CR, frequency domain data were simulated with a reduced change of the fractions at each frequency. Figure 3.9a shows the results of the simulation for LR, CR, and unbleached run data. An examination of Figure 3.9a reveals that there was a mismatch between the unbleached and LR of the phase and modulation data. In contrast, the CR data matched more closely the unbleached phase and modulation data. In addition, one can observe that the experimental errors resulted from the LR is greater than typical experimental errors, while are greatly reduced in the CR.

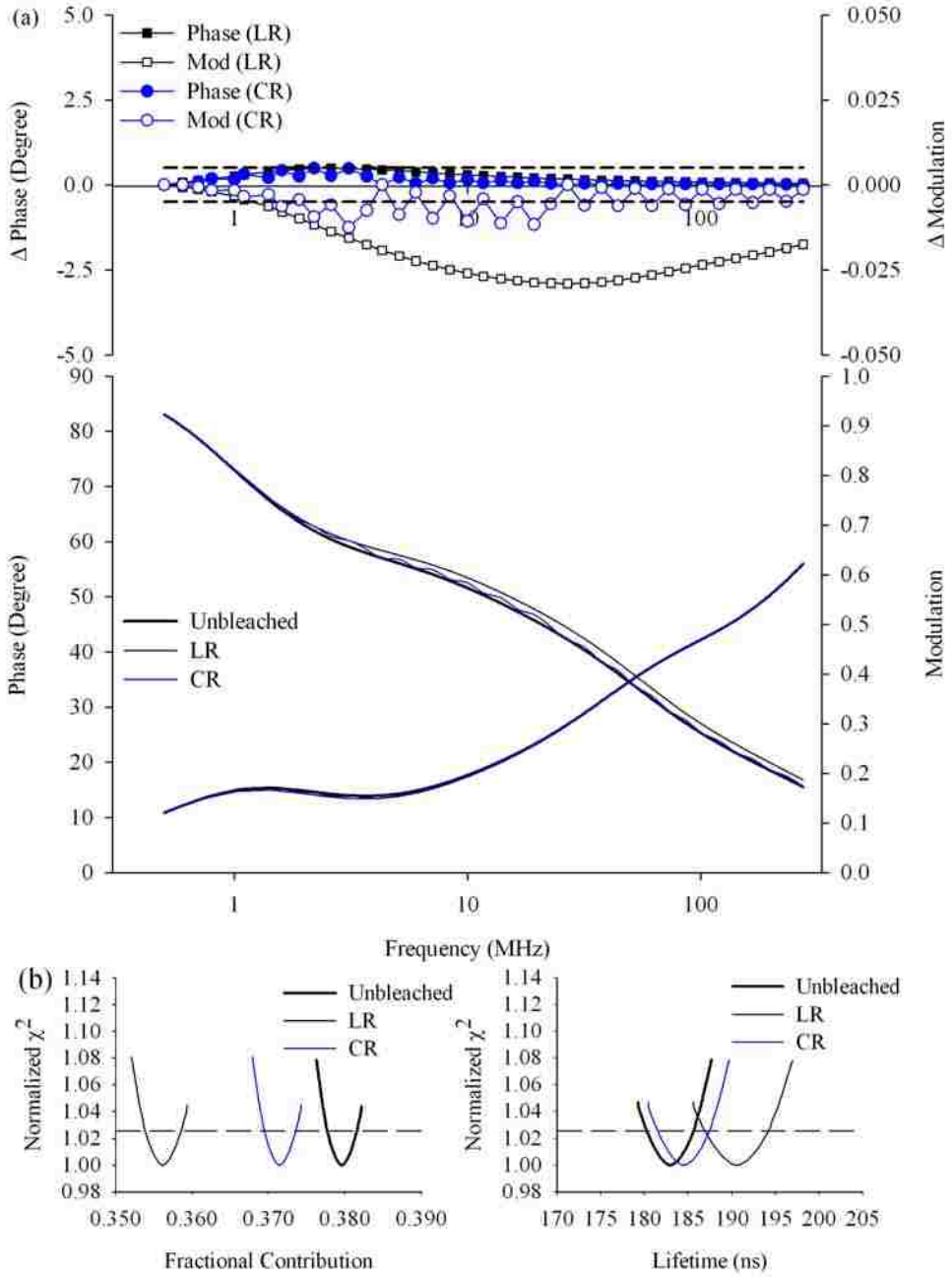

Figure 3.9 (a) Simulated frequency-domain LR and CR data for pyrene (τ= 181.89 ns, $\alpha_{initial}$= 0.379) and SRFAR ($\alpha_{initial}$= 0.621, τ_1= 0.57 ns, α_1= 0.281, τ_2= 3.43 ns, α_2= 0.483, τ_3= 13.71 ns, α_3= 0.236) mixture. Solid and open symbols represent phase and modulation, respectively. Dashed lines in the residual plot represent the 0.5° and 0.005 modulation error values used in the NLLS analyses**.** (b) Normalized χ^2 surfaces for NLLS analyses of the simulated data after 0.5 degree and 0.005 random noise was added. Horizontal dashed lines: one standard deviation from the minima of the χ^2 surface. Corresponding fitting parameters are tabulated in Table 3.4.

Table 3.4 Fluorescence lifetimes and fractional contributions obtained from NLLS analyses for the $(D+D+D)_FD$ model of pyrene and SRFAR mixture after adding different random noises of equivalent magnitude. UB denote the Unbleached run. N represents the added noise. Bolded black parameters are fixed values: same as Figure 3.9.

Set	α_{SRFAR}	α_1	τ_1 (ns)	α_2	τ_2 (ns)	α_3	τ_3 (ns)	α_4	τ_4 (ns)	χ^2
UB N1	0.6208	**0.28**	**0.57**	**0.48**	**3.43**	**0.24**	**13.71**	0.3792	183.5811	1.3065
UB N2	0.6206	**0.28**	**0.57**	**0.48**	**3.43**	**0.24**	**13.71**	0.3794	182.7638	1.4342
UB N3	0.6206	**0.28**	**0.57**	**0.48**	**3.43**	**0.24**	**13.71**	0.3794	183.0103	1.3420
UB N4	0.6198	**0.28**	**0.57**	**0.48**	**3.43**	**0.24**	**13.71**	0.3802	181.0744	1.2725
UB N5	0.6208	**0.28**	**0.57**	**0.48**	**3.43**	**0.24**	**13.71**	0.3792	184.2694	1.2819
UB N6	0.6210	**0.28**	**0.57**	**0.48**	**3.43**	**0.24**	**13.71**	0.3790	183.5453	1.3919
UB N7	0.6196	**0.28**	**0.57**	**0.48**	**3.43**	**0.24**	**13.71**	0.3804	181.7271	1.3030
UB N8	0.6213	**0.28**	**0.57**	**0.48**	**3.43**	**0.24**	**13.71**	0.3787	183.6320	1.3385
UB N9	0.6191	**0.28**	**0.57**	**0.48**	**3.43**	**0.24**	**13.71**	0.3809	182.6028	1.3085
UB N10	0.6202	**0.28**	**0.57**	**0.48**	**3.43**	**0.24**	**13.71**	0.3798	182.7667	1.2440
Average	0.6204	0.28	0.57	0.48	3.43	0.24	13.71	0.3796	182.8973	1.3223
LR N1	0.6427	**0.28**	**0.57**	**0.48**	**3.43**	**0.24**	**13.71**	0.3573	190.7667	2.1746
LR N2	0.6448	**0.28**	**0.57**	**0.48**	**3.43**	**0.24**	**13.71**	0.3552	192.9314	1.9826
LR N3	0.6448	**0.28**	**0.57**	**0.48**	**3.43**	**0.24**	**13.71**	0.3552	192.2744	2.1280
LR N4	0.6445	**0.28**	**0.57**	**0.48**	**3.43**	**0.24**	**13.71**	0.3555	193.2360	2.0078
LR N5	0.6432	**0.28**	**0.57**	**0.48**	**3.43**	**0.24**	**13.71**	0.3568	190.5144	1.9914
LR N6	0.6425	**0.28**	**0.57**	**0.48**	**3.43**	**0.24**	**13.71**	0.3575	187.7311	1.8975
LR N7	0.6454	**0.28**	**0.57**	**0.48**	**3.43**	**0.24**	**13.71**	0.3546	190.9960	1.6453
LR N8	0.6430	**0.28**	**0.57**	**0.48**	**3.43**	**0.24**	**13.71**	0.3570	189.3301	1.9278
LR N9	0.6436	**0.28**	**0.57**	**0.48**	**3.43**	**0.24**	**13.71**	0.3564	189.4139	2.1600
LR N10	0.6433	**0.28**	**0.57**	**0.48**	**3.43**	**0.24**	**13.71**	0.3567	187.5523	1.9304
Average	0.6438	0.28	0.57	0.48	3.43	0.24	13.71	0.3562	190.4746	1.9845
CR N1	0.6272	**0.28**	**0.57**	**0.48**	**3.43**	**0.24**	**13.71**	0.3728	181.3705	1.4083
CR N2	0.6281	**0.28**	**0.57**	**0.48**	**3.43**	**0.24**	**13.71**	0.3719	184.7355	1.5217
CR N3	0.6286	**0.28**	**0.57**	**0.48**	**3.43**	**0.24**	**13.71**	0.3714	184.5163	1.5058
CR N4	0.6289	**0.28**	**0.57**	**0.48**	**3.43**	**0.24**	**13.71**	0.3711	186.1251	1.5661
CR N5	0.6293	**0.28**	**0.57**	**0.48**	**3.43**	**0.24**	**13.71**	0.3707	186.6040	1.3365
CR N6	0.6284	**0.28**	**0.57**	**0.48**	**3.43**	**0.24**	**13.71**	0.3716	182.8157	1.5438
CR N7	0.6285	**0.28**	**0.57**	**0.48**	**3.43**	**0.24**	**13.71**	0.3715	183.6359	1.5385
CR N8	0.6290	**0.28**	**0.57**	**0.48**	**3.43**	**0.24**	**13.71**	0.3710	184.9026	1.5374
CR N9	0.6283	**0.28**	**0.57**	**0.48**	**3.43**	**0.24**	**13.71**	0.3717	184.7760	1.5713
CR N10	0.6285	**0.28**	**0.57**	**0.48**	**3.43**	**0.24**	**13.71**	0.3715	184.6661	1.5493
Average	0.6285	0.28	0.57	0.48	3.43	0.24	13.71	0.3715	184.4148	1.5079

The NLLS analyses of simulated data files were performed after addition of random noise (0.5 degree and 0.005). These analyses allowed the investigation of how pyrene photobleaching would affect the recovered parameters in a LR experiment. The simulation was demonstrated 10

times with different random noise of equivalent magnitude added to each simulation. Recovered parameters for unbleached, LR, and CR simulations using the $(D+D+D)_FD$ model are summarized in Table 3.4. This table contains the results of 10 simulated data files for each run. The results obtained from NLLS analyses of all files within each set are plotted as the χ^2 surfaces shown in Figure 3.9b. Figure 3.9b shows that the pyrene lifetime and fractional intensity contribution of the CR matched more closely those of the unbleached data as compared to the LR. However, a larger magnitude of the pyrene fraction difference between both runs was observed for the simulated data as compared to the NLLS analysis of the experimental data. Furthermore, pyrene lifetimes recovered from the LR were approximately 10 ns longer than those recovered from the CR, while the pyrene fractions were lower for both experimental and simulated data. The agreement between the experimental and simulated data is shown by the similarity of Figures 3.8b and 3.9b. Together, the experimental and simulated LR and CR data illustrate that a decrease in the pyrene intensity over the course of the LR measurement affect the recovered parameters.

3.4 Conclusion

The frequency segmentation and recombination method was demonstrated through both simulation of a two component dye system and comparison of experimental data collected in traditional and segmented fashion. The results displayed clear evidence that the frequency segmentation and recombination experiment of the dye system reduced errors that result from a changing fractional intensity contribution in a multi-component system. NLLS analyses of the dye mixture further confirmed these findings. Better fits, more reasonable χ^2 values, and more random residual plots were obtained from the CR compared to the LR.

In addition, the utility of frequency segmentation and recombination was implemented to both simulations of a more complex pyrene and SRFAR system and comparison of experimental data collected in traditional and segmented fashion. Recovered pyrene fractional contributions and lifetimes differentiated between the LR and CR, confirming that there was a decrease in pyrene intensity over the course of the experiment. These results suggested that the effect of photobleaching, pyrene wall adsorption, or both within multi-component systems may be the cause of the alteration in measured pyrene lifetimes and fractional intensity contributions, which is more pronounced with the LR. On the other hand, the frequency segmentation and recombination experiment appeared to minimize these potential factors, as one can conclude that the alteration on measured lifetimes for both runs can complicate the interpretation of the pyrene quenching mechanism with SRFAR. Finally, the results obtained from both dyes and pyrene with SRFAR systems demonstrated considerable promise for use of segmented frequency-domain lifetime measurements in a range of applications, including biological and environmental.

3.5 References

(1) Lakowicz, J. R. *Principles of Fluorescence Spectroscopy*, Second ed.; Kluwer Academic/Plenum Press: New York, 1999.

(2) Ingle, J. D.; Crouch, S. R. *Spectrochemical Analysis*, First ed.; Prentice-Hall, Inc.: Upper Saddle River, 1988.

(3) Sharma, A., Schulman, Stephen G. *Introduction to Fluorescence Spectroscopy*, First ed.; John Wiley and Sons, Inc.: New York, 1999.

(4) Van den Engh, G.; Farmer, C. *Cytometry* **1992**, *13*, 669-677.

(5) Sandinson, D. R.; R. M. Williams; K. S. Wells; J. Strickler; Webb, W. W. In *In Handbook of Biological Confocal Microscopy,* First ed.; Pawley, J. B., Ed.; Plenum Press: New York, 1995, pp 39-53.

(6) Nakamura, K.; Kowaki, T.; Scully, A. D.; Hirayama, S. *J. Photochem. Photobiol., A* **1997**, *104*, 141-149.

(7) Druzhinin, S. I.; Galievsky, V. A.; Zachariasse, K. A. *J. Phys. Chem. A* **2005**, *109*, 11213-11223.

(8) Bopp, M. A.; Jia, Y.; Li, L.; Cogdell, R. J.; Hochstrasser, R. M. *Proc. Natl. Acad. Sci. U. S. A.* **1997**, *94*, 10630-10635.

(9) Marcu, L.; Grundfest, W. S.; Maarek, J.-M. I. *Photochem. Photobiol.* **1999**, *69*, 713-721.

(10) Chen, Y.; Periasamy, A. *Proc. SPIE-Int. Soc. Opt. Eng.* **2004**, *5323*, 431-439.

(11) Rueck, A.; Dolp, F.; Huelshoff, C.; Hauser, C.; Scalfi-Happ, C. *Proc. SPIE-Int. Soc. Opt. Eng.* **2005**, *5700*, 182-187.

(12) Connelly, J. P.; Botchway, S. W.; Kunz, L.; Pattison, D.; Parker, A. W.; MacRobert, A. J. *J. Photochem. Photobiol., A* **2001**, *142*, 169-175.

(13) Fujimoto, D.; Akiba, K.; Nakamura, N. *Biochem. Biophys. Res. Commun.* **1977**, *76*, 1124-1129.

(14) Deyl, Z.; Macek, K.; Adam, M.; Vancikova *BBA-Protein Struct.* **1980**, *625*, 248-254.

(15) Laor, Y.; Rebhun, M. *Environ. Sci. Technol.* **2002**, *36*, 955-961.

(16) Tiller, C. L.; Jones, K. D. *Environ. Sci. Technol.* **1997**, *31*, 424-429.

(17) Backhus, D. A.; Golini, C.; Castellanos, E. *Environ. Sci. Technol.* **2003**, *37*, 4717-4723.

(18) Chen, S.; Inskeep, W. P.; Williams, S. A.; Callis, P. R. *Environ. Sci. Technol.* **1994**, *28*, 1582-1588.

(19) Holbrook, R. D.; Love, N. G.; Novak, J. T. *Environ. Sci. Technol.* **2004**, *38*, 4987-4994.

(20) Brustlein, S.; Devaux, F.; Wacogne, B.; Lantz, E. *Laser Phys.* **2004**, *14*, 238-242.

(21) Lakowicz, J. R.; Szmacinski, H.; Nowaczyk, K.; Berndt, K. W.; Johnson, M. *Anal. Biochem.* **1992**, *202*, 316-330.

(22) Lakowicz, J. R.; Szmacinski, H.; Nowaczyk, K.; Lederer, W. J.; Kirby, M. S.; Johnson, M. L. *Cell Calcium* **1994**, *15*, 7-27.

(23) Murata, S.-i.; Herman, P.; Lin, H.-J.; Lakowicz, J. R. *Cytometry* **2000**, *41*, 178-185.

(24) Beechem, J. M. *Chem. Phys. Lipids* **1989**, *50*, 237-251.

(25) Beechem, J. M.; Gratton, E. *Proc. SPIE-Int. Soc. Opt. Eng.* **1988**, *909*, 70-81.

(26) Nelson, G.; Patonay, G.; Warner, I. M. *Anal. Chem.* **1988**, *60*, 274-279.

(27) Danielsen, K. M.; Chin, Y.-P.; Buterbaugh, J. S.; Gustafson, T. L.; Traina, S. J. *Environ. Sci. Technol.* **1995**, *29*, 2162-2165.

(28) Cook, R. L.; Langford, C. H. *Anal. Chem.* **1995**, *67*, 174-180.

(29) Hemmingsen, S. L.; McGown, L. B. *Appl. Spectrosc.* **1997**, *51*, 921-929.

(30) Hewitt, J. D.; McGown, L. B. *Appl. Spectrosc.* **2003**, *57*, 256-265.

CHAPTER 4

FREQUENCY-DOMAIN FLUORESCENCE LIFETIME MEASUREMENTS VIA FREQUENCY SEGMENTATION AND RECOMBINATION FOR PYRENE ASSOCIATION WITH DISSOLVED HUMIC MATERIALS

4.1 Introduction

Fluorescence lifetime measurements are one of the most definitive tools in fluorescence spectroscopy.[1] Time-resolved fluorescence measurements provide very useful information such as the rate of excited-state reactions, energy transfer between a donor and acceptor molecules, and fluorescence quenching in a bimolecular process. For example, time-resolved measurements are used for distinguishing static, a non-fluorescent complex formation, from dynamic, collision between the fluorophore and quencher, quenching. In fluorescence lifetime measurements, the decay time of unbound fluorophores does not decrease when static quenching takes place, formation of ground-state complexes. This is due to the fact that only unbound fluorophores can be observed in a fluorescence experiment. In contrast, dynamic quenching decreases the decay time by acting on the entire excited-state population.

In addition, fluorescence lifetime measurements are widely used in different applications of fluorescence. For example, the association mechanism between hydrophobic organic compounds (HOC) and dissolved humic materials (DHM) continues to be of major concern in the environmental field.[2-4] Many studies have indicated that this association is constrained by the contaminant hydrophobicity, chemical characteristic of DHM, and solution chemistry.[5-9] In recent years, there has also been a large discussion on the sorption mechanism of HOC to DHM,[10-15] and a series of proposed models has been investigated. None of these models, however, has been universally accepted, as exemplified by the "glassy/rubber" (hard/soft or condensed/non-condensed) model, and the enthusiastic discussion of this model that has taken

place in the literature. But, one point that was almost universally agreed upon was that HOC sorb into aromatic domains within DHM.[6, 7, 16-20] However, this point of view has become under question, and aliphatic domains within DHM have been implied in the sorption of HOC based on recent studies.[21-23]

In general, static quenching of HOC with DHM has always been assumed based on a steady-state fluorescence technique.[4, 24] However, dynamic quenching has also been implied by other studies.[17, 25, 26] In addition, it has been reported in the literature that photobleaching of HOC with DHM may be one of the major errors affecting the observed probe's fluorescence.[2-4] In one such example, Tiller and Jones[3] have indicated that oxygen and long exposure to radiation can overestimate association constants of HOC with DHM. Other studies have used time-resolved fluorescence measurements in hopes of resolving the debate over the quenching mechanism of HOC with DHM.[16, 27] While time-resolved fluorescence measurements addressed some problems associated with fluorescence steady-state technique, it did not completely resolve the effect of photobleaching. Thus, the seemingly simple question of whether the quenching mechanism of HOC with DHM is static, dynamic, or both is still open. In addition to the effect of photobleaching, HOC adsorption to cell walls has also been reported to be one of encountered problems when measuring fluorescence.[28-30] In fact, adsorption losses of HOC have been indicated to cause a decrease in the fluorescence intensity, resulting in a significant increase in quenching of HOC.[3] Thus, this can complicate the interpretation of fluorescence lifetime results.

This study presents an application of segmented frequency-domain fluorescence lifetime measurements, previously described in Chapter 3 of this dissertation, to the association of pyrene with DHM. Frequency-domain lifetime measurements using a frequency segmentation and recombination method were used to evaluate the chemical effect of DHM on the association

behavior with pyrene, a common fluorescence probe. In addition, experimental considerations, such as the effect of oxygen, wall adsorption, and photobleaching within this multi-component system on changing recovered lifetime parameters, were addressed in order to carefully evaluate the quenching mechanism of pyrene with DHM.

4.2 Experimental

4.2.1 Materials and Reagents

Pyrene (≥ 99%) was purchased from Sigma-Aldrich (Milwaukee, WI) and used as received. Suwannee River fulvic acid reference (SRFAR), Leonardite humic acid standard (LHAS), and Florida peat humic acid standard (FPHAS), were obtained from the International Humic Substances Society (IHSS), Department of Soil, Water, and Climate, University of Minnesota (St. Paul, MN). The peat derived Amherst humic acid (AHA) and a chemically bleached Amherst humic acid (BAHA) were gifts from Professor Baoshan Xing, Department of Plant and Soil Sciences, University of Massachusetts (Amherst, MA). Ethanol and sodium hydroxide were purchased from Fisher Scientific (Fair Lawn, NJ).

4.2.2 Sample Preparation

For the pyrene and DHM study, a stock solution of LHAS (FPHAS, AHA, or BAHA) was prepared in 18.2 MΩ·cm distilled deionized water by first dissolving an appropriate amount of the LHAS (FPHAS, AHA, or BAHA) solution with the aide of a few drops of 0.1 M NaOH and then neutralizing the solution with 0.1 M HCl. The SRFAR stock solution was also prepared in the same manner as well as other DHM but without any addition of NaOH. Pyrene stock solution was also prepared in ethanol. All stock solutions were stored in the dark at 4 °C. A standard reference solution of 0.1 ppm pyrene –below the water solubility limit– was prepared in 18.2 MΩ·cm distilled deionized water by first aliquoting appropriate amounts of pyrene stock

solution and then evaporating ethanol to dryness with nitrogen gas. Standard reference solutions of 12, 16, 20, and 24 ppm DHM were also prepared in 18.2 MΩ·cm distilled deionized water. Pyrene with DHM mixture containing 0.04 ppm pyrene and 0, 12, 16, 20, and 24 ppm DHM were prepared at the same experimental conditions of the standard reference solutions and stored in the dark at 4 °C. Mixtures were allowed to equilibrate in the dark for at least seven days. Solutions were allowed to equilibrate overnight in a quartz fluorometer cell with septum cap and rinsed with fresh solutions prior to fluorescence measurements to reduce losses of pyrene to the cell wall. For such deoxygenated systems, all solutions of pyrene and DHM individual components and their mixture were purged using an argon gas for exactly 15 min, followed by 5 min of equilibration time in the sample compartment with a flow of argon gas over the course of fluorescence measurements. Fluorescence lifetime measurements were also collected for air-equilibrated samples of 24 ppm LHAS to evaluate the effect of oxygen on the recovered fractional intensity contributions and lifetimes of DHM.

4.2.3 Instrumentation

The total carbon (TC) content of DHM solutions was determined using a Shimadzu model TOC-5050A analyzer with an ASI-5000A autosampler (Kyoto, Japan). Steady-state and frequency-domain lifetime measurements were acquired using a Spex Fluorolog-3 spectrofluorometer (model FL3-22TAU3; Jobin Yvon, Edison, NJ, USA) equipped with a 450-W xenon lamp and R928P photomultiplier tube (PMT) detector. Fluorescence measurements were performed in a 10 mm quartz fluorometer cell with septum cap at room temperature. Pyrene, DHM, and their mixture were excited at 333 nm. For characterization of AHA and BAHA, three-dimensional excitation–emission matrices (EEM) fluorescence were collected. The bandwidths for both excitation and emission were 4 nm with an integration time of 0.2 s. The

excitation (Ex) wavelength range was fixed from 250 up to 550 nm in 5 nm intervals, while the emission (Em) wavelength was recorded over the region from 250 up to 600 nm in 1 nm intervals. Absorbance spectra were also collected for correction of both primary and secondary inner-filter effects using equation 1.16 in Chapter 1. Absorbance measurements were performed using the UV-3101PC (UV-VIS-NIR) scanning spectrophotometer (Shimadzu, Columbia, MD).

Frequency-domain fluorescence signals were passed through a 370 long-pass filter. Fluorescence lifetime measurements of pyrene and DHM individual components were performed through single long runs. For the single long run, the frequency range, in the logarithmic scale, was 0.5 up to 275.4 MHz, number of frequencies was 39, and integration time was 15 s. The frequency segmentation and recombination method consists of four individual segments, with a fresh solution used for each segment, and was applied to pyrene and DHM mixture. The number of frequencies for segments 1, 2, 3, and 4 is 13 (4.3-233.3 MHz), 12 (0.5-19.3 MHz), 6 (0.6-3.1 MHz), and 8 (26.9-275.4 MHz), respectively. The integration times were 15 s for segments 1 and 2, 30 s for segment 3, and 7.5 s for segment 4. The data from four segments were recombined onto a single frequency-domain data set for analysis. The number of averages for both long and combined runs was 5 and was calculated using the interleave function such that an average is generated each time the automated sample turret rotates. The experimental details of both single long and combined runs were fully described in Chapter 3 of this dissertation. Frequency-domain measurements were collected for all solutions versus ludox–a scatter reference solution– which shows a lifetime of zero. Frequency-domain phase and modulation decay profiles were analyzed using the Globals software package developed at the Laboratory for Fluorescence Dynamics at the University of Illinois at Urbana-Champaign.[31, 32] In non-linear least squares (NLLS) analysis, various initial guesses of parameters were applied to evaluate the stability of the χ^2 minimization.

Frequency domain data sets were well fit by appropriate models as indicated by visual inspection of residual plots as well as by χ^2 statistics. For consistency and ease of day-to-day data interpretation, fixed errors of 0.5° and 0.005 were used in NLLS analysis. The principles of time-resolved measurements and their data analysis were described in detail in Chapter 1 of this dissertation and will not be discussed further.

The cross polarization magic-angle spinning (CPMAS) ^{13}C NMR experiment of BAHA was performed using a Bruker Avance 400 MHz (9.3T) spectrometer equipped with a 4 mm H(F)XY probe with the standard pulse sequences from the Bruker pulse library. The CPMAS ^{13}C NMR spectrum was acquired at a sample spinning rate of 13 kHz, contact time of 2 ms, and a recycling delay of 1 s. The spectrum was also collected over a set period of time (24 hrs) and processed with 50 Hz linebroadening.

4.3 Results and Discussion

4.3.1 Fluorescence Lifetime Measurements of DHM

In order to obtain a better mechanistic understanding about the association behavior of pyrene and DHM, both recovered fractional contributions and lifetimes of DHM were first evaluated using fluorescence lifetime measurements. In addition, the effect of DHM concentration on the recovered fractional contributions and lifetimes was investigated for all DHM at different concentrations except for BAHA. The BAHA was obtained by bleaching the AHA using hypochlorous acid (HOCl), resulting in the removal of a large percentage of rigid aromatic moieties and retaining the aliphatic species. Therefore, BAHA has very low fluorescence as compared to other DHM, and its fluorescence lifetime measurements were performed at the highest concentration. In general, it is reasonable to expect that each humic displays only three lifetimes but different fractions at different concentrations. Therefore, the

NLLS analyses were obtained by allowing both the fractional intensity contributions and lifetimes to vary (V) but linking (L) the lifetimes at different concentrations of each humic (Figure 4.1). In general, it was previously indicated that humic materials have a three component system, consisting of three fractions and lifetimes.[33-35] In this study, the triple-exponential decay (DDD) model was also found to be consistent with multi-exponential lifetimes of the commercial DHM (SRFAR, LHAS, and FPHAS).

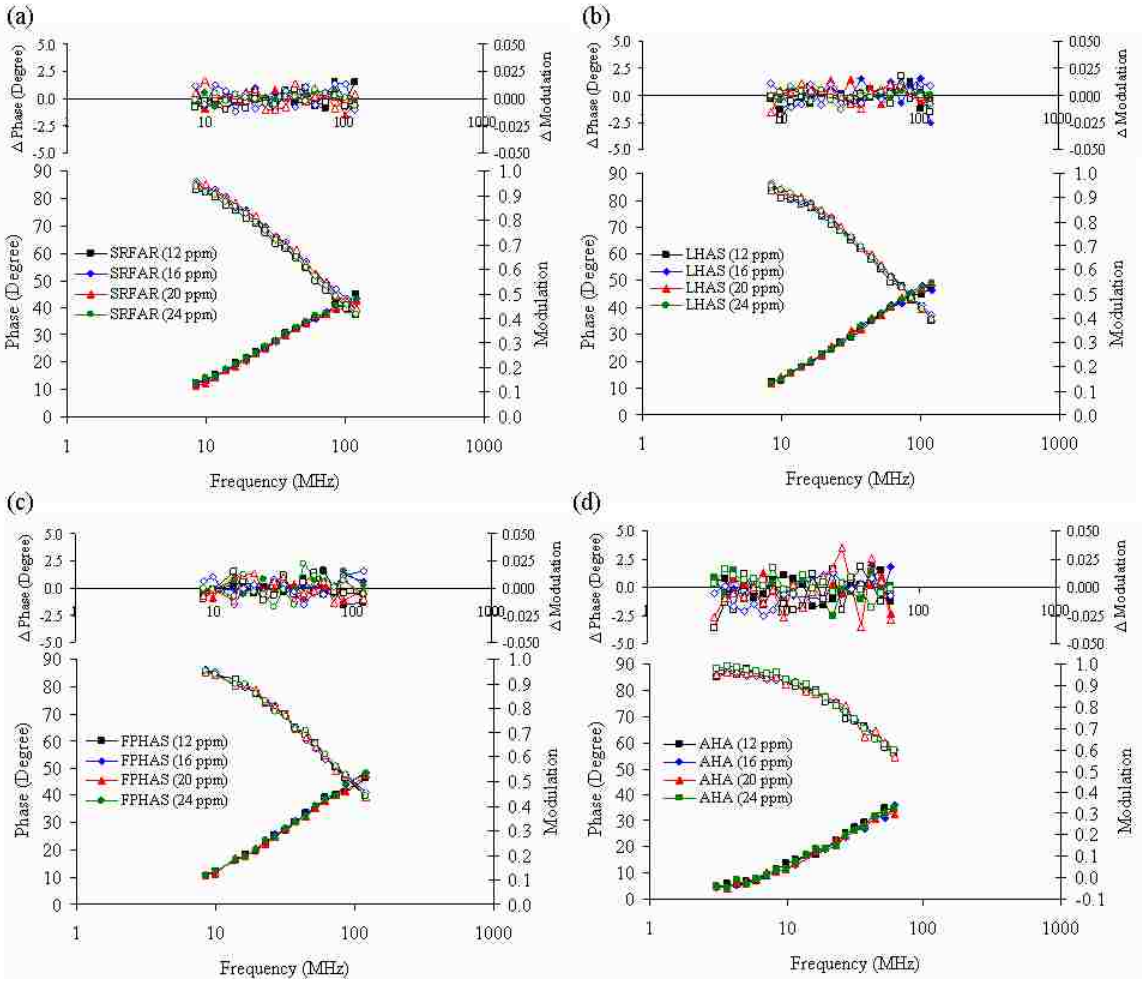

Figure 4.1 Frequency-domain data of (a) SRFAR, (b) LHAS, (c) FPHAS, and (d) AHA. The NLLS analyses were obtained by allowing both the fractional contributions and lifetimes to vary (V) but linking (L) the lifetimes of each humic at different concentrations. Solid and open symbols represent phase and modulation, respectively.

However, a two-exponential decay (DD) model for AHA was found to provide the best fitting parameters and was more stable and robust as compared to the DDD model. The DD model was also found to be the most appropriate model when fitting the data for 24 ppm BAHA. Excellent fits and residual plots were obtained for the commercial DHM and AHA (Figure 4.1). The instability of the DDD model for both AHA and BAHA is further confirmed by the χ^2 surfaces of NLLS analyses. For AHA and BAHA, it can be noted that the χ^2 surfaces of the DDD model are significantly wide (Figure 4.2), indicative to the instability of the DDD model.

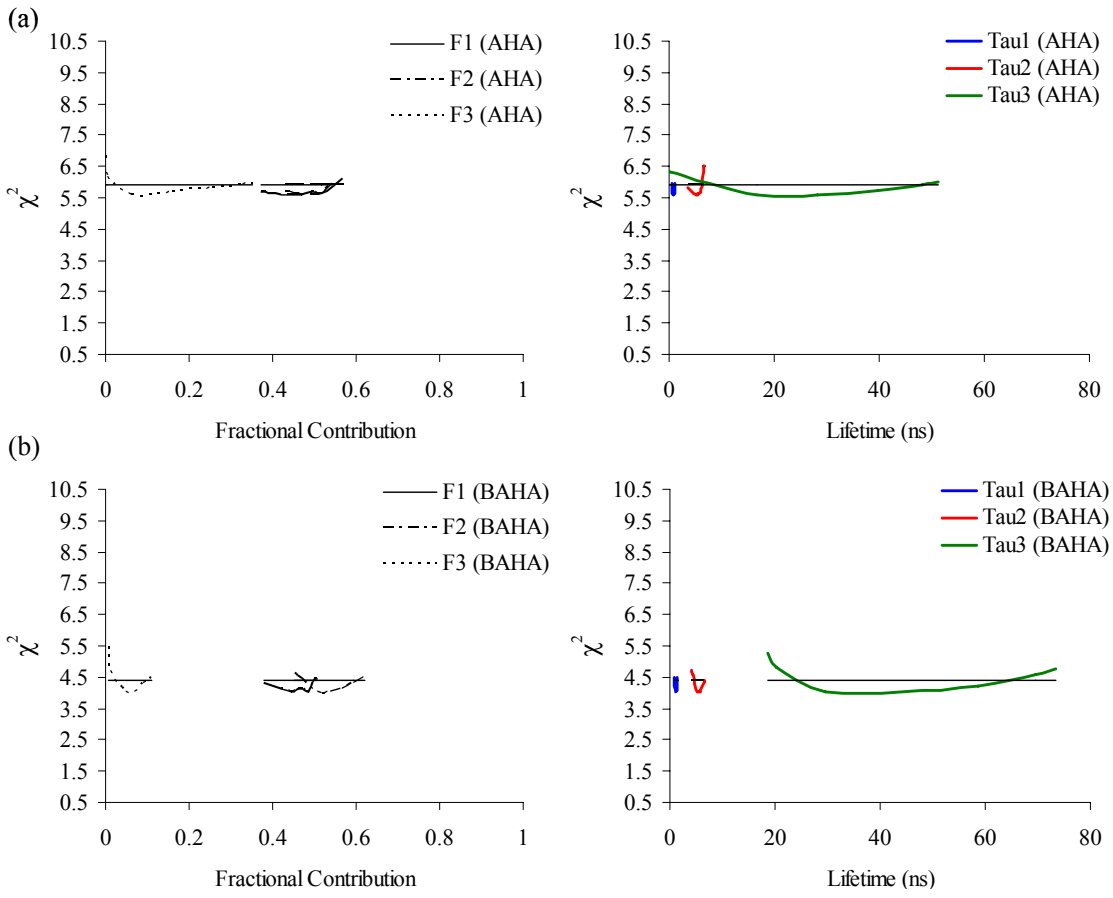

Figure 4.2 The χ^2 surfaces of NLLS analyses for (a) AHA and (b) BAHA. The NLLS analyses were obtained by allowing both the fractional contributions and lifetimes to vary (V) and linking (L) all the parameters at different concentrations of AHA. For BAHA, all the parameters were allowed to vary at the highest concentration (24 ppm). Horizontal solid line: one standard deviation from the minima of the χ^2 surface.

As a result, less confidence should be placed in the DDD model because χ^2 surfaces with a wide range indicate the uncertainty of the recovered fractional contributions and lifetimes. The stability of both DDD and DD models for the commercial DHM and AHA, respectively, were also supported by the χ^2 surfaces of NLLS analyses (Figure 4.3).

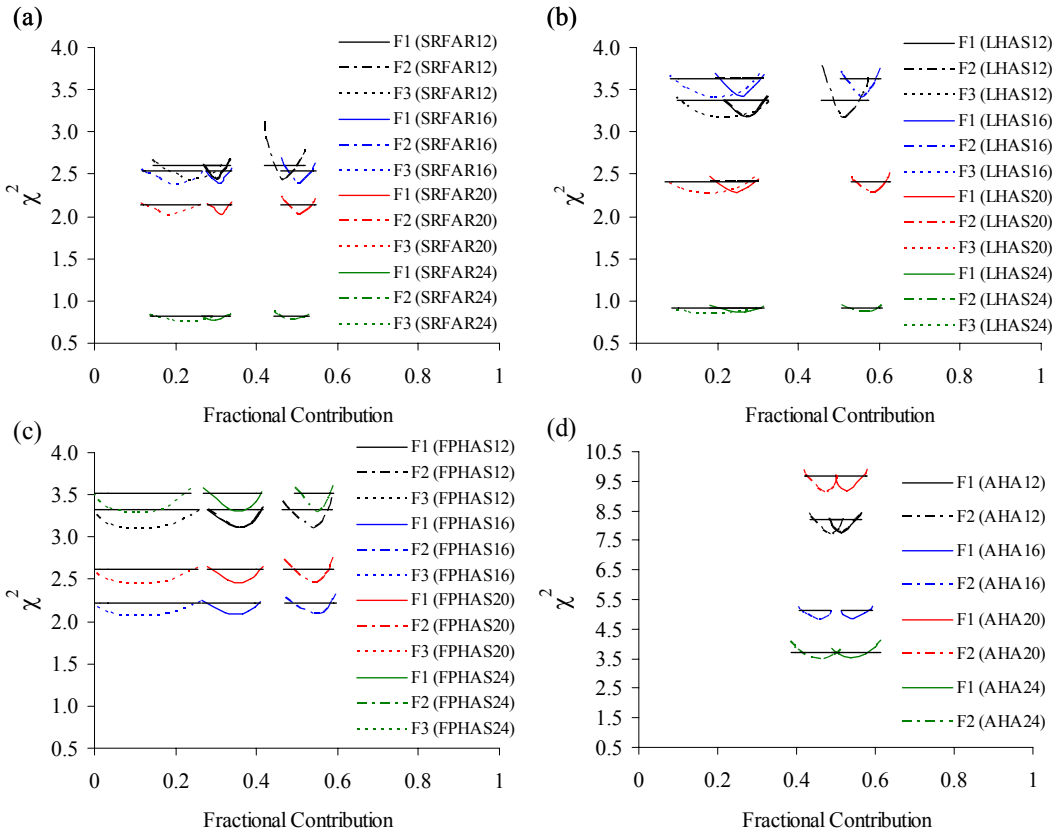

Figure 4.3 The χ^2 surfaces of NLLS analyses for (a) SRFAR, (b) LHAS, (c) FPHAS, and (d) AHA at different concentrations. The NLLS analyses were obtained by allowing both the fractional contributions and lifetimes to vary (V) and linking (L) the lifetimes of each humic at different concentrations. Horizontal solid line: one standard deviation from the minima of the χ^2 surface.

It can be observed from the χ^2 surfaces that both models are stable at all concentrations of each humic. However, a deviation in the fractional contributions of the χ^2 surfaces was noted at the lowest concentration (12 ppm) of the commercial DHM and AHA. In addition, a similar trend in the fractions was obtained with an increase in the humic concentration from 16 up to 24 ppm.

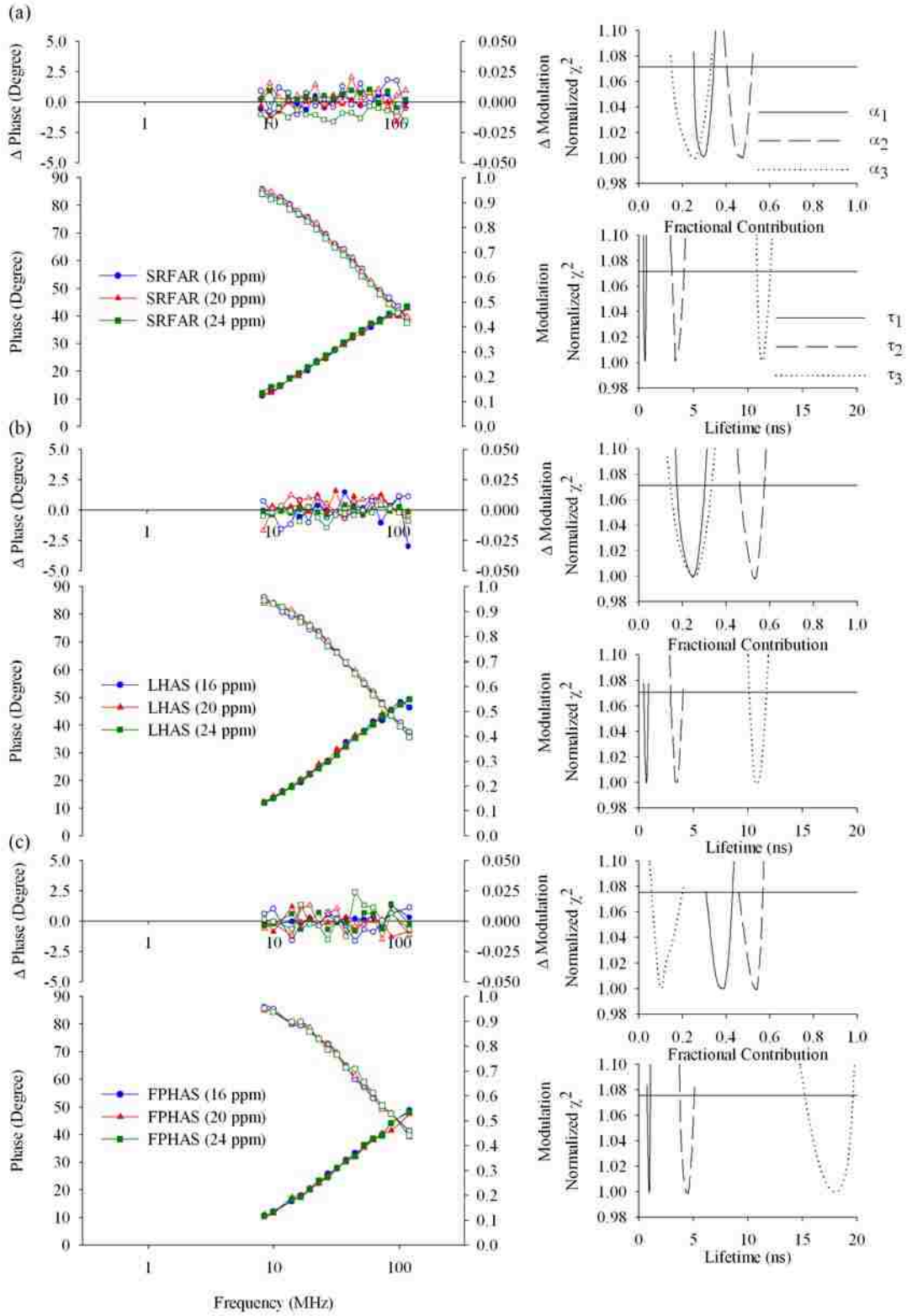

Figure 4.4 Frequency-domain data and normalized χ^2 surfaces of NLLS analyses for (a) SRFAR, (b) LHAS, and (c) FPHAS. Solid and open symbols, in frequency-domain data, represent phase and modulation, respectively. Horizontal solid lines: one standard deviation from the minima of the χ^2 surface. Corresponding fitting parameters are tabulated in Table 4.1.

This indicates that the structural conformation of humic materials is controlled by the nature and concentration of humic materials. It has been previously reported that the structural configuration of humic materials is expanded and stretched to sheet-like structures at a low concentration, while it folds and twist at high concentrations.[36, 37]

To further investigate how NLLS analyses for DHM individual components compensate for the analyses of pyrene and DHM mixture, the NLLS analyses of both DDD and DD models were performed by excluding the lowest concentration (Figures 4.4 and 4.5).

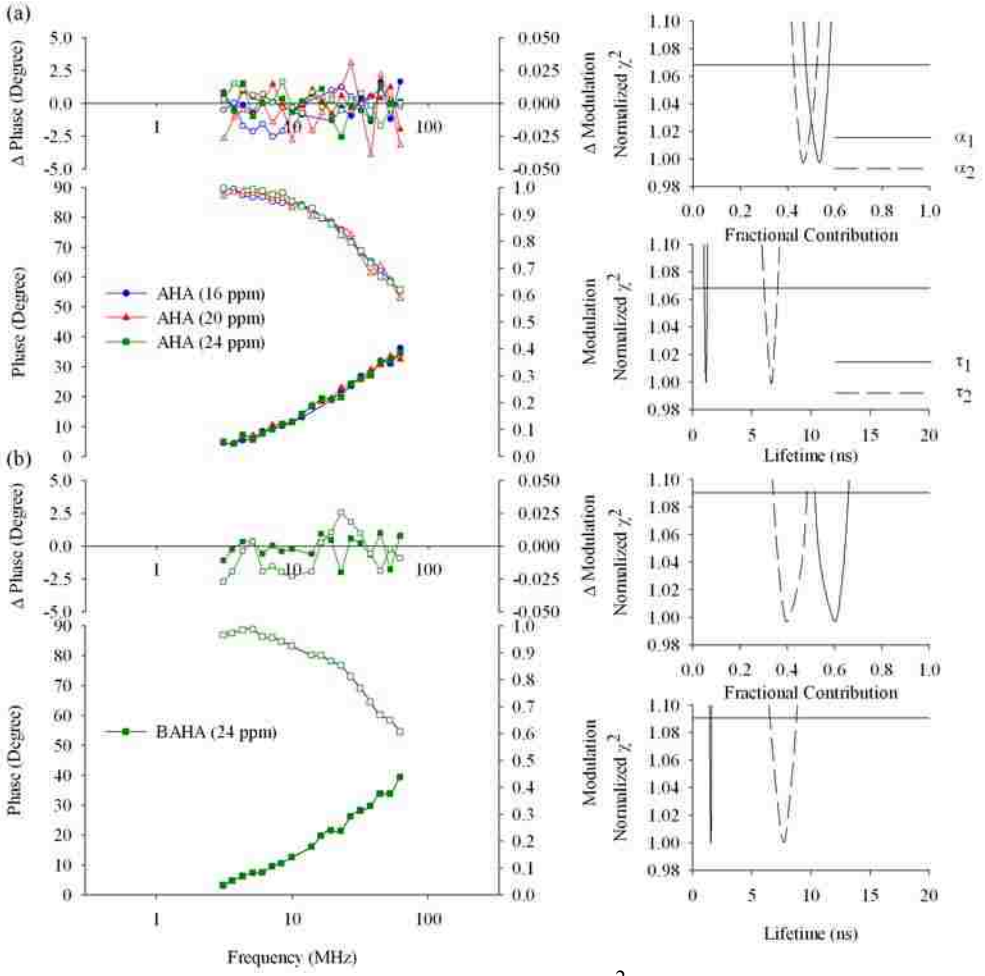

Figure 4.5 Frequency-domain data and normalized χ^2 surfaces of NLLS analyses for (a) AHA and (b) BAHA. Solid and open symbols, in frequency-domain data, represent phase and modulation, respectively. Horizontal solid lines: one standard deviation from the minima of the χ^2 surface. Corresponding fitting parameters are tabulated in Table 4.1.

In the NLLS analyses, both the fractional contributions and lifetimes were allowed to vary (V) but all parameters were linked (L) for all three remaining concentrations of DHM individual components. Excellent fits, χ^2 values, residual plots were obtained (Figures 4.4 and 4.5). The results of measured fractional intensity contributions and lifetime of DHM in argon degassed aqueous solutions are reported in Table 4.1.

Table 4.1 Recovered fluorescence lifetimes and fractional contributions obtained from NLLS analyses of pyrene, DHM, and their mixture. The L subscripts correspond to the fits where both DHM fractional intensity contributions and lifetimes were linked during NLLS analyses. The F subscripts denote the fits where both SRFAR fractional intensity contributions and lifetimes were fixed during NLLS analyses. Bolded black parameters are fixed values: same as Figures 4.4, 4.5, 4.7, and 4.11.

Model	[DHM] (ppm)	Set	α_{DHM}	α_1	τ_1 (ns)	α_2	τ_2 (ns)	α_3	τ_3 (ns)	α_4	τ_4 (ns)	χ^2
D	0	Pyrene	–	1.00	193.74	–	–	–	–	–	–	0.72
$D_LD_LD_L$	16–20–24	SRFAR	–	0.30	0.58	0.46	3.36	0.24	10.98	–	–	2.76
$D_LD_LD_L$	16–20–24	LHAS	–	0.24	0.70	0.52	3.32	0.24	10.59	–	–	2.25
$D_LD_LD_L$	16–20–24	FPHAS	–	0.38	0.95	0.53	4.36	0.09	16.61	–	–	2.52
D_LD_L	16–20–24	AHA	–	0.53	1.09	0.47	6.54	–	–	–	–	5.78
DD	24	BAHA	–	0.59	1.51	0.41	7.51	–	–	–	–	6.38
$(D+D+D)_FD$	16	Pyrene SRFAR mixture	0.41	**0.30**	**0.58**	**0.46**	**3.36**	**0.24**	**10.98**	0.59	185.95	2.27
$(D+D+D)_FD$	20	–	0.46	**0.30**	**0.58**	**0.46**	**3.36**	**0.24**	**10.98**	0.54	192.73	2.93
$(D+D+D)_FD$	24	–	0.73	**0.30**	**0.58**	**0.46**	**3.36**	**0.24**	**10.98**	0.27	178.38	3.33
$(D+D+D)_FD$	16	Pyrene LHAS mixture	0.75	**0.24**	**0.70**	**0.52**	**3.32**	**0.24**	**10.59**	0.25	204.59	3.63
$(D+D+D)_FD$	20	–	0.74	**0.24**	**0.70**	**0.52**	**3.32**	**0.24**	**10.59**	0.26	189.14	2.34
$(D+D+D)_FD$	24	–	0.80	**0.24**	**0.70**	**0.52**	**3.32**	**0.24**	**10.59**	0.20	190.97	3.71
$(D+D+D)_FD$	16	Pyrene FPHAS mixture	0.65	**0.38**	**0.95**	**0.53**	**4.36**	**0.09**	**16.61**	0.35	223.03	5.46
$(D+D+D)_FD$	20	–	0.71	**0.38**	**0.95**	**0.53**	**4.36**	**0.09**	**16.61**	0.29	226.63	4.22
$(D+D+D)_FD$	24	–	0.77	**0.38**	**0.95**	**0.53**	**4.36**	**0.09**	**16.61**	0.23	207.11	4.08
$(D+D+D)_FD$	16	Pyrene AHA mixture	0.36	**0.53**	**1.09**	**0.47**	**6.54**	–	–	0.64	190.11	7.40
$(D+D+D)_FD$	20	–	0.43	**0.53**	**1.09**	**0.47**	**6.54**	–	–	0.57	190.47	4.62
$(D+D+D)_FD$	24	–	0.54	**0.53**	**1.09**	**0.47**	**6.54**	–	–	0.46	193.80	3.80
$(D+D+D)_FD$	16	Pyrene BAHA mixture	0.14	**0.59**	**1.51**	**0.41**	**7.51**	–	–	0.86	192.88	7.17
$(D+D+D)_FD$	20	–	0.17	**0.59**	**1.51**	**0.41**	**7.51**	–	–	0.83	192.41	7.65
$(D+D+D)_FD$	24	–	0.20	**0.59**	**1.51**	**0.41**	**7.51**	–	–	0.80	194.94	5.93

Results of the χ^2 surfaces of NLLS analyses further support the stability of both the DDD and DD models. In addition, it can be noted that the χ^2 surfaces of NLLS analyses for all models are narrow, indicating that these models are stable and robust. In this study, frequency-domain

lifetime measurements were also obtained for 24 ppm LHAS, used as a probe of DHM, to evaluate the effect of oxygen on the recovered fractional contributions and lifetimes of DHM. Frequency-domain data (phase and modulation as a function of frequency) for the air-saturated and argon degassed LHAS solutions show excellent fits and residual plots (Figure 4.6). The results clearly demonstrated LHAS insensitivity to oxygen, indicating that fluorescence of LHAS is interior and highly protected. The χ^2 surfaces of the NLLS analyses were also performed by allowing all parameters to vary (V). Only a small variation in the first and third lived components can be noted. However, the highest probability of both fractional intensity contributions and lifetimes are closely associated with each other for both air-saturated and argon degassed LHAS solutions, which can be observed from the χ^2 surfaces of the NLLS analyses.

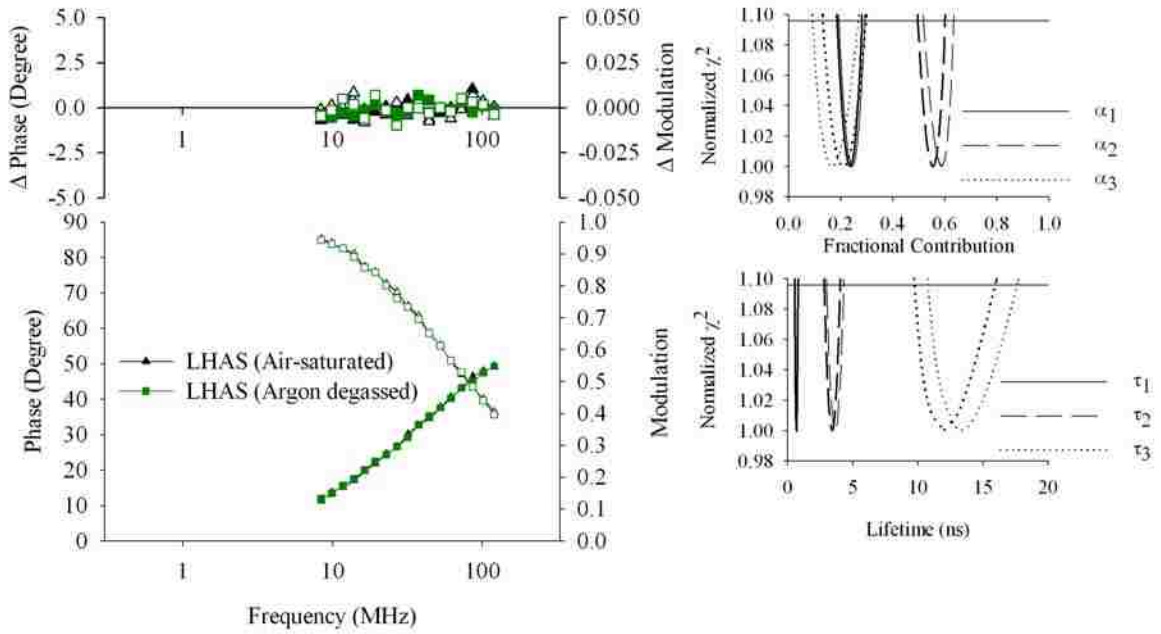

Figure 4.6 Frequency-domain data and normalized χ^2 surfaces of NLLS analyses for air-equilibrated and argon degassed 24 ppm LHAS solutions. The NLLS analyses were obtained by allowing both the fractional contributions and lifetimes to vary (V) for LHAS samples. Solid and open symbols, in frequency-domain data, represent phase and modulation, respectively. In the χ^2 surface, bolded solid, long dash, and dotted lines correspond to the argon degassed 24 ppm LHAS solution. Horizontal solid line: one standard deviation from the minima of the χ^2 surface.

4.3.2 Fluorescence Lifetime Measurements of Pyrene and DHM Mixture

As was discussed in Chapter 3 of this dissertation, the effects of oxygen, HOC adsorption to cell walls, and photobleaching within HOC and DHM mixture, a multi-component system, on changing recovered fractions and lifetimes are problems encountered in previously reported studies. In most studies, these experimental considerations were not fully resolved. As a result, this can easily complicate the interpretation of fluorescence lifetimes and fractional intensity contributions by directly affecting the recovered values. In order to address these issues, the first step was to minimize the effect of pyrene losses to the cell wall on changing the recovered pyrene fractional contributions. All solutions were left to equilibrate overnight in the fluorometer cell with septum cap and rinsed with fresh solution for each segment. In addition, the removal of dissolved oxygen was performed by a 15 min degassing period with ultra high purity argon gas, followed by 5 min of equilibration time in the sample compartment with a flow of argon gas over the course of fluorescence measurements. Finally, frequency-domain lifetime measurements via frequency segmentation and recombination were applied to pyrene and DHM mixture to overcome photobleaching.

For pyrene and the commercial DHM mixture, it is suitable to expect the mixture to show a minimum of four lifetimes consisting of the three DHM and one pyrene lifetime. As was previously discussed in Chapter 3 of this dissertation, the most reasonable model for pyrene and DHM mixture was the $(D+D+D)_F D$ model. Recall that DHM fluorescence was assumed to be independent of pyrene's presence; therefore, DHM fluorescence was considered as a single component within a two component system in this model. In this study, both fractions and lifetimes of the commercial DHM and AHA were all linked at the three remaining concentrations (16, 20, and 24 ppm) to compensate for the analyses of pyrene and DHM mixture (Figure 4.7).

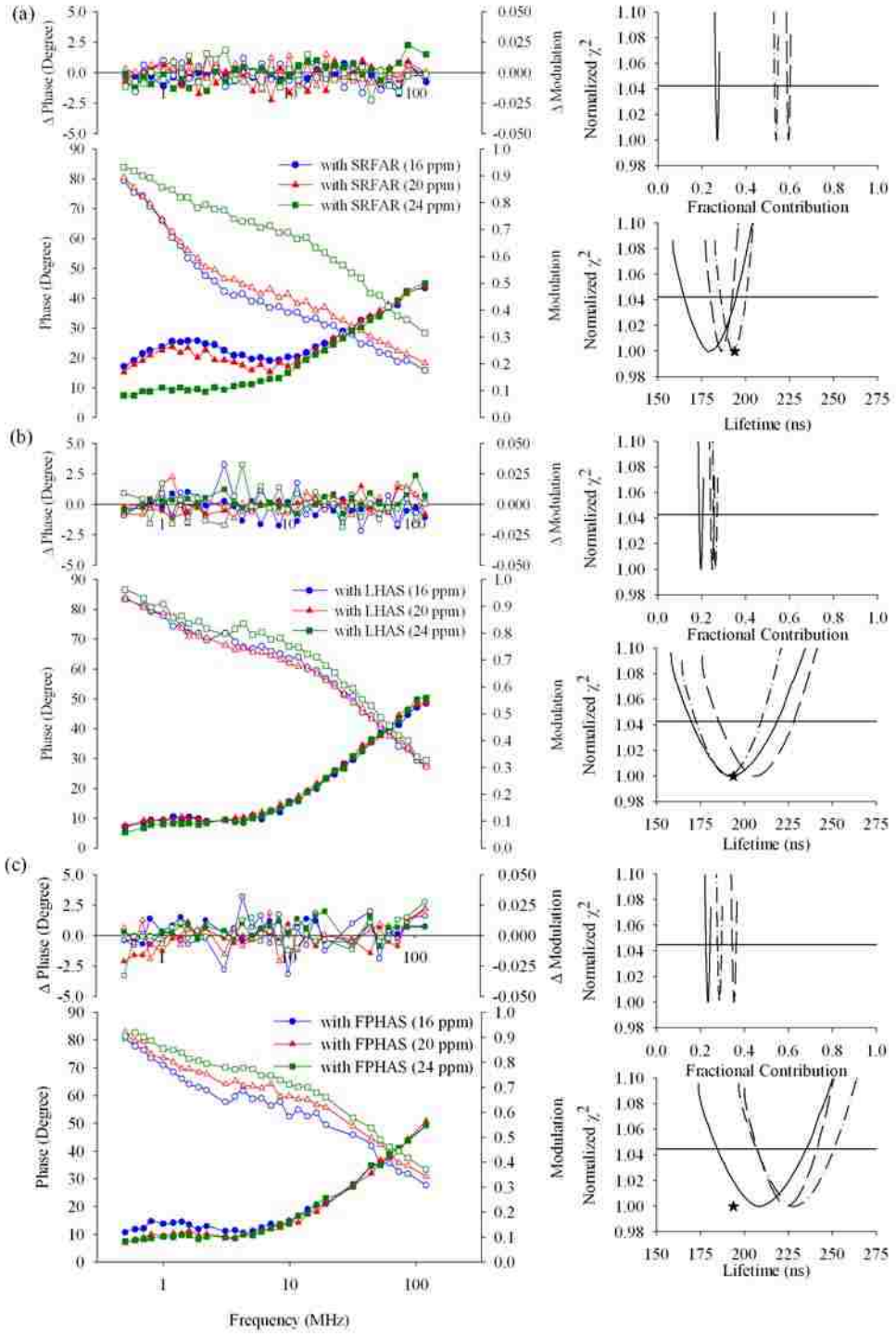

Figure 4.7 Frequency-domain data and normalized χ^2 surfaces of NLLS analyses for 0.04 ppm pyrene and (a) SRFAR, (b) LHAS, or (c) FPHAS mixture. Solid and open symbols, in frequency-domain data, represent phase and modulation, respectively. In the χ^2 surfaces, the long dash, dash-dot, and solid lines correspond to pyrene and DHM mixture at 16, 20, and 24 ppm DHM, respectively. The star indicates the measured pyrene lifetime in the absence of DHM. Horizontal solid lines: one standard deviation from the minima of the χ^2 surface. Corresponding fitting parameters are tabulated in Table 4.1.

For BAHA, the recovered fractional intensity contributions and lifetimes at the highest concentration (24 ppm) were used for the analysis of pyrene and BAHA mixture. Figure 4.7 clearly shows the different behaviors of pyrene in the presence of the commercial DHM. Different frequency-domain profiles for pyrene and DHM mixture, in particular for pyrene and SRFAR mixture, were observed at different DHM concentrations. This indicated that the association of pyrene with DHM is dependent on many factors, such as, the chemical properties and concentrations of DHM. In general, excellent fits and residual plots were obtained for pyrene with the commercial DHM (Figure 4.7). Results of the recovered pyrene fractional intensity contributions and lifetimes are provided in Table 4.1. The χ^2 surfaces of NLLS analyses of pyrene and the commercial DHM were also performed in order to statistically evaluate both recovered pyrene fractions and lifetimes (Figure 4.7). In general, a decrease in the recovered fractional contributions of pyrene with DHM was noted with an increase in DHM concentration. However, the decrease in the recovered pyrene fractions was the most in the presence of LHAS as compared to those with other DHM, indicative of the highest carbon and aromatic content of LHAS. Fluorescence steady-state measurements were also in agreement with the results obtained for pyrene and DHM mixtures. A decrease in pyrene fluorescence intensity was noticed with an increase in the commercial DHM concentration (Figure 4.8). Again, the most significant reduction in the pyrene fluorescence intensity was noted for pyrene in the presence of LHAS.

On the other hand, the results of the χ^2 surfaces of NLLS analyses for measured pyrene lifetimes completely demonstrated different behaviors in the presence of the commercial DHM (Figure 4.7). For the pyrene and SRFAR mixture, the recovered pyrene lifetimes, Table 4.1, increased with an increase in the SRFAR concentration from 16 ppm (185.95 ns) up to 20 ppm (192.73 ns), followed by a decrease at the highest concentration of SRFAR (178.38 ns).

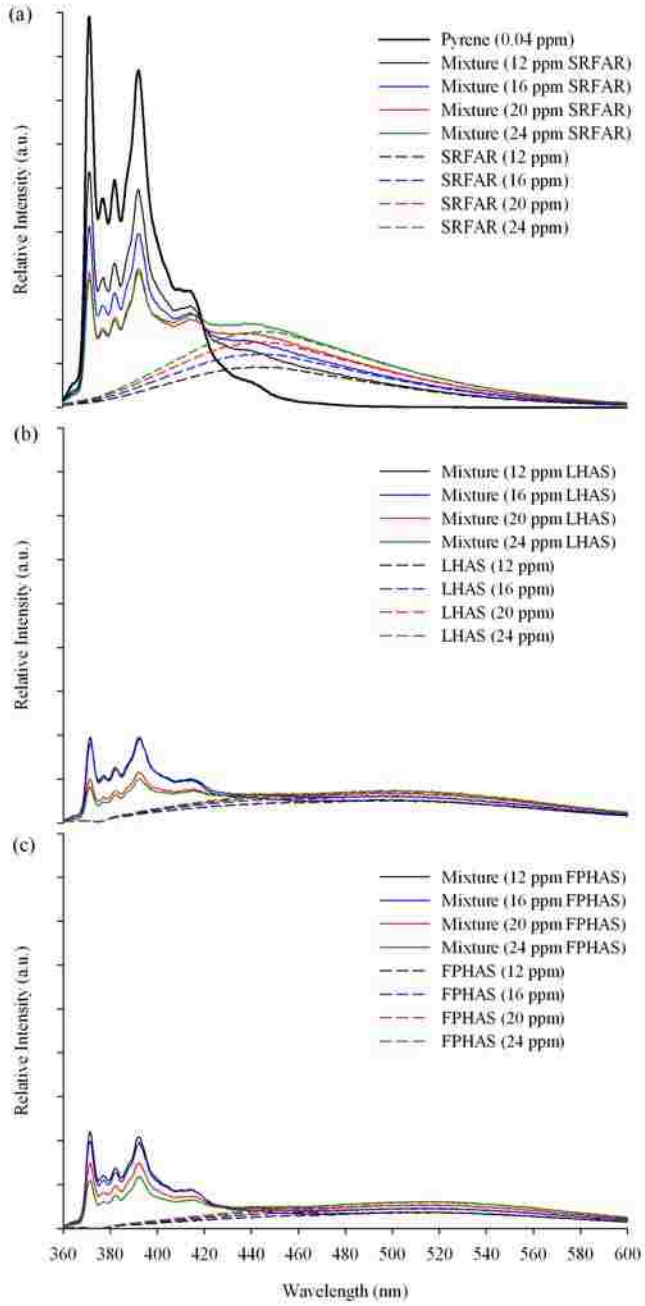

Figure 4.8 Fluorescence emission spectra of 0.04 ppm pyrene and (a) SRFAR, (b) LHAS, or (c) FPHAS mixture in aqueous system at different concentrations of DHM, excited at 333 nm.

However, a decrease in the recovered pyrene lifetimes was noticed when increasing the LHAS concentration from 16 ppm (204.59 ns) up to 20 ppm (189.14 ns), followed by a slight increase at the highest concentration of LHAS (190.97 ns). This is indicative of the pyrene movement

towards different microenvironments in DHM. For the pyrene and FPHAS mixture, it is of a great significance to note that longer recovered pyrene lifetimes were obtained in contrast to those for pyrene and SRFAR (or LHAS) mixture, as reported in Table 4.1. This can be related to the highest aromatic amino acid content of FPHAS, such as phenylalanine and tryptophan, as compared to other commercial DHM. Similar trends in measured pyrene lifetimes with FPHAS to those with SRFAR were also observed.

From the above findings, it is expected that quenched pyrene fluorescence may shorten the recovered pyrene lifetime with an increase in the DHM concentration. However, it is also reasonable to expect that there is more than one population of pyrene in different microenvironments of DHM due to the extremely heterogeneous nature of these naturally occurring materials. Some of these populations can be observed and quenched, resulting in a decrease in the pyrene fluorescence in the presence of DHM. Other portions can be obscure, causing an enhancement of the pyrene intensity with DHM. Therefore, the increase in pyrene recovered lifetimes may be attributed to the static association as a result of pyrene ring currents in π-system above and below pyrene aromatic rings, indicating that this population of pyrene may be fully surrounded by aromatic moieties of DHM. Nelson et al.[38] studied the effect of alcohols on γ-cyclodextrin (CD) inclusion complexes of pyrene by use of time-domain fluorescence measurements. A long pyrene lived component of fluorescence was observed for pyrene and γ-CD mixture in aqueous solutions. However, it was indicated that there was a decrease in the pyrene fractional intensity when increasing the γ-CD concentration. From steady-state fluorescence measurements, the authors also observed that pyrene fluorescence was quenched with an increase in the γ-CD concentration. As a result, it was indicated that the

enhancement in pyrene lifetime can not be related to the increase in pyrene fluorescence if the static interaction occurs.

For pyrene and AHA (or BAHA) mixture, EEM fluorescence spectra were first collected for the humic individual components to obtain the different spectral features between AHA and BAHA (Figure 4.9).

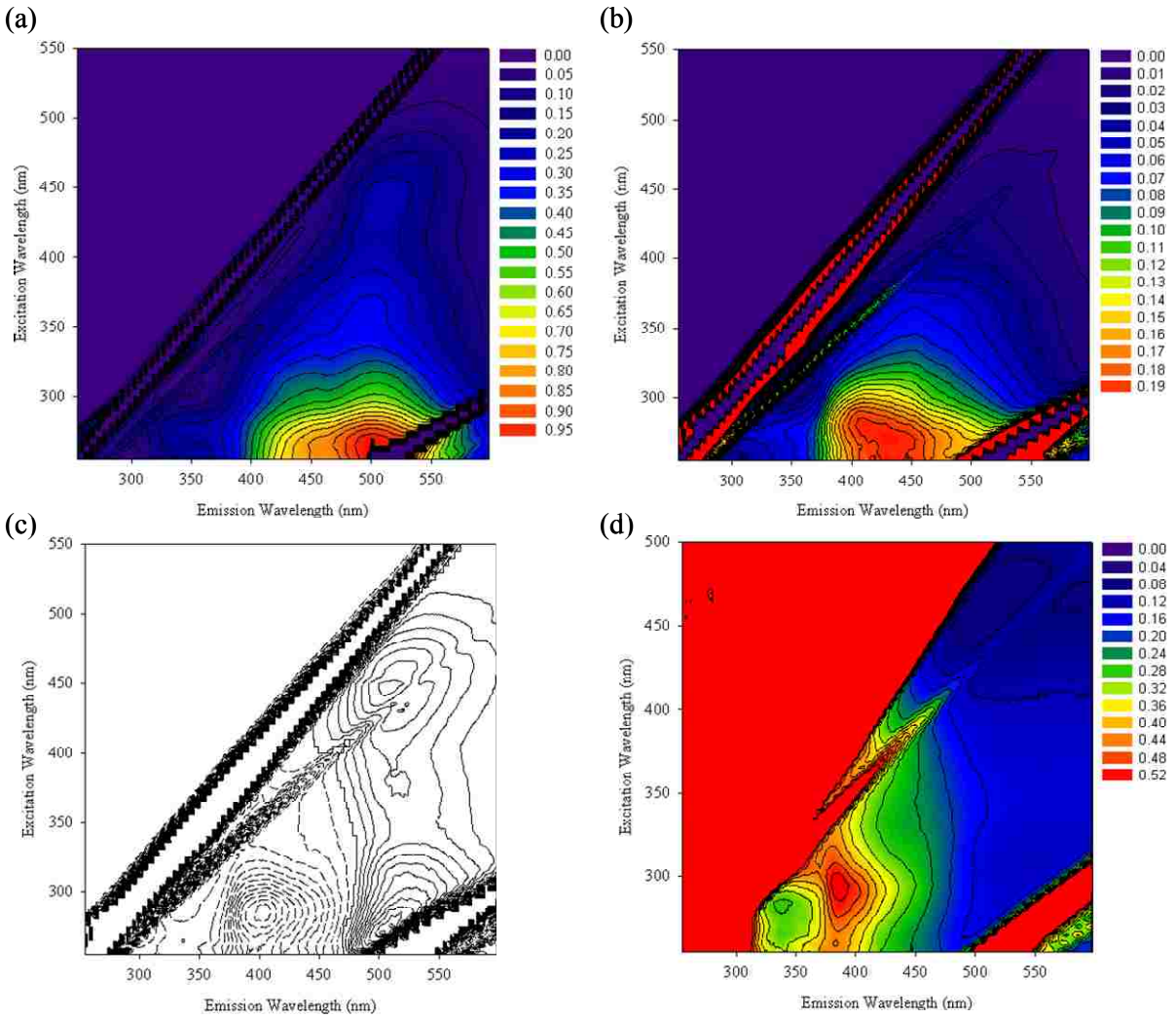

Figure 4.9 EEM spectra of (a) AHA normalized at its fluorescence maximum and (b) BAHA normalized at the maximum fluorescence of AHA EEM spectra. (c) The difference of AHA and BAHA EEM spectra estimated by subtracting the BAHA from AHA normalized EEM spectra at their individual emission maximum. Solid and dash lines represent positive and negative differences, respectively. (d) Fluorescence intensity ratio of BAHA to AHA EEM spectra.

Figures 4.9a and b graphically represent EEM spectra of AHA, normalized to the maximum intensity at Ex265/Em501 nm, and BAHA, normalized at the maximum intensity of AHA EEM, respectively. In the EEM spectra, four fluorophores have been commonly identified in natural organic matter. These fluorophores are tyrosine at Ex (220-235 nm) and Em (290-310 nm), tryptophan at Ex (220-240 nm) and Em (340-360 nm), humic at Ex (220-240 nm) and Em (400-450 nm), and humic-like fluorescence at Ex (300-350 nm) and Em (400-450 nm).[39-44] As shown in Figures 4.9a and b, different EEM spectral profiles of AHA and BAHA were noted. BAHA (Figure 4.9b) was dimmer than AHA (Figure 4.9a), indicative to the low aromatic content of BAHA. There also appeared to be less spectral feature of BAHA in the region at Ex (250-315 nm) and Em (450-500 nm) as compared to that of AHA. The EEM spectral difference between AHA and BAHA, calculated by subtracting the BAHA from AHA EEM spectra normalized at their individual emission maximum, is shown in Figure 4.9c. This figure demonstrates that BAHA is dominated by a component with a spectral feature at Ex285/Em405 nm, while AHA has a dominant feature in the vicinity of Ex270/Em505 nm. The fluorescence intensity ratio of the BAHA to AHA EEM spectra also shows that there is a dominant component in the spectral region at Ex295/388 nm (Figure 4.9d).

In addition to the EEM spectra, the carbon distribution in the BAHA sample was determined by the CPMAS ^{13}C NMR experiment. The CPMAS ^{13}C NMR spectrum of BAHA (Figure 4.10) reveals that the aliphatic moieties are apparently the most dominant content of BAHA. It was found that the functional group distributions of the BAHA are 90.9 (aliphatic, 0-50 ppm), 6.4 (carbohydrate, 50-108 ppm), 0.1 (aromatic, 108-162 ppm), and 2.6 % (carboxylic, 162-220 ppm), further confirming the low fluorescence of BAHA. Mao et al.[45] have previously indicated that the functional group compositions of AHA are 17.3 (aliphatic, 0-50 ppm), 25.0

(carbohydrate, 50-108 ppm), 40.8 (aromatic, 108-162 ppm), and 16.9 % (carboxylic, 162-220 ppm).

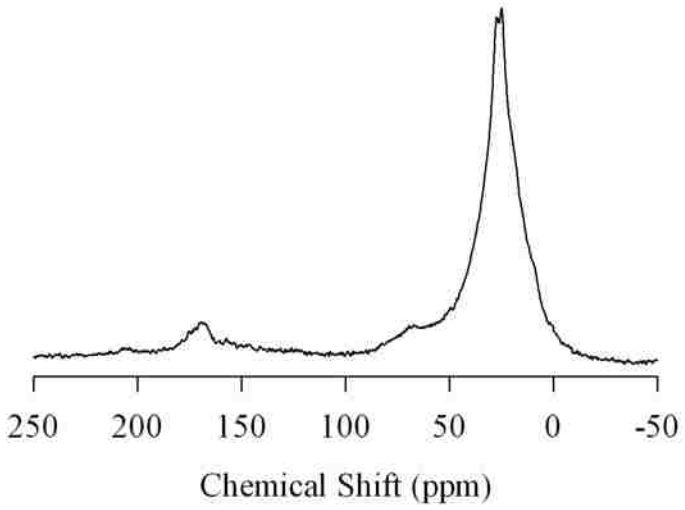

Figure 4.10 The cross polarization magic-angle spinning (CPMAS) ^{13}C NMR spectrum of BAHA.

This further supported the higher EEM spectral feature of AHA in the longer emission wavelength region as compared to that of BAHA, indicative of the high aromatic content of AHA.

Both EEM and CPMAS ^{13}C NMR spectra clearly demonstrated the differences between AHA and BAHA and allowed one to study their association behavior with pyrene using segmented frequency-domain lifetime measurements. Recall that the DD model for both AHA and BAHA was found to be more stable and reproducible as compared to the DDD model. As a result, the $(D+D)_FD$ model was chosen to be the most reasonable model. In this model, both AHA and BAHA fractions and lifetime were allowed to be fixed (F) within the sum of two-exponential decays $(D+D)_F$. In addition, both pyrene fraction and lifetime were allowed to vary as a discrete (D) component model. Frequency-domain phase and modulation data of pyrene and AHA (or BAHA) mixture at different humic concentrations are shown in Figure 4.11 along with

their χ^2 surfaces of NLLS analyses. In general, frequency-domain phase and modulation profiles of the pyrene and BAHA mixture, Figure 4.11b, clearly showed different trends from those of pyrene and AHA (or commercial DHM) mixture.

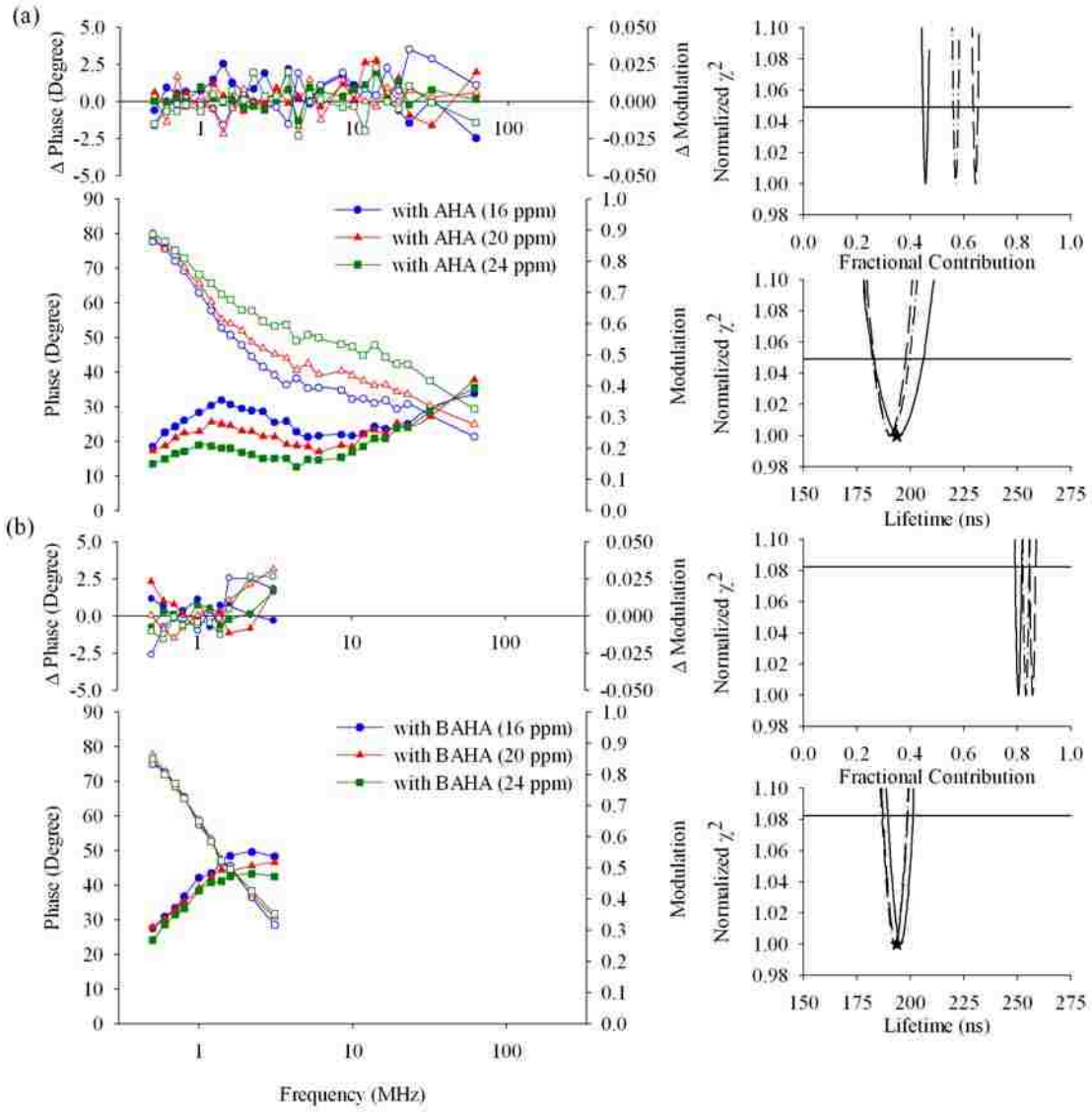

Figure 4.11 Frequency-domain data and normalized χ^2 surfaces of NLLS analyses for 0.04 ppm pyrene and (a) AHA or (b) BAHA mixture. Solid and open symbols, in frequency-domain data, represent phase and modulation, respectively. In the χ^2 surfaces, the long dash, dash-dot, and solid lines correspond to pyrene and DHM mixture at 16, 20, and 24 ppm DHM, respectively. The star indicates the measured pyrene lifetime in the absence of DHM. Horizontal solid lines: one standard deviation from the minima of the χ^2 surfaces. Corresponding fitting parameters are tabulated in Table 4.1.

This further supported the results obtained from the EEM and CPMAS ^{13}C NMR spectra of humic individual components. For the pyrene and AHA mixture, a change in frequency-domain profiles was observed with an increase in the AHA concentration (Figure 4.11a). In contrast, there appeared to be minimal to no change in frequency-domain data for pyrene and BAHA mixture at different BAHA concentrations (Figure 4.11b). In addition, frequency-domain data for this mixture is clearly more dominant by pyrene component as compared to those for pyrene and AHA (or the commercial DHM) mixture. Again, this is indicative of the low fluorescence of this humic among all DHM investigated in this study.

The χ^2 surfaces of NLLS analyses further support these findings (Figure 4.11). Figure 4.11b reveals that pyrene recovered fractional intensities with BAHA were higher than those obtained for pyrene with AHA (Figure 4.11a). The results of the recovered pyrene fractions and lifetimes are summarized in Table 4.1. Fluorescence steady-state data were also consistent with the results obtained for pyrene and AHA (or BAHA) mixture. The decrease in the pyrene fluorescence intensity at different AHA concentrations (Figure 4.12a) was more significant than that with BAHA (Figure 4.12b). Also, it can be observed that the effect of BAHA concentration on pyrene intensity was minimal.

In general, the measured pyrene lifetimes observed at different concentrations of AHA (or BAHA) mixture were similar to those of pyrene in the absence of AHA (or BAHA). However, recovered pyrene lifetimes in the presence of AHA (or BAHA) were found to slightly increase with an increase in the AHA (or BAHA) concentration. In addition, it was observed that recovered pyrene lifetimes for the pyrene and BAHA mixture were slightly higher than those for the pyrene and AHA mixture. This may be attributed to the fact that pyrene is the most dominant component for the pyrene and BAHA mixture as compared to the pyrene and AHA mixture.

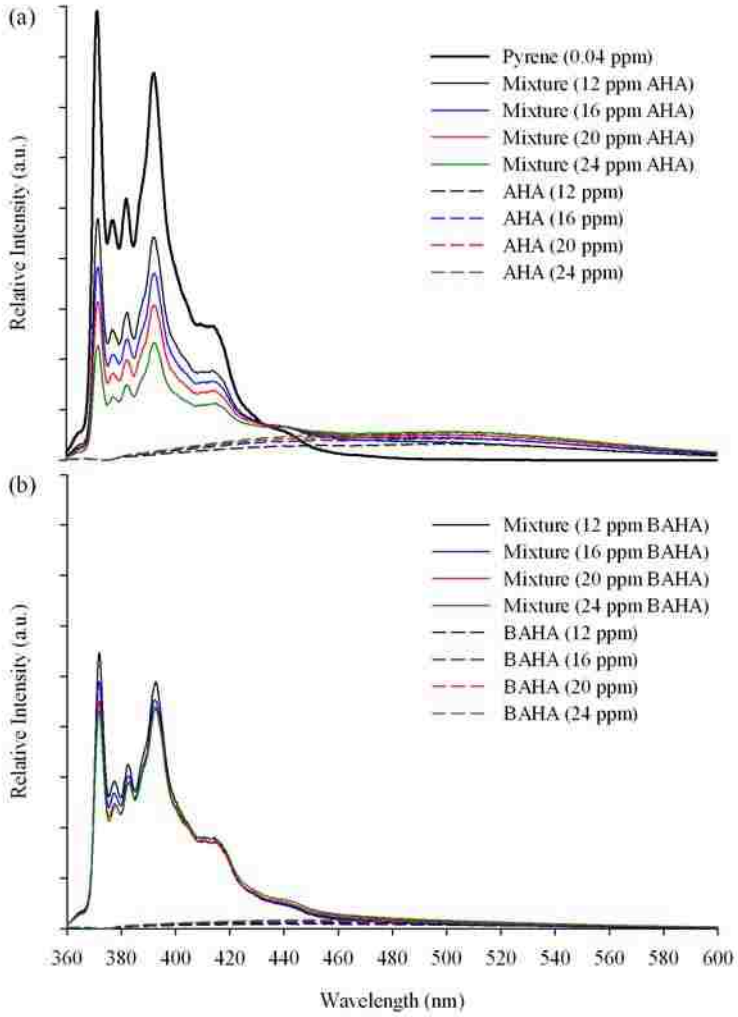

Figure 4.12 Fluorescence emission spectra of 0.04 ppm pyrene and (a) AHA or (b) BAHA mixture in aqueous system at different concentrations of DHM, excited at 333 nm.

4.3.3 Comparison of Measured Pyrene Lifetimes in the Presence of DHM

In general, there were different trends in frequency-domain profiles of pyrene at different concentrations of the commercial DHM and AHA as compared to those with BAHA. From the above results, the NLLS analyses yielded the longest pyrene recovered lifetimes at different concentrations of FPHAS as compared to all DHM investigated in this study. In addition, recall that the removal of one discrete component (D) from the DDD model, used for the commercial

DHM, gave the DD model used for the NLLS analyses of AHA and BAHA. Thus, it could be noted that pyrene measured lifetimes were varied and dominant by different microenvironments within the commercial DHM. However, recovered pyrene lifetimes at different concentrations of AHA (or BAHA) were closely similar to that in the absence of DHM (193.74 ns), indicating that pyrene may be associated with a simpler microenvironment within AHA (or BAHA) as compared to the commercial DHM. As a result, static quenching is more dominant than dynamic quenching for pyrene in the presence of AHA (or BAHA) as compared to that with the commercial DHM.

4.4 Conclusion

The results presented in this study demonstrated that the association behavior of pyrene with DHM is controlled by various factors, such as, the nature and concentration, aliphatic or aromatic content, and elemental composition of DHM. There is, however, no simple answer stating that the quenching mechanism of pyrene with DHM is either static or dynamic quenching, in particular when studying systems as complex as HOC and DHM. Yet, the association mechanism could be a combination of both static and dynamic quenching. This is further supported by the results obtained from the measured pyene lifetimes in the presence of DHM included in this study.

In general, pyrene is affected by different microenvironments of DHM because of the extremely heterogeneous nature of these naturally occurring materials. The results also displayed clear evidence that not all DHM have similar association accessibilities with pyrene. The association behavior of pyrene with the commercial DHM was comparatively different from that for pyrene with AHA (or BAHA). The NLLS analyses of pyrene and DHM mixture further

confirmed these findings as one can observe that there was a variation in the recovered pyrene lifetimes with different DHM.

4.5 References

(1) Lakowicz, J. R. *Principles of Fluorescence Spectroscopy*, Second ed.; Kluwer Academic/Plenum Press: New York, 1999.

(2) Laor, Y.; Rebhun, M. *Environ. Sci. Technol.* **2002**, *36*, 955-961.

(3) Tiller, C. L.; Jones, K. D. *Environ. Sci. Technol.* **1997**, *31*, 424-429.

(4) Backhus, D. A.; Golini, C.; Castellanos, E. *Environ. Sci. Technol.* **2003**, *37*, 4717-4723.

(5) Peuravuori, J. *Anal. Chim. Acta* **2001**, *429*, 75-89.

(6) Perminova, I. V.; Grechishcheva, N. Y.; Petrosyan, V. S. *Environ. Sci. Technol.* **1999**, *33*, 3781-3787.

(7) Chin, Y.-P.; Aiken, G. R.; Danielsen, K. M. *Environ. Sci. Technol.* **1997**, *31*, 1630-1635.

(8) Jones, K. D.; Tiller, C. L. *Environ. Sci. Technol.* **1999**, *33*, 580-587.

(9) Schlautman, M. A.; Morgan, J. J. *Environ. Sci. Technol.* **1993**, *27*, 961-969.

(10) Xing, B.; Pignatello, J. J.; Gigliotti, B. *Environ. Sci. Technol.* **1996**, *30*, 2432-2440.

(11) Weber, W. J., Jr.; Huang, W. *Environ. Sci. Technol.* **1996**, *30*, 881-888.

(12) Huang, W.; Weber, W. J., Jr. *Environ. Sci. Technol.* **1997**, *31*, 2562-2569.

(13) Huang, W.; Young, T. M.; Schlautman, M. A.; Yu, H.; Weber, W. J., Jr. *Environ. Sci. Technol.* **1997**, *31*, 1703-1710.

(14) Xing, B.; Pignatello, J. J. *Environ. Sci. Technol.* **1997**, *31*, 792-799.

(15) Graber, E. R.; Borisover, M. D. *Environ. Sci. Technol.* **1998**, *32*, 3286-3292.

(16) Holbrook, R. D.; Love, N. G.; Novak, J. T. *Environ. Sci. Technol.* **2004**, *38*, 4987-4994.

(17) Engebretson, R. R.; von Wandruszka, R. *Environ. Sci. Technol.* **1994**, *28*, 1934-1941.

(18) Chiou, C. T.; McGroddy, S. E.; Kile, D. E. *Environ. Sci. Technol.* **1998**, *32*, 264-269.

(19) Perminova, I. V.; Grechishcheva, N. Y.; Kovalevskii, D. V.; Kudryavtsev, A. V.; Petrosyan, V. S.; Matorin, D. N. *Environ. Sci. Technol.* **2001**, *35*, 3841-3848.

(20) Drewes, J. E.; Croue, J. P. *Water Sci. Technol.: Water Supply* **2002**, *2*, 1-10.

(21) Chefetz, B.; Deshmukh, A. P.; Hatcher, P. G.; Guthrie, E. A. *Environ. Sci. Technol.* **2000**, *34*, 2925-2930.

(22) Hu, W.-G.; Mao, J.; Xing, B.; Schmidt-Rohr, K. *Environ. Sci. Technol.* **2000**, *34*, 530-534.

(23) Wang, K.; Xing, B. *J. Environ. Qual.* **2005**, *34*, 342-349.

(24) Kumke, M. U.; Frimmel, F. H.; Ariese, F.; Gooijer, C. *Environ. Sci. Technol.* **2000**, *34*, 3818-3823.

(25) Puchalski, M. M.; Morra, M. J.; Von Wandruszka, R. *Environ. Sci. Technol.* **1992**, *26*, 1787-1792.

(26) Morra, M. J.; Corapcioglu, M. O.; Von Wandruszka, R. M. A.; Marshall, D. B.; Topper, K. *Soil Sci. Soc. Am. J.* **1990**, *54*, 1283-1289.

(27) Chen, S.; Inskeep, W. P.; Williams, S. A.; Callis, P. R. *Environ. Sci. Technol.* **1994**, *28*, 1582-1588.

(28) Backhus, D. A.; Gschwend, P. M. *Environ. Sci. Technol.* **1990**, *24*, 1214-1223.

(29) Schlautman, M. A.; Morgan, J. J. *Environ. Sci. Technol.* **1993**, *27*, 2523-2532.

(30) Herbert, B. E.; Bertsch, P. M.; Novak, J. M. *Environ. Sci. Technol.* **1993**, *27*, 398-403.

(31) Beechem, J. M. *Chem. Phys. Lipids* **1989**, *50*, 237-251.

(32) Beechem, J. M.; Gratton, E. *Proc. SPIE-Int. Soc. Opt. Eng.* **1988**, *909*, 70-81.

(33) Cook, R. L.; Langford, C. H. *Anal. Chem.* **1995**, *67*, 174-180.

(34) Hemmingsen, S. L.; McGown, L. B. *Appl. Spectrosc.* **1997**, *51*, 921-929.

(35) Hewitt, J. D.; McGown, L. B. *Appl. Spectrosc.* **2003**, *57*, 256-265.

(36) Piccolo, A.; Conte, P.; Trivellone, E.; van Lagen, B.; Buurman, P. *Environ. Sci. Technol.* **2002**, *36*, 76-84.

(37) Lee, C.-L.; Kuo, L.-J.; Wang, H.-L.; Hsieh, P.-C. *Water Res.* **2003**, *37*, 4250-4258.

(38) Nelson, G.; Patonay, G.; Warner, I. M. *Anal. Chem.* **1988**, *60*, 274-279.

(39) Coble, P. G.; Green, S. A.; Blough, N. V.; Gagosian, R. B. *Nature* **1990**, *348*, 432-435.

(40) Coble, P. G.; Schultz, C. A.; Mopper, K. *Mar. Chem.* **1993**, *41*, 173-178.

(41) Coble, P. G. *Mar. Chem.* **1996**, *51*, 325-346.

(42) Sierra, M. M. D.; Giovanela, M.; Parlanti, E.; Soriano-Sierra, E. J. *Chemosphere* **2005**, *58*, 715-733.

(43) Lead, J. R.; De Momi, A.; Goula, G.; Baker, A. *Anal. Chem.* **2006**, *78*, 3609-3615.

(44) Marhuenda-Egea, F. C.; Martinez-Sabater, E.; Jorda, J.; Moral, R.; Bustamante, M. A.; Paredes, C.; Perez-Murcia, M. D. *Chemosphere* **2007**, *68*, 301-309.

(45) Mao, J. D.; Hu, W. G.; Schmidt-Rohr, K.; Davies, G.; Ghabbour, E. A.; Xing, B. *Soil Sci. Soc. Am. J.* **2000**, *64*, 873-884.

CHAPTER 5

INVESTIGATION OF THE ENANTIOSELECTIVITY OF DISSOLVED HUMIC MATERIALS WITH CHIRAL COMPOUNDS

5.1 Introduction

Humic substances (HS) are formed by the degradation of dead biomass with plant, animal, fungal, and bacterial biopolymers residue being the most important components of organic materials in aquatic and terrestrial environments.[1, 2] Investigation of the significant role of HS association with pollutants in the environment is a complex task due to the extremely heterogeneous nature of these naturally occurring materials.[3] In the environment, these materials may influence the fate and transport of hydrophobic organic compounds (HOC), such as, polycyclic aromatic hydrocarbons (PAHs) and pesticides, and polychlorinated biphenyls.[4-9]

Several studies have been focused on the investigation of the association behavior between synthetic organic compounds and humic materials (HM). For example, studies have shown that the solubility of HOC in the presence of dissolved humic materials (DHM) in water is enhanced.[10-16] Fluorescence quenching method has also been applied to examine the association of DHM with several HOC, for example, pyrene, naphthalene, phenanthrene, anthracene, and triphenylene.[17-23] These studies have indicated that such association is due to a partition-like interaction between HOC and the hydrophobic domains within DHM.

In addition, it has been suggested that the sorption of HOC to DHM may be due to a hydrophobic solid-phase partitioning.[5, 24-29] In the partitioning model, it was indicated that HM can solubilize and distribute HOC uniformly inside their matrix because HM behave like non-polar liquid phases. However, other studies, such as, nonlinear isotherms,[30-33] solute-solute competition,[6, 34] and desorption hysteresis[35-37] have been explained by dual-mode sorption properties to HM instead of the partitioning model. In addition, a series of proposed models have

been developed by many studies.[30, 32, 34, 38-42] In these models, HM have been described to have rubbery and glassy regions, assigning nonlinear sorption to the presence of a small amount of high surface area containing carbonaceous material (hard). This condensed organic matter has the ability to sorb HOC in relationship with the soft, geologically immature HM. However, none of these models has been fully accepted, and aromatic domains within HM have been implied to be the sorption sites for HOC.[11, 43-46] In addition, aliphatic domains within HM have been involved in the sorption of HOC based on recent studies.[47-49]

Fluorine nuclear magnetic resonance (^{19}F NMR) spectroscopy has also been applied to examine the association of fluorine organic compounds, used as probes, with HM.[50-52] For example, Chein et al.[50] have investigated a membrane micelle model of HM by solubilizing atrazine, labeled by a trifluoromethyl group, in aqueous solutions containing humic acid. It was indicated that atrazine was solubilized by concentrated humic acid solutions, which can form a hydrophobic domain leading to the association with HOC. In addition, Khalaf et al.[52] have investigated the sorption behavior of hexafluorobenzene with humic acid by solid-state ^{19}F NMR spectroscopy after fractionation of the humic acid to eight different molecular size components. It was indicated that humic acid molecules have different chemical environments, accessible for the sorption to HOC, such as hexafluorobenzene. In addition, their results suggested that there were at least three homogeneous sorption sites in the smaller fractions and two sorption sites in the larger fractions, dominated by a rigid sorption domain. It was proposed that this sorption domain resulted from regions containing aliphatic moieties.

While extensive time has been spent on investigating the association behavior between HOC as described above, little is known about the enantiomeric selectivity of DHM and their association behavior with chiral compounds. For example, pesticides are one of the most

important pollutants, and DHM play an important role in the accumulation, mobilization, and transformation process of pesticides.[1, 53] The chirality of these contaminants determines their behavior in a biological environment. Pesticide steric properties are also important with respect to their biological interest. In addition, HM absorb sunlight in soil and aquatic environments.[54, 55] They generally absorb radiation between 300 and 500 nm. As a result, they induce photochemical processes, that generate peroxy and hydroxyl radicals, hydrated electrons, hydrogen peroxide, singlet oxygen and superoxide.[56] In addition, it has been shown that HM can affect the photochemical degradation of several HOC by acting as a photosensitizer or as absorbing chromophor.[57, 58] For example, previous studies have investigated the enantioselective degradation of chiral pesticides, such as metalaxyl, in soils by use of chromatographic technigues.[59-62] It was shown that the enantioselective degradation of enantiomers in soils have different or similar behavior based on the chemical conditions.

In accordance, the purpose of this study was to investigate the chemical effect of chiral pesticides (coumachlor, difenacoum, warfarin, and napropamide) on the sorption mechanism with Leonardite humic acid standard (LHAS) by monitoring changes in fluorescence intensities of each chiral pesticide. In addition, the enantioselectivity of LHAS was examined with chiral compounds, used as probes for the interaction, by use of liquid-state ^{19}F NMR spectroscopy and high performance liquid chromatography (HPLC). In ^{19}F NMR study, the interaction of enantiopure *R*- or *S*-compounds, 1-(9-anthryl)-2,2,2-trifluoroethanol and 1,1'-bi-2-naphthol bis (trifluoro - methanesulfonate), with LHAS was monitored on a day time scale. To further investigate the enantiomeric selectivity of LHAS with chiral compounds, the effect of LHAS on the photochemical degradation of *R*- and *S*-1-(9-anthryl)-2,2,2-trifluoroethanol was investigated

by use of HPLC. The enantioselectivity of LHAS towards both enantiomers was evaluated for samples monitored in the dark and exposed to light.

5.2 Experimental

5.2.1 Materials and Reagents

LHAS was obtained from the International Humic Substances Society (IHSS), Department of Soil, Water, and Climate, University of Minnesota (St. Paul, MN). Chiral pesticides (coumachlor, difenacoum, warfarin, and napropamide), with 99% purity, were obtained from Fluka (Buchs SG, Switzerland) and used as received. Deuterated water (D_2O, 99.9% d) and pure enantiomers of 1-(9-anthryl)-2,2,2-trifluoroethanol [TFAE] and 1,1'-bi-2-naphthol bis (trifluoro - methanesulfonate) [BNF], with 98% purity, were obtained from Sigma-Aldrich (Milwaukee, WI). Monobasic sodium phosphate (NaH_2PO_4), dibasic sodium phosphate (Na_2HPO_4), sodium acetate ($C_2H_3O_2Na$), acetonitrile (ACN), ethanol, and sodium hydroxide (NaOH) were purchased from Fischer Scientific (Fair Lawn, NJ).

5.2.2 Sample Preparation

For the association study of chiral pesticides with LHAS, a stock solution of LHAS was prepared in 18.2 MΩ·cm distilled deionized water by first dissolving an appropriate amount of the LHAS solution with the aide of a few drops of 0.1 M NaOH and then neutralizing the solution with 0.1 M HCl. Stock solutions of each chiral pesticide were prepared in ethanol. All stock solutions were stored in the dark at 4 °C. Six standard solutions of each chiral pesticide with different concentrations of LHAS were prepared by adding appropriate amounts of the chiral pesticide stock solution, evaporating the ethanol to dryness with nitrogen gas (N_2), and followed by adding proper amounts from LHAS stock solution. The final concentration of standard solutions contained 0.5 ppm chiral pesticide and 0, 5, 10, 15, 20, and 25 ppm LHAS. In

addition, individual reference solutions of LHAS (5, 10, 15, 20, and 25 ppm) were also prepared under the same experimental conditions of the chiral pesticide and LHAS mixture. All standard solutions were adjusted to pH 7.0 with buffered aqueous solutions (1 mM of NaH_2PO_4 and 1 mM Na_2HPO_4) and kept in the dark for seven days. In addition, they were purged with N_2 to remove oxygen prior to analysis. Absorbance measurements, required for inner-filter corrections, were obtained directly following fluorescence measurements using the same standard solutions.

For the enantioselectivity study of LHAS by use of ^{19}F NMR, standard solutions of *R*- or *S*-enantiomer of BNF (or TFAE) in the absence and presence of LHAS were prepared in 18.2 MΩ·cm distilled deionized water. The final concentrations of standard solutions contained 0.5 mM of each enantiomer and 0, 8, 10, and 12 mg/mL LHAS. The concentration of 0.5 mM for fluorine labeled chiral compounds was used as a practical concentration limit because of the low concentration sensitivity of ^{19}F NMR measurements. All standard solutions were prepared with the addition of 30% ACN and 16% D_2O. The addition of 30% ACN was the lowest amount required in order to ensure a complete solubility of chiral compounds included in this study. All solutions were adjusted to pH 4.0 with sodium acetate buffer and kept in the dark. The *R*- and *S*-enatiomer in the absence and presence of LHAS were individually incubated under laboratory conditions at different temperatures. All solutions were also deoxygenated purged with nitrogen gas before ^{19}F NMR measurements.^{19}F NMR spectra were collected at a temperature of 298 K. In addition, temperature studies required for evaluating the kinetic interaction of *R*- or *S*-BNF in the absence and presence of LHAS were obtained at 288, 293, and 303 K.

For the enantioselective degradation study of LHAS, *R*- or *S*-TFAE and LHAS mixtures were prepared as described above in the fluorescence study for chiral pesticides. The final concentrations of these standard solutions contained 0.15 ppm *R*- or *S*-TFAE and 0, 15, 30, 45,

and 60 ppm LHAS. Reference solutions of LHAS (15, 30, 45, and 60 ppm) were also prepared. A first set of standard solutions of *R*- or *S*-TFAE in the absence and presence of LHAS was incubated in the dark at 25 °C. In addition, a second set of these solutions was incubated under exposure to light for different time periods on a rotary shaker (70 rpm) at 25 °C. All solutions were covered by caps and light transparent materials for the first and second sets, respectively, to avoid losses by evaporation. In this study, two approaches were used. In the first approach, HPLC measurements were done without sample handling procedures. Secondly, sample pretreatments were performed in order to isolate LHAS so that the interaction of LHAS with the stationary phase of HPLC column could be minimized. The isolation method of LHAS was preformed as described by IHSS.[63] All solutions were first equilibrated at room temperature to a pH value between 1 and 2 with 1 M HCl in order to precipitate LHAS. The suspensions were shaken for 1 hr, and supernatants were collected by use of centrifugation, followed by neutralization to pH 6 with 1 M NaOH.

5.2.3 Instrumentation

Steady-state fluorescence measurements were acquired in triplicate using a Spex Fluorolog-3 spectrofluorimeter (model FL3-22TAU3; Jobin Yvon, Edison, NJ, USA) equipped with a 450-W xenon lamp and R928P photomultiplier tube (PMT) emission detector. The excitation and emission spectra were recorded in a 10 mm quartz fluorescence cuvette with slit widths set for entrance and exit bandwidths of 2 and 4 nm on both excitation and emission monochromators, respectively, for napropamide and 3.5 and 3 nm for coumachlor, difenacoum, and warfarin, respectively. Fluorescence emission spectra were monitored at 290 nm for napropamide and at 309 nm for coumachlor, difenacoum, and warfarin. All fluorescence spectra were blank subtracted before data analysis. Absorbance measurements were also performed in

triplicate using the UV-3101PC (UV-VIS-NIR) scanning spectrophotometer (Shimadzu, Columbia, MD). Absorbance spectra were recorded using 10 mm quartz cuvette.

One-dimensional ^{19}F NMR spectra were acquired in the single-pulse mode by use of a Bruker Avance 400 MHz (9.3T) spectrometer at a frequency of 376.39 MHz. ^{19}F NMR spectra were obtained by applying a 7 μs over a spectral width of 67567.57 Hz and 128 scans. Data points were typically 16 K, accumulated as the sum of 64 transients and separated between pulses by 5 s relaxation delay intervals. In addition, the FIDs were zero filled to 32 K and apodized before Fourier transformation. Chemical shifts were calibrated relative to an external reference of hexafluorobenzene at -160.00 ppm.

HPLC measurements were preformed in triplicate using a liquid chromatography system equipped with 1100 thermostatted autosampler, 1100 quaternary pump with degasser, and 1100 diode array detector and fluorescence detector. A ZORBAX Eclipse XDB-C18 column (5 μm particle diameter, stainless-steel cartridge, 150 mm length, and 4.6 mm inner diameter) was used. The fluorescence detector was set at 364 and 414 nm excitation and emission wavelengths, respectively. The autosampler temperature was controlled at 40 °C. An isocratic elution was established with a mobile phase composition of 60% ACN and 40% water. The flow rate of the gradient was 1 mL/min, and the volume of sample injection was 20 μL.

5.3 Results and Discussion

5.3.1 Fluorescence Associative Study of Chiral Pesticides

The interaction of chiral pesticides with LHAS was studied at pH 7 because the studied pesticides are stable at this pH and cannot undergo the hydrolysis process at pH 7-9.[64] In addition, all solutions were kept in the dark for seven days in order to insure that the interaction

of chiral pesticides with LHAS could take place. The structures of chiral pesticides investigated in this study are shown in Figure 5.1.

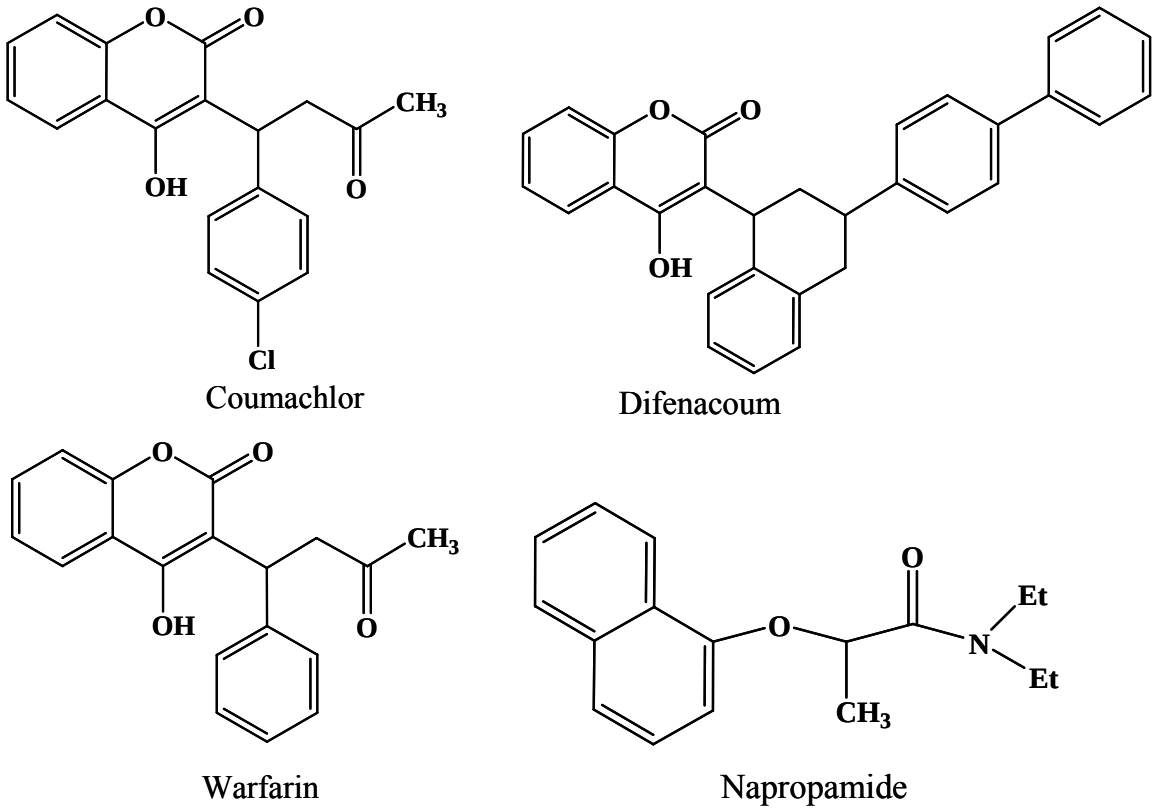

Figure 5.1 Structures of the chiral pesticides.

Steady-state fluorescence measurements were performed to investigate the association behavior between chiral pesticides and LHAS. Figure 5.2 shows fluorescence emission spectra of 0.5 ppm coumachlor, difenacoum, or warfarin in the absence and presence of LHAS (5, 15, and 25 ppm), respectively. Figures 5.2a_1, b_1, and c_1 reveal that the fluorescence intensity of chiral pesticides showed marked decrease with increase in the LHAS concentration from 5 up to 25 ppm. Fluorescence intensities of coumachlor, difenacoum, or warfarin in the absence and presence of LHAS (25 ppm) were also normalized as shown in Figures 5.2a_2, b_2, and c_2.

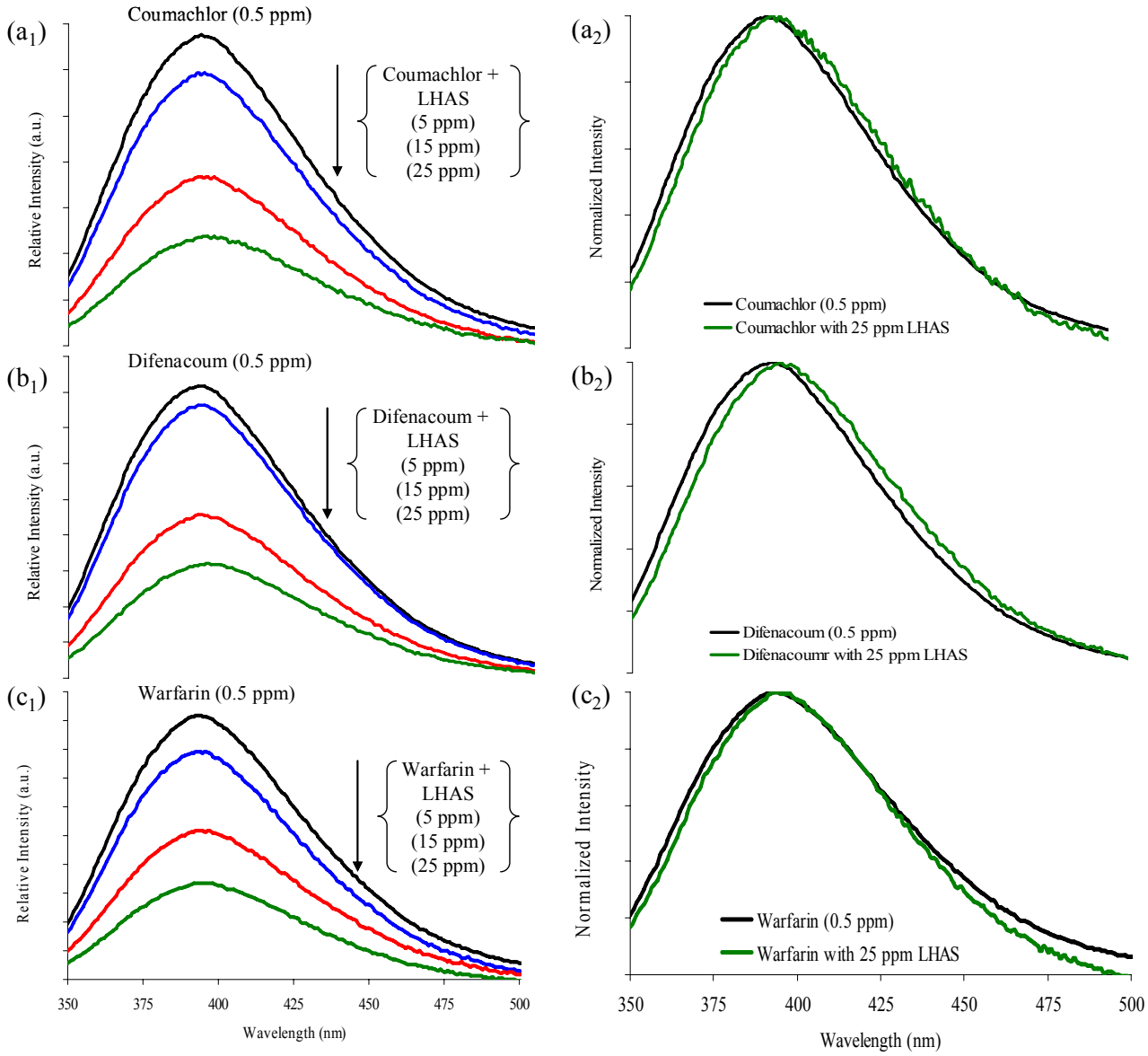

Figure 5.2 Fluorescence emission spectra of 0.5 ppm (a) coumachlor, (b) difenacoum, or (c) warfarin with LHAS (0, 5, 15, and 25 ppm) at pH 7.

A close examination of Figures 5.2a_2, b_2, and c_2 reveal that fluorescence emission of chiral pesticides in the presence of LHAS showed distinct shifts as compared to that in the absence of LHAS, indicative of the association of chiral pesticides with LHAS. In addition, the same trend was observed in the fluorescence intensity of napropamide with LHAS (Figure 5.3). However,

the decrease in the napropamide intensity was the greatest in the presence of LHAS as compared to other chiral pesticides.

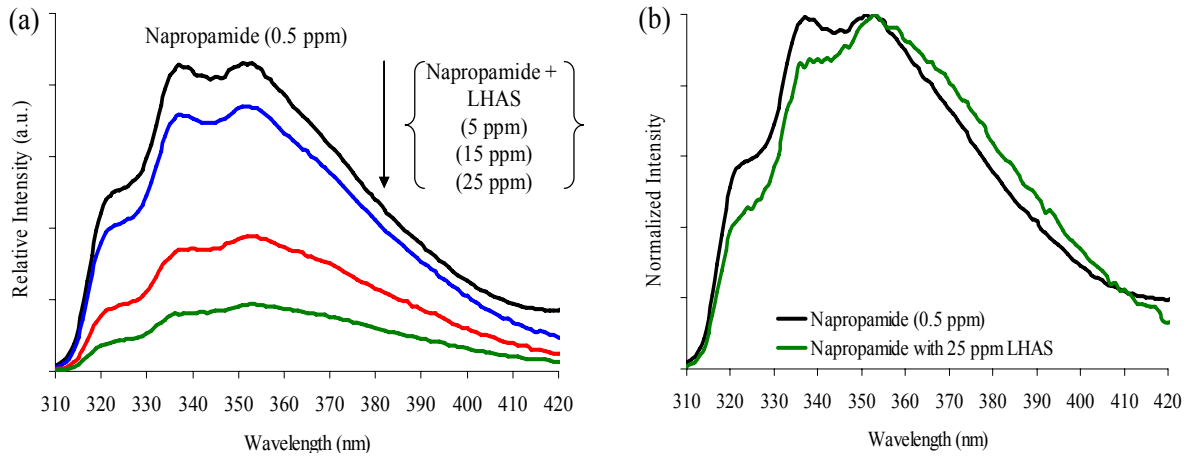

Figure 5.3 Fluorescence emission spectra of 0.5 ppm napropamide with LHAS (0, 5, 15, and 25 ppm) at pH 7.

This may be attributed to structural microenvironment differences between napropamide and other chiral pesticides investigated in this study. This quenching of chiral pesticides at fixed concentrations (0.5 ppm) with an increase of the LHAS concentration may likely be ascribed to associations of chiral pesticides with LHAS. LHAS has the highest aromatic content (0.58) as compared to other soil humic acids.[65] Thus, the hydrophobic domain within LHAS may be the association site of these chiral compounds. In addition, all chiral pesticides have distinctive compositions involving aromatic rings, which afford (π-π) associations with LHAS.

However, fluctuations of the measured fluorescence intensities of chiral pesticides in the presence of LHAS were observed. These fluctuations were due to the fact that LHAS can absorb radiation at both excitation and emission regions of chiral pesticides. This phenomenon, known as the inner-filter effect, can complicate the interpretation of fluorescence results, particularly at higher concentrations of LHAS. Therefore, it was important to correct the measured fluorescence

intensities in order to eliminate these interferences and examine the quenching mechanism of chiral pesticides with LHAS. The corrections of the observed fluorescence intensities for primary and secondary inner-filter effects were performed using equation 1.16 in Chapter 1 of this dissertation.

Figure 5.4 represents Stern-Volmer plots of coumachlor, difenacoum, warfarin, or napropamide in the absence and presence of LHAS after correcting the observed fluorescence intensities for inner-filter effects. As shown in Figure 5.4, Stern-Volmer plots of F_o/F versus [LHAS] showed upward curvatures even after correcting the observed fluorescence intensities.

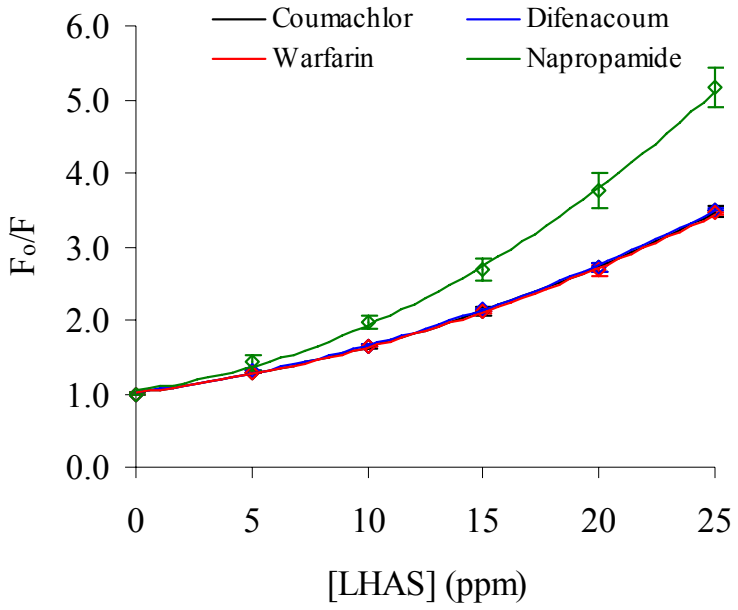

Figure 5.4 Stern-Volmer plots of 0.5 ppm chiral pesticide with LHAS at pH 7.

However, fluorescence quenching of napropamide was the most efficient, as compared to other chiral pesticides, in the presence of LHAS. The upward curvature in Stern-Volmer plot usually indicates that both static and dynamic quenching may take place between the fluorophore and quencher.[66] In addition, this curvature in the Stern-Volmer plot has been previously reported for HOC with HM, which is indicative of the micellar nature of HM.[67]

To further investigate the observed quenching mechanism, the effect of temperature on the fluorescence quenching ratio (F_o/F) of chiral pesticides by LHAS was evaluated, which allows one to determine the primary quenching mechanism. Figure 5.5 shows the effect of temperature on the fluorescence quenching ratio of each chiral pesticide with LHAS.

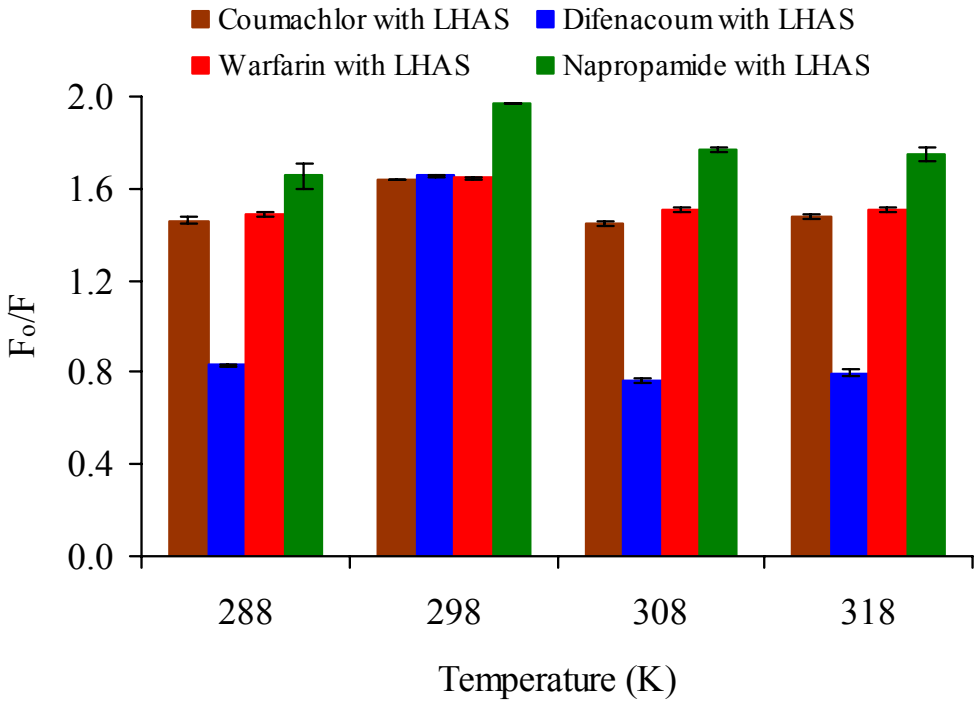

Figure 5.5 The effect of temperature on fluorescence quenching ratio (F_o/F) of 0.5 ppm chiral pesticide with 10 ppm LHAS at pH 7.

In this experiment, the concentration of LHAS remained constant at 10 ppm. In general, it could be observed that the fluorescence quenching ratio of all chiral pesticides showed insignificant change with an increase in the temperature except at 298 K (Figure 5.5). At this temperature, there appeared to be an increase in the fluorescence quenching ratio of the chiral pesticides. A similar finding in the fluorescence quenching ratio of napropamide with a humic acid has also been reported by Chen et al.[68] It was indicated that the increase in fluorescence quenching ratio of napropamide with an increase in the temperature may be attributed to the presence of small

dynamic components or to the thermal instability of napropamide associated with the humic acid. The authors concluded that static quenching was the primary quenching mechanism of napropamide with the humic acid. Their results were also supported by fluorescence lifetime measurements of napropamide in the absence and presence of the humic acid. Accordingly, the trend observed in the fluorescence quenching ratio of chiral pesticides with an increase in the temperature may indicate that the quenching mechanism of chiral pesticides with LHAS is more dominant by static than dynamic quenching.

5.3.2 Enantioselectivity Study of Humic Materials by Use of ^{19}F NMR

^{19}F NMR spectra of *R*- or *S*-BNF were collected and followed up on a day time scale based on the interaction of each enantiomer with LHAS, as DHM model. It can be noted that only one ^{19}F NMR peak was observed, and no change was noticed on this peak for both *R*-BNF and *S*-BNF in the absence of LHAS when the run time increased from 0.2 up to 24 hr (Figure 5.6). This originated signal from 6 fluorine atoms is as a result of the fast rotation around the three bonds of the CF_3 group, averaging the chemical shift of the two CF_3 signals into a single sharp and intense ^{19}F NMR peak.[69, 70] This can be expected since all substituted fluorine atoms of BNF are in the same microenvironment. However, it can be noted that the association of *R*- or *S*-BNF with LHAS retained the original ^{19}F NMR signal observed for the *R*- or *S*-BNF in the absence of LHAS. In addition, it resulted in the appearance of new two signals, the second and third peaks. Both the second and third ^{19}F NMR peaks showed an upfield shift by approximately 0.1 and 3.6 ppm, respectively. This indicates that there is more than one association site within LHAS, having different association accessibility for *R*- or *S*-BNF. In general, this would be expected due to the extremely heterogeneous nature of HM.

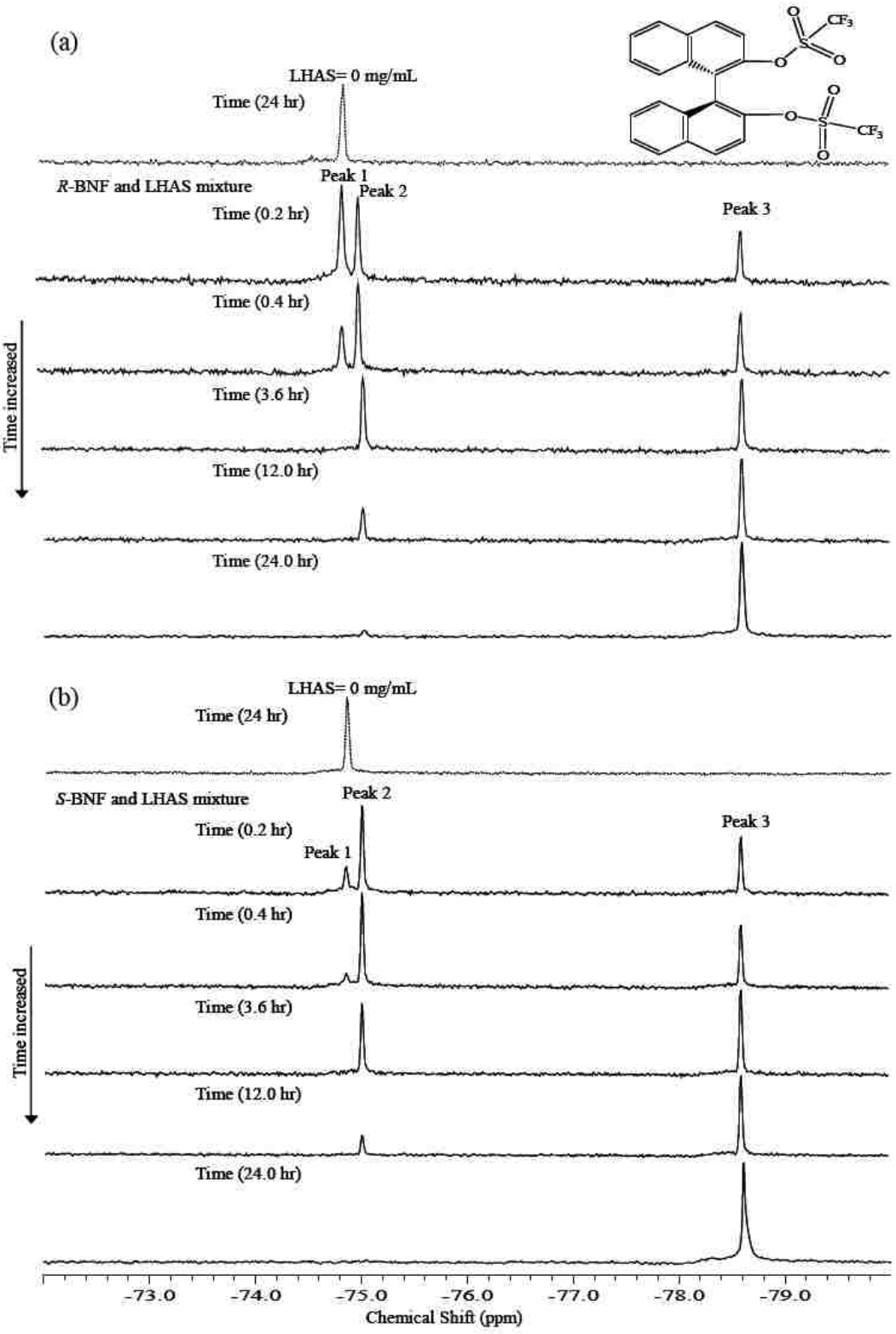

Figure 5.6 ^{19}F NMR spectra of (a) *R*- or (b) *S*-BNF in the absence and presence of 8 mg/mL LHAS at 298 K and pH 4.

The large upfield shift in the third peak may be related to the higher electron density of the fluorine nucleus or ring currents in π-systems for *R*- or *S*-BNF upon association with LHAS as compared to that in the absence of LHAS.

Cornelissen et al.[71] have investigated the interaction of hexafluorobenzene (HFB) with two organic sediments by use of solid-state ^{19}F NMR. There was only one ^{19}F NMR signal at -169 ppm of HFB in the absence of the sediment. For HFB in the presence of the organic sediment without Tenax extraction, only a single ^{19}F NMR of HFB at -126 ppm was observed. It was indicated that the significant difference between the peaks at -169 ppm and -126 ppm could be the result of non-covalent interaction between HFB and the organic sediment. However, two signals at -125.5 and -165.6 ppm were observed for HFB with the organic sediment after Tenax extraction. The authors suggested that the intense peak at -165.6 ppm may be attributed to slowly desorbing HFB. It was also indicated that the small peak at -125.5 ppm may be due to either small residues of rapidly desorbing HFB or a little amount of HFB desorbed from the slow into a rapidly desorbing fraction. In addition, the sorption of HFB with active carbon (a very aromatic matrix), polyacetal (rubbery polymer matrix), or polystyrene (a glassy polymer matrix) was studied to evaluate the similarities between these model sorbents and organic sediments. It was noted that there was two HFB signals with the active carbon at -125.5 and -176.6 ppm. The intensity of the upfield shift peak at -176.6 ppm was 50 times larger than the intensity at -125.5 ppm peak. The authors suggested that the large upfield shift of HFB peak at -176.6 ppm was due to ring currents in π-systems of the HFB aromatic ring.

In addition, a similar behavior of the ^{19}F NMR chemical shift in biological applications has also been reported. For example, Kwon et al.[72] have studied the binding of DNA substrates with the wild-type or Y274F topoisomerase. ^{19}F NMR experiments were performed for the DNA

duplex with wild-type or Y274F topoisomerase. A single ^{19}F NMR peak was observed for free single-stranded 24U^{F}-mer and the duplex 24U^{F}/24-mer. When binding with wild-type or Y274F topoisomerase, the original signal of the free DNA was observed, and a new ^{19}F NMR peak appeared that was upfield shifted by 3 ppm. However, the relative intensity and the ratio of peak area of the DNA duplex with wild-type topoisomerase showed a significant increase as compared to Y274F topoisomerase. It was indicated that the large upfield shift of 3 ppm in ^{19}F NMR peak is attributed to the fact that fluorine nucleus has a greater electron density in the complex as compared to the free DNA duplex. It was also suggested that the large change in the chemical shift upon topoisomerase binding could be the result of a combination of changes in van der Waals interactions, ring current effects, interactions with magnetically anisotropic groups, or dipole interactions. In addition, a much larger magnitude of 11 ppm upfield shift than 3 ppm was reported for the flipped out 5-fluorocytosine from a stacked duplex environment into the active site of *Hha*I cytosine-5-methyltransferase.[73]

In this study, it is of great significance to also note that the third peak is not only upfield shifted, but also the ratio of the peak area and relative intensity were significantly increased with time as compared to the first and second peaks for *R*- or *S*-BNF and LHAS mixture (Figures 5.6 and 5.7c). There was also a decrease in the peak area and relative intensity of the first peak when increasing the time from 0.2 up to 24 hr (Figures 5.6 and 5.7a). However, a different trend was observed for the second ^{19}F NMR peak. An increase followed by a decrease was observed in the peak area and relative intensity of the second peak with the time (Figures 5.6 and 5.7b). This is indicative of the kinetic interaction of *R*- or *S*-BNF with LHAS association sites. When the time increased, the third ^{19}F NMR peak became more dominant compared to the first and second

peaks, evident in its peak area and relative intensity. This is also seen in the disappearance of the first peak followed by the second peak as shown in Figure 5.7.

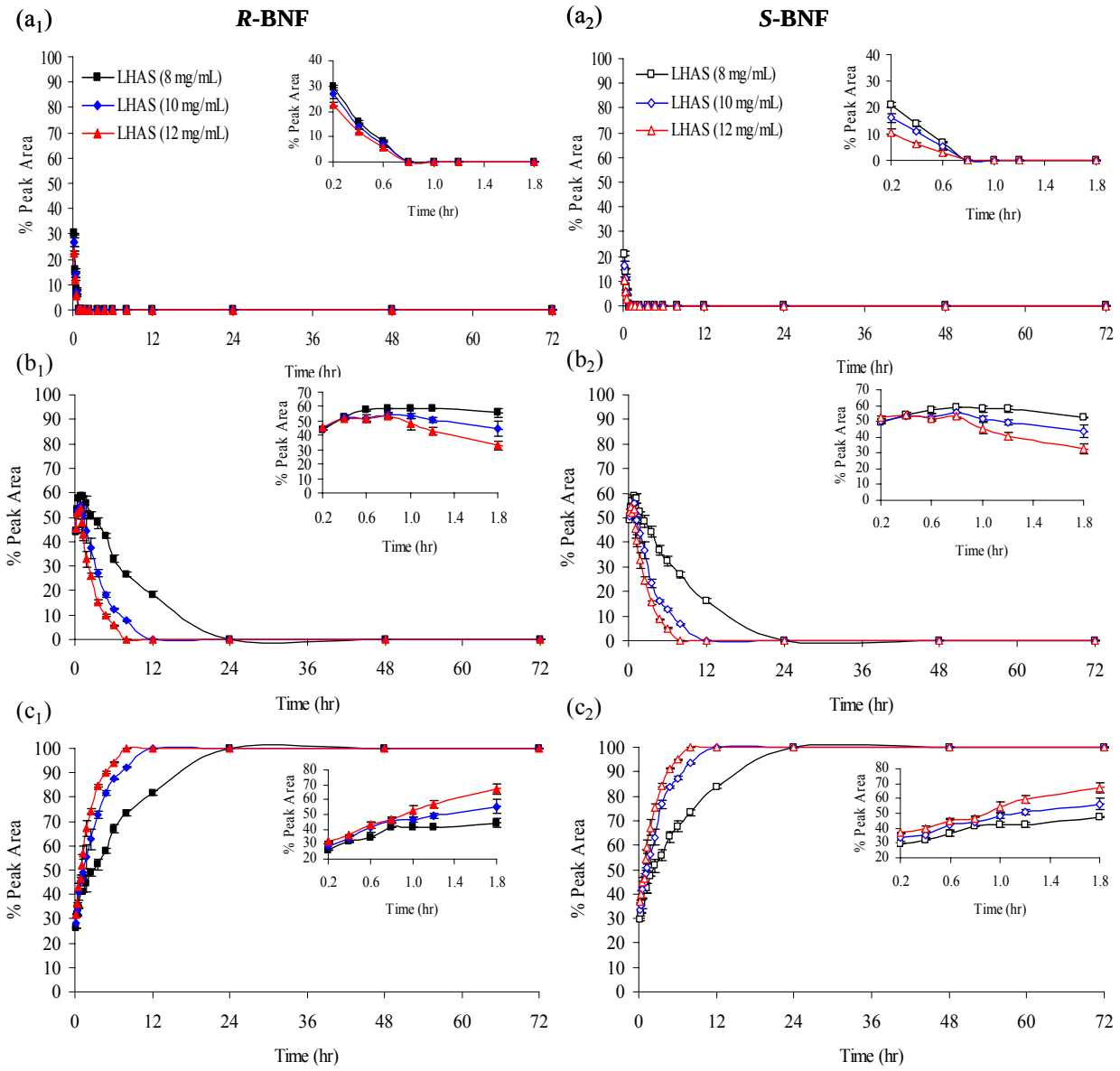

Figure 5.7 The effect of LHAS concentration on the kinetic interaction of 0.5 mM *R*- or *S*-BNF for the (a) first, (b) second, and (c) third peaks at 298 K and pH 4. Corresponding fitting parameters are tabulated in Table 5.1.

This indicated that the movement of *R*- or *S*-BNF towards one of the association site, the third peak, of LHAS became more favorable as compared to other sites when the interaction of *R*- or *S*-BNF with LHAS increased.

To investigate the enantioselectivity of LHAS with *R*- and *S*-BNF enantiomers, the interaction was also monitored at different concentrations of LHAS (Figure 5.7). In general, *R*- and *S*-BNF interactions with LHAS were maximized when LHAS concentration increased from 8 up to 12 mg/mL. This is indicative of the change in LHAS environment with increase in concentration in order to compensate for *R*- and *S*-BNF. It can also be noted that *R*- and *S*-BNF come into more frequent contact with the association site of LHAS, in particular at higher LHAS concentrations. In regards to the enantiomeric selectivity of LHAS towards *R*- and *S*-BNF, similar trends were observed for both enantiomers. However, there appeared to be some differences in the calculated peak areas of the first peak between *R*- and *S*-BNF with an increase in the LHAS concentration (Figure 5.7). It could be observed that the decrease in *S*-BNF peak areas of the first peak was more pronounced as compared to those of *R*-BNF. This indicates that LHAS may have some enantioselectivity towards *R*- and *S*-BNF because *S*-BNF interaction with LHAS was comparatively faster than that of *R*-BNF.

Corresponding rate constants of *R*- or *S*-BNF were determined for the second peak. A linear range of logarithmic plots can be obtained as follows:

$$\ln [BNF]_o - \ln [BNF]_t = k\,t \qquad (5.1)$$

where $[BNF]_o$ and $[BNF]_t$ denote BNF concentration between time (t) = 0 and $t = x$, respectively. The rate constants (k) were determined from the slopes of the corresponding logarithmic plots, ($\ln [BNF]_o - \ln [BNF]_t$) versus t. Linear plots were obtained from equation 5.1, indicating that the kinetic interaction of *R*- or *S*-BNF with LHAS is a first-order kinetic. The calculated rate

constants along with their correlation coefficients (R^2) are reported in Table 5.1. In general, estimated rate constants for both enantiomers increased when increasing LHAS concentration. This indicates that the association of *R*- or *S*-BNF with LHAS is maximized at higher concentrations of LHAS. In regards to LHAS enantiomeric selectivity towards *R*- and *S*-BNF, it was noted that minimal or no change in the calculated rate constants could be observed between both enantiomers when the concentration of LHAS increased.

Table 5.1 The estimated rate constants (*k*) and correlation coefficients (R^2) of *R*- and *S*-BNF at different LHAS concentrations: same as Figure 5.7.

Compound	[LHAS] (mg/mL)	*k* (hr^{-1})	R^2
***R*-BNF**	8	0.107 ±(0.033)	0.986
***S*-BNF**	8	0.114 ±(0.057)	0.996
***R*-BNF**	10	0.274 ±(0.032)	0.998
***S*-BNF**	10	0.291 ±(0.027)	0.997
***R*-BNF**	12	0.415 ±(0.012)	0.999
***S*-BNF**	12	0.436 ±(0.004)	0.998

However, there appeared to be a very slight difference in the calculated rate constants between both enantiomers at the highest concentration of LHAS, may be indicative of LHAS enantioselectivity towards *R*- and *S*-BNF.

To gain further insight into the enantiomeric selectivity of LHAS with both enantiomers, the effect of temperature on the association behavior of these enantiomers with LHAS was also investigated at fixed concentration of LHAS (8 mg/mL), as shown in Figure 5.8. In this study, this concentration of LHAS was chosen because the interactions of *R*- or *S*-BNF with LHAS were the slowest at this concentration. Thus, it allows more time to monitor the kinetic interactions and obtain more information. As previously discussed, in the concentration study, a similar trend in the interaction of *R*- or *S*-BNF with LHAS was also observed with an increase in

the temperature (Figure 5.8). In addition, a more significant decrease was noted in *S*-BNF peak areas of the first peak in comparison to those of *R*-BNF when increasing the temperature. Again, this may be indicative of LHAS enantiomeric selectivity towards *R*- and *S*-BNF.

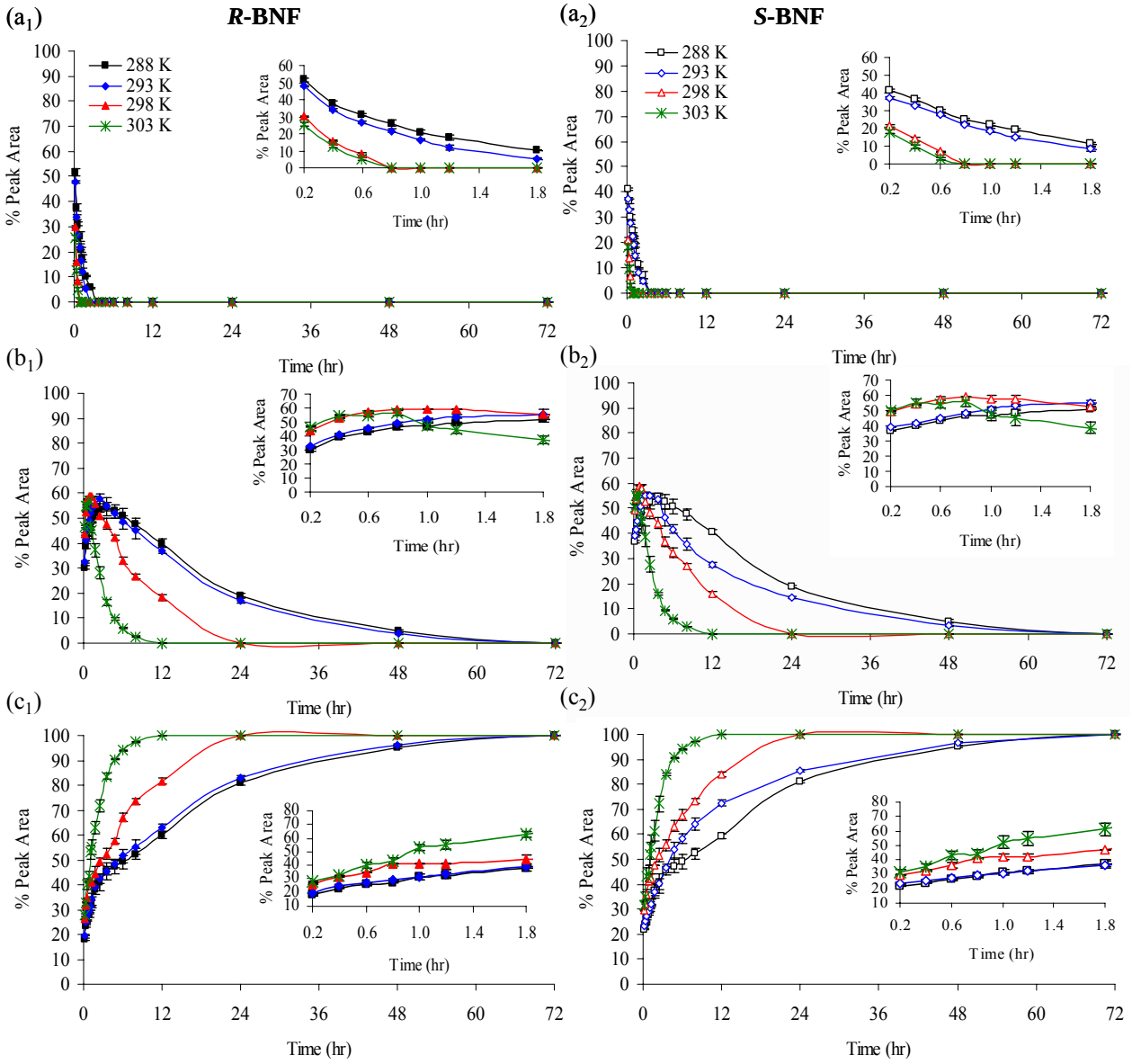

Figure 5.8 The effect of temperature on the kinetic interaction of 0.5 mM *R*- or *S*-BNF with 8 mg/mL LHAS for the (a) first, (b) second, and (c) third peaks at pH 4. Corresponding fitting parameters are tabulated in Table 5.2.

In general, it could be observed from Figure 5.8 that the interaction of *R*- or *S*-BNF with LHAS increased with an increase in temperature from 288 up to 303 K. This suggested that LHAS may change its configuration, leading to an increase in the association with *R*- or *S*-BNF. The calculated rate constants along with the correlation coefficients (R^2) of both enantiomers at different temperatures are summarized in Table 5.2. These findings are also supported by the calculated rate constants. For both *R*- and *S*-BNF, it can be noted that the calculated rate constants increased with an increase in the temperature. In regards to the enantioselectivity of LHAS with *R*- and *S*-BNF, minimal or no change was noted in the calculated rate constants for both enantiomers when the temperature increased from 288 up to 303 K.

Table 5.2 The estimated rate constants (*k*) and correlation coefficients (R^2) of *R*- and *S*-BNF at different temperatures: same as Figure 5.8.

Compound	Temperature (K)	*k* (hr^{-1})	R^2
***R*-BNF**	288	0.055 ±(0.027)	0.997
***S*-BNF**	288	0.055 ±(0.027)	0.996
***R*-BNF**	293	0.061 ±(0.012)	0.998
***S*-BNF**	293	0.062 ±(0.022)	0.998
***R*-BNF**	298	0.107 ±(0.033)	0.986
***S*-BNF**	298	0.114 ±(0.057)	0.996
***R*-BNF**	303	0.423 ±(0.025)	0.999
***S*-BNF**	303	0.414 ±(0.025)	0.997

The activation energy of *R*- or *S*-BNF in the presence of LHAS was also investigated by use of the Arrhenius equation, which can be expressed as follows:

$$k = Ae^{-E_a/RT} \tag{5.2}$$

where *A* is the frequency factor, E_a denotes the activation energy (J/mol), *R* is the ideal gas constant (8.314 $Jmol^{-1}K^{-1}$), and *T* is the temperature (K). A downward curvature was obtained from this equation as shown in Figure 5.9. This further confirmed that there is more than one

association site in LHAS due to the heterogeneous nature of humic materials. In addition, the interaction of *R*- or *S*-BNF with LHAS is constrained by other factors such as LHAS chemical and physical properties. In general, there appeared to be no statistical differences between *R*- and *S*-BNF, which can be observed from the Arrhenius plot in Figure 5.9.

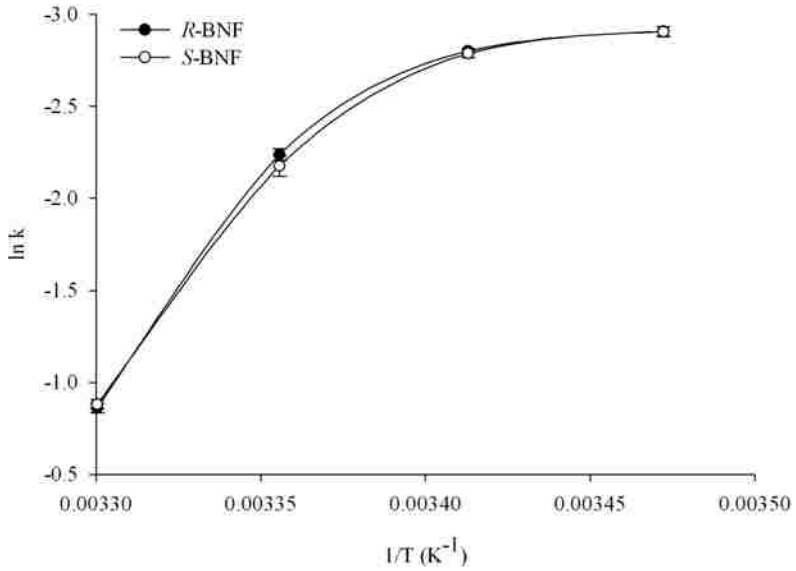

Figure 5.9 Arrhenius plot of the kinetic interactions of 0.5 mM (a) *R*- or (b) *S*-BNF with 8 mg/mL LHAS at pH 4.

^{19}F NMR spectra were also monitored on a day time scale for *R*- or *S*-TFAE in the absence and presence of LHAS. No such kinetic interaction of *R*- or *S*-TFAE was observed in the presence of LHAS. In addition, a completely different behavior was noticed for *R*- or *S*-TFAE with LHAS as compared to *R*- or *S*-BNF. In the absence of LHAS, one ^{19}F NMR signal was noted, and no change was observed in this signal over a course of ^{19}F NMR measurements when increasing the time from 0.2 up to 168 hr (Figure 5.10). However, a downfield shift of the^{19}F NMR signal can be observed for *R*- or *S*-TFAE and LHAS mixture with an increase in the time. It is also interesting to note that *R*- or *S*-TFAE in the presence of LHAS showed a return toward an environment similar to that when *R*- or *S*-TFAE is in the absence of LHAS.

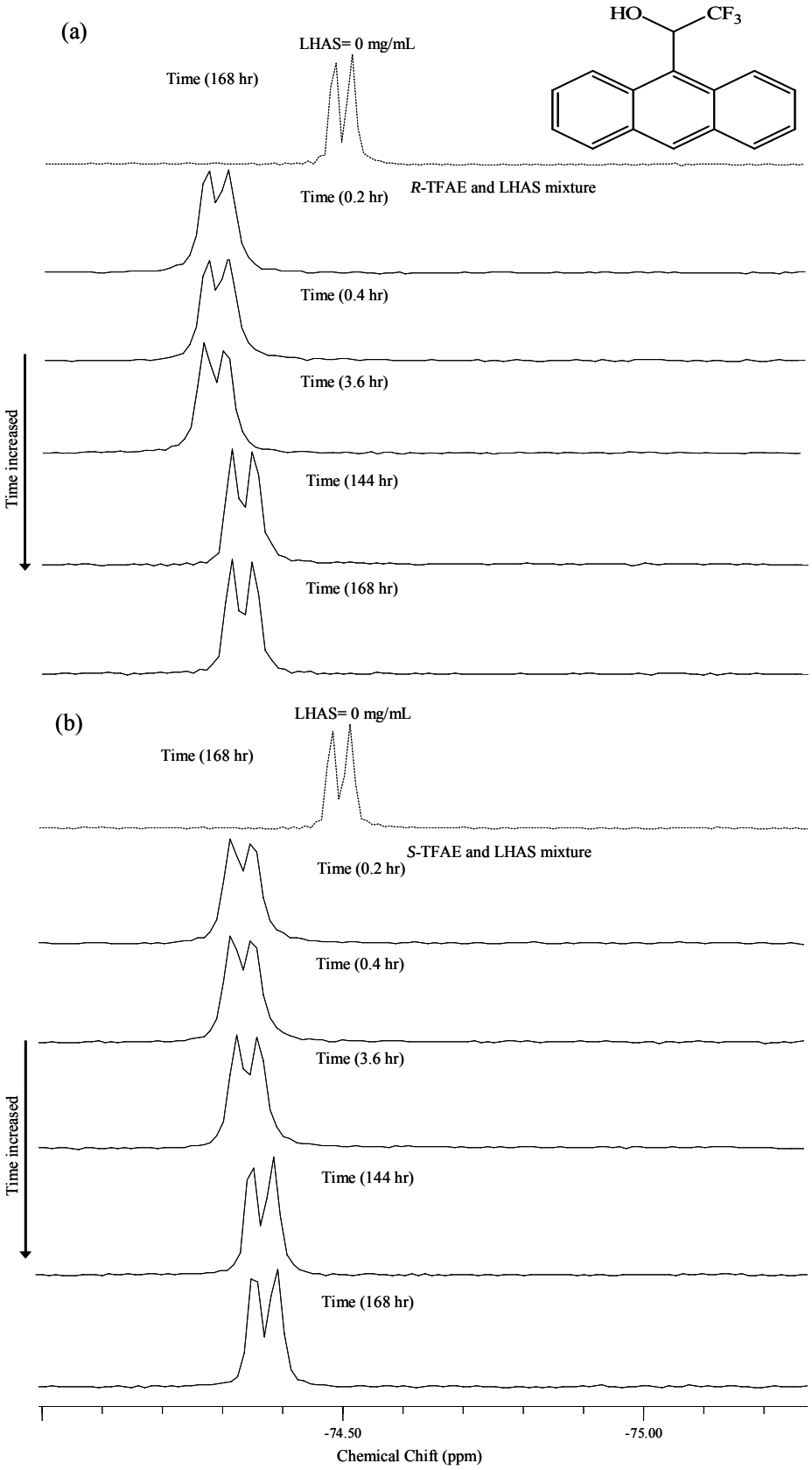

Figure 5.10 ^{19}F NMR spectra of (a) *R*- or (b) *S*-TFAE in the absence and presence of 8 mg/mL LHAS at 298 K and pH 4.

To evaluate the enantiomeric selectivity of LHAS towards *R*- and *S*-TFAE, the effect of LHAS concentration on the association behavior with *R*- or *S*-TFAE was also investigated (Figure 5.11). In general, it can be noted that the interaction of *R*- or *S*-TFAE with LHAS was more prevalent at the lowest concentration of LHAS. At higher LHAS concentrations, both *R*- and *S*-TFAE showed a similar trend to that when the time increased as indicated above. This can likely be ascribed to the hydrophilic property of TFAE that increases its mobility in aqueous environments.

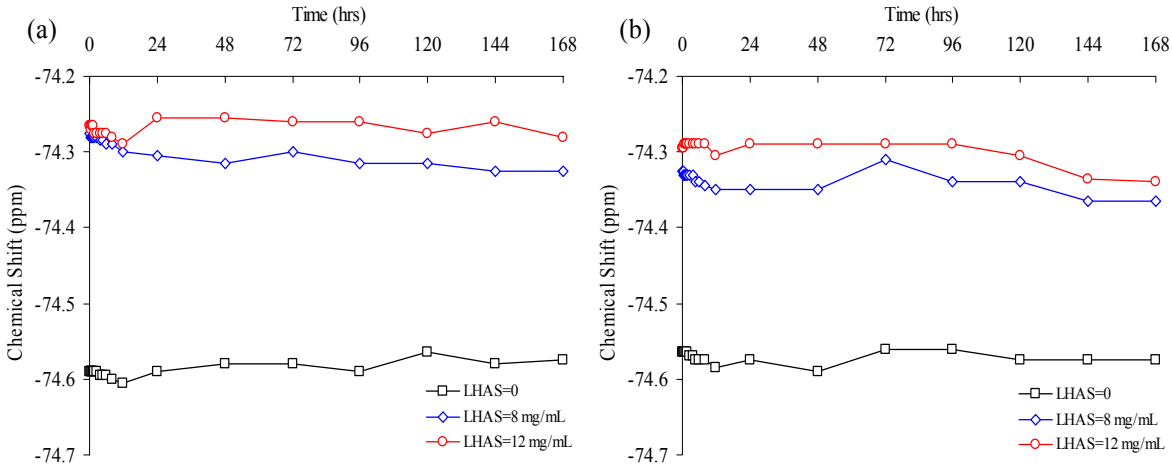

Figure 5.11 ^{19}F NMR chemical shift of 0.5 mM (a) *R*- or (b) *S*-TFAE in the absence and presence of LHAS at 298 K and pH 4.

However, this trend was more pronounced with *S*-TFAE as compared to that with *R*-TFAE. In regards to the chemical shift between *R*- and *S*-TFAE, there appeared to be some differences in the chemical shift at the lowest concentration of LHAS. This may be indicative to the enantioselectivity of LHAS when the association sites were at premium. It could also be observed when there was no such effect at higher LHAS concentrations.

Differences in the association behavior of BNF and TFAE with LHAS can be attributed to the differences in their structural microenvironments and chemical properties. Both BNF and

TFAE have different types of stereoisomerism. The former has an axial-chrality because of the presence of an asymmetric plane. The latter has C-chirality due to the presence of an asymmetrically substituted carbon atom in the alkyl moiety. In addition, BNF is comparatively more hydrophobic than TFAE. Therefore, the interaction of BNF with the hydrophobic domain of LHAS was more prevalent in comparison to that of TFAE. In contrast, the hydrophilic character of TFAE makes it more mobile in aqueous environments. This trend was observed for both *R*- and *S*-TFAE in the presence of LHAS as was discussed above.

5.3.3 Enantioselective Degradation Study of Humic Materials

As was previously discussed in ^{19}F NMR study, minimal or no change was observed in the enantioselectivity of LHAS towards chiral compounds. Therefore, HPLC measurements were performed to gain further insight into the chiral recognition ability and enantioselectivity of LHAS towards *R*- or *S*-TFAE. In this study, the interaction of *R*- or *S*-TFAE with LHAS was investigated for samples monitored in the dark and exposed to light for different time periods. In addition, two approaches were used.

In the first approach, HPLC measurements were performed without any sample pretreatments. Figure 5.12 shows HPLC chromatograms for *R*-TFAE with and without LHAS for solutions monitored in the dark after 21 days and exposed to light from 7 up to 21 days. It can be observed that LHAS is eluted first at ~1.2 min, followed by *R*-TFAE between 5 and 6 min. In general, the eluted peak of LHAS, as shown in Figure 5.12, has an asymmetrical shape with some tailing at a high retention time. Cabaniss et al.[74] have studied the molecular weight distribution in aquatic fulvic acids to investigate the role of HS size in environmental processes by use of high pressure size exclusion chromatography. A similar behavior in the peaks of the fulvic acid and hydrophobic acid fraction was reported.

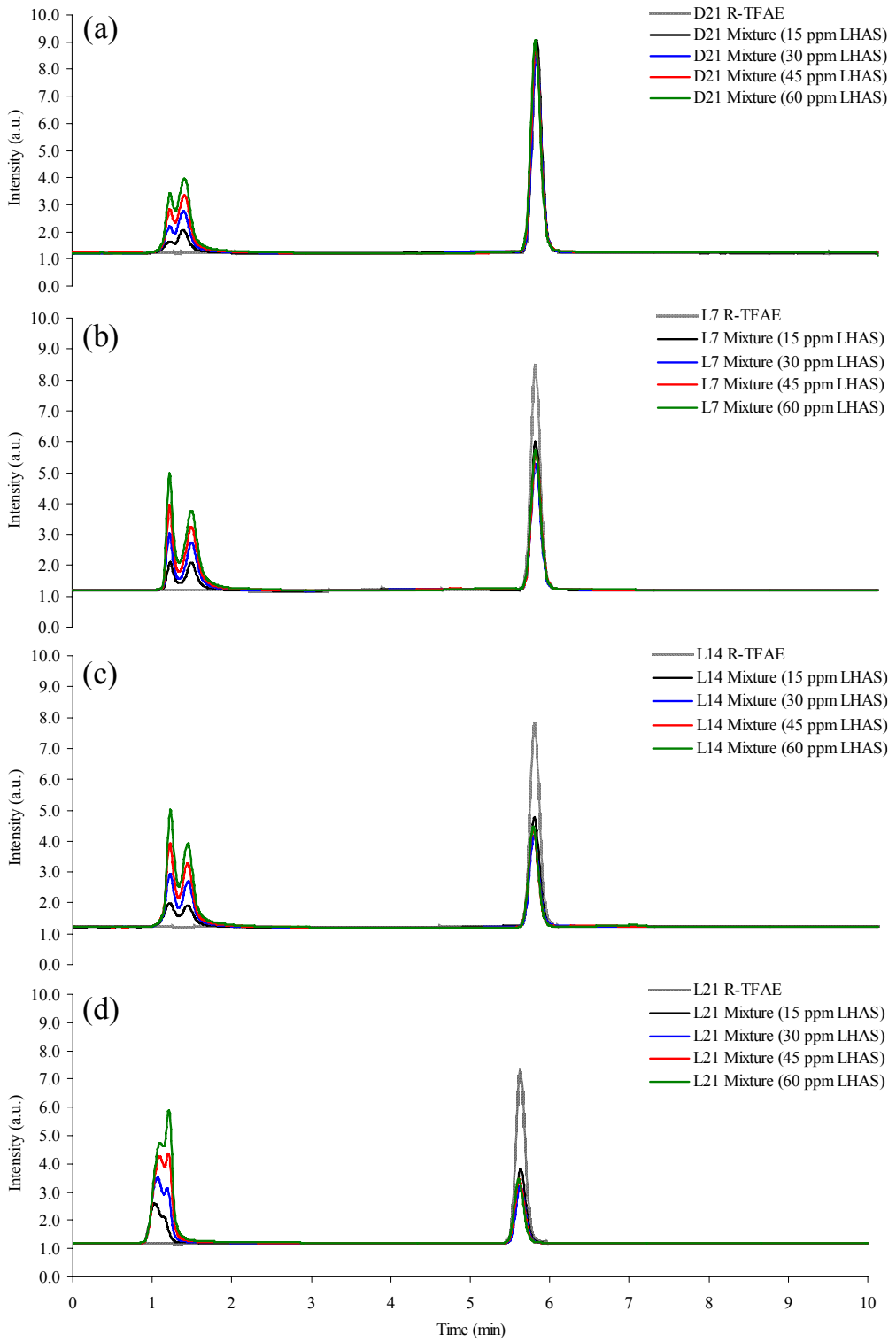

Figure 5.12 HPLC chromatograms of the first approach for 0.15 ppm *R*-TFAE in the absence and presence of LHAS for samples monitored in the dark (D) after (a) 21 days and exposed to light (L) after (b) 7, (c) 14, and (d) 21 days. LHAS is eluted first at ~1.2 min, followed by *R*-TFAE between 5 and 6 min.

It was indicated that the tailing in the peaks may be attributed to either an asymmetrical mass distribution or to undesired interactions of the sample with the column stationary phase. In this study, it was also noted that the elution time of *R*-TFAE slightly decreased when increasing the exposure time to light from 7 up to 21 days (Figure 5.12), strongly indicative of the LHAS interaction with the stationary phase of HPLC column.

In general, no changes were observed in the relative intensity and calculated peak areas of *R*- or *S*-TFAE in the absence and presence of LHAS with increase in the incubation time from 0 up to 21 days (Figures 5.12 and 5.13). In addition, minimal to no changes were observed on LHAS enantioselectivity towards *R*-TFAE for samples monitored in the dark even after 21 days periods. A similar trend was also noticed for *S*-TFAE. This is further supported by a plot of the calculated peak areas versus the concentration of LHAS for both enantiomers, as illustrated in Figure 5.13. These results are in agreement with those obtained in ^{19}F NMR study. For samples exposed to light, photochemical degradation was observed for both *R*- and *S*-TFAE and LHAS individual components. However, the degradation of both enantiomers in the absence of LHAS was less significant as compared to *R*- or *S*-TFAE with LHAS (Figures 5.12 and 5.13). For *R*- or *S*-TFAE and LHAS mixture, it can be noted that the decrease in the relative intensities and peak areas increased with increase in the incubation time and LHAS concentration, indicative of the photochemical degradation of *R*- and *S*-TFAE and their interaction with LHAS.

In addition, it could be observed that the lowest concentration of LHAS (15 ppm) prompted the photochemical degradation of *R*- and *S*-TFAE to the active site within LHAS. However, there was minimal to no change in *R*- or *S*-TFAE relative intensities and peak areas with an increase in the concentration of LHAS from 30 up to 60 ppm. This indicated that less

light reached *R*- or *S*-TFAE at high concentrations of LHAS, which can also be absorbed by LHAS.

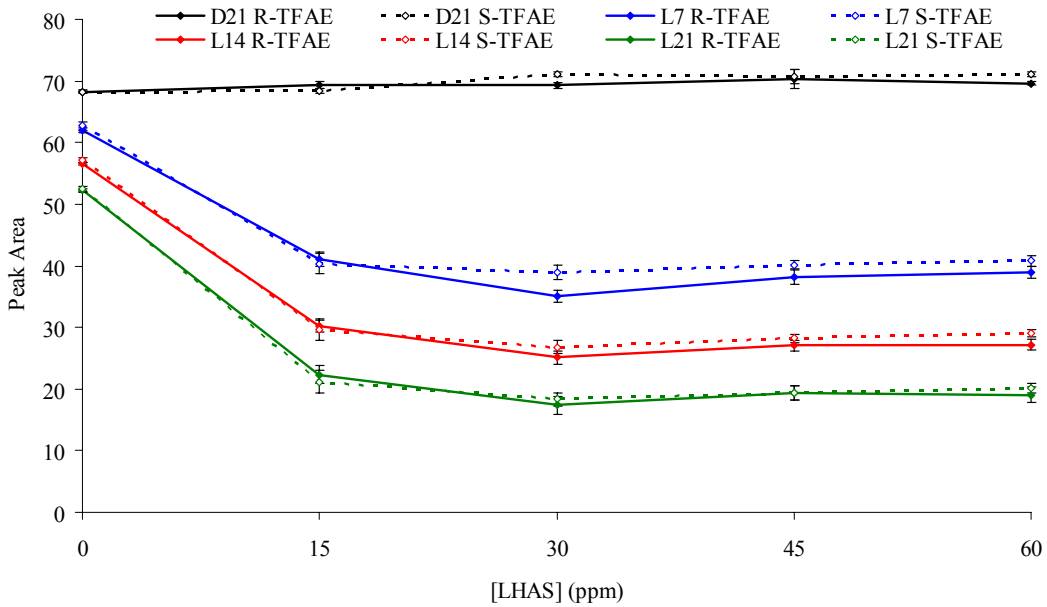

Figure 5.13 Calculated peak areas of the first approach for 0.15 ppm *R*- or *S*-TFAE in the absence and presence of LHAS for samples monitored in the dark (D) after 21 days and exposed to light (L) after 7, 14, and 21 days.

In addition, similar trends were observed in the photochemical degradation of LHAS individual components, in particular at 45 and 60 ppm, with an increase in the incubation time (Figure 5.12). Thus, both *R*- and *S*-TFAE can undergo a more protected environment within LHAS, causing their photochemical degradation to be less as compared to that at lower concentrations of LHAS.

In regards to the enantioselectivity of LHAS with *R*- and *S*-TFAE, both enantiomers showed a similar photochemical degradation behavior in the presence of LHAS as a result of exposure to light and interaction with LHAS (Figure 5.13). However, it could be noted that there was a difference in the calculated peak area of *R*- or *S*-TFAE in the presence of 30 ppm LHAS

after 7 days of the incubation time. This may hint out to the chiral recognition ability and enantiomeric selectivity of LHAS towards both *R*- or *S*-TFAE. However, the enantioselectivity of LHAS with *R*- or *S*-TFAE became less significant when increasing the incubation time from 7 up to 21 days. This can likely be attributed to the diffusion of the photochemical degradation products away from the active site within LHAS. In general, this trend in the LHAS enantiomeric selectivity with *R*- or *S*-TFAE was also observed at different LHAS concentrations with an increase in the incubation time.

In the second part of this study, HPLC measurements were performed for samples monitored in the dark and exposed to light, but a high percentage of LHAS was removed from the sample matrix by acidification with 1M HCl, followed by neutralization with 1 M NaOH. Recall that there was some peak tailing in the eluted peak of LHAS and a slight decrease in the elution time of *R*- or *S*-TFAE in the presence of LHAS, possibly indicating to the undesired interaction between LHAS with the stationary phase of the HPLC column. Therefore, the acidification of the sample matrix can reduce the interaction between LHAS in the stationary phase. Based on this approach, a high percentage of the LHAS individual components and *R*- or *S*-TFAE that is associated with LHAS can be removed from the sample matrix. As a result, it is expected that *R*- or *S*-TFAE individual components to be the most dominant components in the sample matrix. Figure 5.14 displays HPLC chromatograms of *R*-TFAE in the absence and presence of LHAS for samples monitored in the dark after 21 days and exposed to light from 7 up to 21 days. It could be observed that the relative peak intensity of LHAS decreased for both samples monitored in the dark and exposed to light with an increase in the incubation time, indicative of the removal of the high percentage of LHAS.

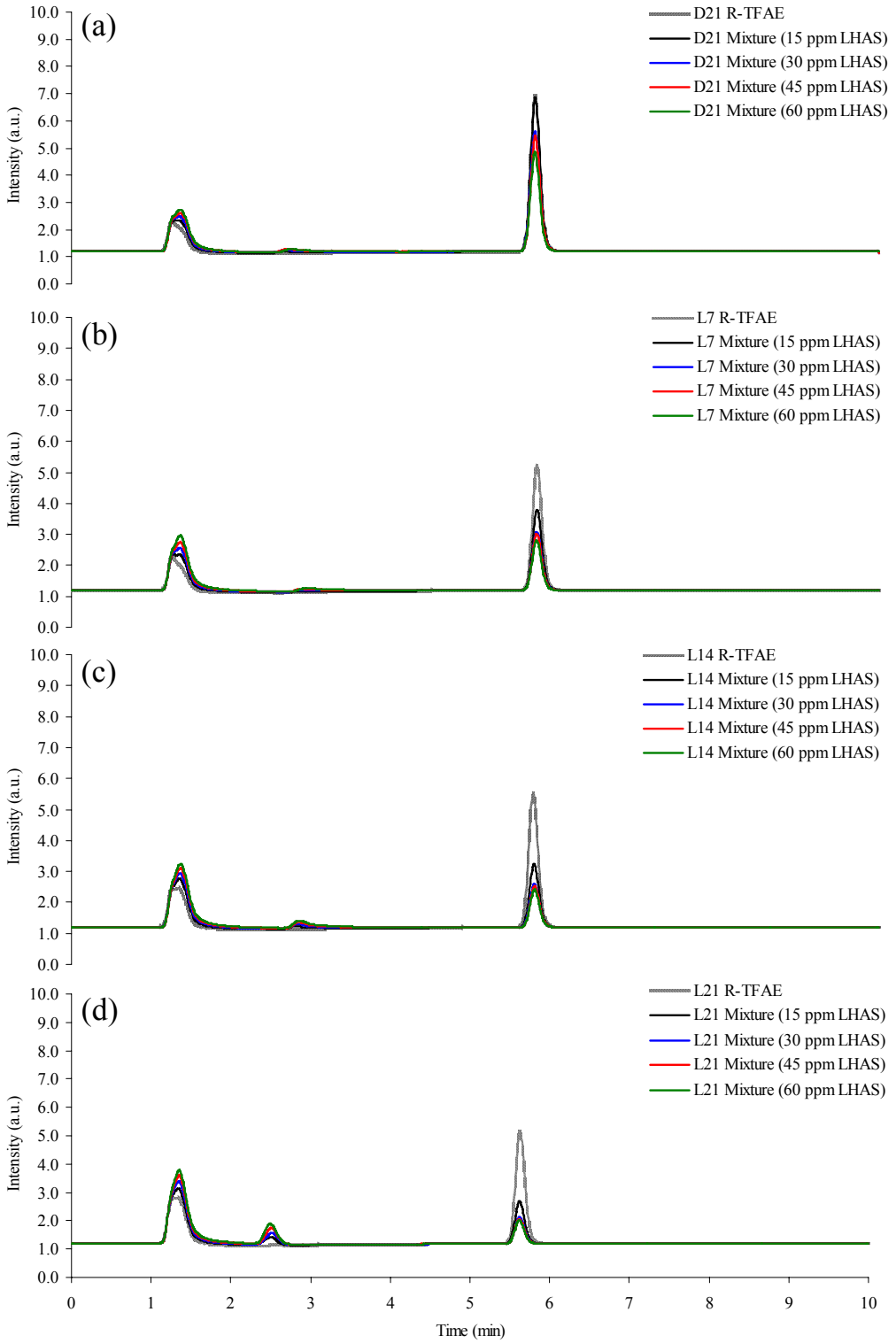

Figure 5.14 HPLC chromatograms of the second approach for 0.15 ppm *R*-TFAE in the absence and presence of LHAS for samples monitored in the dark (D) after (a) 21 days and exposed to light (L) after (b) 7, (c) 14, and (d) 21 days. LHAS is eluted first at ~1.2 min, followed by *R*-TFAE between 5 and 6 min.

In regards to the enantiomeric selectivity of LHAS with *R*- or *S*-TFAE, similar results in the second approach to those obtained in the first approach were also observed for samples monitored in the dark and exposed to light (Figures 5.14 and 5.15). However, in the dark, there was a consistent decrease in the relative intensity of *R*- or *S*-TFAE with an increase in the LHAS concentration in the second approach as compared to the first approach. In addition, it could be noted that the calculated peak areas of both enantiomers decreased when increasing the concentration of LHAS and incubation time for samples monitored in the dark and exposed to light (Figure 5.15). These results suggested that the association of *R*- or *S*-TFAE with LHAS is maximized when increasing the concentration of LHAS because less *R*- or *S*-TFAE molecules were detected with an increase in the LHAS concentration. This decrease in the peak areas of *R*- or *S*-TFAE with LHAS, in the second approach, was more consistent than that in the first approach.

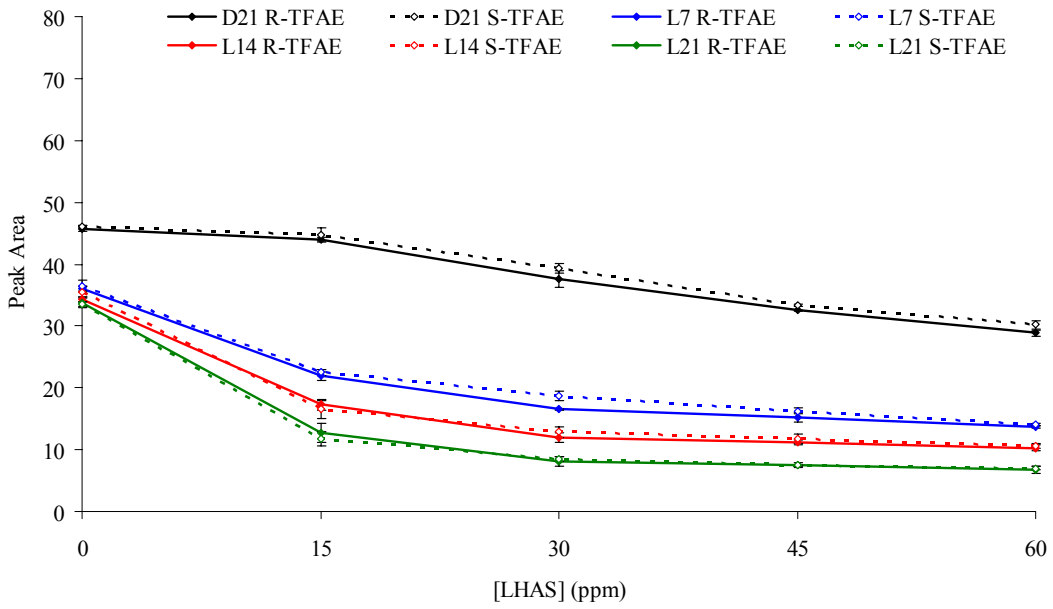

Figure 5.15 Calculated peak areas of the second approach for 0.15 ppm *R*- or S-TFAE in the absence and presence of LHAS for samples monitored in the dark (D) after 21 days and exposed to light (L) after 7, 14, and 21 days.

This further confirmed the effect of LHAS high concentrations (30 to 60 ppm) on the photochemical degradation of both enantiomers, which was observed in the first approach.

However, in the second approach, there appeared to be a new peak in HPLC chromatograms in the region between 2 and 4 min for samples monitored in the dark and exposed to light. This is indicative of LHAS chemical decomposition as a result of sample pretreatments. In the second approach, it could also be noted that there was a more decrease in the relative intensity and calculated peak area of *R*- or *S*-TFAE in the absence of LHAS for solutions monitored in the dark and exposed to light as compared to the first approach. This indicates that sample pretreatments can influence the recovery of both *R*- or *S*-TFAE. In addition, minimal change was observed in the elution time for both enantiomers in the second approach for samples exposed to light after 21 days. This may be attributed to the presence of small percentage of LHAS or to sample handling procedures.

Experimental data of *R*- and *S*-TFAE in the absence of LHAS were evaluated for both approaches in order to study the effect of sample pretreatments on the recovery of both enantiomers (Figure 5.16). In the first approach, no influence was noted on the recovery of *R*- or *S*-TFAE in the absence of LHAS for solutions monitored in the dark (Figure 5.16a). For samples exposed to light, the decrease in peak areas was due to photochemical degradation of both enantiomers as a result of exposure to light. In addition, a consistent trend was observed for samples monitored in the dark and exposed to light. In contrast, it can be noted from Figure 5.16b that there was an effect on the recovery of *R*- or *S*-TFAE for samples monitored in the dark and exposed to light in the second approach. In the dark, there was a decrease in the peak areas of both *R*- or *S*-TFAE in the absence of LHAS, indicative to the effect of sample handling procedures in the recovery of both enantiomers.

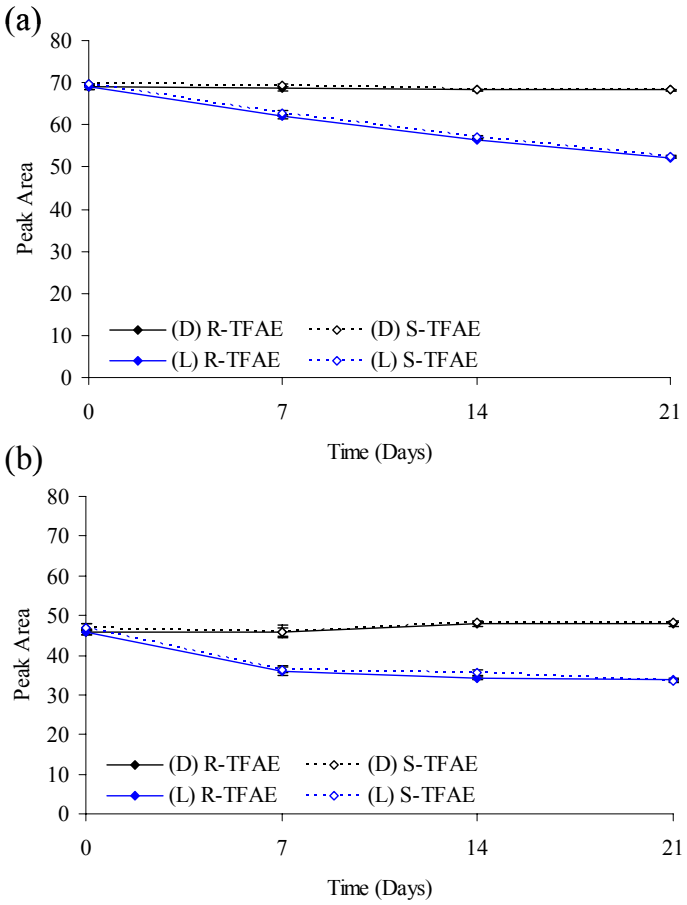

Figure 5.16 Calculated peak areas of 0.15 ppm *R*- or *S*-TFAE in the absence of LHAS for samples monitored in the dark (D) and exposed to light (L) for (a) first and (b) second approaches.

For samples exposed to light, it could be observed that there was a decrease in the calculated peak areas of *R*- or *S*-TFAE in the absence of LHAS as a result of the photochemical degradation. However, the decrease in the peak areas was more significant in the second approach as compared to the first approach, also indicating to the effect of sample pretreatments on the recovery of *R*- or *S*-TFAE.

5.4 Conclusion

Fluorescence characterization of the association behavior between chiral pesticides and LHAS demonstrated that both the high aromaticity of LHAS and distinctive composition of

chiral pesticides can be major contributors of such association. Significant reductions were observed in the fluorescence intensity of chiral pesticides with an increase in the LHAS concentration. From Stern-Volmer plots, fluorescence quenching of napropamide was the most efficient as compared to coumachlor, difenacoum, or warfarin in the presence of LHAS. In addition, upward curvatures were observed in Stern-Volmer plots of all chiral pesticides, indicative of both static and dynamic quenching mechanisms of chiral pesticides in the presence of LHAS. For further investigation of the quenching mechanism, the effect of temperature on the fluorescence quenching ratio of these compounds in the absence and presence of LHAS was investigated. The results suggested that the association mechanism of chiral pesticides with LHAS was more dominant by static than dynamic quenching.

The results of the association between *R*- and *S*-enantiomers with LHAS using ^{19}F NMR showed clear evidence that chirality may play a role in the association of organic pollutants with HM. ^{19}F NMR results suggested that humic materials have a heterogeneous nature, and more than one association site can have different accessibilities for organic pollutants. In general, the calculated rate constants for *R*- or *S*-BNF increased with increasing the temperature or LHAS concentration. In regards to the enantioselectivity of LHAS towards *R*- and *S*-BNF, minimal or no change was observed in the calculated rate constants between both enantiomers. However, there appeared to be a very slight difference in the rate constant between *R*- and *S*-BNF at the highest LHAS concentration. This may indicate that LHAS has some enantioselectivity towards these enantiomers.

In contrast, a different trend was noted for TFAE in the association behavior with LHAS as compared to that of BNF. This can likely be ascribed to the structural microenvironment differences of compounds investigated in this study. Generally, the

association behavior of *R*- or *S*-TFAE with LHAS was more pronounced at the lowest concentration of LHAS. In regards to LHAS enantioselectivity with *R*- and *S*-TFAE, a slight difference in ^{19}F NMR chemical shift was observed between *R*- and *S*-TFAE at the lowest LHAS concentration. Finally, results demonstrated considerable promise of ^{19}F NMR in studying the kinetics of association between fluorine labeled pollutants and humic materials.

The enantiomeric selectivity of LHAS was further investigated by use of HPLC. Two approaches were used to examine the enantiomeric selectivity of LHAS towards *R*- and *S*-TFAE. In the dark, minimal to no change was observed on the chiral recognition ability and enantiomeric selectivity of LHAS with *R*- and *S*-TFAE for the first and second approaches. In contrast, the interaction of *R*- or *S*-TFAE with LHAS for solutions exposed to light showed that LHAS may have a slight enantioselectivity towards both enantiomers at 30 ppm LHAS in both approaches. In the second approach, results showed that the association of *R*- or *S*-TFAE with LHAS is maximized with an increase in the LHAS concentration. Finally, both the first and second approaches have advantages and disadvantages and can be considered as complementary approaches in providing detail into the enantiomeric selectivity of DHM with chiral compounds.

5.5 References

(1) Maqueda, C.; Morillo, E.; Martin, F.; Undabeytia, T. *J. Environ. Sci. Heal. B* **1993**, *B28*, 655-670.

(2) Phillips, S. L.; Olesik, S. V. *Anal. Chem.* **2003**, *75*, 5544-5553.

(3) Hemmingsen, S. L.; McGown, L. B. *Appl. Spectrosc.* **1997**, *51*, 921-929.

(4) Mingelgrin, U.; Gerstl, *Z. J. Environ. Qual.* **1983**, *12*, 1-11.

(5) Chiou, C. T.; Porter, P. E.; Schmedding, D. W. *Environ. Sci. Technol.* **1983**, *17*, 227-231.

(6) McGinley, P. M.; Katz, L. E.; Weber, W. J., Jr. *Environ. Sci. Technol.* **1993**, *27*, 1524-1531.

(7) Xing, B.; Pignatello, J. J. *Environ. Sci. Technol.* **1997**, *31*, 792-799.

(8) Xing, B.; Pignatello, J. J. *Environ. Sci. Technol.* **1998**, *32*, 614-619.

(9) Kohl, S. D.; Rice, J. A. *Chemosphere* **1998**, *36*, 251-261.

(10) Carter, C. W.; Suffet, I. H. *Environ. Sci. Technol.* **1982**, *16*, 735-740.

(11) Chin, Y.-P.; Aiken, G. R.; Danielsen, K. M. *Environ. Sci. Technol.* **1997**, *31*, 1630-1635.

(12) McCarthy, J. F.; Jimenez, B. D. *Environ. Sci. Technol.* **1985**, *19*, 1072-1076.

(13) Chiou, C. T.; Malcolm, R. L.; Brinton, T. I.; Kile, D. E. *Environ. Sci. Technol.* **1986**, *20*, 502-508.

(14) Webster, G. R. B.; Muldrew, D. H.; Graham, J. J.; Sarna, L. P.; Muir, D. C. G. *Chemosphere* **1986**, *15*, 1379-1386.

(15) Chiou, C. T.; Kile, D. E.; Brinton, T. I.; Malcolm, R. L.; Leenheer, J. A.; MacCarthy, P. *Environ. Sci. Technol.* **1987**, *21*, 1231-1234.

(16) Johnson-Logan, L. R.; Broshears, R. E.; Klaine, S. J. *Environ. Sci. Technol.* **1992**, *26*, 2234-2239.

(17) Gauthier, T. D.; Shane, E. C.; Guerin, W. F.; Seitz, W. R.; Grant, C. L. *Environ. Sci. Technol.* **1986**, *20*, 1162-1166.

(18) Tiller, C. L.; Jones, K. D. *Environ. Sci. Technol.* **1997**, *31*, 424-429.

(19) Danielsen, K. M.; Chin, Y.-P.; Buterbaugh, J. S.; Gustafson, T. L.; Traina, S. J. *Environ. Sci. Technol.* **1995**, *29*, 2162-2165.

(20) Perminova, I. V.; Grechishcheva, N. Y.; Petrosyan, V. S. *Environ. Sci. Technol.* **1999**, *33*, 3781-3787.

(21) Kumke, M. U.; Frimmel, F. H.; Ariese, F.; Gooijer, C. *Environ. Sci. Technol.* **2000**, *34*, 3818-3823.

(22) Laor, Y.; Rebhun, M. *Environ. Sci. Technol.* **2002**, *36*, 955-961.

(23) Backhus, D. A.; Golini, C.; Castellanos, E. *Environ. Sci. Technol.* **2003**, *37*, 4717-4723.

(24) Karickhoff, S. W.; Brown, D. S.; Scott, T. A. *Water Res.* **1979**, *13*, 241-248.

(25) Wu, S. C.; Gschwend, P. M. *Environ. Sci. Technol.* **1986**, *20*, 717-725.

(26) Rutherford, D. W.; Chiou, C. T.; Kile, D. E. *Environ. Sci. Technol.* **1992**, *26*, 336-340.

(27) Rutherford, D. W.; Chiou, C. T. *Environ. Sci. Technol.* **1992**, *26*, 965-970.

(28) McGroddy, S. E.; Farrington, J. W.; Gschwend, P. M. *Environ. Sci. Technol.* **1996**, *30*, 172-177.

(29) Maruya, K. A.; Risebrough, R. W.; Horne, A. J. *Environ. Sci. Technol.* **1996**, *30*, 2942-2947.

(30) Xing, B.; Pignatello, J. J. *Environ. Toxicol. Chem.* **1996**, *15*, 1282-1288.

(31) LeBoeuf, E. J.; Weber, W. J., Jr. *Environ. Sci. Technol.* **1997**, *31*, 1697-1702.

(32) Huang, W.; Young, T. M.; Schlautman, M. A.; Yu, H.; Weber, W. J., Jr. *Environ. Sci. Technol.* **1997**, *31*, 1703-1710.

(33) Chiou, C. T.; Kile, D. E. *Environ. Sci. Technol.* **1998**, *32*, 338-343.

(34) Xing, B.; Pignatello, J. J.; Gigliotti, B. *Environ. Sci. Technol.* **1996**, *30*, 2432-2440.

(35) Kan, A. T.; Fu, G.; Tomson, M. B. *Environ. Sci. Technol.* **1994**, *28*, 859-867.

(36) Aochi, Y. O.; Farmer, W. J. *Environ. Sci. Technol.* **1997**, *31*, 2520-2526.

(37) Cornelissen, G.; Van Noort, P. C. M.; Govers, H. A. J. *Environ. Sci. Technol.* **1998**, *32*, 3124-3131.

(38) Weber, W. J., Jr.; McGinley, P. M.; Katz, L. E. *Environ. Sci. Technol.* **1992**, *26*, 1955-1962.

(39) Young, T. M.; Weber, W. J., Jr. *Environ. Sci. Technol.* **1995**, *29*, 92-97.

(40) Weber, W. J., Jr.; Huang, W. *Environ. Sci. Technol.* **1996**, *30*, 881-888.

(41) Huang, W.; Weber, W. J., Jr. *Environ. Sci. Technol.* **1997**, *31*, 2562-2569.

(42) Graber, E. R.; Borisover, M. D. *Environ. Sci. Technol.* **1998**, *32*, 3286-3292.

(43) Gauthier, T. D.; Seitz, W. R.; Grant, C. L. *Environ. Sci. Technol.* **1987**, *21*, 243-248.

(44) Chiou, C. T.; McGroddy, S. E.; Kile, D. E. *Environ. Sci. Technol.* **1998**, *32*, 264-269.

(45) Drewes, J. E.; Croue, J. P. *Water Sci.Technol.: Water Supply* **2002**, *2*, 1-10.

(46) Holbrook, R. D.; Love, N. G.; Novak, J. T. *Environ. Sci. Technol.* **2004**, *38*, 4987-4994.

(47) Chefetz, B.; Deshmukh, A. P.; Hatcher, P. G.; Guthrie, E. A. *Environ. Sci. Technol.* **2000**, *34*, 2925-2930.

(48) Hu, W.-G.; Mao, J.; Xing, B.; Schmidt-Rohr, K. *Environ. Sci. Technol.* **2000**, *34*, 530-534.

(49) Wang, K.; Xing, B. *J. Environ. Qual.* **2005**, *34*, 342-349.

(50) Chien, Y.-Y.; Kim, E.-G.; Bleam, W. F. *Environ. Sci. Technol.* **1997**, *31*, 3204-3208.

(51) Chien, Y.-Y.; Bleam, W. F. *Langmuir* **1997**, *13*, 5283-5288.

(52) Khalaf, M.; Kohl, S. D.; Klumpp, E.; Rice, J. A.; Tombacz, E. *Environ. Sci. Technol.* **2003**, *37*, 2855-2860.

(53) Hewitt, J. D.; McGown, L. B. *Appl. Spectrosc.* **2003**, *57*, 256-265.

(54) Malcolm, R. L. *Anal. Chim. Acta* **1990**, *232*, 19-30.

(55) Schmitt-Kopplin, P.; Hertkorn, N.; Schulten, H.-R.; Kettrup, A. *Environ. Sci. Technol.* **1998**, *32*, 2531-2541.

(56) Cooper, W. J.; Zika, R. G.; Petasne, R. G.; Fischer, A. M. In *Aquatic Humic Substances: Influence on Fate and Treatment of Pollutants*; Suffet, I. H., P. MacCarthy, Eds.; American Chemical Society: Washington, DC, 1989, pp 333-362.

(57) Khan, S. U.; Schnitzer, M. *J. Environ. Sci. Heal. B* **1978**, *B13*, 299-310.

(58) Minero, C.; Pramauro, E.; Pelizzetti, E.; Dolci, M.; Marchesini, A. *Chemosphere* **1992**, *24*, 1597-1606.

(59) Mueller, M. D.; Buser, H.-R. *Environ. Sci. Technol.* **1995**, *29*, 2031-2037.

(60) Marucchini, C.; Zadra, C. *Chirality* **2002**, *14*, 32-38.

(61) Buser, H.-R.; Mueller, M. D.; Poiger, T.; Balmer, M. E. *Environ. Sci. Technol.* **2002**, *36*, 221-226.

(62) Buerge, I. J.; Poiger, T.; Mueller, M. D.; Buser, H.-R. *Environ. Sci. Technol.* **2003**, *37*, 2668-2674.

(63) Swift, R. S. In *Organic matter characterization (chap 35),* First ed.; Soil Science Society of America: Madison, 1996, pp 1018-1020.

(64) Desiderio, C.; Palcaro, C. M.; Fanali, S. *Electrophoresis* **1997**, *18*, 227-234.

(65) Engebretson, R. R.; Amos, T.; von Wandruszka, R. *Environ. Sci. Technol.* **1996**, *30*, 990-997.

(66) Lakowicz, J. R. *Principles of Fluorescence Spectroscopy*, Second ed.; Plenum Press: New York, 1999.

(67) Puchalski, M. M.; Morra, M. J.; Von Wandruszka, R. *Environ. Sci. Technol.* **1992**, *26*, 1787-1792.

(68) Chen, S.; Inskeep, W. P.; Williams, S. A.; Callis, P. R. *Environ. Sci. Technol.* **1994**, *28*, 1582-1588.

(69) Papeo, G.; Giordano, P.; Brasca, M. G.; Buzzo, F.; Caronni, D.; Ciprandi, F.; Mongelli, N.; Veronesi, M.; Vulpetti, A.; Dalvit, C. *J. Am. Chem. Soc.* **2007**, *129*, 5665-5672.

(70) Jackson, J. C.; Hammill, J. T.; Mehl, R. A. *J. Am. Chem. Soc.* **2007**, *129*, 1160-1166.

(71) Cornelissen, G.; Van Noort, P. C. M.; Nachtegaal, G.; Kentgens, A. P. M. *Environ. Sci. Technol.* **2000**, *34*, 645-649.

(72) Kwon, K.; Jiang, Y. L.; Song, F.; Stivers, J. T. *J. Biol. Chem.* **2002**, *277*, 353-358.

(73) Klimasauskas, S.; Szyperski, T.; Serva, S.; Wuthrich, K. *EMBO J.* **1998**, *17*, 317-324.

(74) Cabaniss, S. E.; Zhou, Q.; Maurice, P. A.; Chin, Y.-P.; Aiken, G. R. *Environ. Sci. Technol.* **2000**, *34*, 1103-1109.

CHAPTER 6

CONCLUSIONS AND FUTURE STUDIES

In this research, the association of hydrophobic organic compounds (HOC) with dissolved humic materials (DHM) was investigated using a series of analytical techniques. In Chapter 2 of this dissertation, the association of pyrene with DHM, including Leonardite humic acid standard (LHAS), Amherst humic acid (AHA), and Suwannee River fulvic acid reference (SRFAR), was investigated using steady-state fluorescence spectroscopy. Quenching in the fluorescence intensity of pyrene was observed in the presence of DHM. In addition, the effects of temperature, pH, and ionic strength on the association behavior of pyrene with DHM were discussed. Results obtained showed that steady-state fluorescence spectroscopy alone may not resolve the issue over the quenching mechanism of pyrene with DHM.

In contrast, lifetime based fluorescence measurements allow for a deeper mechanistic understanding into the association behavior of HOC with DHM. In Chapter 3, a new method to frequency-domain lifetime measurements, based on frequency segmentation and recombination, was developed. The effects of photobleaching, dissolved oxygen, and cell walls adsorption within multi-component systems on recovered fluorescence lifetimes and fractional intensity contributions were addressed. The frequency segmentation and recombination method was described and evaluated through both simulation of a two component dye system, consisting of fluorescein and rhodamine B mixture, and comparison of experimental data collected in traditional and segmented fashion. In addition, this newly developed method was applied to a more complex system consisting of pyrene and SRFAR to improve recovered lifetimes and fractional contributions. Results demonstrated clear evidence that frequency segmentation and recombination experiments of multi-component systems reduced errors that result from a

changing fractional contribution and provide more reliable results as compared to traditional fashion (single long run).

For further investigation of the fluorescence quenching mechanism of pyrene with DHM, the newly developed method was applied to pyrene and DHM mixtures in Chapter 4. In general, results of recovered pyrene lifetimes suggested that the association behavior of pyrene with DHM is dependent upon several factors, such as, the nature and concentration, aliphatic or aromatic content, and elemental composition of DHM. In addition, DHM have different association accessibilities for pyrene due to the extremely heterogeneous nature of these naturally occurring materials. Consequently, there is no simple answer stating that the quenching mechanism of pyrene with DHM is either static or dynamic quenching; yet, it could be a combination of both.

In Chapter 5, the association of chiral pesticides (coumachlor, difenacoum, warfarin, napropamide) with LHAS was investigated by use of steady-state fluorescence spectroscopy. In general, a decrease in the fluorescence intensity of chiral pestisides was observed with an increase in the LHAS concentration. Stern-Volmer plots and the effect of temperature on fluorescence quenching ratio of these compounds with LHAS were also discussed. Results showed that the quenching mechanism of chiral pesticides with LHAS is more dominant by static than dynamic quenching.

To investigate the chiral recognition ability of LHAS with chiral compounds, liquid-state ^{19}F NMR spectroscopy and high performance liquid chromatography (HPLC) were applied in the second part of this study. In ^{19}F NMR study, both 1-(9-anthryl)-2,2,2-trifluoroethanol [TFAE] and 1,1'-bi-2-naphthol bis (trifluoro - methanesulfonate) [BNF] were used as probes of the interaction with LHAS. The effects of concentration and temperature on the interaction of *R*- or

S-BNF with LHAS were discussed. Results obtained indicated that both *R*- and *S*-BNF are associated with more than one site of LHAS, confirming the heterogeneous nature of humic materials. In regards to the enantioselectivity of LHAS towards *R*- and *S*-BNF, minimal or no change in the rate constants was observed between both enantiomers. In contrast to the association behavior of BNF with LHAS, a different trend was noted in the interaction of TFAE with LHAS. This can likely be attributed to structural microenvironment differences of chiral compounds. In regards to the enantioselectivity of LHAS with *R*- and *S*-TFAE, a slight difference in ^{19}F NMR chemical shift was observed between *R*- and *S*-TFAE at the lowest LHAS concentration.

The enantiomeric selectivity of LHAS was further investigated by use of HPLC. In this study, two approaches were applied to evaluate the interaction of *R*- or *S*-TFAE with LHAS. In general, minimal or no change was observed in the enantioselectivity of LHAS towards *R*- and *S*-TFAE for mixtures monitored in the dark for both approaches. In contrast, the interaction of *R*- or *S*-TFAE with LHAS for samples exposed to light showed that LHAS may have a slight enantioselectivity towards these enantiomers for both approaches at a concentration of 30 ppm LHAS. In addition, results obtained from the second approach suggested that the association of *R*- or *S*-TFAE with LHAS is maximized when increasing the LHAS concentration. Finally, both the first and second approaches have advantages and disadvantages. In addition, they can be used as complementary approaches in providing detailed insight into the enantioselectivity of DHM towards chiral compounds.

The studies discussed earlier confirmed that the association of HOC with DHM is dependent on many factors, including the pH, ionic strength, temperature, chemical property of HOC, and nature and concentration of DHM. In Chapter 5, future studies for investigation of the

DHM enatiomeric selectivity with chiral compounds will focus on studying additional DHM with different chiral compounds. In general, as was previously discussed in steady-state fluorescence spectroscopy, DHM absorb radiation at both excitation and emission regions of HOC. As a result, HOC and DHM mixtures usually yield overlapping fluorescence spectra. Steady-state fluorescence spectroscopy, a single wavelength measurement, has the limitation of not providing a deep mechanistic understanding of multi-component systems. This limitation of steady-state fluorescence spectroscopy can be resolved by simultaneously measuring different fluorescence properties of the fluorophore in single measurements, which will also minimize the analysis time. The use of individual fluorescence parameters, including excitation, emission wavelength, time, and their combination will provide more valuable information of multi-component systems. For example, it was previously observed, in Chapters 3 and 4, how powerful the time-resolved fluorescence spectroscopy is in providing a deeper mechanistic understanding of multi-component systems as compared to steady-state fluorescence technique.

Therefore, future directions for investigation of the HOC association behavior with DHM should be focused on the use of various characterization techniques, for example excitation emission matrix (EEM) fluorescence,[1-3] synchronous fluorescence scan (SFS),[4, 5] time-resolved fluorescence spectroscopy, fluorescence correlation spectroscopy (FCS),[6, 7] multi-dimensional fluorescence detection for chromatography,[8, 9] and solid phase extraction with fluorescence detection.[10, 11] In addition, more humic substances will be isolated, fractionated, and characterized from different regions around the world. Different characterization techniques of humic materials will be applied, such as NMR spectroscopy, EEM, SFS, Fourier transform infrared (FTIR) spectroscopy, dynamic light scattering (DLS),[12, 13] transmission electron microscopy (TEM),[14] and atomic force microscopy (AFM).[15, 16]

6.1 References

(1) JiJi, R. D.; Cooper, G. A.; Booksh, K. S. *Anal. Chim. Acta* **1999**, *397*, 61-72.

(2) Westerhoff, P.; Chen, W.; Esparza, M. *J. Environ. Qual.* **2001**, *30*, 2037-2046.

(3) Sun, W. L.; Ni, J. R.; Xu, N.; Sun, L. Y. *Chemosphere* **2007**, *66*, 700-707.

(4) Patra, D.; Mishra, A. K. *Trends Anal. Chem.* **2002**, *21*, 787-798.

(5) Patra, D. *Luminescence* **2003**, *18*, 97-102.

(6) Nakashima, K.; Yashuda, S.; Ozaki, Y.; Noda, I. *J. Phys. Chem. A* **2000**, *104*, 9113-9120.

(7) Geng, L.; Cox, J. M.; He, Y. *Analyst* **2001**, *126*, 1229-1239.

(8) Kaneta, T.; Imasaka, T. *Anal. Chem.* **1995**, *67*, 829-834.

(9) Pino, V.; Ayala, J. H.; Afonso, A. M.; Gonzalez, V. *J. Chromatogr. A* **2002**, *949*, 291-299.

(10) Algarra, M.; Radin, C.; De Violet, P. F.; Lamotte, M.; Garrigues, P.; Hardy, M.; Gillard, R. *J. Fluoresc.* **2000**, *10*, 355-359.

(11) Whitcomb, J. L.; Campiglia, A. D. *Talanta* **2001**, *55*, 509-518.

(12) Muller, F. L. L. *Anal. Chim. Acta* **1996**, *331*, 1-15.

(13) Kretzschmar, R.; Holthoff, H.; Sticher, H. *J. Colloid Interface Sci.* **1998**, *202*, 95-103.

(14) Baalousha, M.; Motelica-Heino, M.; Galaup, S.; Le Coustumer, P. *Microscopy Research and Technique* **2005**, *66*, 299-306.

(15) Maurice, P. A.; Namjesnik-Dejanovic, K. *Environ. Sci. Technol.* **1999**, *33*, 1538-1541.

(16) Gibson, C. T.; Turner, I. J.; Roberts, C. J.; Lead, J. R. *Environ. Sci. Technol.* **2007**, *41*, 1339-1344.

VITA

Hadi M. Marwani was born in Jeddah, Saudi Arabia. He attended a public high school and graduated in 1994. After high school, he joined King Abdulaziz University, Jeddah, Saudi Arabia, in 1994. He majored in chemistry and received a Bachelor of Science degree in chemistry with first class honor (upper division) in 1998. In 1998, he worked as a demonstrator in the chemistry department of King Abdulaziz University. His teaching was specialized in analytical, general, and organic chemistry laboratories. In addition, he worked as research assistant in the organic chemistry under the direction of Professor Hasan Albar. On July 7, 2001, he got married to Nouf Alrobi.

In the spring of 2002, he was admitted to Louisiana State University in Baton Rouge to pursue a degree of Doctor of Philosophy in chemistry, under the guidance of Professors: Isiah M. Warner and Robert L. Cook. On May 9, 2007, he received a chemistry departmental research scholar award for his outstanding achievements in research. His dissertation focuses on the investigation of the association behavior between hydrophobic organic compounds and dissolved humic materials using a series of analytical methods. He graduated with a Doctor of Philosophy degree in chemistry from Louisiana State University in December 2007. He was actively involved in the publication of his dissertation research work in scientific journals prior to his graduation. The articles he published and submitted for publication are listed below:

- **Marwani, H. M.**; Lowry, M.; Keating, P.; Warner, I. M.; Cook, R. L. Segmented Frequency-Domain Fluorescence Lifetime Measurements: Minimizing the Effects of Photobleaching within a Multi-component System. *On-line, Journal of Fluorescence* 2007.

- **Marwani, H. M.**; Lowry, M.; Warner, I. M.; Cook, R. L. Frequency-Domain Fluorescence Lifetime Measurements via Frequency Segmentation and Recombination Method for Pyrene with Dissolved Humic Materials. *In preparation for publication*.

- **Marwani, H. M.**; Fakayode, S. O.; Lowry, M.; Warner, I. M.; Cook, R. L. Application of ^{19}F Nuclear Magnetic Resonance Spectroscopy for Monitoring the Kinetics of Chiral Compounds Interaction with Dissolved Humic Acid. *In preparation for publication.*

- Bwambok, D. K.; **Marwani, H. M.**; Fernand, V. E.; Fakayode, S. O.; Lowry, M.; Negulescu, I.; Strongin, R.; Warner, I. M. Synthesis and Characterization of Novel Chiral Ionic Liquids and Investigation of their Enantiomeric Recognition Properties. *Submitted for publication.*

- Richard, G. I.; **Marwani, H. M.**; Jiang, S.; Fakayode, S. O.; Lowry, M.; Strongin, R. M.; Warner, I. M. The Use of a Fluorescent Resorcinarene for the Chiral Recognition and Determination of Enantiomeric Composition of Amino Acids. *In preparation for publication.*

During his graduate studies, he presented his work at a number of national scientific conferences including:

- "Frequency Domain Fluorescence Lifetime Measurements via Frequency Segmentation and Recombination as Applied to Pyrene Sorption to Dissolved Humic Materials" **Hadi M. Marwani**, Mark Lowry, Isiah M. Warner, and Robert L. Cook. 231st National Annual Meeting of the American Chemical Society, Division of Analytical Chemistry, Atlanta, GA, March 2006.

- "Application of ^{19}F Nuclear Magnetic Resonance Spectroscopy for Monitoring the Kinetics of Xenobiotic Chemical Interactions with Natural Organic Matter" **Hadi M. Marwani**, Robert L. Cook, and Isiah M. Warner. Pittsburgh Conference of Analytical Chemistry and Applied Spectroscopy, Orlando, FL, March 2006.

- "Fluorescence Characterization of Pyrene Associated with Dissolved Humic Materials" **Hadi M. Marwani**, Kristin A. Fletcher, Mark Lowry, Robert L. Cook, and Isiah M. Warner. Pittsburgh Conference of Analytical Chemistry and Applied Spectroscopy, Orlando, FL, March 2005.

- "Associative Study of Chiral Pesticides with Dissolved Humic Acid Using Fluorescence Spectroscopy" **Hadi M. Marwani**, Kristin A. Fletcher, Mark Lowry, Robert L. Cook, and Isiah M. Warner. Pittsburgh Conference of Analytical Chemistry and Applied Spectroscopy, Chicago, IL, March 2004.